INFORMATION TO USERS

Phase Transitions in Superionic PbSnF$_4$

Maria Cecilia S. Madamba

A Thesis

in

The Department

of

Chemistry

Presented in partial Fulfillment of the Requirements
for the Degree of Master of Science at
Concordia University
Montréal, Québec, Canada

December 1998

The author has granted a non-exclusive licence allowing the National Library of Canada to reproduce, loan, distribute or sell copies of this thesis in microform, paper or electronic formats.

L'auteur a accordé une licence non exclusive permettant à la Bibliothèque nationale du Canada de reproduire, prêter, distribuer ou vendre des copies de cette thèse sous la forme de microfiche/film, de reproduction sur papier ou sur format électronique.

The author retains ownership of the copyright in this thesis. Neither the thesis nor substantial extracts from it may be printed or otherwise reproduced without the author's permission.

L'auteur conserve la propriété du droit d'auteur qui protège cette thèse. Ni la thèse ni des extraits substantiels de celle-ci ne doivent être imprimés ou autrement reproduits sans son autorisation.

Canada

NOTE TO USERS

Page(s) not included in the original manuscript are unavailable from the author or university. The manuscript was microfilmed as received.

ii

ABSTRACT

Phase Transitions in Superionic PbSnF$_4$

Maria Cecilia S. Madamba

PbSnF$_4$ is the highest performance fluoride ion conductor known to date. We have studied the phase transitions it undergoes under three different conditions: (i) versus the amount of hydrofluoric acid used for the preparation by the aqueous route, (ii) upon application of mechanical energy, and (iii) versus temperature.

The addition of an aqueous solution of lead(II) nitrate to a fresh aqueous solution of SnF$_2$ results in the precipitation of α-PbSnF$_4$(aq$_1$), which is very highly strained in the $(\bar{a},\bar{b})$ plane of the tetragonal unit-cell. If a very minor amount of hydrofluoric acid is used, the strain increases and o-PbSnF$_4$ is obtained. The α-PbSnF$_4$ $\rightarrow$ o-PbSnF$_4$ transition is mostly a bidimensional phase transition, which includes a highly disordered intermediate *"transitional phase"*.

Ball milling results in a phase transition, giving microcrystalline disordered $\mu\gamma$-PbSnF$_4$, a cubic β-PbF$_2$ like phase. Tests were performed to make sure the $\mu\gamma$-PbSnF$_4$ samples are indeed microcrystalline cubic PbSnF$_4$ and not a mixture of microcrystalline β-PbF$_2$ and amorphous SnF$_2$.

Milling α- and β-PbF$_2$ for comparison and testing showed that both $\beta \rightarrow \alpha$ and $\alpha \rightarrow \beta$ transitions take place upon milling. Stirring α-PbF$_2$ in an aqueous solution of SnF$_2$

iii

results in the formation of α-PbSnF$_4$(aq$_2$) or Pb$_2$SnF$_6$ depending on the conditions whereas no reaction occurs with β-PbF$_2$. When all the phases of PbSnF$_4$ are heated, phase changes take place versus temperature and time.

Our findings provide key knowledge that will have to be taken into account in the fabrication of practical devices using PbSnF$_4$ for guaranteed reproducible results, long term stability and stable output of the device.

ACKNOWLEDGEMENTS

thank my colleagues in our group for their input, friendship and encouragement during my stay.

Finally, all of these would not have been possible without the tremendous support of my family. I would like to thank my brother, Victor and most especially my mother, Merlinda for believing in me and for the encouragement, understanding and patience they showed throughout my studies.

To my mother, Merlinda

and

in memory of my late father, Robert

Table of Contents

List of Figures

List of Tables

CHAPTER 1

INTRODUCTION

1.1. HISTORY OF EARLY WORKS ON PbSnF$_4$

The studies carried out on PbSnF$_4$ obtained by precipitation prior to this work are summarized in Table 1.

1.1.1. Synthesis and Crystal System

A pioneering work on the MF$_2$-SnF$_2$ systems in both aqueous and molten states was carried out by Donaldson and Senior in 1967[1]. This group was the first to prepare PbSnF$_4$. Two methods were used; (i) the addition of an aqueous solution of Pb(NO$_3$)$_2$ to an aqueous solution of SnF$_2$ (30% w/v), and (ii) by cooling from the melt a stoichiometric mixture of α-PbF$_2$ and α-SnF$_2$. The PbSnF$_4$ phases obtained from both methods were found to be identical. They found it crystallizes in the tetragonal system regardless of the method of preparation.

In 1975, Dénès et al. repeated the preparation both by precipitation and by direct reaction of α-PbF$_2$ and α-SnF$_2$ at 250°C, and also found the same product which they characterized by X-ray powder diffraction[2]. They found them to be identical to Donaldson's and Senior's[1], with the same crystal system. In the same study, Dénès et al. determined on a single crystal that the space group was P4/nmm-D4h, No. 129, tetragonal. Dénès et al. also prepared isotypic SrSnF$_4$ and BaSnF$_4$ by direct solid state

Table I: History of the Symmetry of the Unit-cell of PbSnF$_4$ Obtained by Precipitation

Year	Authors	Crystal System[**]	Reference
1967	Donaldson and Senior	Tetragonal	1
1975	Dénès et al.	Tetragonal	2
1978	Réau et al.	Orthorhombic	3
1979	Pannetier, Dénès et al.	Tetragonal	4
1980	Pérez et al.	Monoclinic	5
1986	Birchall, Dénès et al.	Tetragonal	6
1988	Parris and Dénès	Tetragonal and Orthorhombic	7

[**] = PbSnF$_4$ phase obtained by precipitation of a solution of Pb(NO$_3$)$_2$ to an aqueous solution of α-SnF$_2$.

2

reaction at 500°C[2], in gold or copper containers and established that the $MSnF_4$ structures (M = Pb, Ba, Sr) were closely related to the PbClF-type with ordering between M and Sn along $\vec{c}$, whereas there is an anion ordering in PbClF. In 1978, Réau et al. confirmed the preparation of $PbSnF_4$ by the addition of a solution of $Pb(NO_3)_2$ to a solution of SnF_2 with a molar ratio of $Pb(NO_3)_2 / SnF_2$ 1:4 and also confirmed the solid state synthesis of $PbSnF_4$ in gold containers[3]. However, the product formed from the aqueous solution was found to have an orthorhombic symmetry, which is in conflict with the previous results[1,2].

In 1979, Pannetier et al.[4], on the other hand, confirmed that their earlier findings[2] and Donaldson et al.'s[1] as being correct i.e. the $PbSnF_4$ phase obtained by both methods crystallizes in the tetragonal symmetry. They reported that, in addition, to the tetragonal α-phase, two other high temperature phases exist, tetragonal $β-PbSnF_4$ and cubic $γ-PbSnF_4$, however no orthorhombic phase was observed. The low symmetry compound reported by Réau[3] was interpreted as originating possibly from a mixture of phases.

In 1980, Pérez et al.[5], reported that previous findings from their own group[3] were incorrect and claimed that there were five phases of $PbSnF_4$. The room temperature phase obtained by precipitation found by Dénès' and Donaldson's groups as being tetragonal and claimed previously by their own group[3] as being orthorhombic, was now found to be monoclinic. High temperature phases (β and $γ-PbSnF_4$) were also reported in these studies[3-5].

In 1988, Parris, and Dénès[7], clarified the controversy about the symmetry of the unit-cell of the material obtained by precipitation. They scrutinized the conditions of

preparation from aqueous solutions reported in the literature and found out that the conditions were not all exactly the same and often were not well specified. Such conditions as temperature and Pb/Sn ratio were not always given. In addition, the SnF_2 solution used was acidified with the addition of HF by Réau et al. but not by the others. Parameters such as time (SnF_2) and time ($PbSnF_4$) (Table II) had not been established yet and were not mentioned in any of the earlier reports. This induced Parris and Dénès to establish precise reaction parameters by the use of very well defined conditions and vary only one condition at a time in order to determine its influence.

Parris and Dénès[7] found that the addition of HF to the solution is the key factor regarding the symmetry of the phase obtained. They established that a transition from tetragonal to orthorhombic symmetry takes place as a function of the amount of HF added to the aqueous solution of SnF_2 used in the preparation, and they defined other experimental parameters that have a strong influence on the transition from tetragonal to orthorhombic. In the same study, they also observed that the magnitude of the orthorhombic distortion is a function of the amount of HF used[7] and no monoclinic distortion was observed. These findings were recently corroborated by us[8] and two Japanese groups[9-11].

In 1991, R. Kanno et al.[9] found that the preparation of $PbSnF_4$ from aqueous solution results in two phases: tetragonal and monoclinic. However, the preparative conditions necessary for the reaction was not mentioned, particularly the presence of HF. The monoclinic phase they obtained was consistent with that of Pérez et al.[5] which seemed to be identical to what Dénès et al.[7] called o-$PbSnF_4$ where $a = b$. Since the X-ray powder diffraction pattern is indexable in orthorhombic with equal success as in

Table II : Preparation Parameters used in this work

Parameter	Description	Range
X	$Pb(NO_3)_2$ / SnF_2 molar ratio in the reaction mixture	0.2
t (SnF_2)	time between the dissolution of SnF_2 in H_2O (and HF where indicated) and the beginning of addition of first drop of $Pb(NO_3)_2$	0 hour
t ($PbSnF_4$)	time between the end of the addition of $Pb(NO_3)_2$ and the filtration of the product	0 hour
C (SnF_2)	concentration of SnF_2	1.5M
C ($Pb(NO_3)_2$)	concentration of $Pb(NO_3)_2$	1.7M
VR	$V_{(H_2O)}/V_{(HF - H_2O)}$ Total volume = 11ml.	0 - 0.57
Beaker	nature of the beaker used for reaction	teflon
Gas	degassing the water solvent and gas blanket over the reaction	air
Rate	rate of addition of one solution into the other	5.0mL/min.
Order	$Pb(NO_3)_2$ solution is added to the SnF_2 solution	Pb in Sn
T	temperature of the reaction (°C)	RT
Stirring Rate	rate of stirring of the reaction mixture	Med to Fast

monoclinic, there is no reason to use the monoclinic cell, since it requires an extra variable parameter (β angle) and has accidentally $a = b$ not constrained by symmetry. Other means could justify choosing the monoclinic unit-cell, like single crystal diffraction, unfortunately, quality single crystals have not been obtained from precipitation.

1.1.2. Crystal Structure

The resolution of the crystal structure of α-PbSnF$_4$ was difficult and one of the reasons was that good quality single crystals are difficult, if not impossible, to prepare. The strong preferred orientation of PbSnF$_4$ and low scattering of X-rays by F$^-$ compared to the heavy metal Pb, together with low crystal quality made the structure resolution by X-ray diffraction (XRD) impossible[6]. The very highly enhanced preferred orientation also made the analysis of neutron powder diffraction data difficult since it modifies the line intensities by very large factors. This was mainly due to the very strong texture caused by the sheet-like structure of the materials, which gave an inadequate Bragg peak intensity. In addition, the high F$^-$ mobility resulted in TDS (Thermal Diffuse Scattering) which adds some broadening at the base of the neutron Bragg peak and thereby modifies both their intensity and lineshape. Since the refinement of the structure of α-PbSnF$_4$ was not entirely successful due to the difficulties encountered, the refinement was carried out on BaSnF$_4$ (isotypic with α-PbSnF$_4$), by Birchall et al. in 1986[6]. This study was confirmed and completed by Dénès et al. in 1991[12] using a combination of

6

methods such as XRD, Mössbauer Spectroscopy, and EXAFS (Extended X-ray Absorption Fine Structure). The structure of α-PbSnF$_4$ is closely related to that of β-PbF$_2$[12]. The metal ions are ordered parallel to the $\bar{c}$ axis according to the following sequence....Pb Pb Sn Sn Pb Pb.... Figure 1 shows a projection of the fluorite-type β-PbF$_2$ and α-PbSnF$_4$ in the same orientation. In β-PbF$_2$ (fluorite-type), Pb is located in the center of a PbF$_8$ cube (fig. 2a).

The tin(II) coordination is a SnF'$_4$E pseudo-octahedron (fig. 2b) with four equivalent Sn-F' equatorial bonds about equal to the sum of the ionic radii, and a short axial Sn-F bond which is strongly covalent. Tin(II) can be considered as being sp^3d^2 hybridized and the lone pair E is located opposite the short axial Sn-F bond. Tin can also be viewed as being located in a cube, a face of which is missing, and with the opposite remaining face being perforated through its center by the short Sn-F covalent bond. (fig. 2b). In this case, one can view tin(II) as being sp hybridized, with the cation [ESnF]$^+$ binding ionically to a face of the F$_8$ cubes not containing Pb. The coordination of lead(II), on the other hand, is more closely related to that found in β-PbF$_2$ i.e. distorted cubic PbF''$_4$F$_4$ with four additional Pb-F bonds that are secondary weaker bonds to the fluorine atoms that are strongly axially bonded to four adjacent tin atoms to make a total coordination PbF''$_4$F'$_4$F$_4$ (fig. 2c & 2d)[6,12]. Table III shows the M-F distances of β-PbF$_2$, BaF$_2$ and BaSnF$_4$ (isotypic with PbSnF$_4$).

The tin lone pairs are oriented parallel to the $\bar{c}$ axis of the unit-cell and away from the lead/fluorine layers in order to make four equivalent Sn-F-Pb bridges possible[6,12]. The lone pairs from two adjacent tin planes are located in a plane perpendicular to $\bar{c}$ (fig.1b). This plane replaces a fluorine plane of the β-PbF$_2$ structure
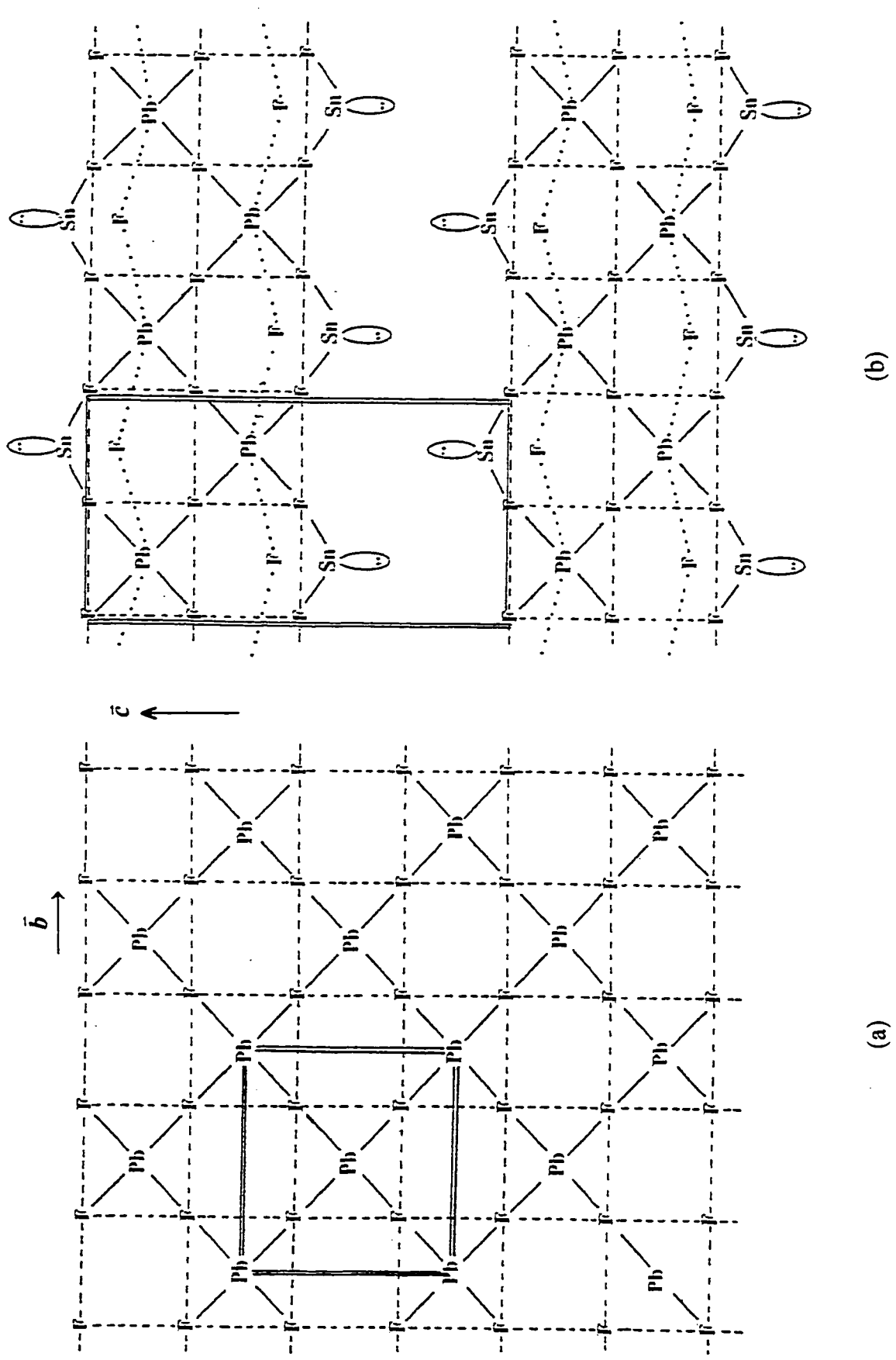
Figure 1: Projection of the structures of (a) β-PbF$_2$ and (b) α-PbSnF$_4$ onto the ($\bar{b}$, $\bar{c}$) plane (β-PbF$_2$ axes).

8
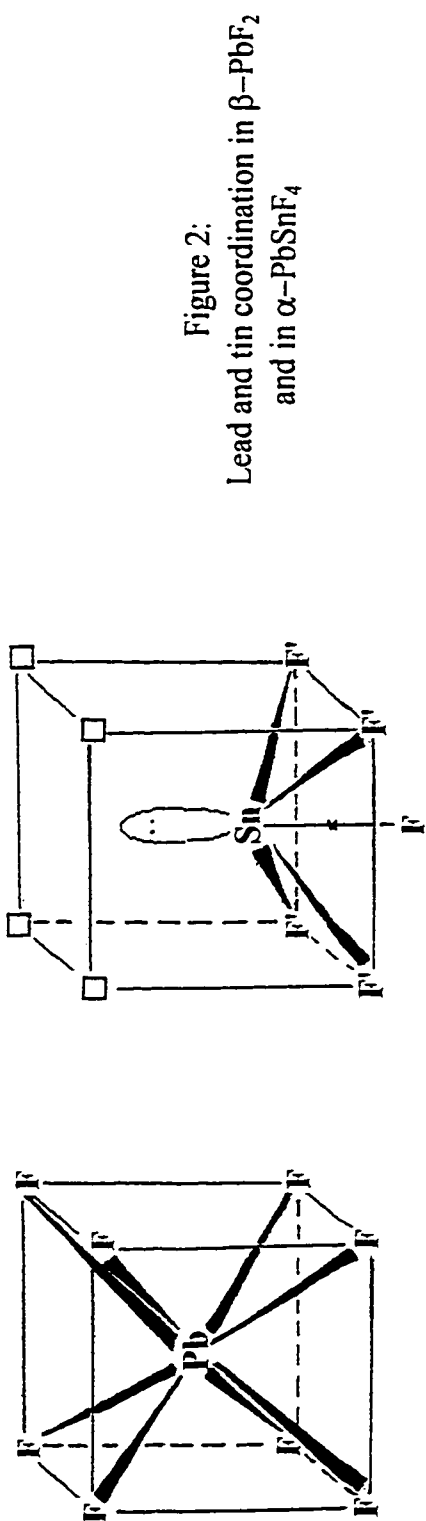
Figure 2:
Lead and tin coordination in β–PbF₂
and in α–PbSnF₄

[a]
PbF₈ cube in β–PbF₂

[b]
SnFF′₄E pseudo-octahedron
in α–PbSnF₄
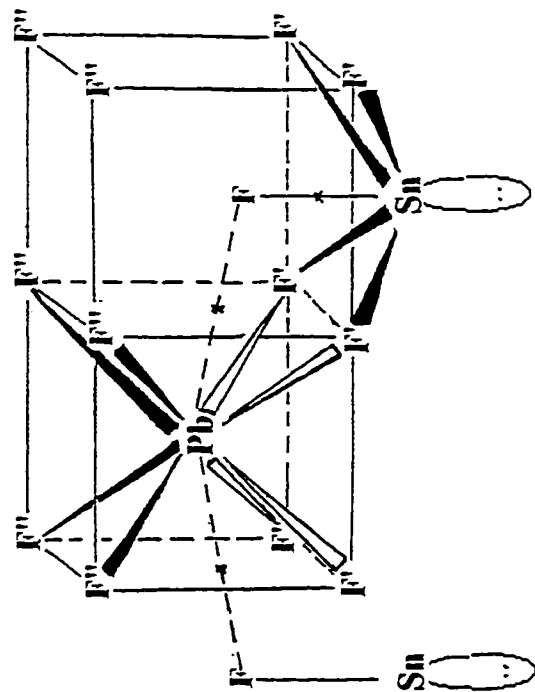
[c]
PbF″₄F′₄F₄ unit in
α–PbSnF₄

(d) Top view of the lead
coordination in α–PbSnF₄
(F′ and F″ are superimposed)

9

Table III : M-F Distances of β-PbF$_2$, BaF$_2$ and BaSnF$_4$[12]

M-F	β-PbF$_2$	BaF$_2$	BaSnF$_4$*
Pb-F distances (Å)	2.578	-	-
Ba-F distances (Å)			
Ba-F"	-	2.68	2.626
Ba-F'	-	-	2.955
Ba-F	-	-	3.148
Sn-F distances (Å)			
Sn-F	-	-	2.029
Sn-F'	-	-	2.282

* = BaSnF$_4$ is isotypic with PbSnF$_4$

and contains the missing face of the cube in the coordination sphere of Sn. This results in a 2-D (two dimensional) structure, which is in agreement with the sheet-like crystallites and strong preferred orientation of α-PbSnF$_4$[6]. Two recent structural studies of PbSnF$_4$, one by R. Kanno et al.[9] and the other by Ito et al.[10] corroborate Dénès et al.'s results[6,12]. Ito et al. carried out a single crystal X-ray diffraction measurements of a tetragonal form PbSnF$_4$ however, the single crystal was prepared at a high temperature (i.e. annealing at 280°C). The c parameter of 11.744 Å is clearly higher than the value reported by others[1-5,7-12] for α-PbSnF$_4$. From the results of Dénès et al.[4,12], heating at high temperature results in β-PbSnF$_4$ which is also tetragonal but has a much larger superstructure and a tetragonal distortion that is slightly different from α-PbSnF$_4$.

On the other hand, R. Kanno et al.[11] carried out a Reitveld analysis (profile refinement) of neutron powder diffraction patterns at different temperatures -253°,-103°

and -27°C and they found that the structure of α-PbSnF$_4$ is the same as that found by Dénès et al.[6,12].

1.1.3. Phase Transitions

PbSnF$_4$ is to date the highest performance fluoride ion conductor. Its structure is derived from the fluorite-type (CaF$_2$) and it undergoes a number of phase transitions. Phase transitions are physical or structural changes without any change in chemical composition, taking place as some physical parameter (e.g. temperature, pressure, magnetic field, electrical field or applied stress) is varied. Changes of chemical composition within a solid solution i.e. without a structural change, but with a change in the statistical population of some sites, can have the same effect.

A few examples of phase transitions are:
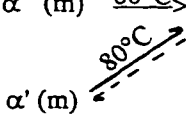
1. Ice $\rightarrow$ water : this is a phase transition with a change of physical state (solid $\rightarrow$ liquid)

2. α-PbF$_2$ $\rightarrow$ β-PbF$_2$ a solid state phase transition involving symmetry and coordination changes; there is no change of physical states;

3. Insulator $\rightarrow$ Superconductor at low temperature;

4. ferromagnetic $\rightarrow$ paramagnetic.

Cases 3 and 4 are phase transitions with changes in a physical property with or without structural changes.

Since many of the physical properties of a solid are related to its crystal structure, a structural phase transition results in a change of some properties. The study of phase transitions in solids is important in order to understand the properties of solids when structural changes takes place as medium conditions change.

Several authors have reported phase transitions in $PbSnF_4$. Table IV shows the different phase transitions reported in the literature. In sequence (i), Réau et al. reported an orthorhombic symmetry below 80°C which is in contradiction with previous studies by Donaldson and Senior[1] and Dénès et al.[2]. In 1979, Pannetier et al. reported another sequence of phase transitions for $PbSnF_4$ which is different from that of Réau's group. In sequence (ii), the room temperature phase is tetragonal (α), no phase transition was observed at 80°C, a second tetragonal phase (β) with a larger superstructure exists above 260-280°C, and a cubic high temperature phase (γ) is obtained at 390°C, and its melts in closed inert containers or decomposes in open containers above 420°C[4]. β-$PbSnF_4$ is a high temperature phase, however, it is quenchable to ambient temperature and it can be stored at ambient conditions in the metastable state for a fairly long time (days or weeks), whereas the γ-phase is non-quenchable since the $\beta \rightleftarrows \gamma$-transition is reversible without hysteresis. However in sequence (iii), the partial transition of $\beta \rightarrow \alpha$ back to the stable state was observed in-situ by recording the X-ray diffraction pattern versus temperature (T = 170° - 260°C)[4]. It was also observed to occur sometimes spontaneously at ambient condition, and in that case it was very sluggish (sequence iv)[4]. In sequence (v), it was also observed to occur once very rapidly, when cooled to liquid nitrogen temperature[4]. A sequence of phase transitions (vi), more complex than in their earlier work[3], involving two monoclinic phases α and α' was reported in 1980 by Pérez et al.[5].

Table IV : Sequence of Phase Transitions Reported in the Literature

	REF. NO.
(i) α (orthorhombic) $\xrightarrow{80°C}$ β (tetragonal) $\xrightarrow{355°C}$ γ (cubic) $\xrightarrow{390°C}$ melt	3
(ii) α (tetragonal) $\xrightarrow{260\text{-}280°C}$ β (tetragonal) $\xrightarrow{390°C}$ γ (cubic) $\xrightarrow{\geq420°C}$ melt or decomposition if in open containers (iii) β (tetragonal) $\rightarrow$ α (tetragonal) on heating (T = 170° - 260°C) sluggish (iv) β (tetragonal) $\rightarrow$ α (tetragonal) at ambient temperature, sometimes only, very sluggish (v) β (tetragonal) $\rightarrow$ α (tetragonal) at 77K, sometimes only, fast	4
(vi) α (m) $\xrightarrow{80°C}$ β (t) $\xrightarrow{350°C}$ β' (t) $\xrightarrow{380°C}$ γ (cubic) $\xrightarrow{390°C}$ melt α' (m) $\xrightarrow{80°C}$ where: m = monoclinic t = tetragonal	5
(vii) α (tetragonal) $\xrightarrow{25°C}$ o (orthorhombic) versus VR = $V_{HF}/V_{(HF - H_2O)}$ in the SnF_2 solution used for precipitation reaction	7
(viii) β (tetragonal) $\xrightarrow{50°C}$ α' (monoclinic) versus time	9,11

In 1988, (vii) Parris and Dénès published the α-(tetragonal) $\rightarrow$ o-(orthorhombic) phase transition upon the addition of a minor amount of HF to the aqueous SnF_2 solution used for the synthesis[7]. In the same year, two heat capacity anomalies were observed by another group, Callanan et al.[13]. These are (i) between -143 and -113°C where they assumed that the heat capacity was due to some structural rearrangement not reported before, (ii) the range from 27 to 79°C was assumed to be

13

the monoclinic (α) $\rightarrow$ tetragonal (β) phase transition which was reported in 1980 by

Pérez et al.[5]. R. Kanno et al. in 1991[9], reported they were unable to observe the

(β) tetragonal $\rightarrow$ (α') monoclinic transition upon annealing (sequence viii) as reported by

Pérez et al.[5] earlier. In addition, they also found that at 80°C, no symmetry change

occurs, which is inagreement with Dénès et al.[4], and in contrast with the phase

transitions reported by Réau et al.[3] and Pérez et al.[5].

In 1994, R. Kanno et al.[11] found that tetragonal PbSnF$_4$ undergoes a transition to

monoclinic where a $\approx$ b upon cooling from -103 to -253°C, using the Rietveld analysis of

TOF (Time of Flight) neutron diffraction from -253° to 27°C to determine the structure

of PbSnF$_4$.

1.2. STRUCTURE OF α-PbSnF$_4$ AND HIGH FLUORIDE ION MOBILITY

Fluorides crystallizing in the fluorite-type structure (CaF$_2$) are the best solid

fluoride-ion conductors for binary metal fluorides. The high mobility of fluoride ions in

these materials is due to the ability of the fluorite structure to accommodate a large

number of Frenkel defects in the fluoride sublattice. Frenkel defects are a combination

of vacancies (vacant sites that would be normally occupied in a defect-free crystal) and

interstitials (occupied site that should be vacant) for the same type of ions (Figure 3).

PbSnF$_4$ is to date the highest performance fluoride ion conductor and its structure

is derived from the fluorite type. Replacing half of the lead ions by divalent tin in β-PbF$_2$

gives PbSnF$_4$. Ordering of the metal ions along the $\vec{c}$ direction results in the doubling

of the c parameter of the unit cell, the loss of the cubic symmetry and of the F lattice
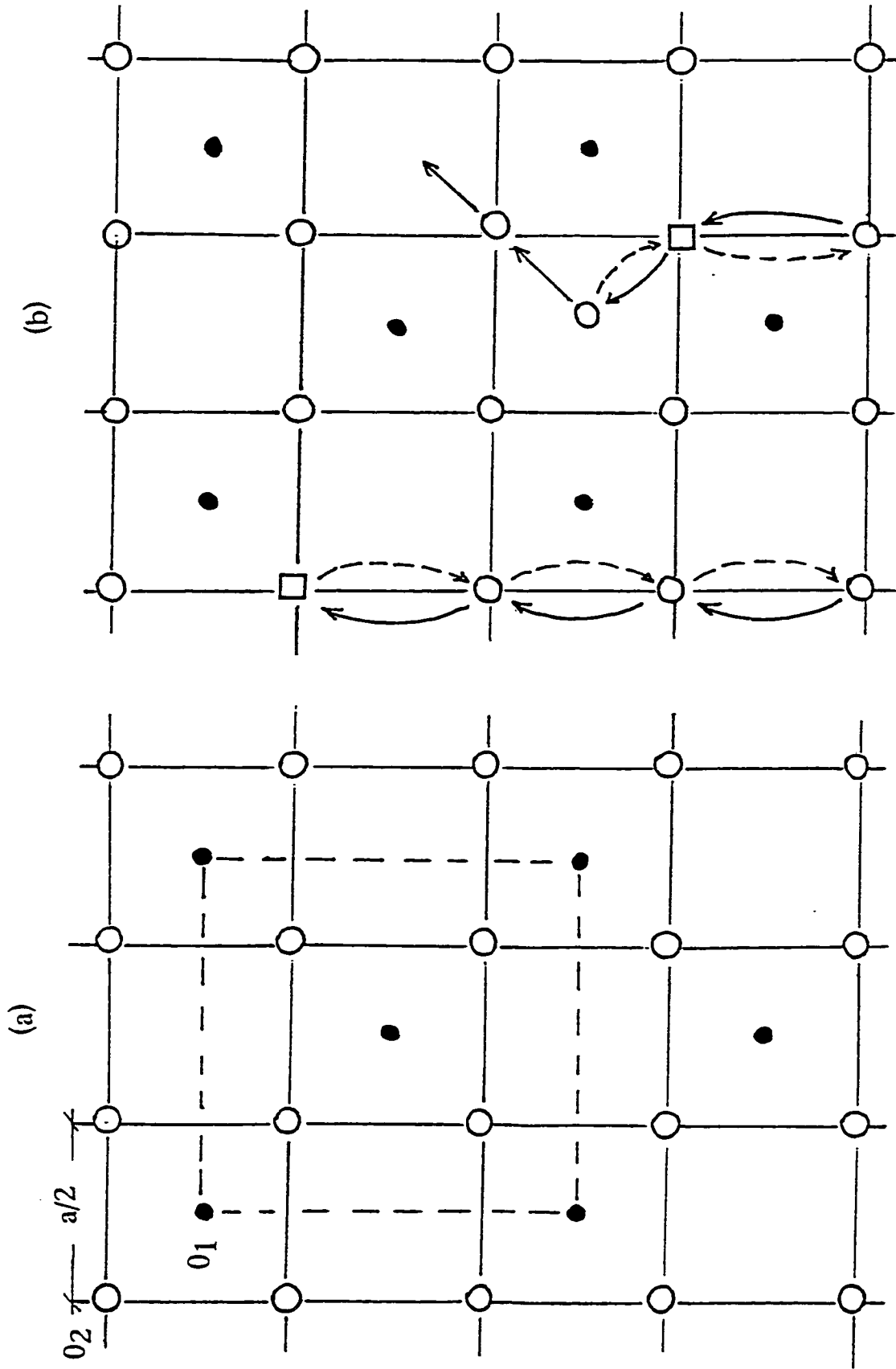
Figure 3: (a) The fluorite-type: rows of F_8 cubes and (b) Conduction by Frenkel defects in fluorite

translations. The layer of fluorine ions separating the adjacent tin layers is missing thereby forming a layered structure (fig. 1b). This results in an increase in conductivity by three orders of magnitude (Fig. 4). α-PbSnF$_4$ structure shows a tetragonal distortion relative to the cubic fluorite type and a very strong anisotropy with Pb and Sn being ordered[6,12].
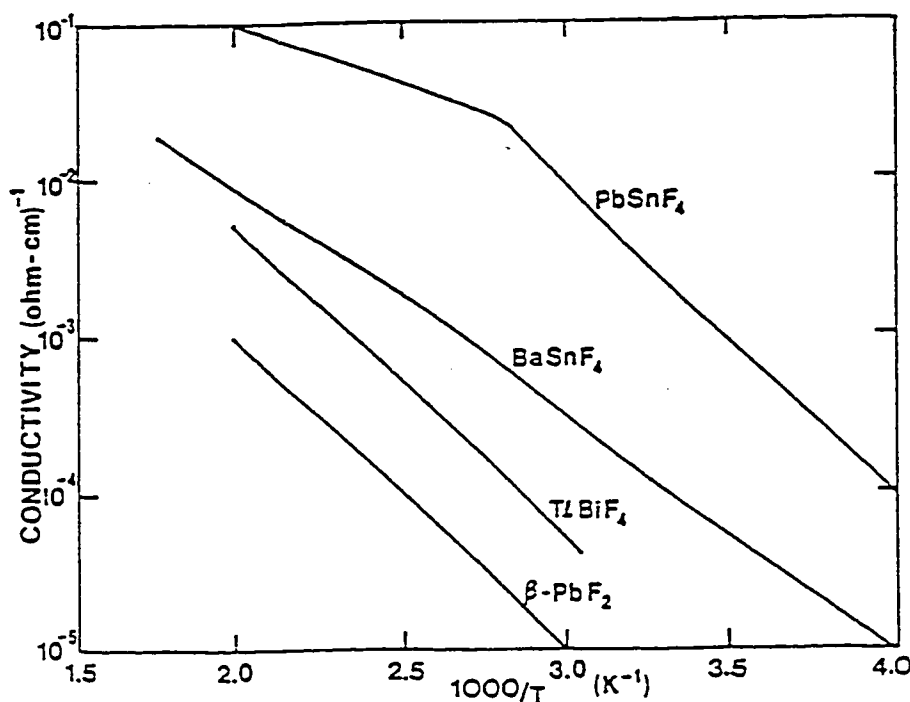
Figure 4: Log of conductivity versus 1000/T for several fluoride ion conductors[14]

Figure 1 shows a projection of the structure of β-PbF$_2$ and α-PbSnF$_4$. In the fluorite-type β-PbF$_2$ the metal ions are located at the origin of the unit-cell and in the middle of each face and thus describe a face-centered cubic lattice. The F$^-$ anions, on the

other hand, are located at the x,y,z coordinates with x, y and z all equal to ¼ or ¾, i.e. there are 2 F⁻ ions on each of the four body diagonals of the cube, shifted by ¼ and ¾ from the origin. The F⁻ ions describe primitive cubes wherein the edge of each is half the edge of the unit-cell. These cubes of fluoride ions form a three dimensional network parallel to the three axes of the unit-cell. The F⁻ ions also describe two face centered cubic lattices (edge equal to the unit-cell edge) shifted ½, ½, ½ apart, in agreement with the Fm3m space group.

Empty F_8 cubes in each row alternate with cubes having a metal ions in their center along the three axes of the unit-cell, giving an occupancy factor of 50%. The presence of such a large number of vacant metal positions in the fluorite structure allows for the presence of a large number of Frenkel defects, and thus has been held responsible for the high ionic conductivity. The availability of such vacant sites allows the F⁻ ions to have a high mobility. However, it was recently established that this model cannot fully account for the high conductivity of β-PbF$_2$, and not at all for PbSnF$_4$[15]. Indeed, the empty F_8 cubes in β-PbF$_2$ are barely large enough to accommodate a fluoride ion, without strain when BaF$_2$ can very easily, therefore, contrary to observations, BaF$_2$ should be more conducting. In the α-PbSnF$_4$ structure, all the F_8 cubes are filled, since those that are empty in BaF$_2$ contain the fluorine atom axially bonded to tin in α-PbSnF$_4$. Since the axial bond is strongly covalent, there is little opportunity for the axial fluorine to be mobile, and there is no empty F_8 cube to make possible the creation of a large number of Frenkel defects. The high polarizability of the Pb^{2+} ion, making possible large local distortion to accommodate F⁻ ions, is accounted for the high conductivity of β-PbF$_2$. The presence of covalently bonded Sn(II) in the structure of α-PbSnF$_4$ derived from ionic type

β-PbF$_2$ seems to generate a large number defects on the fluoride sublattice, which are responsible for its high ionic conductivity.

Tetragonal α-PbSnF$_4$ as shown on Figure 1 has the same cationic sublattice, as that of β-PbF$_2$ except that half of the lead(II) is replaced by tin(II), which are located in a five-fold coordination since tin(II) can not take a cubic coordination because of its stereoactive lone pair. The lone pair stereoactivity, and hence covalency of Sn-F bonding, with the stereoactive lone pair located on one of the tin hybrid orbitals, has been proven by ^{119}Sn Mössbauer spectroscopy[6,12,16]. This situation contrasts with the case of ionic bonding, with the lone pair on the Sn^{2+} cation being located on the unhybridized 5s orbital, like in SnCl$_2$ and Ba$_{1-x}$Sn$_x$Cl$_{1+y}$F$_{1-y}$[17,18]. An unhybridized lone pair can be partially transferred to the conduction band to give semiconducting properties. There is even a known case of total transfer of the unhybridized lone pair to the conduction band to give metal conduction, i.e. in CsSnBr$_3$[19]. This is not possible for a hybridized lone pair, which is locked in the valence shell of tin[18,20].

1.3. CONDUCTING PROPERTIES AND APPLICATIONS OF PbSnF$_4$

The exceptionally high F$^-$ ion mobility in the MSnF$_4$ structure has been studied by the complex impedance method on polycrystalline samples of PbSnF$_4$[3,10] and BaSnF$_4$[14], including more recent measurements on our own PbSnF$_4$ samples[21,22]. They have a conductivity about three orders of magnitude higher than that of the corresponding MF$_2$. PbSnF$_4$ is the highest performance fluoride ion conductor known to date. Dénès et al. have shown that, in the α-PbSnF$_4$ structure, the fluorine atoms axially bonded to tin

occupy all the previously (in β-PbF$_2$) empty F$_8$ cubes (half of the total F$_8$ cubes) which are not occupied by a metal ion, and thus are not available for the formation of Frenkel defects like in the MF$_2$ fluorite-type structure[6,12]. Various X-ray and neutron diffractions, EXAFS, NMR and Mössbauer spectroscopic studies have established that: (i) some of the fluorine sites are underpopulated, therefore, there is a significant amount of fluorine in interstitial positions, (ii) there is no exchange between frozen fluorine sites and disordered sites, (iii) as temperature increases, more and more fluoride ions leave their normal sites to go to interstitial positions, (iv) the very high F$^-$ ion conductivity of MSnF$_4$ is related to the distortions created by the stereoactivity of the tin(II) lone pair and the covalency of the Sn-F bonds, in contrast with typically ionic Pb-F bonds[10-12,15,23,24].

The exceptionally high conductivity of PbSnF$_4$ has recently been used for the design of chemical sensors that could have practical applications. An amperometric oxygen sensor with fast response at room temperature was designed by Wagaki and Kuwano[25] and applied for the fabrication of iron(II) phthalocyanine-based sensing electrodes containing carbon microbeads[26].

1.4. PREPARATION OF PbSnF$_4$ AND UNIT-CELLS

There are two known main routes to prepare PbSnF$_4$. They are the following:

1. From solution:

$$2SnF_2 + Pb(NO_3)_2 \xrightarrow{\ H_2O\ } \alpha\text{-PbSnF}_4 + Sn^{2+} + 2NO_3^- \qquad (I)$$

[α- PbSnF$_4$ is (tetragonal)]

19

$$2SnF_2 + Pb(NO_3)_2 \xrightarrow{H_2O/HF} \text{o-PbSnF}_4 \text{ or m-PbSnF}_4 + Sn^{2+} + 2NO_3^- \qquad (II)$$
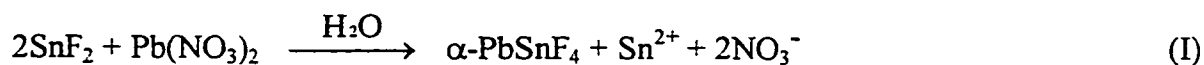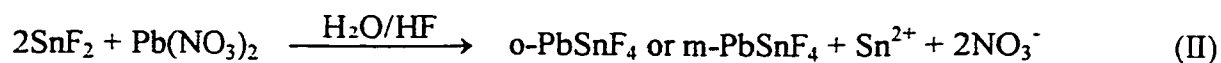
[o- PbSnF$_4$ is orthorhombic, m-PbSnF$_4$ is monoclinic]

2. By direct reaction at high temperature:

$$\alpha\text{-PbF}_2 + \alpha\text{-SnF}_2 \quad \begin{cases} \xrightarrow{250°C} \alpha\text{-PbSnF}_4 \text{ (tetragonal)} \\[2em] \xrightarrow{>270°C} \beta\text{-PbSnF}_4 \text{ (tetragonal)} \end{cases} \qquad (III)$$
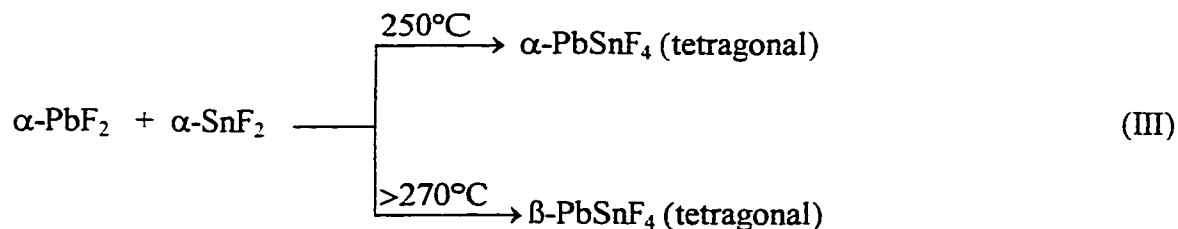
In the preparations from aqueous solutions, PbSnF$_4$ precipitates as soon as the two solutions are mixed. Two moles of SnF$_2$ are required for each of lead nitrate, since SnF$_2$ is the only source of fluorine. The reason most authors use an excess of SnF$_2$ is to avoid the formation of Pb$_2$SnNO$_3$F$_5$·2H$_2$O, which has been reported to form under a local or global excess of lead nitrate [1,7]. The solid state synthesis of PbSnF$_4$ from α-PbF$_2$ and α-SnF$_2$ gives α-PbSnF$_4$ at 250°C and β-PbSnF$_4$ above ca. 270°C. Although β-PbSnF$_4$ is also tetragonal, it has a different supercell than the α-phase; it is much larger with a longer periodicity along the three axes of the unit-cell.

Figure 5 shows the relationships between the unit-cells of β-PbF$_2$, α-PbSnF$_4$, o-PbSnF$_4$, β-PbSnF$_4$ and γ-PbSnF$_4$[4,12]. It can be seen that a_α (= b_α) is about equal to half the diagonal of the ($\bar{a},\bar{b}$) face of β-PbF$_2$ ($a_\alpha \approx a_F/\sqrt{2}$), whereas c_α is about double that of β-PbF$_2$ ($c_\alpha \approx 2c_F$), due to the ......Pb Pb Pb Sn Sn...... ordering. The unit-cell axes of β-PbSnF$_4$ have the same direction as for α-PbSnF$_4$ with

a_F, a_γ

b_F, b_γ

β-PbF$_2$ and γ-PbSnF$_4$

b_α a_α

α-PbSnF$_4$

a_o

b_o

o-PbSnF$_4$

a_β

b_β

β-PbSnF$_4$

c_β

c_α, c_o

c_γ, c_F

Figure 5: Relationships between the unit-cells of cubic β-PbF$_2$ and γ-PbSnF$_4$(a_F, b_F, c_F), tetragonal α-PbSnF$_4$ (a_α, b_α, c_α), orthorhombic o-PbSnF$_4$ (a_o, b_o, c_o) and tetragonal β-PbSnF$_4$ (a_β, b_β, c_β).

21
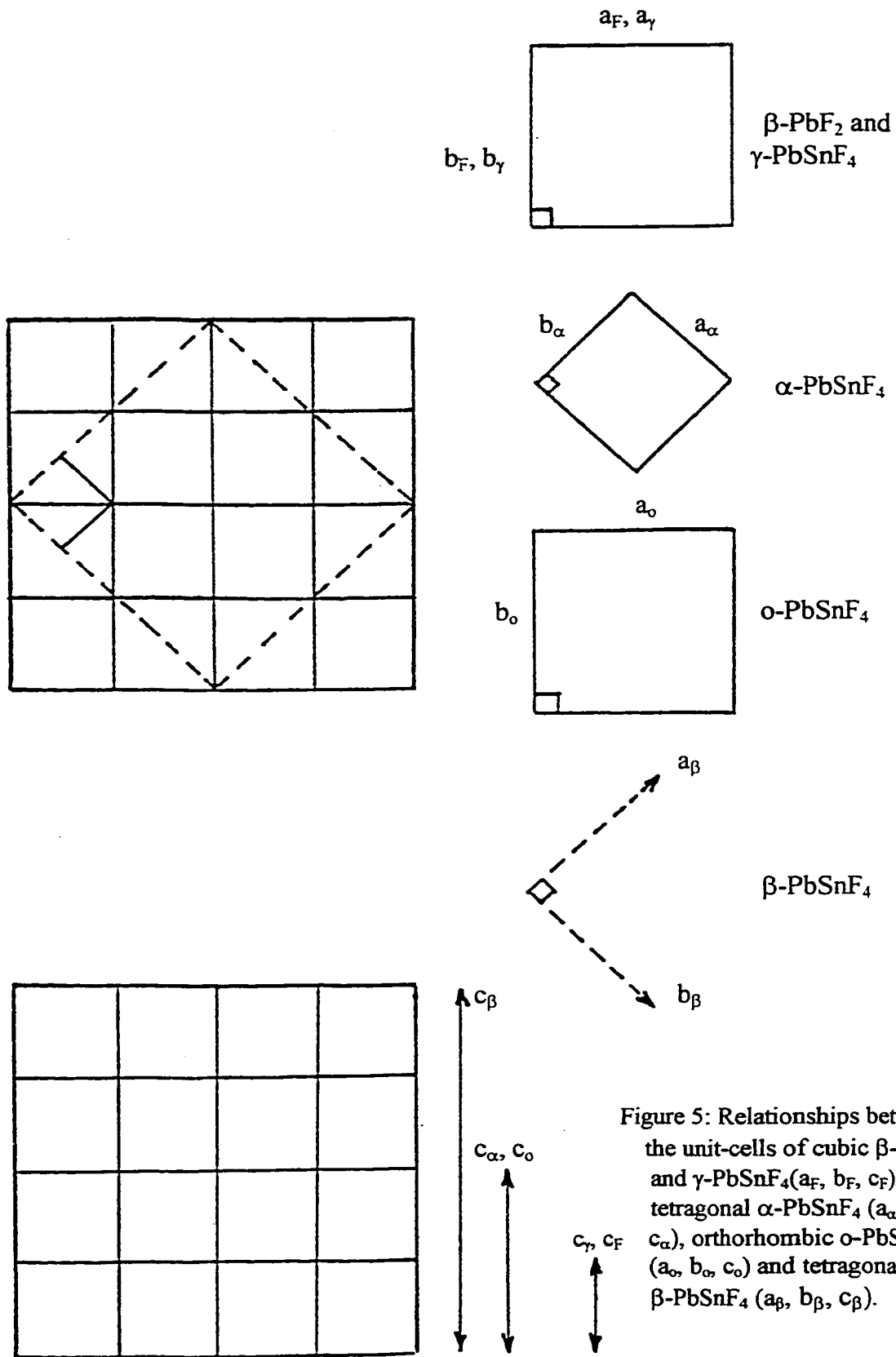
a_β ($= b_\beta$) $\approx 4a_\alpha$ and $c_\beta \approx 2c_\alpha$, resulting in a volume $V_\beta \approx 32V_\alpha$. For o-PbSnF$_4$,

a_o and b_o ($a_o \neq b_o$) $\approx a_\alpha\sqrt{2}$ (i.e. a_o and $b_o \approx a_F$), and $c_o \approx c_\alpha$, which give $V_o \approx V_F \approx 2V_\alpha$. The unit-cell axes for β-PbF$_2$ and o-PbSnF$_4$ are colinear.

Figures 6 and 7 show the influence of symmetry changes and superstructures on the X-ray powder diffraction pattern, which result in peak splittings and low angle superstructure reflections. For α-PbSnF$_4$ (aq$_1$), precipitated from an aqueous solution of SnF$_2$ (fig. 6b), and α-PbSnF$_4$ (ssr) i.e. solid state synthesis of SnF$_2$ and PbF$_2$ (fig. 7b), the following changes are observed[12], relative to β-PbF$_2$ (fig. 6a &7a):

(i). a splitting of the all (hkl) Bragg peaks is caused by the tetragonal distortion, (i.e) with $l \neq h$

(ii). the h and k indices of all the peaks except (001) change upon the 45° rotation of the axes in the ($\bar{a}, \bar{b}$) plane with the MSnF$_4$ axes having half the length of the diagonals of the ($\bar{a}, \bar{b}$) face of MF$_2$;

(iii). the l index doubles due to the doubling of the c parameter;

(iv). new peaks appear due to the superstructure along $\bar{c}$ and the lower symmetry (i.e. from Fm3m to P4/nmm)

It results in the change of indexation and splitting of the fluorite peaks such as :

(111)$_F$ → (102)$_\alpha$

(200)$_F$ → (110)$_\alpha$ and (004)$_\alpha$

(220)$_F$ → (200)$_\alpha$ and (114)$_\alpha$ and

also the appearance of the following new peaks :
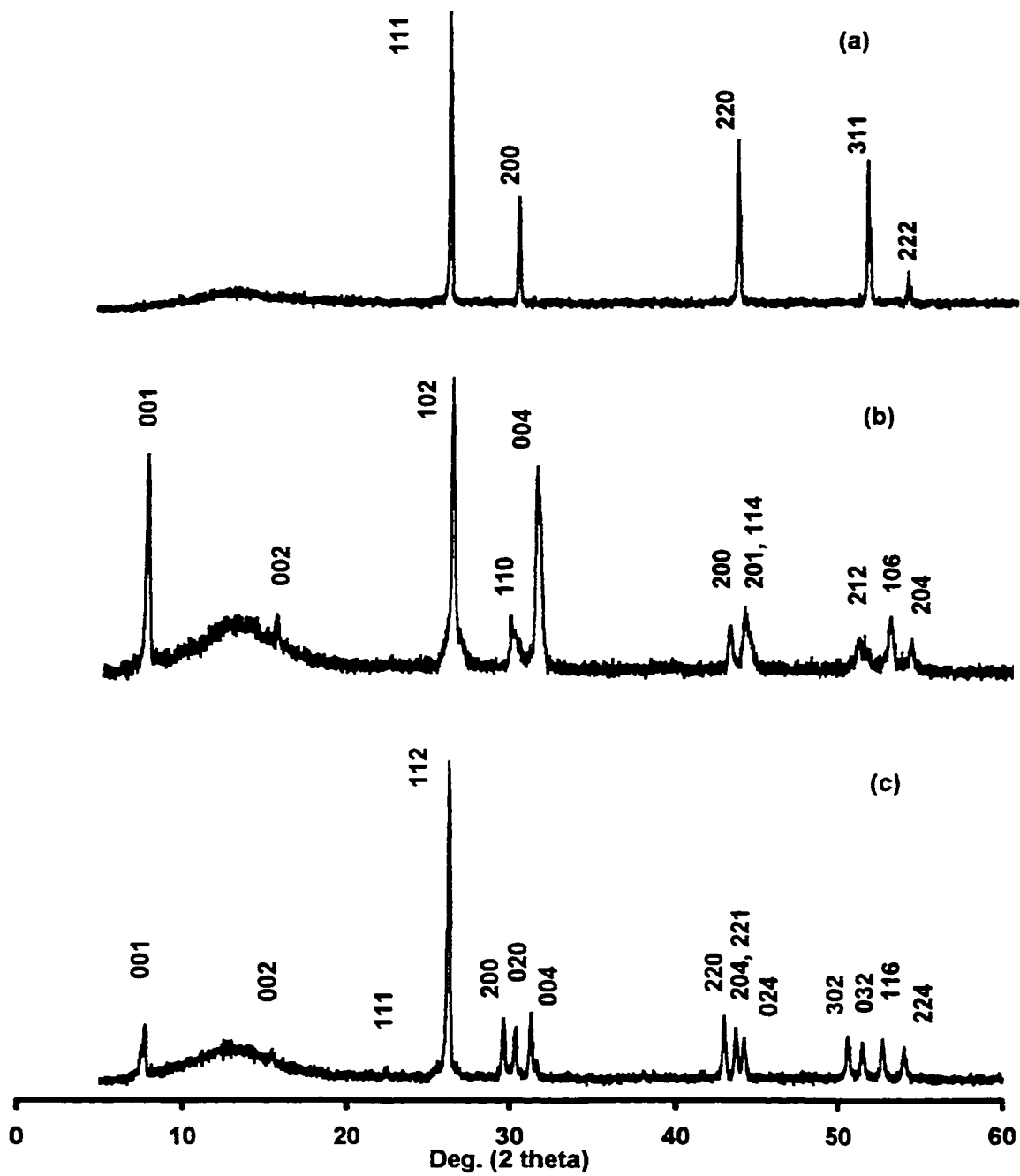
Figure 6: Relationships between the X-ray powder patterns of (a) β-PbF$_2$, (b) α-PbSnF$_4$(aq$_1$), and (c) o-PbSnF$_4$.
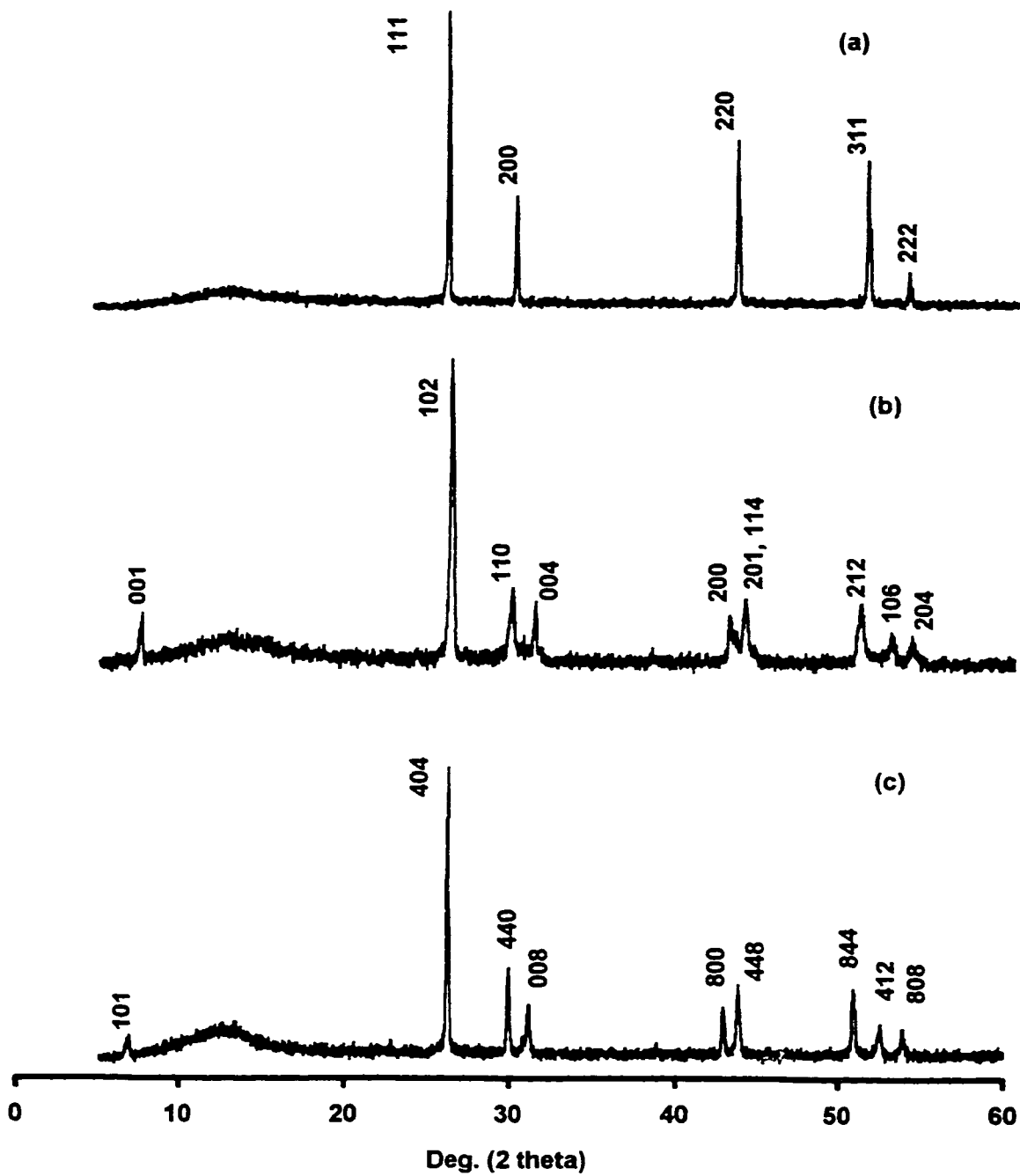
Figure 7: Relationships between the X-ray powder patterns of (a) β-PbF₂, (b) α-PbSnF₄(ssr), and (c) β-PbSnF₄.

$(001)_\alpha$, $(002)_\alpha$, $(113)_\alpha$, $(104)_\alpha$, $(005)_\alpha$, $(201)_\alpha$, and $(006)_\alpha$.

where: $(hkl)_F$ and $(hkl)_\alpha$ peaks are the Miller indices for β-PbF_2 and α-$PbSnF_4$, respectively

Fig. 7 also shows the relationship of the X-ray powder patterns of α-$PbSnF_4$ (ssr) and β-$PbSnF_4$. The changes of Miller indices of β-$PbSnF_4$ (fig. 7c) relative to β-PbF_2 are due to the following[27]:

(i). the **a** and **b** parameters of β-$PbSnF_4$ have twice the length of the diagonal of the $(\bar{a},\bar{b})$ face of β-PbF_2 and thus four times the **a** and **b** parameters of α-$PbSnF_4$.

(ii). the length of the unit-cell of β-$PbSnF_4$ along the $\bar{c}$ axis (and thus the l index) is quadrupled relative to β-PbF_2 and thus is doubled relative to α-$PbSnF_4$.

(iii). new peaks appear due to the lowering of symmetry (i.e. from cubic to tetragonal) and the large unit-cell formed. The superstructure reflections observed for β-$PbSnF_4$ are different from those of α-$PbSnF_4$.

The change of the $(hkl)_F$ indexation of β-PbF_2 and of the $(hkl)_\alpha$ indexation of α-$PbSnF_4$ peaks to the $(hkl)_\beta$ peaks for β-$PbSnF_4$ are as follows:

$(111)_F \rightarrow (102)_\alpha \rightarrow (404)_\beta$

$(200)_F \rightarrow (110)_\alpha$ and $(004)_\alpha \rightarrow (440)_\beta$ and $(008)_\beta$

$(220)_F \rightarrow (200)_\alpha$ and $(114)_\alpha \rightarrow (800)_\beta$ and $(448)_\beta$

For o-PbSnF$_4$ (fig.6c), the X-ray diffraction pattern is similar to that of α-PbSnF$_4$ wherein the main difference is the splitting of all peaks with $h \neq k$ in the β-PbF$_2$ axes, e.g. of the (110)$_\alpha$ peak to (200)$_o$ and (020)$_o$ peaks for example, which are characteristic of further symmetry loss. These changes observed on o-PbSnF$_4$ are in agreement with Réau et al.[3].

1.5. GOALS OF THIS WORK

The main goals of this work were to study the phase transitions of PbSnF$_4$ in further depth and if possible, discover new phase transitions.

Reaction (IV) was used versus the amount of HF added to the aqueous solution of SnF$_2$ for the preparation of α- and o-PbSnF$_4$, the amount of HF being nil for the preparation of α-PbSnF$_4$. Reaction (III) was used to prepare α-PbSnF$_4$ and β-PbSnF$_4$ by direct reaction at high temperature.

$$5SnF_2 + Pb(NO_3)_2 \xrightarrow{\quad H_2O\ HF \quad} PbSnF_4 + 3SnF_2 + Sn^{2+} + 2NO_3^- \qquad (IV)$$
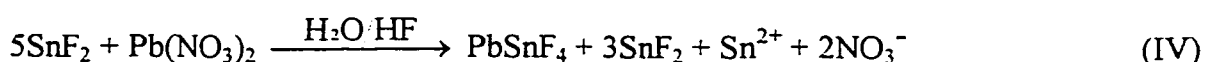
A coarse study of reaction (IV) was done by Parris and Dénès[7] who studied the influence of a large number of reaction parameters (Table II) on the material obtained and established that the presence of HF in the SnF$_2$ solution used for the synthesis was responsible for the orthorhombic distortion. In the present work, a detailed study of the phase transition from tetragonal to orthorhombic vs. a larger number of HF values has

been carried out and the influence of thermal and mechanical energies on the stability of each phase: stable or metastable, at ambient conditions (o-, α- and β-PbSnF$_4$) has been undertaken.

Therefore, knowing that the addition of hydrofluoric acid in the reaction mixture changes the cell symmetry from tetragonal to orthorhombic, we aimed at understanding and studying this transition in greater details. The following was studied:

(i) the mechanism of the transition from tetragonal to orthorhombic symmetry ($\alpha \longrightarrow$ o- transition);

(ii) the differences between the two phases;

(iii) the effect of mechanical energy followed by annealing on crystallinity, structure, texture and phase transitions of the various phases of PbSnF$_4$

(iv) the mechanism of the phase transitions upon annealing.

This study has also resulted in the discovery of a new method for preparing PbSnF$_4$, the preparation of a new tin(II)/Pb(II)fluoride material, and the design of a way to control the texture of PbSnF$_4$.

CHAPTER 2

EXPERIMENTAL PROCEDURES: THEORY, INSTRUMENTATION AND APPLICATIONS

2.1. SYNTHESIS

2.1.1. Reagents

SnF_2	:99.8% Ozark Mahoning
$Pb(NO_3)_2$	: Sharpe Chemicals
α-PbF_2	: 99% Alfa
HF (40%)	: Mallinckrodt
Certified Atomic Absorption	
Standards (1000ppm) Sn and Pb	: Fisher Scientific

2.1.2. Preparation of PbSnF₄

2.1.2.1. Preparation of α- and o-PbSnF₄ by precipitation from aqueous solution

All preparations of both α- and o-PbSnF₄ were carried out in air at ambient temperature in deionized water. The beakers used were made of polyethylene or polytetrafluoroethylene (teflon) in order to prevent etching of the glass due to hydrofluoric acid if glass beakers were used. Reactions were performed in glass beakers only when no HF was used.

A saturated aqueous solution of $Pb(NO_3)_2$ (1.7M) was added to a freshly prepared (t $_{(SnF2)}$ = 0) 1.5M aqueous (pure water or aqueous HF) solution of SnF_2 on stirring.

The volumes of the two solutions were chosen in order to give an overall Pb/Sn ratio of 0.2[2]. The ratio of the volume of HF to the total volume of the SnF$_2$ aqueous solution was varied from 0 to 0.57. Upon contact between the two solutions (i.e. aqueous SnF$_2$ and aqueous Pb(NO$_3$)$_2$) a white precipitate immediately formed. The precipitate was filtered immediately after the end of addition of the SnF$_2$ solution (t$_{(product)}$ = 0), washed several times with water and allowed to dry in air at room temperature. We have named tetragonal and orthorhombic PbSnF$_4$ obtained from precipitation α-PbSnF$_4$(aq$_1$) and o-PbSnF$_4$ respectively.

2.1.2.2. Preparation of α-PbSnF$_4$ by reaction of a slurry of α-PbF$_2$ with an aqueous solution of SnF$_2$

A slurry of solid α-PbF$_2$ in an aqueous solution of SnF$_2$ at a molar ratio of α − PbF$_2$/SnF$_2$ < 1 was stirred for a minimum of 1 hour at ambient temperature. The suspension was suction filtered immediately, washed with water and then, allowed to dry in air at room temperature. X-ray diffraction showed that the solid obtained was α-PbSnF$_4$. In order to differentiate this solid from α-PbSnF$_4$(aq$_1$), we name it α-PbSnF$_4$(aq$_2$).

2.1.2.3. Preparation of α- and β- PbSnF$_4$ by solid state synthesis

A stoichiometric mixture of SnF$_2$ and PbF$_2$ was placed in the port of a dry nitrogen glove box which was evacuated and filled with nitrogen twice. The mixture was thoroughly mixed and ground together in an agate mortar inside the glove box. Then, it

was loaded into a copper tube previously sealed at one end and temporarily sealing of the tube inside the glove box was carried out. The final sealing of the second end was performed outside the glove box, according to literature procedure[28]. Then, the copper tube was preheated at 200°C for 1 hour, i.e. just below the melting point of SnF_2. With this procedure, SnF_2 reacts with PbF_2 in the solid state, thereby avoiding possible corrosion of the copper tube by liquid SnF_2 and also hydrolysis/oxidation of a minor amount of SnF_2 by residual H_2O/O_2 in nitrogen. In a second step, the tube was heated at the reaction temperature for 3 hours to complete the reaction and obtain the phase of interest. The reaction temperature was 250°C for α-$PbSnF_4$ and 350°C for β-$PbSnF_4$. Then, the tube was quenched by quick immersion in cold water in order to stabilize the high temperature metastable phase of β-$PbSnF_4$, or simply removed from the furnace and allowed to cool in air for α-$PbSnF_4$[2,4]. We have named α-$PbSnF_4$ obtained by direct reaction α-$PbSnF_4$(ssr).

2.2. CHARACTERIZATION OF THE MATERIALS
2.2.1. X-Ray Powder Diffraction (XRD)
2.2.1.1. Principles

This method utilizes X-rays wherein the sample to be studied is reduced to a fine powder and placed in a beam of monochromatic X-rays. The tiny particles of a powder are small crystals called "crystallites".

Set of families of equidistant parallel planes, each defined by its (*hkl*) Miller indices, can be defined for each crystalline material. Each family of planes acts like a grating with an interplanar distance of the order of magnitude of the Å, and thus can give

rise to diffraction when irridiated by a monochromatic beam of radiations with a wavelength similar to the interplanar spacing. Such radiations can be obtained for X-ray, neutrons and electrons. When the angle between the incident beam and a given family of planes has a given θ value (Bragg angle) diffraction will occur provided Bragg law is satisfied (equation i) (fig. 8).

$$2d\sin\theta = n\lambda \qquad\qquad\qquad (i)$$

where:

d = the interplanar spacing (d-spacing)

θ = diffraction angle = incident angle

n = order of diffraction (integer number)

λ = radiation wavelength

From the geometric point of view, diffraction is similar to the reflection of light on a mirror, i.e. the diffraction angle is equal to the incident angle, and both the incident beam and the diffracted beam are coplanar. However, contrary to reflection, diffraction occurs only for a selected number of θ angles that satisfy Bragg law.

The d-spacing is a function of the unit-cell size and crystal system and therefore, the position of the diffracted beam is a function of these parameters. The intensity of each diffracted beam is a function of: (i) the scattering power f of each atom (which is itself a function of Z for X-ray diffraction), Z being the atomic number, (ii) of the Bragg angle θ, (iii) of the x,y,z fractional coordinates of each atom in the unit-cell and (iv) of the (hkl) Miller indices of the family of planes giving rise to the diffracted beam. The

Crystal planes (h, k, l)
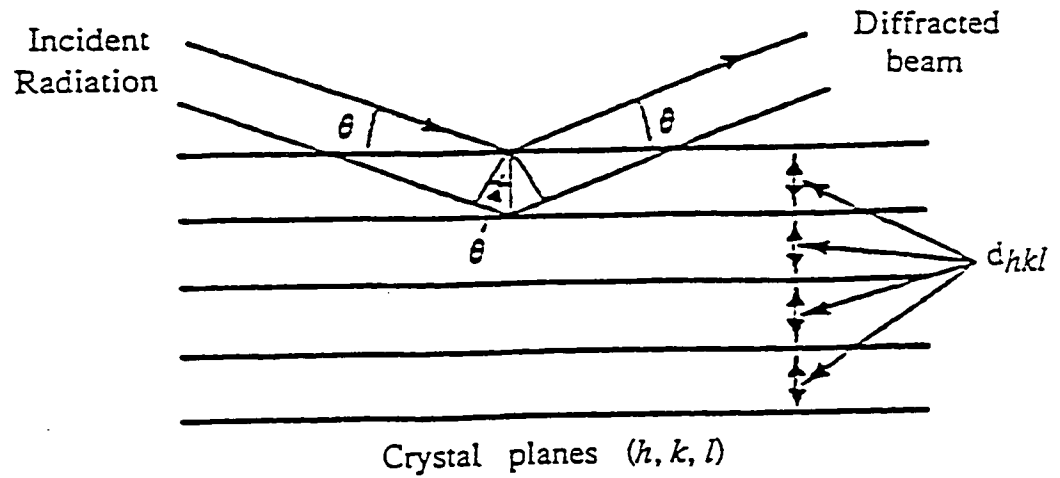
Bragg condition: $n\lambda = 2d_{hkl} \sin \theta$

(a)
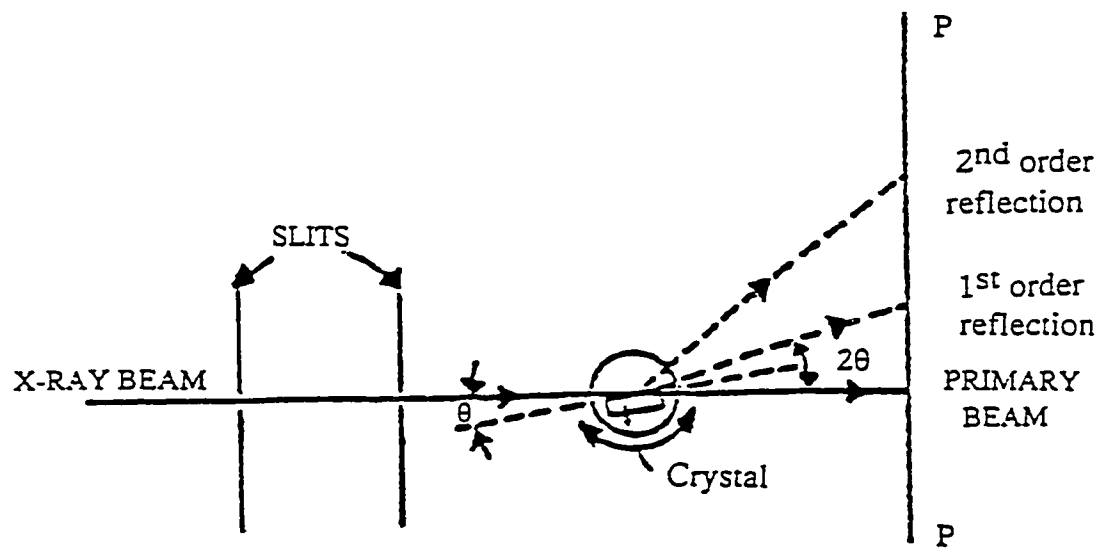
(b)

Figure 8: (a) reflection analogy of X-ray diffraction;
(b) diffraction of radiation from a crystal

intensity I_{hkl} of each diffracted beam is the product of the structure factor F_{hkl} by its complex conjugate F^*_{hkl} ($I_{hkl} = F_{hkl} \cdot F^*_{hkl}$) where:

$$F_{hkl} = \sum_{j=1}^{N} f_j \exp^{-2\pi i (h_{x_j} + k_{y_j} + l_{z_j})} \tag{ii}$$

where: f_j is the scattering factor of the jth atom,

x_j, y_j, and z_j are the fractional coordinates of the jth atom in the unit-cell,

i is the imaginary number ($i = \sqrt{-1}$)

In addition, the intensity of each diffracted beam is affected by the following:

(i) thermal vibrations of the atoms (the higher the amplitude of the thermal vibration, the lower the intensity)

(ii) temperature T and pressure p, since the atomic coordinates and the thermal vibrations vary with T and p

For polycrystalline samples (including powders), (i) the relative amount of the phase of concern in the sample, if it is a mixture of phases, and (ii) texture, also modify the line intensity. Texture effect occurs if the crystallites are not randomly oriented; then preferred orientation enhances the intensity for the family of planes lying in the preferred direction, and reduces those perpendicular to it. This phenomenon can be very highly enhanced when the crystals are plate- or needle-shaped.

In summary, the direction of the diffracted beams is a function of the d-spacing, and hence, of the unit-cell parameters **a**, **b**, **c**, α, β, γ, and also their temperature and

pressure dependence since these parameters change with T (thermal expansion) and p (compressibility). The intensity of the diffracted beams is a function of (i) the x,y,z fractional coordinate of the atoms in the unit-cell, (ii) Z^2, the square of the atomic number for X-ray diffraction, (iii) thermal vibrations (and hence, temperature and pressure), (iv) the abundance of the crystalline phase in the sample, (v) the texture i.e. preferred orientation of the particles , and (vi) temperature and pressure, which modify the atomic coordinates and the amplitude of thermal vibrations. The width of the Bragg peaks is related to microcrystallinity (small crystallite size) and non-uniform strain, both of which give line broadening.

Furthermore, since each (hkl) Bragg peak is representative of a direction in space (direction of the (hkl) family of planes), the shift of a given (hkl) Bragg peak gives the change of d-spacing perpendicularly to the (hkl) plane i.e. thermal expansion or compressibility is obtained as a function of direction in the crystal, and can be related to bonding, packing and to some phase transitions. Similarly, broadening of a given (hkl) Bragg peak gives the average particle dimension perpendicular to the (hkl) plane or indicates the presence of strain in the plane. Again, these can be related to bonding, packing and also to cooperative phenomena in some phase transitions (ferroic transition).

Finally, since each crystalline material has a set of different Bragg peaks, these can be used very efficiently for identifying the crystalline phase(s) in the material. Amorphous and microcrystalline (particularly < ca. 30 Å) materials give no diffraction pattern and are not detected by diffraction. An X-ray powder diffraction pattern is a set of peaks, each of different intensity and position (i.e. d-spacing or Bragg angle), and for a given material the line positions and to a lesser extent the relative intensities are

essentially fixed and are characteristic of that material and its crystal structure.

2.2.1.2. Instrumentation

The X-ray powder patterns were obtained using a Philips PW 1050/25 diffractometer with the monochromatic radiation K_α line of Cu (λ = 1.54178 Å) which was isolated using a Ni filter. The diffractometer uses a focusing goniometer, whereby the source collimator, the sample and the detector collimator are located on a circle, in order to minimize the effect of beam divergence and maximize the count rate (fig. 9). The SIE RAY112 X-ray diffractometer automation system and software for IBM PC manufactured by SIETRONICS was used for data accumulation and analysis. The detector is positioned in such a way as it makes an angle 2θ with the incident beam when the sample makes an angle θ with the incident beam. During data accumulation, the sample is rotated at an angular velocity of $\theta°$ min.$^{-1}$ while at the same time, the detector is rotated at a velocity of $2\theta°$ min.$^{-1}$ ($\theta/2\theta$ mode), in order to keep the surface of the sample tangent to the focussing circle and thereby, maximize the beam focussing in the detector collimator. The detector rotates around the center of the goniometer; and the sample is located at its center. Each time the θ angle abides with Bragg law for one of the d-spacings of the materials, the diffracted beam is measured by the detector and gives a Bragg peak. For each position of the X-ray detector which corresponds to a Bragg peak, a fraction of the crystallites of the powder is oriented such that the (hkl) planes are in diffraction positions. This fraction is reduced or enhanced by preferred orientation, depending on the angle between the (hkl) planes and
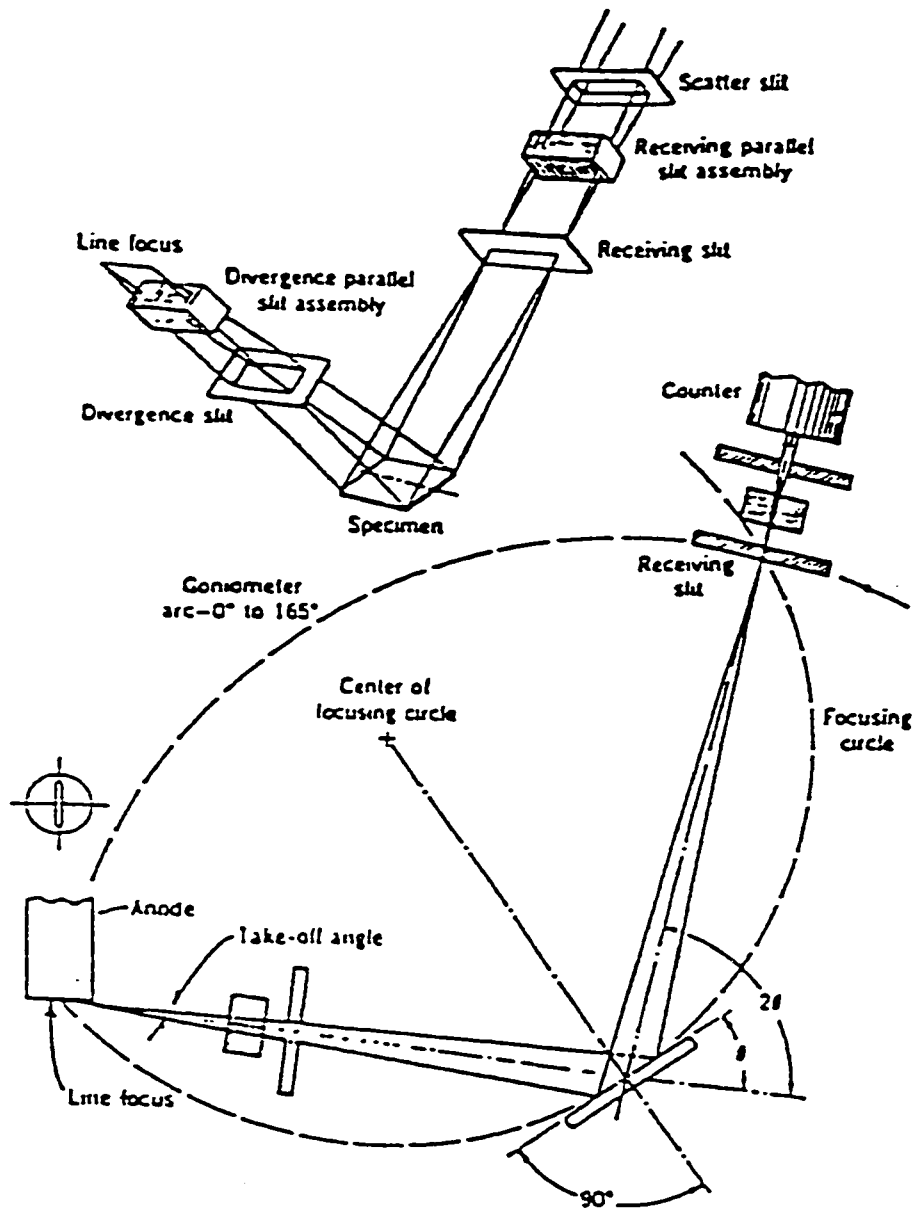
Figure 9: A Schematic Arrangement of the line Focusing X-ray Powder Diffractometer[29]

the direction of preferred orientation. The powder diffraction patterns were obtained by step scanning from 5° to 60° (2θ) at a velocity of 1° (2θ) per minute with a step size of 0.02°.

Data collection and processing were carried out using the SIE112 software. Phase identification was carried out by comparing the peaks of the samples to that of the expected phases. In some cases, computer search-match was carried out by comparing the experimental diffraction pattern with the JCPDS database[30], with the help of the μPDSM (Micro-Powder Diffraction Search-Match) software manufactured by Fein-Marquat[31].

2.2.1.3. Phase Identification and use of the line position and width

The best technique for identifying crystalline phases is X-ray powder diffraction. The diffraction patterns are a function of the crystal periodicity and they are also very sensitive to small changes in the size and shape of the crystal lattice. An X-ray powder pattern is a one-dimensional projection of the three dimensional reciprocal lattice.

The diffraction lines observed in a powder pattern provide a finger-print of the crystalline phase and usually allow a unambiguous identification of the phases in the material. If the sample contains crystalline impurities they will give characteristic lines that allow their identification since there is no interference between the lines of different crystalline species, except line intensity or shape modification due to overlap. However, amorphous or microcrystalline (diameter < ca. 30 Å) materials will not be detected. Once the powder pattern is indexed, i.e. (hkl) Miller indices have been assigned to each

Bragg peak, the unit-cell parameters (a, b, c, α, β, γ) can be calculated, and the crystal system is obtained. In addition, lattice translations can be identified from the absence conditions and the possible space groups usually be narrowed down to a short list of half a dozen or less. The line splitting will show any cell distortion present and the line positions are used to calculate the unit-cell dimensions. The linewidth are used for particle size determination and identification of any strain that maybe present in the material being studied.

2.2.1.4. Texture Effects

In ideal polycrystalline samples, crystallites are randomly oriented, i.e. there are the same number of crystallites oriented in every direction of space. However, in real cases, texture effects are often observed. Perfectly randomly oriented samples can be hard to obtain since some crystal shapes favor preferred orientation of the crystallites. Crystallites with a platelet or a needle shape tend to stack parallel to each other causing texture effects. In the case of $PbSnF_4$, the $\bar{c}$ axis is perpendicular to the plates and many more crystallites are oriented perpendicularly to $\bar{c}$ than in any other direction. It results that the $(00l)$ Bragg peaks are strongly enhanced. On the other hand, the $(hk0)$ reflections become weaker, since they are representative of the direction perpendicular to the direction of the preferred orientation.

2.2.1.5. Determination of accurate unit cell parameters

The unit-cell parameters are often determined by single crystal diffraction on films (Weissenberg and precession methods) are accurate to only two or three significant figures. The powder pattern provides more accurate cell parameters provided the positions of the lines have been accurately measured. Unit-cell parameters that are accurate enable complex powder patterns to be indexed, measuring of thermal expansion coefficients (if measurements were taken versus temperature) and the effects of the composition on the cell parameters. Often, a least-squares refinement of the unit-cell parameters is carried out using a large number of d-spacings, since the number of observables (d-spacings) is usually larger than the number of unit-cell parameters[32]. However, in this case, this method was not used since only a few peaks can be measured accurately: (i) the (001) peak is at very low angle, where the accuracy of θ is lower (at grazing angle) and where a small error of θ gives a large error of d-spacing due to the non-linearity of Bragg law; (ii) for 2θ > ca. 16°, peak broadening and overlap makes difficult the precise measurement of peak position. Therefore, only a few relevant peaks in the range of $2\theta = 24 - 34°$ were used for the determination of the unit-cell parameters.

Interplanar d-spacing is a function of both the plane Miller indices (hkl) and the unit-cell parameters. The relation between the d-spacing and the unit-cell parameters depends on the crystal system (Table V).

2.2.1.6. Sample preparation

The product was ground using a mortar and pestle into a fine powder and mixed with KCl (internal standard). Overgrinding was avoided, except for the study of the effect of grinding. For the study of texture in the samples, preferred orientation was enhanced by vacuum filtration and the samples were used without grinding. In some cases, the samples were vacuum filtered directly onto a X-ray holder constructed for this purpose. The ground powder was then pressed into the window of a plexiglass holder with the use of a glass slide in order to have a smooth flat surface.

Table V : Unit-Cell Parameters and Interplanar d-spacing

CRYSTAL SYSTEM	INTERPLANAR SPACING (d)	$V\ (\text{Å})^3$
CUBIC	$d = \dfrac{a}{\sqrt{h^2 + k^2 + l^2}}$	a^3
TETRAGONAL	$d = \dfrac{1}{\left(\dfrac{h^2 + k^2}{a^2} + \dfrac{l^2}{c^2}\right)^{\frac{1}{2}}}$	a^2c
ORTHORHOMBIC	$d = \dfrac{1}{\left(\dfrac{h^2}{a^2} + \dfrac{k^2}{b^2} + \dfrac{l^2}{c^2}\right)^{\frac{1}{2}}}$	abc
MONOCLINIC	$\dfrac{1}{d} = \dfrac{1}{\sin\beta}\left[\dfrac{h^2}{a^2} + \dfrac{k^2\sin^2\beta}{b^2} + \dfrac{l^2}{c^2} - \dfrac{2hl\cos\beta}{ac}\right]^{\frac{1}{2}}$	$abc\sin\beta$

This, however, often induce preferred orientation (i.e. uneven distribution of orientations of the crystallites), due to the fact that the crystallites are very thin plates.

The area of the sample irradiated by the incident beam varies with the Bragg angle, therefore, it was important to ensure the homogeneity of each sample. The dimensions of the surface used in all the analyses carried out were fixed by the sample holder used, the window dimensions of which were 2 cm wide and 1 cm high, in order to minimize direct irradiation of plexiglass by the X-ray beam. Plexiglass holder was chosen as the holder material, for it gives no Bragg peak. However, it gives a curved background with a typical broad scattering ring in the range of $2\theta = 10 - 20°$.

2.2.2. Atomic Absorption Spectrometry

Atomic absorption spectrometry was used for the analysis of the metals, i.e. Pb and Sn. For atomic absorption spectrometry, the sample solution is aspirated into a flame and the sample element to be analyzed is converted to atomic vapor. The flame contains atoms of the element to be analyzed and some are thermally excited by the flame, but most remain in the ground state. These ground state atoms can absorb radiation given off by a special source made from that element and the wavelengths of radiation given off by the source are the same as those absorbed by the atoms in the flame[33].

2.2.2.1. Instrumentation

The instrument used for the atomic absorption studies was the PERKIN-ELMER atomic absorption spectrometer model 503. A light source beam, a cell (i.e. flame), a

monochromator, and a detector are necessary for carrying out atomic absorption spectrometry. A schematic diagram of dual beam atomic absorption spectrometer used in this study is illustrated in (Figure 10) for a system with a signal detector shared by both beams.

The source beam was alternately directed through the flame and around the flame by the chopper. The two beams then pass through a monochromator to a detector and a readout system after recombination. The difference between the two beams was integrated over 3 seconds and then displayed. The source used for a specific element is a hollow cathode tube that emits the light at a specific wavelength. A premixed chamber burner is used in which the fuel and support gas are mixed before entering the burner head where the combustion takes place. The sample solution is then aspirated through a capillary by the Venturi effect using the support gas for aspiration. Large droplets of the sample condense, drain out of the chamber and the remaining fine droplets mix with the gases and enter the flame.

2.2.2.2. Sample Preparation

In the preparation of standards, the matrix used was the same as for the sample (i.e. 10% HCl). Two main factors affected the method of preparation for $PbSnF_4$ samples for atomic absorption spectrometry. $PbSnF_4$ is insoluble in water and therefore, a strongly acidic solution has to be used. Precautions must be taken to ensure accurate results and since it has been established that tin tends to be lost from aqueous solution during storage, up to 80% overnight from glass vessels in highly dilute non-acidic
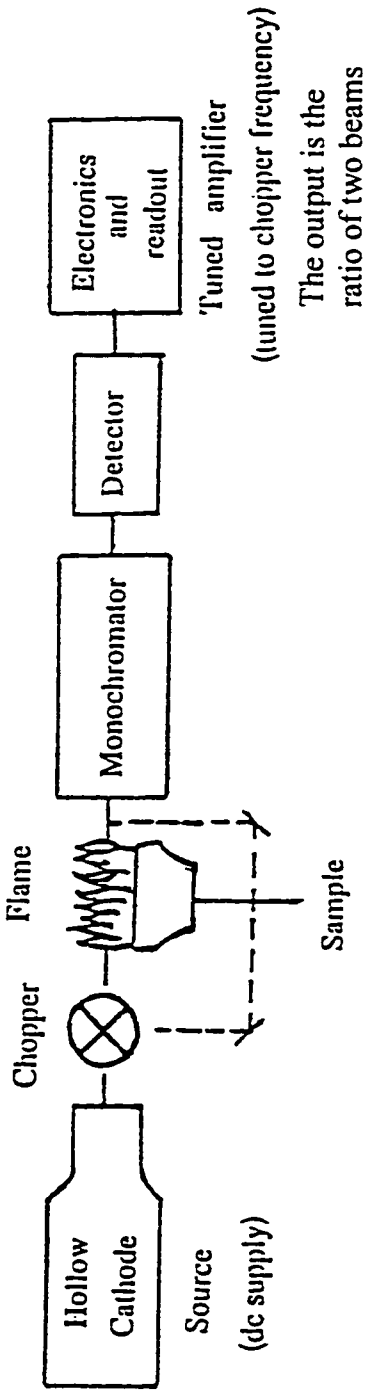
Figure 10: Schematic diagram of an atomic absorption instrument[32].

media[34]. However, these losses are reduced to <10 % loss per week from plastic containers, and are negligible in a strongly acidic and more concentrated solution stored in plastic containers. Therefore, it is imperative to use plastic or teflon vessels and to acidify the samples. The samples were, as an additional precaution, dissolved less than 24 hours before analysis, in order to eliminate the loss of tin.

All samples were prepared by dissolving $PbSnF_4$ in a minimum amount of concentrated HCl, and then diluting to 10 % HCl with deionized water. The samples were diluted with 10% HCl until they came into the linear range of the instrument. The sample size of $PbSnF_4$ was taken between 100-150 mg. The standard solutions used were prepared using certified 1000ppm stock solutions of Sn and Pb.

For the analysis of Sn, a wavelength of 284nm giving an absorption of 200 for a 300 ppm solution was used. A Cathodeon Ltd. type C hollow cathode lamp was used as the source. The flame was nitrous oxide-acetylene reducing. For Pb, the wavelength was 180.5nm giving an absorption of 100 for a 20 ppm solution. A Perkin-Elmer intensitron hollow cathode lamp was used and the flame was air-acetylene oxidizing.

2.2.3. Bulk Density Measurements[35, 36]

The density of a substance is its mass divided by its volume. The bulk density of a material contains information about the chemical composition (which affects the mass) and the efficiency of packing of atoms or ions (which affects the volume). For example, the volume change taking place at a reconstructive phase transition results in a change of density, whereas second order phase transitions, often displacive, occurs with no volume

change, and therefore no change of density at the transition point.

Bulk density measurements were carried out at room temperature using Archimedean's method of displacement in a liquid. The liquid that was used for the measurements was carbon tetrachloride because it is non-reactive with the powders being analyzed, it does not dissolve them, and it has a low viscosity, and thus is a good wetting agent.

The principle of this method is based on the measurement of the volume or the mass of the liquid (i.e. CCl_4) displaced by the powder. A specially designed apparatus (fig. 11) for minimizing air bubbles trapped between the particles was used. The apparatus of figure 11 is connected to a vacuum line (figure 12b) for evacuating slowly the air contained in the powder and a modified analytical balance was used for weighing (fig. 12a). The sequence of measurements is as follows:

(i) the empty crucible mass is measured, m_1

(ii) the mass of the empty crucible immersed in CCl_4 is measured, m_2

(iii) the mass of the crucible with the sample is taken, m_3

(iv) the sample is placed under vacuum for approximately 30 minutes with the use of a rotary and diffusion pumps.

Evacuation of air has to be done very slowly in order to avoid sucking powder out of the crucible. The sample is then immersed in CCl_4 while still under vacuum and the mass m_4 is measured after breaking the vacuum (only after the sample is completely immersed in CCl_4).
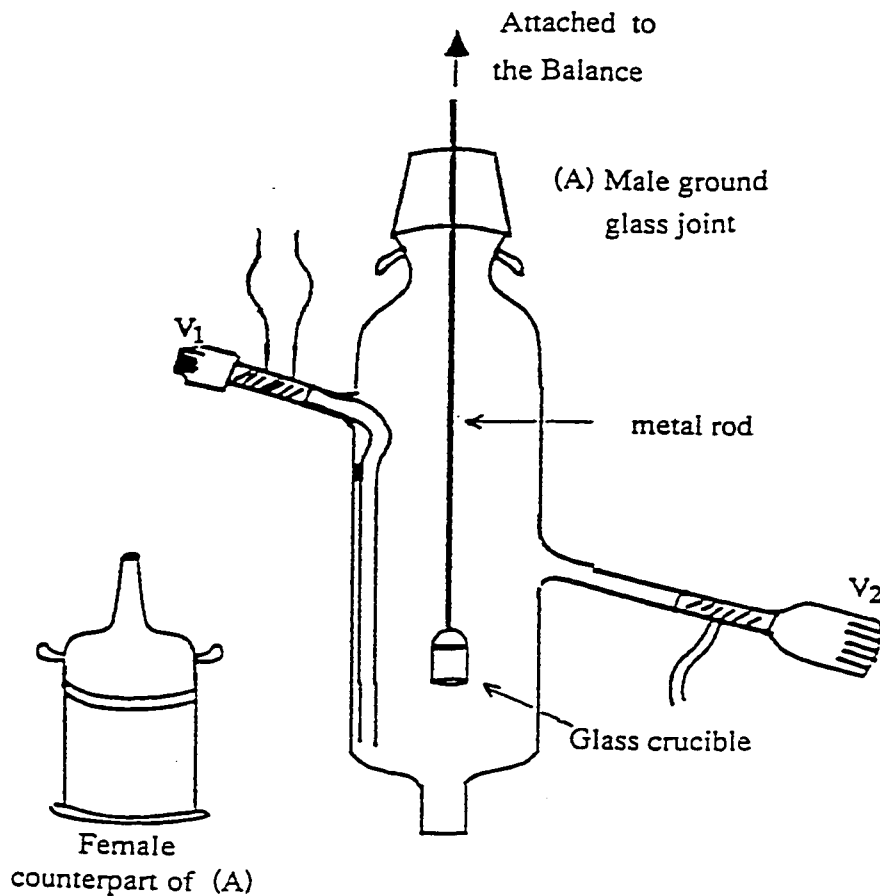
Figure 11: Vessels used for the Bulk density measurement[35].

The evacuation of the sample is very important in order to remove the trapped air between the powder particles which would lead to an overestimation of the volume. Therefore, the sample has to be covered with liquid CCl_4 while still under vacuum.

For this type of technique, it is important to (i) avoid temperature fluctuations (since the density of CCl_4 varies with temperature) and (ii) keep the level of CCl_4 constant in order to have the same length of rod immersed for the measurements of m_2 and m_4. The density of the powder is defined as :
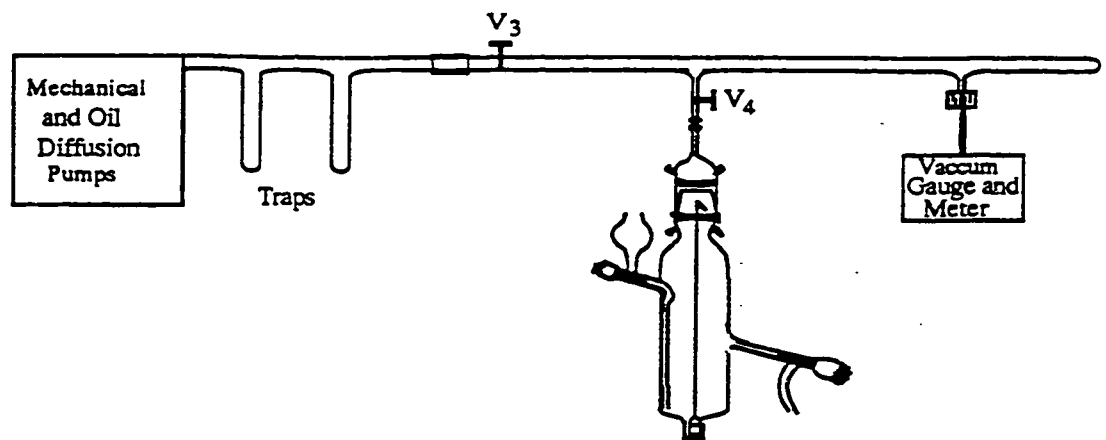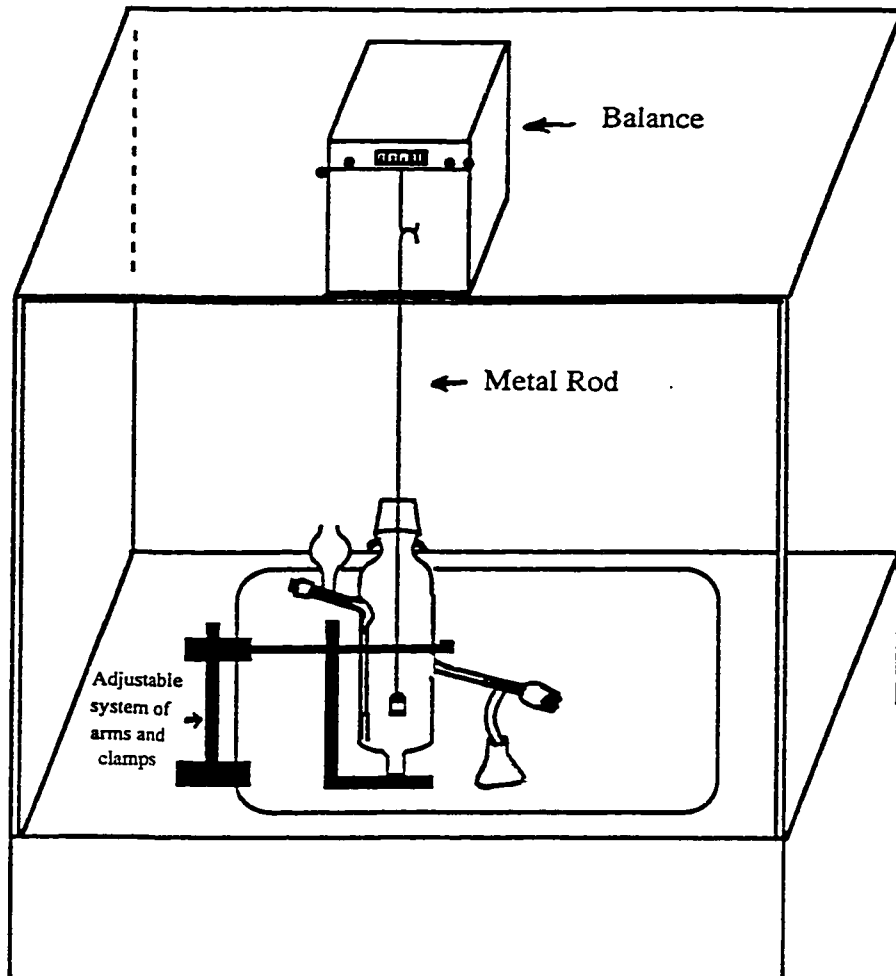
Figure 12: (a) weighing setting, and (b) vacuum setting for the Bulk density measurements[36].

$$\rho = m/V \qquad \text{(iii)}$$

where m = m_3-m_1 and the volume is :

$$V = \frac{(m_3 - m_1) - (m_4 - m_2)}{\rho_{CCl_4}} \qquad \text{(iv)}$$

The volume of the sample is equal to the volume of CCl_4 it displaces, provided there is no air trapped between the powder particles. The density of the sample can then be calculated as :

$$\rho = \frac{(m_3 - m_1)\rho_{CCl_4}}{(m_3 - m_1) - (m_4 - m_2)} \qquad \text{(v)}$$

The amount of $PbSnF_4$ sample needed for these type of measurements is between 1-2 grams. It is important to remember to tare the balance before each weighing. Problems that are usually encountered when measuring the density of the powder are: (i) the removal of trapped air remaining between the particles, and (ii) imperfect degassing although this method is designed to minimize this type of problem. Slow degassing and sufficient wetting of the sample minimize these problems.

Bulk density measurements were carried out in order to determine if there is a change in the Pb/Sn stoichiometry at the $\alpha \rightarrow$ o-$PbSnF_4$ transition. This is because Pb is denser than Sn therefore, any change would lead to a significant change in the density. In addition, a significant change in the compactness of the material, this can also be detected by measuring the density.

48

2.2.4. Scanning Electron Microscopy (SEM)

This technique was used in order to determine the particle shape and size of the material being studied, and to investigate if there is any change that occurs at the transition from tetragonal to orthorhombic ($\alpha \rightarrow o$), and also if the change in texture can be related to the macroscopic observations of the sample. To avoid charge build up, the samples were gold coated by vacuum deposition. The scanning electron micrographs were recorded on a Hitachi S-S20 SEM instrument energized by 15kV equipped with a polaroid camera.

2.2.5. Fluoride Ion Analysis
2.2.5.1. Principles

Fluoride in a water sample is determined by measurement with a Fluoride-ion selective combination electrode.

The analysis for fluoride ion was carried out using a MODEL 94-09 Fluoride ion selective electrode manufactured by Orion Research Laboratories, and a pH 220 digital pH meter manufactured by Corning. The pH meter is switched to its mV position, and all readings are taken in millivolts. The fluoride ion selective technique is very sensitive to interferences, and many precautions must be taken. The temperature of all solutions must be identical as must be their pH. In addition, since the electrode measures only free F^- ions, all fluorine must be decomplexed in order to be measured. Furthermore, since OH^- ions interfere with the functioning of the electrode, measurements must be carried

out in acidic conditions.

2.2.5.2. Preparation of required Chemicals and solutions

Total ionic strength adjustment buffer (TISAB II) solution was prepared with 52mL glacial acetic acid, 58 grams NaCl and 4 grams CDTA (Cyclohexylenedinitrotetraacetic acid) in about 500 mL of water, adjusted to pH 5-5.5 with 5M NaOH and diluted to a total volume of 1 liter. It provides a high ionic strength and it also serves as a buffer at pH 5.0 - 5.5 since in an acid medium HF forms, and in an alkaline medium OH^- ion interfere with the electrode response. In addition, CDTA preferentially complexes with polyvalent cations present in water (e.g. Si^{4+}, Al^{3+}, Fe^{2+}, etc) which would otherwise complex with F^- and make it undetectable since the electrode measures only free F^- ions.

2.2.6. Thermal Analysis

Thermal analysis is the measurement of physical and chemical properties of materials as a function of temperature[37]. The two thermal analysis techniques used in this work are thermogravimetric analysis (TGA), which records the change of mass of a material as a function of temperature or time, and differential thermal analysis (DTA) which measures the difference of temperature, ΔT, between the material under study and an inert reference material as a function of temperature. DTA, therefore, detects exchanges of heat between the sample and its environment.

Thermal analysis was performed on a Thermal Sciences Combined DTA/TGA instrument equipped with a STA 1000/1500 module and ATII hardware and software.

Thermal analysis was carried out in order to identify heat exchanges at phase transitions, since first-order transitions usually involve an enthalpy change similar to the latent heat for melting or vaporization ($\Delta H \neq 0$), however, for solid state phase transitions, the enthalpy change is usually much smaller. Nevertheless, it can usually be detected by DTA (Differential Thermal Analysis), unless the transition is very sluggish, in which case the heat exchange is too much spread in time and, instead of giving a peak, it merges with the background, which is often curved. For second order transitions, no enthalpy change is involved, however, a change of heat capacity C_p usually occurs at the transition ($\Delta H = 0$, $\Delta C_p \neq 0$). DTA is usually unable to detect such transitions.

2.2.7. Mössbauer Spectroscopy[38]

2.2.7.1. Principles

(a) The isomer shift

The isomer shift δ can be expressed as follows:

$$\delta = [(2 \pi Z e^2)/3] \{|\psi_s (0)_A|^2 - |\psi_s (0)_S|^2\} \{<R_e^2> - <R_g^2>\} \tag{vi}$$

where: e is the charge of the proton

$|\psi_s (0)_A|$ and $|\psi_s (0)_S|$ are the absolute values of the s-electron density at the nucleus in the absorber and in the source, respectively

$<R_e^2>$ and $<R_g^2>$ are the root mean square radii of the nucleus in the excited state and in the ground state, respectively.

51

For ^{119}Sn, since $I_g = \frac{1}{2}$, the nucleus is spherical in the ground state and $<R_g^2>$ is the square of the radius in the ground state. It can be seen that the isomer shift δ is the product of three terms: a constant, a chemical term (s-electron densities), and a nuclear term (root mean square radii of the nucleus). For a given nuclear transition of a given Mössbauer nuclide, only the chemical term is variable and when the same γ-ray source is used, only $\psi_s (0)_A$ is variable. The ψ functions are the electron densities "at the nucleus", i.e., they are a function of not only the valence s-electron density, but also of the screening effects of p-, d-, and f-electrons, and by bond covalency, i.e. by the chemical bonding of the atom and electronegativity of the ligands.

Since $\{<R_e^2> - <R_g^2>\}$ is positive for the $\frac{1}{2} \rightarrow \frac{3}{2}$ transition of ^{119}Sn, an increase of 5s-electron density in the immediate neighborhood of tin in the absorber results in an increase of isomer shift.

(b). The quadrupole splitting

Mössbauer spectroscopy is the resonant emission of γ photons by a radionuclide in a radioactive source and their resonant reabsorption by the same type of nuclide in an absorber. In order for both processes to be resonant, they have to be recoilless, i.e. both the source and the absorber must be solids, since it is a zero-phonon process. In Mössbauer spectroscopy, the modulation of the γ-ray energy is provided by Doppler effect, i.e. in most cases by vibrating the γ-ray source relative to the fixed absorber. The absorption of the 23.8 keV photon by tin excites the nucleus from the nuclear ground state (spin $I_g = \frac{1}{2}$) to the nuclear first excited state (spin $I_e = \frac{3}{2}$). The degeneracy of the

nuclear energy sublevels can be removed in an electric field gradient (e.f.g.) or in a magnetic field. Since tin(II) and tin(IV) are diamagnetic and no applied magnetic field will be used, only the e.f.g. is relevant here. The e.f.g. acting at the nucleus is the tensor $E_{ij} = -V_{ij}$, where V_{ij} is the electrical potential.

$$E_{ij} = -V_{ij} = (\delta^2 V/\delta x_i x_j), (x_i, x_j = x, y, z) \qquad \text{(vii)}$$

The stereoactivity of the tin(II) lone pair creates a very large e.f.g. at tin(II), which interacts with the nuclear quadrupole moment Q. For spins $\leq \frac{1}{2}$, $Q = 0$, i.e. the nuclear electric charge is spherically distributed. This is the case of the ground state ($I_g = \frac{1}{2}$), which is therefore not split by an e.f.g. On the other hand, for spins $> \frac{1}{2}$, Q is not equal to zero, and the nuclear electric charge has a non-spherical distribution, which can be approximated by a quadrupole term. For $Q < 0$, the nucleus is oblate, i.e. flattened along the spin axis; for $Q > 0$, the nucleus is prolate, i.e. elongated along the spin axis. When Q is not equal to zero, it interacts with the e.f.g. and partially removes the degeneracy of the nuclear sublevels. This is the case of the first excited state ($I_e = \frac{3}{2}$). Of course, if e.f.g. = 0, then there is not energy level splitting, regardless of Q, i.e. regardless of the value of the nuclear quadrupole moment. The interactions of the e.f.g. with the nuclear quadrupole moment are summarized on fig. 13.

(c) Probing the stereoactivity of the tin lone pair by Mössbauer spectroscopy

The presence of local distortions at the tin site will be evidenced by Mössbauer spectroscopy. Indeed, a regular cubic coordination of tin, like that of lead(II) in $\beta\text{-PbF}_2$
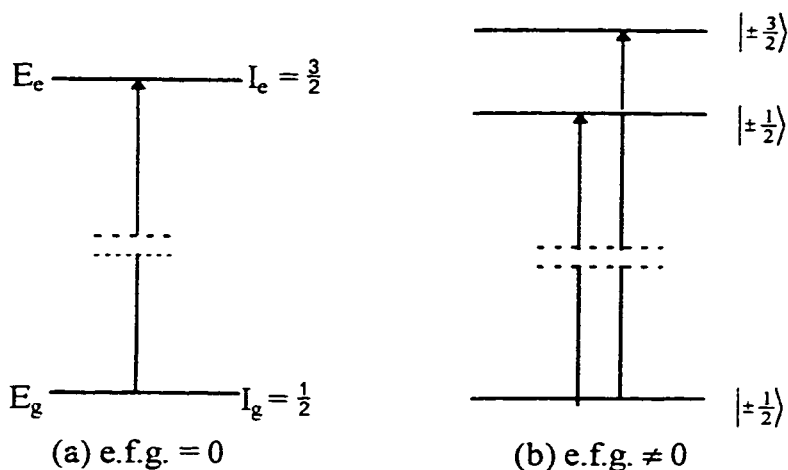
Figure 13: Interaction of the e.f.g. acting at the nucleus with the nuclear quadrupole moment. $\left|\pm\tfrac{1}{2}\right\rangle$ and $\left|\pm\tfrac{3}{2}\right\rangle$ are the spin operators.

would require the tin(II) lone pair to occupy the unhybridized 5s orbital, which would generate no $(V_{zz})_{val}$, $(V_{zz})_{val}$ being the V_{zz} generated by the valence electrons, because of the spherical distribution of the s electrons. This would make Sn(II) be a spherical Sn^{2+} ion, which could take a regular cubic coordination, hence $(V_{zz})_{latt} = 0$, where $(V_{zz})_{latt}$ is the V_{zz} generated by the atoms surrounding tin. Therefore, if tin(II) were in a cubic coordination, both contributions to V_{zz} would be nil, the total e.f.g. would be zero, and there would be no splitting of the nuclear first excited state. No quadrupole splitting would result ($\Delta = 0$), and a single Mössbauer line would be observed (fig. 13a). Of course, Sn^{2+} is a soft ion because the filled 5s orbital is in the valence shell. This will make it susceptible to polarization by the surrounding ions if the coordination is not quite regular. This could result in a small e.f.g., which would result in a small quadrupole splitting (e.g. up to ca. 0.5 mm/s), which would not be resolved, and thus give

a broadened line.

In the case of the Sn^{2+} ion, the $5s^2$ lone pair is concentrated around the tin core shell, and it results in a highly positive isomer shift: $\delta \approx$ ca. 4 mm/s. Therefore, ionic Sn^{2+} in cubic coordination, thus with a non-stereoactive lone pair, gives $\delta \approx$ ca. 4 mm/s and $\Delta \approx$ ca. 0 mm/s.

On the other hand, for covalently bonded tin(II), the lone pair is located in one of the hybrid orbitals (usually sp^3, sp^3d or sp^3d^2). Contrary to the unhybridized 5s orbital, the hybridized orbitals are highly axial, therefore, a significant amount of the 5s electron density is shifted away from the tin core, hence it results in a lower isomer shift, typically $\delta = 2.5$ to 3.7 mm/s. In addition, the highly directional stereoactive lone pair creates a very high $(V_{zz})_{val}$. The presence of the stereoactive lone pair results in a highly distorted tin coordination, that generates a large $(V_{zz})_{latt}$. $(V_{zz})_{latt}$ may add to $(V_{zz})_{val}$ or subtract from it, however, since $|(V_{zz})_{val}| \gg |(V_{zz})_{latt}|$ for the tin(II) stereoactive lone pair, in contrast with the Sn^{2+} ion, the total e.f.g. is enormous. It results in a large splitting of the sublevels of the nuclear first excited state, and a large quadrupole splitting, typically $\Delta = 1.2$ to 2.0 mm/s, is observed (fig. 13b).

In summary, Mössbauer spectroscopy provides a convenient method for testing the stereoactivity of the tin lone pair, and of the possibility for a regular coordination of tin, e.g cubic in the $M_{1-x}Sn_xF_2$ solid solution and in $PbSn_4F_{10}$, i.e.:

- If $\delta \approx$ 4mm/s and $\Delta \approx$ 0 mm/s: spherical Sn^{2+} ion, non-stereoactive lone pair, fairly regular coordination;

- if $\delta \approx$ 2.5 to 3.7 mm/s and $\Delta = 1.2$ to 2.0 mm/s: covalently bonded tin(II), stereoactive lone pair, highly distorted tin coordination.

It has been shown by Mössbauer spectroscopy in earlier works that tin(II) has a stereoactive lone pair, hence a highly distorted coordination, in the following cubic fluorite type disordered systems: $Pb_{1-x}Sn_xF_2$ (x = 0-0.30), $PbSn_4F_{10}$ and microcrystalline $Ca_{1-x}Sn_xF_2$, and it is suspected to be the case in γ-$PbSnF_4$[20,27,39,40,41]. In addition, the values of the isotropic Debye-Waller factors B_M and B_F in $Pb_{1-x}Sn_xF_2$, where: B_M stands for (1-x)Pb + xSn statistically disordered on the metal site (4 a Wyckoff site of the Fm3m space group), and B_F for F located in site 8 c, have been fitted from ambient temperature X-ray and neutron powder diffraction data. Both B_M and B_F increase rapidly when x increases, from 0.8(2) and 1.3(4) for x = 0, to 8 and 20, for B_M and B_F respectively. This shows clearly that the high values of B_M and B_F have a static origin (disorder) rather than dynamic (thermal vibrations) and therefore tin is not located in the center of F_8 cubes like Pb.

2.2.7.2. Instrumentation and experimental procedures[40]

The [119]Sn Mössbauer spectroscopic study was carried out using a Harshaw (TI)NaI scintillation detector. The γ-ray source used was a nominally 5mCi $Ca^{119m}SnO_3$ pellet supplied by Tenex-Uranservice. The Doppler velocity was obtained using an Elscint driving system working in the constant acceleration mode (triangular waveform). All spectra were taken at ambient temperature and accumulated in a quarter of the 2K Tracor Northern 7200 multichannel analyzer operating in the multiscanning mode. The data were transferred to an IBM compatible computer after accumulation and saved on a diskette. About 200mg of the sample was used and pressed in a Teflon holder with a

tight fitting cap. Isomer shifts were referenced to $CaSnO_3$ at room temperature as velocity zero.

CHAPTER 3

RESULTS AND DISCUSSION: THE STRAIN-DRIVEN
$\alpha- \rightarrow$ o-PbSnF$_4$ FERROIC TYPE TRANSITION

3.1. LINE BROADENING IN POWDER DIFFRACTION

Experimental difficulties involved in the measuring of particle size from line broadening increase for very small and for very large particles. The maximum size measurable by line broadening is determined by the instrumental broadening and usually placed at around 1000Å. Line broadening is chiefly used to measure the particle size of loose powders rather than the size of the individual crystals in a solid aggregate[42].

There are a few reasons why Bragg peaks cannot have an infinitely small line width. One is instrumental broadening, another is that the K_α emission line of copper is not a single line but a doublet i.e. $K_{\alpha 1}$ and $K_{\alpha 2}$. Since the geometry of the X-ray powder diffractometer uses the line focussing arrangement, high intensities and good resolution are observed. However, the slits which prevent radiations scattered at angles other than the Bragg angles to enter the detector cannot be infinitely narrow, otherwise the intensity reaching the detector would be infinitely small. This finite width of the slits will give rise to a finite linewidth for the Bragg peaks[42]. In addition, the non resolved (or partially resolved) lines due to $K_{\alpha 1}$ and $K_{\alpha 2}$ result in further broadening. An absolute physical limit is due to the width of the X-ray emission lines, which is limited by Heisenberg's uncertainty principle i.e. by the precision on the energy of the electronic

level involved in the production of X-ray photons. This then results in peaks with a natural linewidth, therefore, if there is no other cause of broadening, the peaks are very narrow. The third reason is due to sample broadening[32]. Line broadening by the sample can be due to the following different factors:

(i) **microcrystallinity** - i.e. broadening in addition to instrumental broadening that can occur if the size of the crystallites is too small, usually below 1000Å in diameter. Below an average particle size of about 40Å , the peaks are so broad that they can hardly be distinguished from the background counts and therefore, no diffraction pattern can be observed.

From the measurements of this extra broadening, the average particle size may be obtained by using the accepted formula for particle size broadening known as Scherrer formula:

$$t = 0.9\lambda \, / \, B\cos\theta_B \, .$$

(viii)

where: t = average thickness of the crystallites, Å

λ = X-ray wavelength (λ = 1.54178 Å for K_α Cu)

θ_B = Bragg angle

B = broadening due to small particle size

The linewidth is measured at half the peak height. The extra broadening B, the instrumental broadening and the experimental linewidth are related by Warrens' formula:

$$B^2 = B^2_M - B^2_S$$

(ix)

where: B_M = measured peakwidth, in radians, at half height, for the sample

B_S = measured peakwidth, in radians, at half height, for a standard crystalline material at a similar θ angle

One very interesting feature is that, since each Bragg peak is representative of a particular direction in the crystal, the particle dimension versus direction can be measured, therefore the anisotropy of the particle dimensions is obtained. This is particularly useful in highly anisotropic structures such as $PbSnF_4$.

(ii)   **strain** - when a crystal is subjected to a strain, changes results in the d-spacing or in the linewidth which can have a marked effect on the diffraction pattern.

A uniform strain results in a uniform change of d-spacing and therefore, shifts the Bragg peak without broadening. A non-uniform strain, on the other hand, distorts the crystals. It results in domains with variable values of d-spacing and the resulting distribution of d-spacings gives a distribution of Bragg angles therefore, it results in a highly broadened peak. The direction of the strain is obtained from the Miller indices of broadened peaks. The strain responsible for the line shift or broadening can be external (i.e. applied) or internal (i.e. due to bonding in the crystal structure or some physical properties driven by cooperative phenomena such as ferroelectricity, antiferroelectricity, ferroelasticity, or piezoelectricity.

3.2. UNIT-CELL PARAMETERS, VOLUME AND DISTORTION

The X-ray powder diffraction patterns of β-PbF$_2$ and PbSnF$_4$ obtained by precipitation from aqueous solution (α-PbSnF$_4$(aq$_1$) and o-PbSnF$_4$) are shown on figure 6 and the X-ray powder pattern of α-PbSnF$_4$ prepared from solid state reaction is shown on figure 7. Table VI compares the unit-cell parameters of β-PbF$_2$ and the various phases of PbSnF$_4$.

The unit-cell parameters of α-PbSnF$_4$ are the same within experimental error, regardless of the method of preparation. The (200) peak of β-PbF$_2$ splits into 2 peaks, (110) and (004) to give the tetragonal distortion observed in α-PbSnF$_4$. The (004) peak is representative of the $\bar{c}$ direction and the (110) peak is representative of the ($\bar{a}$, $\bar{b}$) plane, which is perpendicular to $\bar{c}$. The tetragonal distortion for α-PbSnF$_4$ (aq$_1$) is $\sqrt{2a}/c$ = 0.957, using the β-PbF$_2$ axes, compared to 1 in cubic therefore a 4.1% flattening along $\bar{c}$ occurs. The changes of the Miller indices relative to β-PbF$_2$ are due to: (i) the splitting of (200) β-PbF$_2$ to (110) and (004) of α-PbSnF$_4$, and of (220) β-PbF$_2$ to (200) and (114) in tetragonal, as mentioned earlier, (ii) the 45° rotation of the axes in the ($\bar{a}$, $\bar{b}$) plane which is due to the loss of the F Bravais lattice, and (iii) the length of the unit-cell along the $\bar{c}$ axis is doubled resulting in l in α-PbSnF$_4$ being doubled. This is due to the ordering of Pb/Sn along the $\bar{c}$ axis.

The transition from α → o-PbSnF$_4$ is mostly bidimensional, taking place in the ($\bar{a}$, $\bar{b}$) plane of the unit-cell. The a parameter increases by 0.86%, b decreases by 1.38% whereas only a very minor change in c (-0.088%) is observed (Table VI).

Table VI: Unit-cell parameters of β-PbF$_2$, and the various phases of PbSnF$_4$ at ambient temperature

		a(Å)	b(Å)	c(Å)	V(Å)	c/a[1]	c/b[1]	b/a
β-PbF$_2$	unit-cell	5.924	$= a^{(2)}$	$= a^{(2)}$	207.9	1	$\simeq 1^{(2)}$	$1^{(2)}$
α-PbSnF$_4$(aq$_1$)	unit-cell	4.219	$= a^{(2)}$	11.420	203.3	0.957	$= c/a^{(2)}$	$1^{(2)}$
	% change from β-PbF$_2$	0.719	0.719	-3.612	-2.222	-	-	-
α-PbSnF$_4$(aq$_2$)	unit-cell	4.221	$= a^{(2)}$	11.428	203.6	0.957	$= c/a^{(2)}$	$1^{(2)}$
	% change from β-PbF$_2$	0.766	0.766	-3.545	-2.061	-	-	-
α-PbSnF$_4$(ssr)	unit-cell	4.222	$= a^{(2)}$	11.416	203.5	0.956	$= c/a^{(2)}$	$1^{(2)}$
	% change from β-PbF$_2$	0.790	0.790	-3.646	-2.118	-	-	-
o- PbSnF$_4$	unit-cell	6.018	5.884	11.410	202.0	0.948	0.970	0.978
	% change from β-PbF$_2$	1.587	-0.675	-3.697	-2.829	-	-	-
	% change from α-PbSnF$_4$(aq$_1$)	0.862	-1.384	-0.088	-0.621	-	-	-
β-PbSnF$_4$	unit-cell	16.864	$= a^{(2)}$	22.928	6520.6	0.961	$= c/a^{(2)}$	$1^{(2)}$
	% change from β-PbF$_2$	0.647		-3.241	-1.985	-	-	-
	% change from α-PbSnF$_4$(aq$_1$)	-0.071		0.385	-0.242	-	-	-

[1]Ratio of unit cell lengths and % changes are given relative to the β-PbF$_2$ axes for all phases.
[2]Restricted by symmetry

Figure 14 shows the c parameter decreasing up to a VR $\approx$ 0.005 then, it remains constant. The slight shrinkage along $\bar{c}$ results in a slight improvement of packing along the $\bar{c}$ direction due to the shifting of the atoms within the layers when the tetragonal symmetry is broken and the ($\bar{a},\bar{b}$) plane shrinks. The increase of a and the decrease of b and c versus VR = Vol.$_{(HF)}$/Vol.$_{(HF + H_2O)}$ result in a decrease of the volume of the unit-cell with increasing volume ratio, up to $\approx$ 0.5% decrease for a volume ratio of 0.002 (fig. 15). The volume change is completed by VR = 0.002 when the orthorhombic symmetry has reached its maximum. The orthorhombic symmetry has more degrees of freedom and thus allows a more efficient packing of the ions than the α-phase.

A plot of the tetragonal distortion is shown on figure 16. As the Vol.$_{(HF)}$/Vol.$_{(HF + H_2O)}$ increases up to $\approx$ 0.002, the c/(a+b) ratio increases i.e. the tetragonal distortion decreases, since no tetragonal distortion would be observed for c/(a+b) = $\sqrt{2}/2$ = 0.707. Above VR = Vol.$_{(HF)}$/Vol.$_{(HF + H_2O)}$ = 0.002 a plateau is reached and a slightly reduced, but still significant tetragonal distortion persists in the orthorhombic phase.

The X-ray powder pattern of o-PbSnF$_4$ is similar to that of α-PbSnF$_4$ (fig. 6). The (110) peak of α-PbSnF$_4$ (tetragonal) splits further into two lines, the (200) and (020) where the a and b parameters are different. This is characteristic of further symmetry loss i.e. as the unit-cell goes from cubic (β-PbF$_2$) to tetragonal (α-PbSnF$_4$) and to orthorhombic (o-PbSnF$_4$) the symmetry decreases. This is in agreement with earlier results of Réau et al[3]. The magnitude of the splitting of (110)$_\alpha$ to (200)$_o$ and (020)$_o$ was used to measure the orthorhombic distortion.

Figure 14 : c vs. Vol.$_{HF}$/Vol.$_{(HF + H_2O)}$

c (Å)
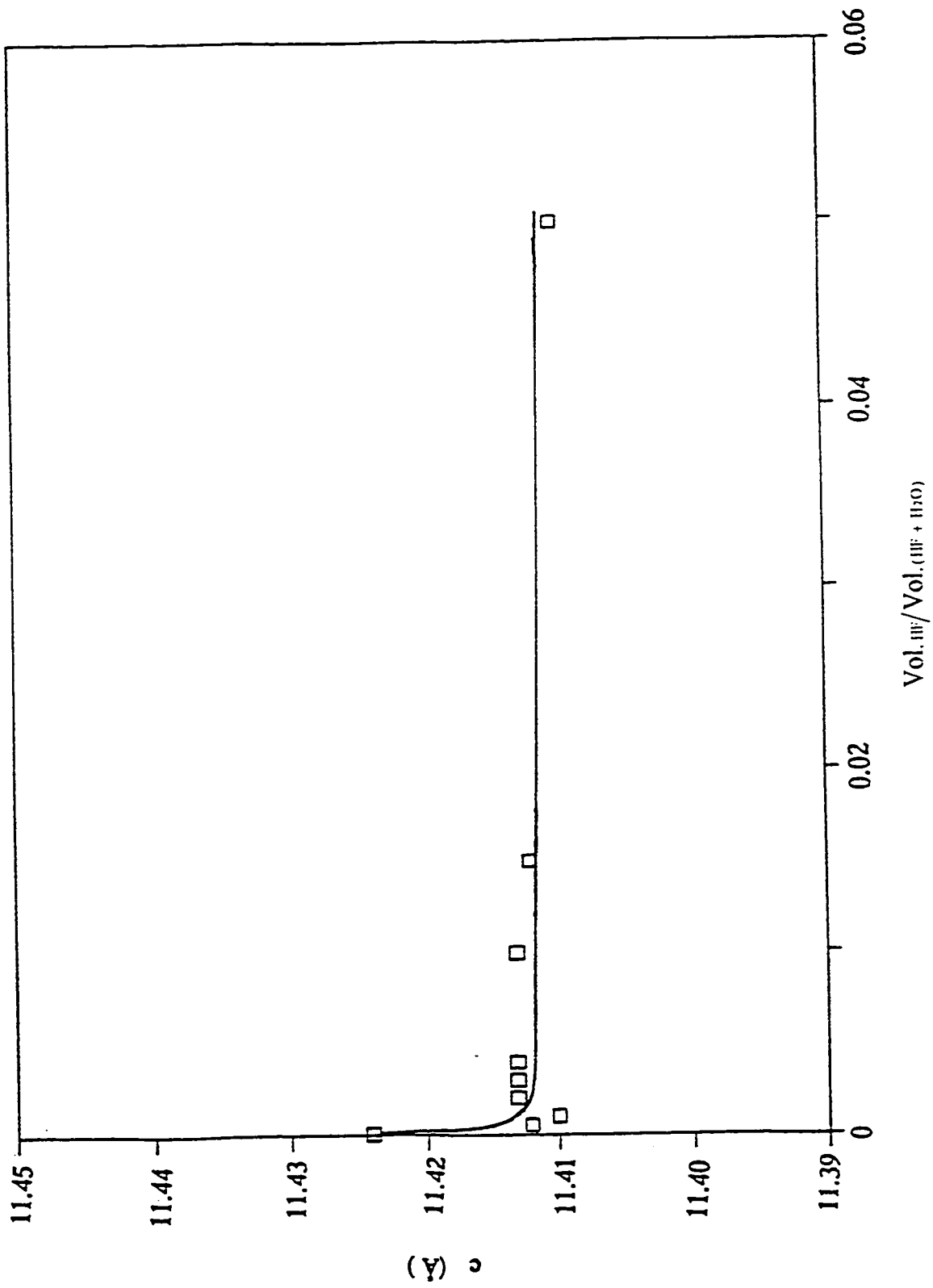
Vol.$_{HF}$/Vol.$_{(HF + H_2O)}$

Figure 15 : Volume vs. $Vol._{HF}/Vol._{(HF + H2O)}$

$Vol._{HF}/Vol._{(HF + H2O)}$

$V (\mathring{A})$
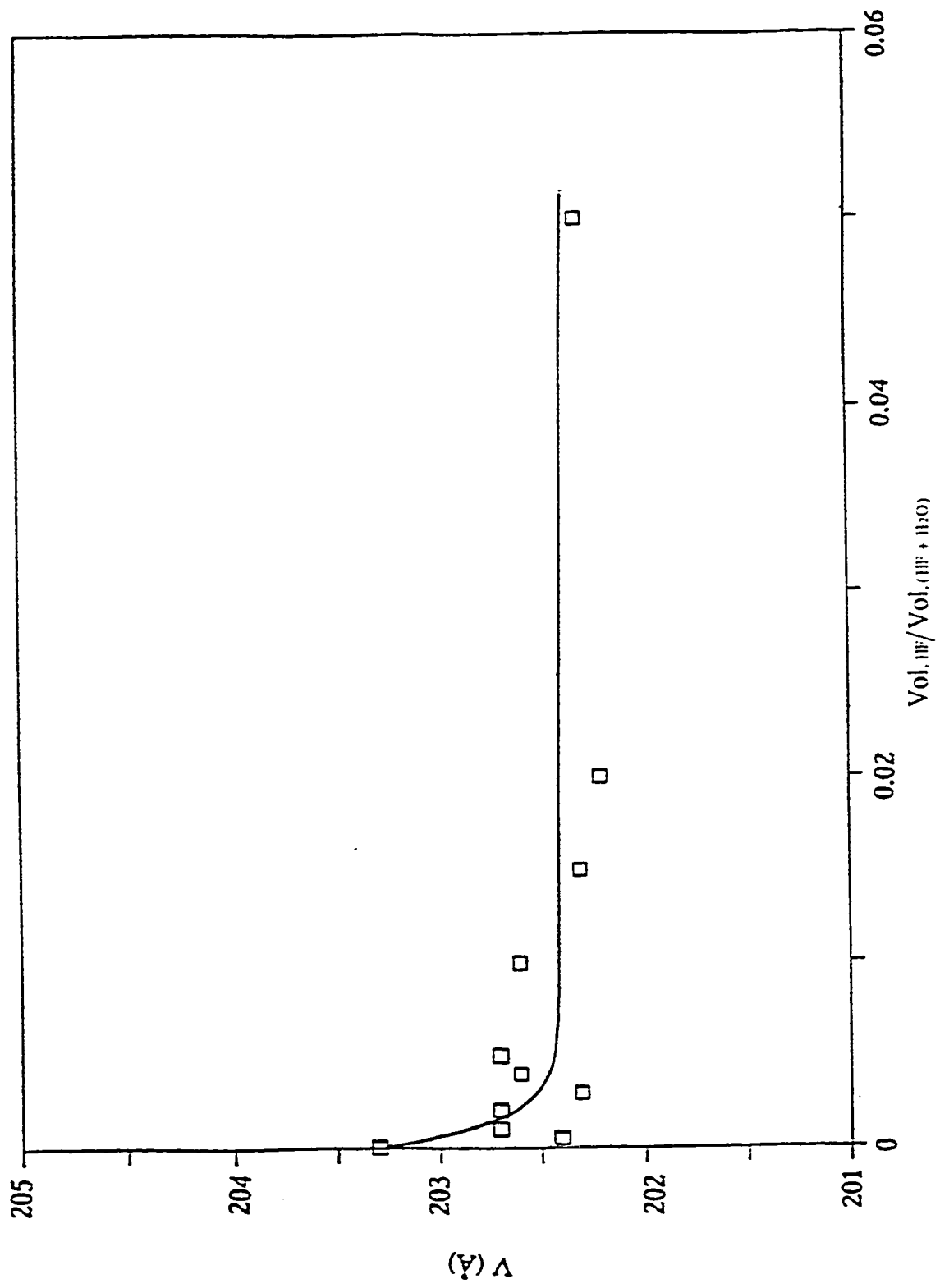
Figure 16 : Tetragonal Distortion $c/(a+b)$ vs. $Vol._{HF}/Vol._{(HF+H_2O)}$

$Vol._{HF}/Vol._{(HF+H_2O)}$

$c/(a+b)$
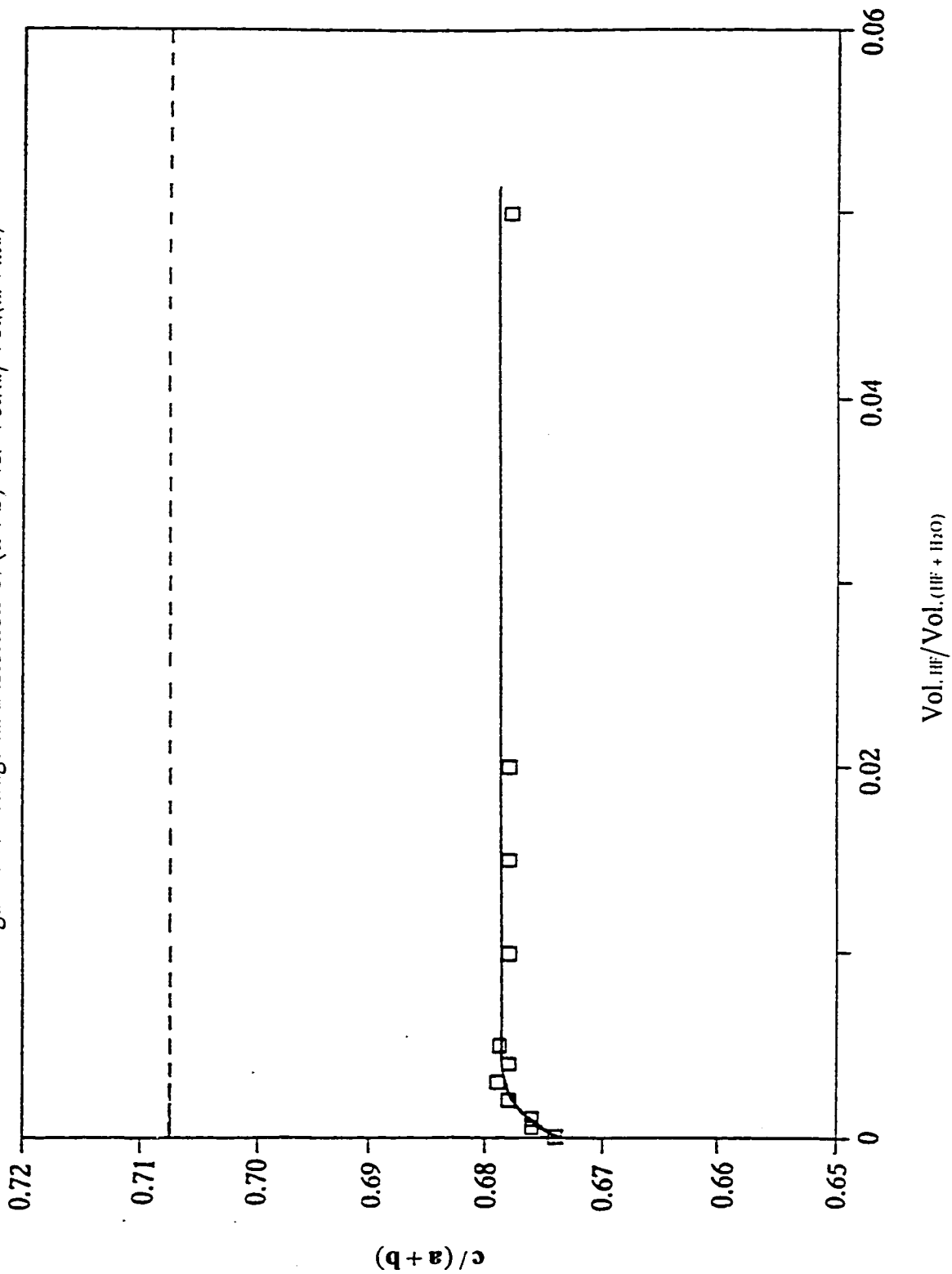
Orthorhombic distortion starts as a small perturbation of the tetragonal distortion. Figure 17 shows a plot of the orthorhombic distortion observed with increasing VR. At VR = 0 (i.e. for tetragonal α-PbSnF$_4$) b/a = 1. A sharp decrease is observed when VR increases until a maximum is reached for a VR = 0.005. Then, it remains constant at b/a $\approx$ 0.98. However, the orthorhombic distortion (-2%) still remains smaller than the tetragonal distortion (-4.1%).

3.3. INFLUENCE OF THE AMOUNT OF HYDROFLUORIC ACID ON THE $\alpha \rightarrow$ o-PbSnF$_4$ TRANSITION IN THE $(\bar{a}, \bar{b})$ PLANE

The transition from $\alpha \rightarrow$ o-PbSnF$_4$ starts with the use of a very minor amount of HF (VR = 0.0005) used for the synthesis. The orthorhombic splitting increases up to a VR = 0.002 when constant unit-cell parameters are reached (figure 18). The average of a and b (i.e. (a+b)/2) shows that an overall shrinkage of 0.26% of the $(\bar{a}, \bar{b})$ plane takes place. Figure 19 shows the profile of the (110) peak of α-PbSnF$_4$ versus the amount of HF. As the HF volume ratio increases to 0.003, the (110) peak of α-PbSnF$_4$ starts broadening asymmetrically towards higher angle with unresolved splitting. This can be attributed to the near equivalence of a and b and thus, a possible exchange between them, or hesitation about which is which, possibly resulting in fluctuations between the definition of the two axes. For a VR of 0.003, the combined (200) and (020) peak is very broadened asymmetrically, and seems to have more than two maxima (fig. 19). This could be due to the presence of crystallites with a distribution of a and b values, more particularly of b, since the asymmetric broadening takes place towards higher angles,

Figure 17 : Orthorhombic Distortion **b/a** vs. Vol.$_{\text{IIF}}$/Vol.$_{(\text{IIF} + \text{H}_2\text{O})}$
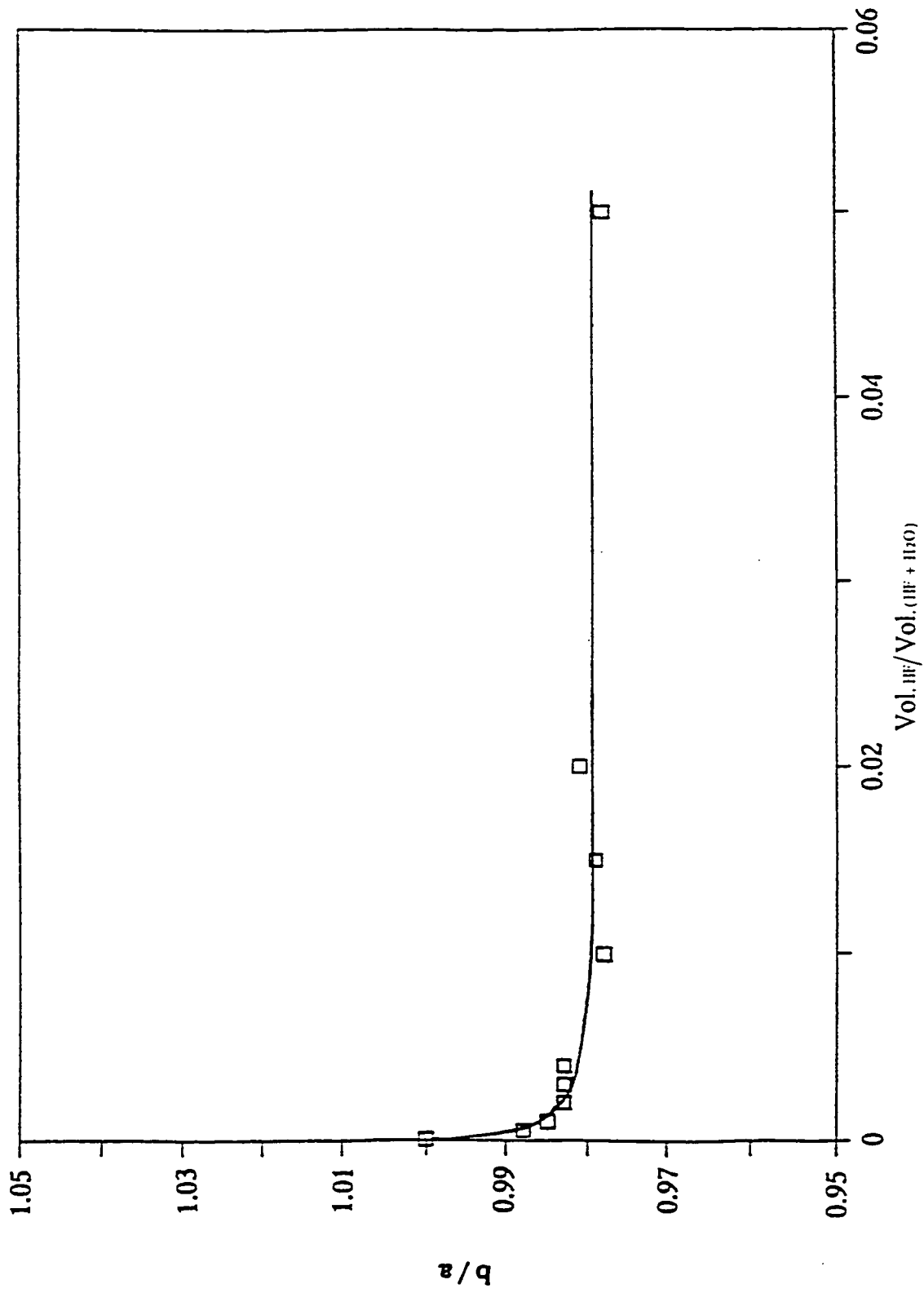
Figure 18 :Unit-cell parameters **a** and **b** (in the orthorhombic axes) vs. $Vol._{HF}/Vol._{(HF + H_2O)}$
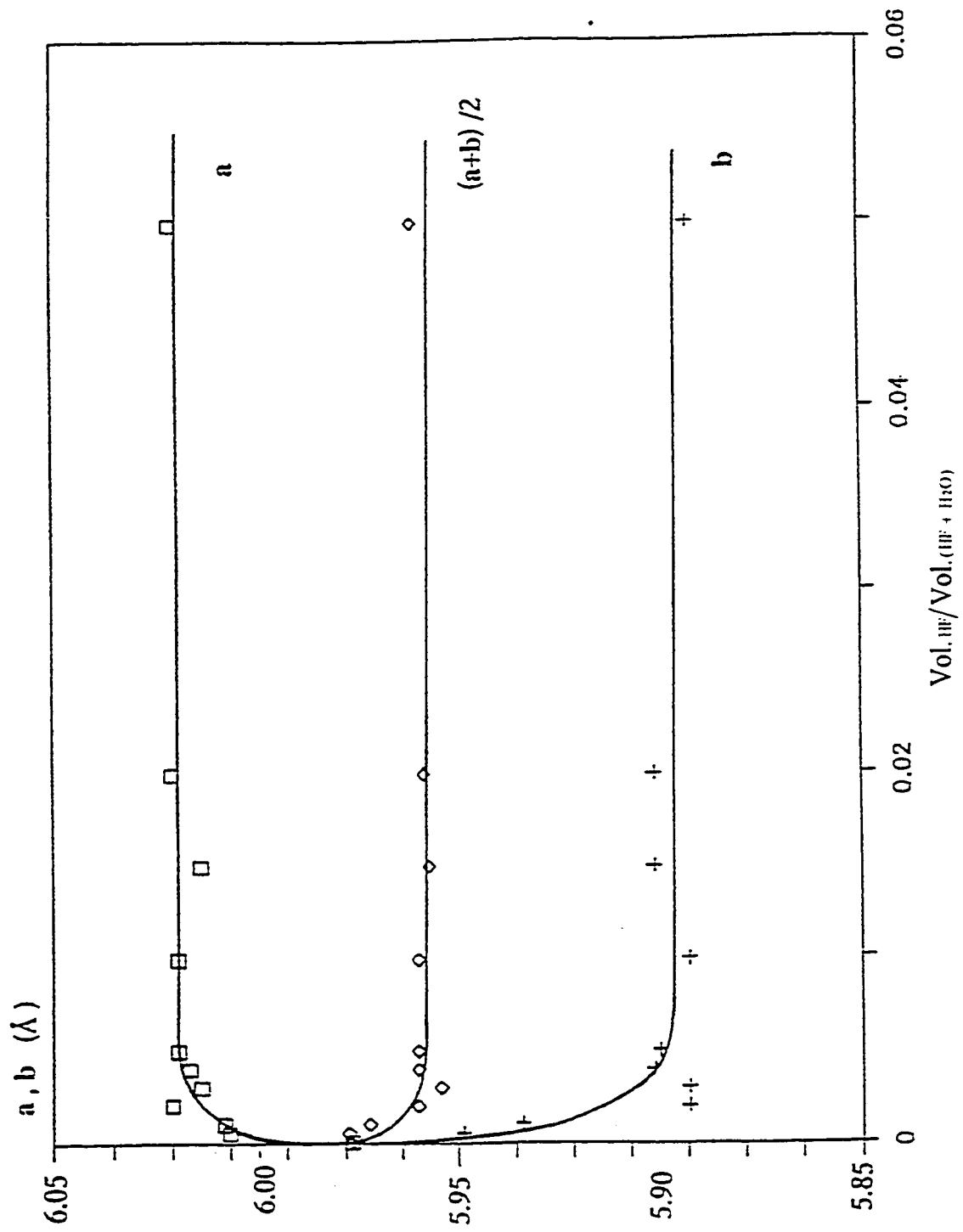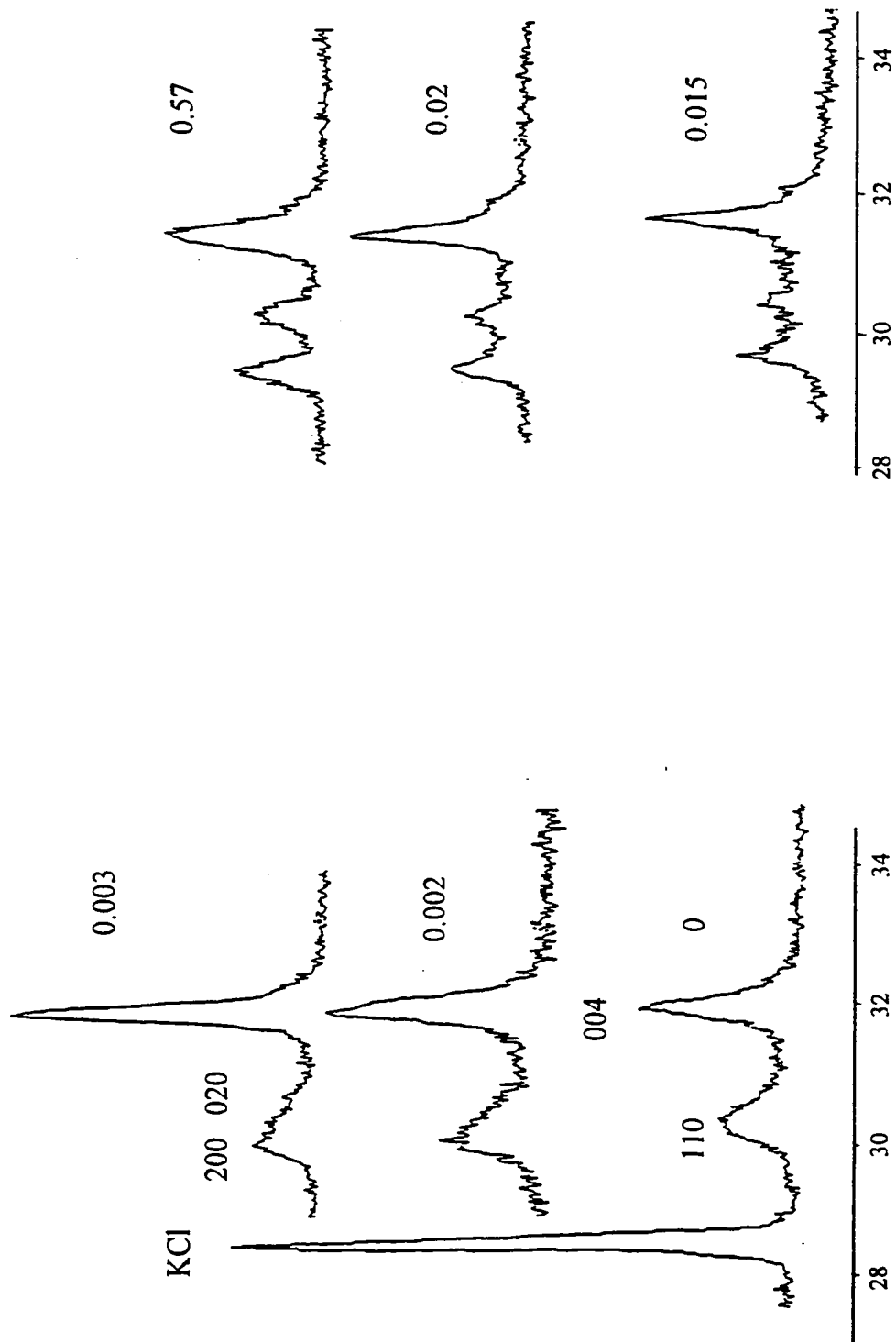
Figure 19: Profile of the (110) peak of α-PbSnF$_4$ vs. Vol.$_{\text{HF}}$/Vol.$_{\text{(HF + H}_2\text{O)}}$

70

when the (020) peak splits from (200). The presence of multiple values of a and b would not be surprising since it takes place in the narrow range of VR values where the value of the orthorhombic splitting is very sensitive to VR. It is quite possible that the crystallites formed at the beginning of the $Pb(NO_3)_2$ addition to the SnF_2 solution have a given value of a and b, and as more $Pb(NO_3)_2$ is added, since the composition of the reaction mixture changes (SnF_2 is used in the reaction and maybe HF as well), the values of a and b vary. In this region, precise values of a and b cannot be obtained. The (004) peak shows little change as the HF volume ratio increases, except a very slight shift to higher angles therefore, there is no significant transformation taking place in the $\bar{c}$ direction which, then, confirms the bidimensionality of the transition. At higher HF volume ratios (0.003-0.015), the (110) peak clearly splits up to give (200) and (020) peaks as $(020)_o$ grows at the expense of the wide high angle tail of $(110)_\alpha$. At this stage, there is probably enough HF to make all the particles have full orthorhombic splitting. However, a very high background is present between the two peaks. This is assumed to be due to the fact that the a and b parameters are no longer equal, although there is still a considerable distribution of values and maybe even fluctuations between the $\bar{a}$ and $\bar{b}$ directions. At higher HF volume ratio, the splitting remains the same, however the $\bar{a}$ and $\bar{b}$ directions are now better defined and the fluctuations between $\bar{a}$ and $\bar{b}$ directions are decreasing. For VR = 0.57, much of the background has disappeared, therefore the $\bar{a}$ and $\bar{b}$ directions are now well defined and there is no more spread of values.

The (110) peak for the α-phase i.e. when no HF is added to the SnF_2 solution, is broad compared to the (200) peak of the KCl internal standard (fig.19). The slight

broadening of the (004) peak is most likely due to the small dimension of the particles in the $\bar{c}$ direction. The thickness of the platelet-like crystallites is calculated from the broadening of (004) to be $\approx$ 700-800 Å. This is not surprising, since cleavage originates in the lack of bonding between the sheets and the high repulsions due to the adjacent layers of lone pairs facing each other (figure 1). The layers of sheets are polymerized in $(\bar{a},\bar{b})$ and contain strong metal-fluorine bonds which gives rise to large surface area particles parallel to the $(\bar{a},\bar{b})$ plane of the unit-cell, therefore, broadening of the (110) peak of α-PbSnF$_4$ cannot be due to the small size of the crystallites in any direction within the $(\bar{a},\bar{b})$ plane[8].

It should be pointed out that, in the tetragonal α-phase, crystal symmetry forces the material to be isotropic in $(\bar{a},\bar{b})$. Therefore, the main reason for the line broadening is non-uniform stress. It results in domains with variable values of d-spacing, whereas a uniform stress results in a uniform change in d-spacing which, therefore, shifts the Bragg peaks without broadening[43]. The broadening of (110) indicates that the α-phase is stressed in the $(\bar{a},\bar{b})$ plane and that this stress is non-uniform. When HF is added in the reaction mixture, the stress in the $(\bar{a},\bar{b})$ plane increases since the broadening increases. However, since the peak broadening is asymmetric, the material also starts to overcome the tetragonal symmetry constraints, and orthorhombic splitting occurs. As the HF volume ratio is increased, first the stress remains very high, then further, the stability of the orthorhombic phase increases and the stress decreases. For very high HF volume ratios, the orthorhombic structure is very stable and much of the stress in the $(\bar{a},\bar{b})$ plane has disappeared (figure 19).

3.4. SEQUENCE AND DIAGRAM OF THE $\alpha \rightarrow$ o-PbSnF₄ PHASE TRANSITION

The sequence of changes leading to the $\alpha \rightarrow$ o-PbSnF₄ phase transition is shown on figure 20. It shows what happens to the $\bar{a}$ and $\bar{b}$ directions during the transition from tetragonal (α-phase) to orthorhombic. In the α-phase, a = b, and the (110) peak representative of the $(\bar{a}, \bar{b})$ plane is observed. When a minor amount of HF is added, a transitional phase is observed i.e. a and b are no longer equal and are changing to different values, with the difference increasing with the amount of HF. Since the $\bar{a}$ and $\bar{b}$ axes of tetragonal α-PbSnF₄ are identical, and therefore fully interchangeable, the symmetry change from tetragonal to orthorhombic can occur according to two different orientations of the $\bar{a}$ and $\bar{b}$ axes:

(i) a_t goes to a_o and b_t goes to b_o, or

(ii) a_t goes to b_o and b_t goes to a_o

where: a_o and b_o are the $\bar{a}$ and $\bar{b}$ axes of o-PbSnF₄, and a_t and b_t are the values of α-PbSnF₄.

The presence of these two possibilities which have equal probability in tetragonal symmetry, creates a strain in the $(\bar{a}, \bar{b})$ plane which is non-uniform since it acts in two perpendicular directions (along $\bar{a}$ and $\bar{b}$) and thus, it causes line broadening. This is observed in the form of the asymmetric broadening of (110)$_\alpha$ on figure 19. As HF is added, the probability $a_t \rightarrow a_o$ and $b_t \rightarrow b_o$ is no longer equal to $a_t \rightarrow b_o$ and $b_t \rightarrow a_o$,
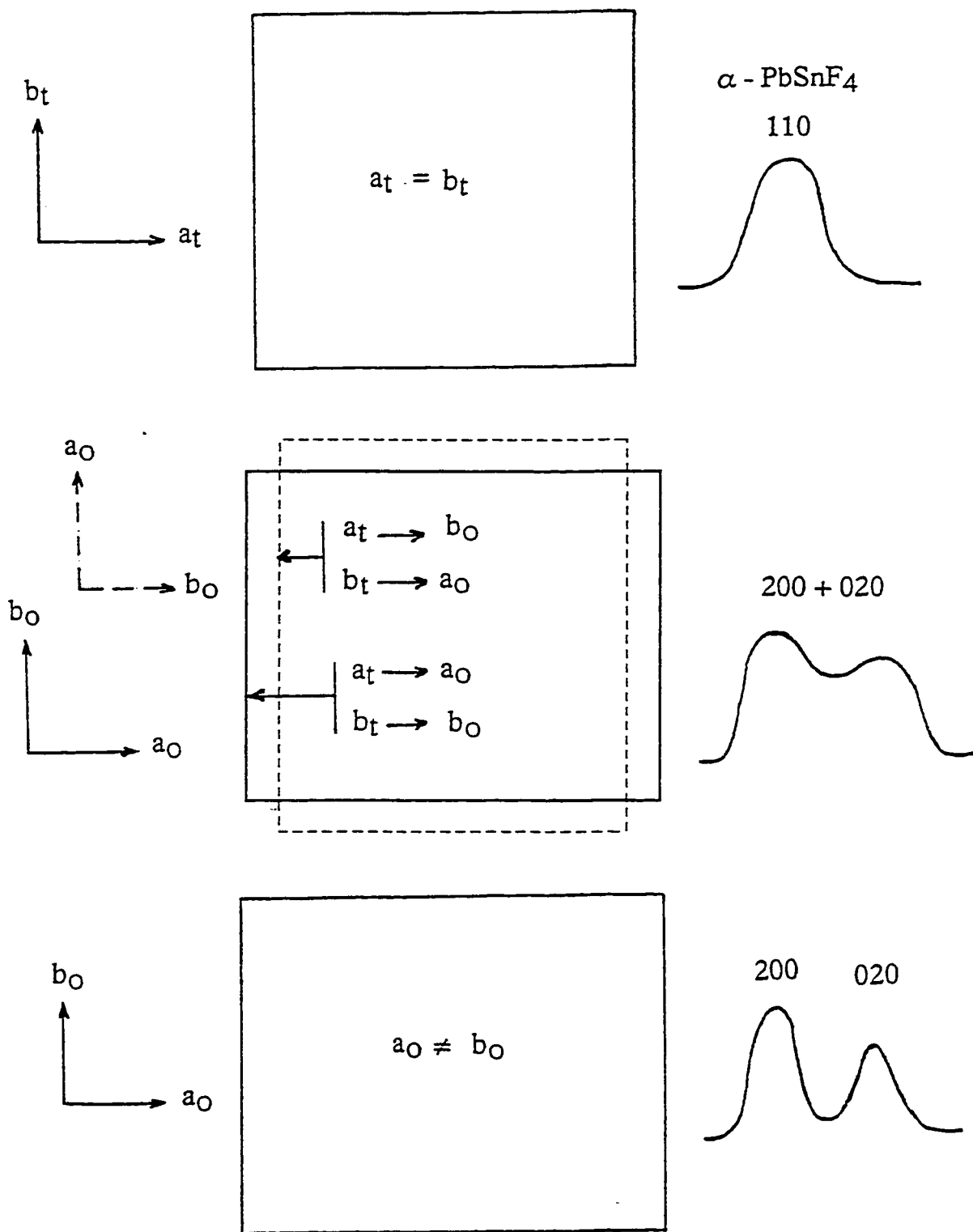
Figure 20: Sequence of the stages of the phase transition from tetragonal
α-PbSnF$_4$ $\rightarrow$ o- PbSnF$_4$

therefore the probability of having a_o in one direction and b_o in the perpendicular direction increases, giving a finite orthorhombic splitting. However, the choice of the directions of a_o and b_o remains largely unresolved, as can be seen by the fact the $(110)_\alpha$ peaks broadens asymmetrically to give $(200)_o$ and $(020)_o$, which are unresolved at this stage due to the large linewidth caused by the still large strain and most likely interchanging $\bar{a}$ and $\bar{b}$ directions, with possibly a distribution of a and b values. The asymmetry of the broadening is due to the fact that $(020)_o$ is weaker than $(200)_o$, as can be seen at higher VR, when the splitting is larger and the lines are narrower (fig. 19). As the amount of HF used increases, the orthorhombic splitting increases up to a maximum and the line gets narrower, indicating that the strain has decreased since there is at this stage lower probability of a/b permutation and a narrow distribution of a and b values. However, for low amounts of HF, the orthorhombic splitting is small, i.e. it is still close to the tetragonal symmetry. The nearly equal probability of having $a_t \rightarrow a_o$ and $b_t \rightarrow b_o$, compared to $a_t \rightarrow b_o$ and $b_t \rightarrow a_o$, increases the strain. At this stage, the line broadening is due to the sum of the effects of increased non-uniform strain and small line splittings. It results that the values of a_o and b_o are nearly impossible to measure from the X-ray diffraction pattern. At higher amount of HF, a fully split orthorhombic unit-cell is observed with narrower peaks which means that much of the strain observed has drastically decreased, since the probabilities of $a_t \rightarrow a_o$ and $b_t \rightarrow b_o$ is now sufficiently different from that of $a_t \rightarrow b_o$ and $b_t \rightarrow a_o$. The system has chosen the $\bar{a}$ and $\bar{b}$ directions out of the two possibilities that are described above. This dual choice of direction distribution is common in all materials exhibiting ferroic properties (ferromagnetic, ferroelectric and ferroelastic), particularly in ferroelastic - paraelastic

75

transitions where a broadening of Bragg peaks due to spontaneous internal strain has been reported[44,45]. In such a case, the transition is usually driven by a change of temperature (e.g. β-SnF$_2$ $\rightleftarrows$ γ-SnF$_2$) or pressure (tetragonal paratellurite TeO$_2$ $\rightleftharpoons$ high pressure TeO$_2$)[46-49]. In addition, it could also be due to a change in chemical composition, since some ion substitution can be approximated to local pressure because of change of size or electronic interactions. Such an example is found in cubic $\rightarrow$ tetragonal distortion of the Pb$_{1-x}$Sn$_x$F$_2$ solid solution at x $\approx$ 0.30[39].

The diagram of figure 21 summarizes the sequences of changes occurring during the phase transition. The different stages of the transition are the following:

(i) The (110) Bragg peak of α-PbSnF$_4$ is symmetrically broad. The symmetry is tetragonal when no HF is added however, it is not strain-free, i.e. even α-PbSnF$_4$ is a potential orthorhombic phase that has not managed to decide whether a should increase and b decrease or vice-versa.

(ii) the (110) peak of the α-phase broadens further as HF is added and splits to give (200)$_o$ and (020)$_o$ due to increasing strain making tetragonal symmetry unstable. This is called a "*transitional phase*" where the start of orthorhombic splitting is increasing rapidly and is observed in the form of a highly asymmetrically broadened peak, which makes it is very hard to measure the peaks positions, and therefore, results in highly inaccurate a and b unit-cell parameters.

(iii) in this region, the orthorhombic splitting is constant but the broadening is still large. The VR in the region is equal to 0.005 to 0.015. This is still a "*transitional phase*" since there is still peak broadening and high background between the (200) and

76
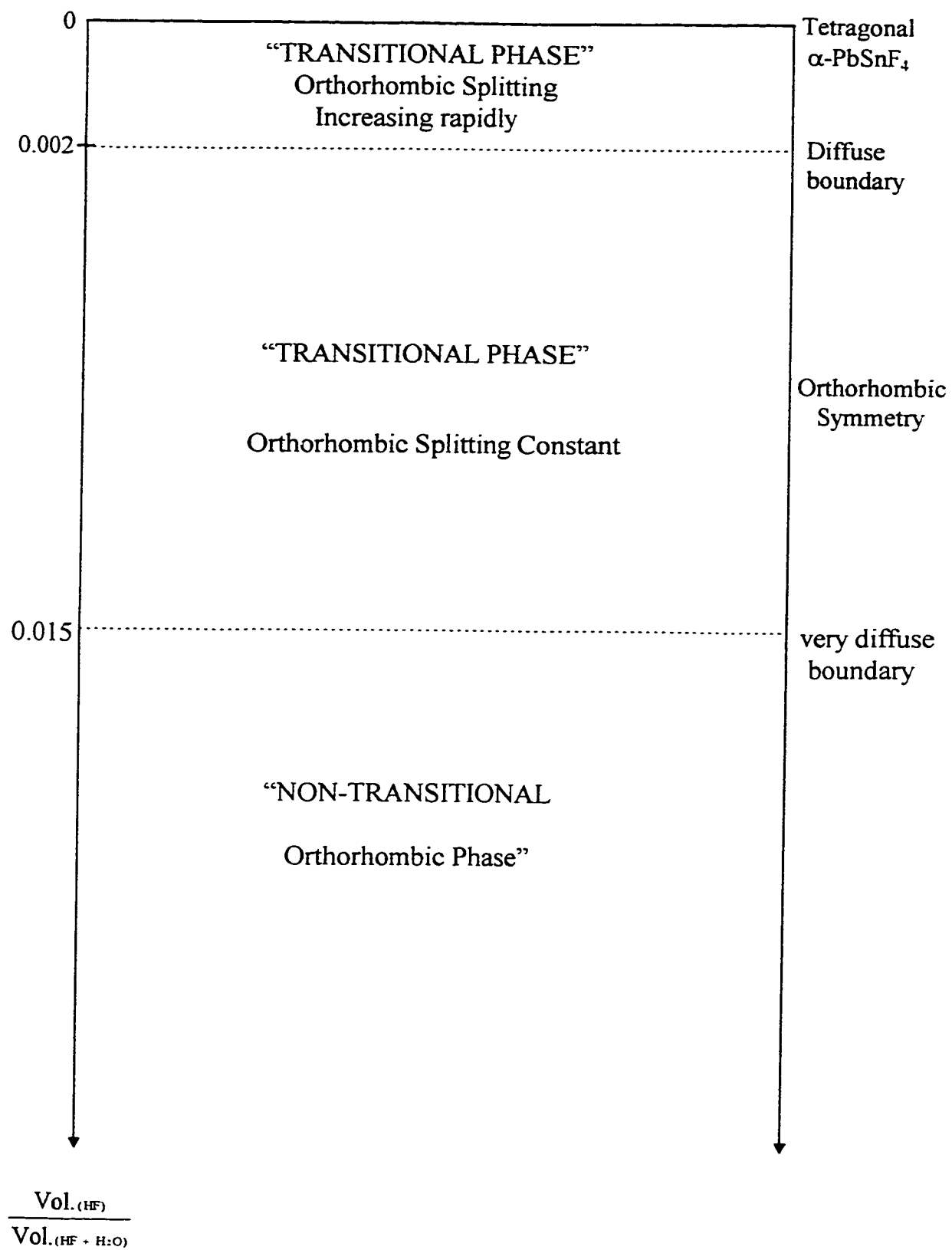
Figure 21: Diagram of the phase transition from α-PbSnF$_4$ $\rightarrow$ o- PbSnF$_4$

(020) peaks observed in this region. The high background might be an indication of disorder and/or microcrystallinity in the $(\bar{a},\bar{b})$ plane, due to fragmentation of the crystallites caused by the strain, which usually leads to the formation of polydomain crystals in ferroic phases[44,45].

(iv) This region, at higher HF volume ratio, ≥ 0.015 is called the "*non-transitional*" orthorhombic phase since, the peaks are more clearly defined and much of the strain has disappeared. In summary, the tetragonal $\rightarrow$ orthorhombic symmetry change at the $\alpha \rightarrow$ o-PbSnF$_4$ phase transition is a ferroelastic transition which is driven by increasing non-uniform strain in the $(\bar{a},\bar{b})$ plane. The transition is a complex phenomenon involving strain acting in two perpendicular directions ($\bar{a}$ and $\bar{b}$), particle fractioning and maybe even disorder between $\bar{a}$ and $\bar{b}$ with the two axes fluctuating, and a distribution of a and b values in the intermediate stage called "*transitional phase*" until less strained orthorhombic symmetry sets in.

3.5. CHEMICAL COMPOSITION AND DENSITY OF PbSnF$_4$ VERSUS Vol.$_{(HF)}$/Vol.$_{(HF - H_2O)}$

Ferroic transitions of the type observed in PbSnF$_4$ are usually caused by a change in the physical parameters the sample is subjected to, such as temperature, pressure, electrical field, magnetic field or applied strain. For example, this is the case of the ferroelastic - paraelastic $\beta \rightleftarrows \gamma$-SnF$_2$ transition occurring when temperature is varied[46,47]. In other cases, changes of chemical composition within a solid solution can

cause similar transition, for example, the cubic $\rightarrow$ tetragonal transition in $Pb_{1-x}Sn_xF_2$ occurring at $x \approx 0.30^{[39]}$.

Through the $\alpha \rightarrow$ o-PbSnF$_4$ transition, no physical parameter such as external strain or a change of temperature or pressure was applied. However, since the transition is caused by the presence of HF in the SnF_2 solution used for the synthesis, it is reasonable to suspect that some chemical change may occur in the sample when HF is used. Possible changes could include the Pb/Sn ratio which is supposed to be 1:1 in $PbSnF_4$, or the formation of fluorohydrates $PbSnF_4.nHF$. Such changes can be detected by chemical analysis, and also by bulk density measurements, provided they are large enough to give rise to measurable effects.

3.5.1. Elemental Analysis

Figure 22 shows that the atomic (%) content of tin and lead measured by atomic absorption spectrometry are equal to one another and to the theoretical values for $PbSnF_4$ at all HF volume ratios. The same is true for fluorine measured by the use of a F^- ion selective electrode. In addition, DTA/TGA showed no weight loss which could be attributed to the loss of HF molecules. The horizontal lines on figure 22 are the theoretical values for the formula $PbSnF_4$. The theoretical values (at%) for Sn is 16.7%, for Pb is 16.7% and for F is 66.7%, and the sum of tin and lead is 33.33%. Table VII shows that the measured values are close to the theoretical values for $PbSnF_4$ and no trend is observed versus VR. Therefore, there is no significant change in composition with the amount of HF used in the reaction and the material has the $PbSnF_4$ composition
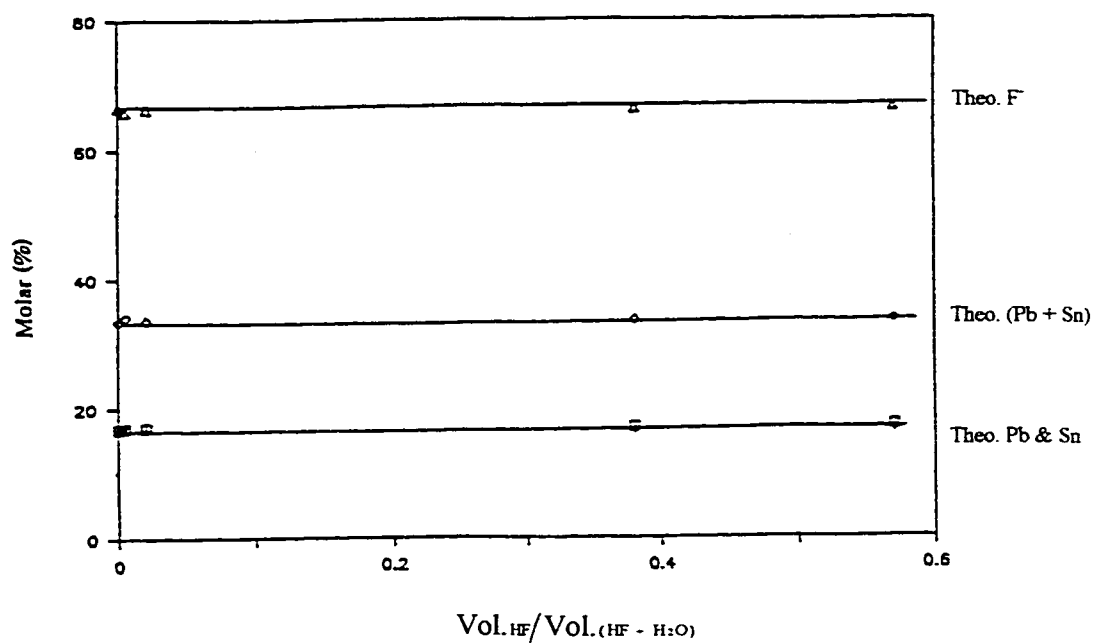
Figure 22: Molar Percent (%) of Pb, Sn, F and (Pb+Sn) versus Vol.$_{HF}$/Vol.$_{(HF - H_2O)}$
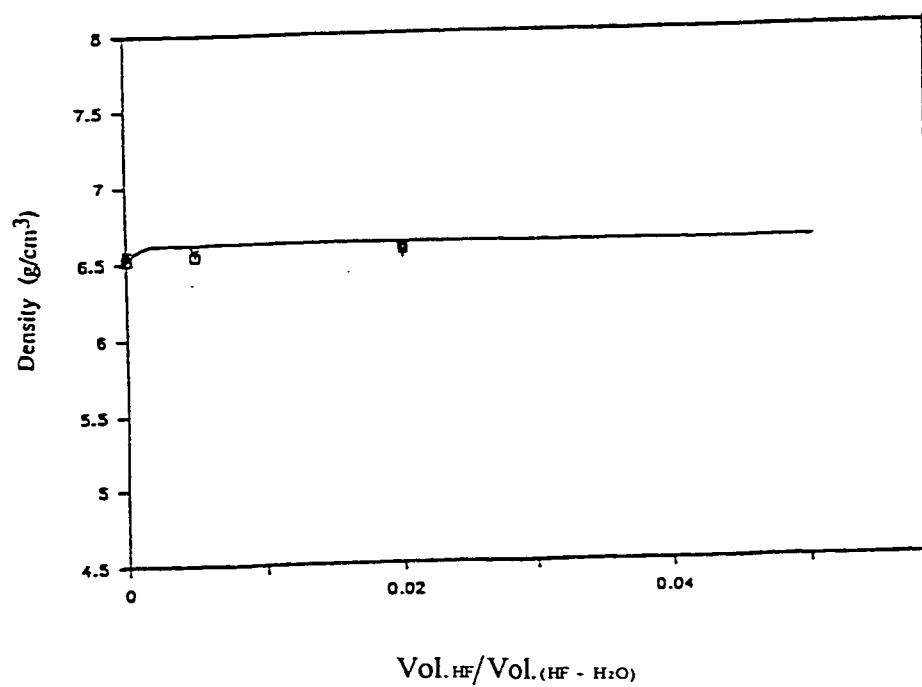
Figure 23: Density versus Vol.$_{HF}$/Vol.$_{(HF + H_2O)}$

regardless of VR. One can conclude that there is no detectable change of chemical composition within the precision of the methods used. Therefore, the $\alpha \rightarrow$ o-transition is really a phase transition, and not a chemical change, unless it involves minor amounts of compositional defects below the detection limit of analytical methods used. It is well known that when SnF_2 is dissolved in water, a portion of it hydrolyzes to $Sn(OH)_2$ according to reaction (V)[49]:

$$SnF_2 + H_2O \rightleftharpoons Sn(OH)_2 + 2HF \qquad (V)$$

Since $Sn(OH)_2$ is insoluble in water, aqueous solutions of SnF_2 are slightly cloudy. HF slowly evaporates, which leads to further hydrolysis by shifting the equilibrium to the right. This is one of the reasons why freshly prepared solutions were used in all cases. If HF is added to the solution, the equilibrium shifts to the left, i.e. the hydrolysis is reversed and this can be easily observed as the solution becomes clear.

Table VII: Molar Percent (%) of Pb, Sn, F, and Pb+Sn compared to the theoretical values

Vol. HF/Vol. HF + H₂O	Pb	Sn	F	Pb+Sn
0	16.71	16.67	66.61	33.38
0.005	16.85	17.23	65.93	34.08
0.020	17.02	16.62	66.36	33.64
0.380	17.03	16.57	66.40	33.60
0.570	17.14	16.45	66.41	33.59
AVERAGE	16.95	16.71	66.34	33.66
THEORETICAL	16.70	16.70	66.70	33.30

In the preparation of tetragonal α-PbSnF$_4$, there is a possibility of hydrolysis of a fraction of SnF$_2$ to Sn(OH)$_2$ since no HF is used, and it is possible that some of the fluoride ions are replaced by a hydroxide ion or that two F are replaced by one O. If this occurred, it would have to be in low amount since it was not detected in the fluoride ion determination. For some compounds a minor impurity is sufficient to induce a phase transition and if this is the case, maybe some OH$^-$ ion replacing F$^-$ ion force the symmetry to be tetragonal. When a minor amount of HF is added to the SnF$_2$ solution, maybe only a fraction of Sn(OH)$_2$ is changed back to SnF$_2$, and the reduced amount of O/OH in the PbSnF$_4$ structure increases the strain and induces the symmetry break. With larger amounts of HF, all Sn(OH)$_2$ is reversed to SnF$_2$; as a result, no O/OH is present in the PbSnF$_4$ structure, and this makes it fully split orthorhombic with lower strain. The O/OH content would have to be minor since no F deficit is detected by chemical analysis. It has been shown by N.M.R that aqueous solutions of SnF$_2$ contain SnF$_2$·OH$_2$ molecules, and that addition of F$^-$ generates SnF$_3^-$ ions[50]. Whether these SnF$_3^-$ ions are responsible for the phase transitions is not known at this point.

In order to check further for the possible roles played by F$^-$ anions or protons when HF is used in the SnF$_2$ solution, a large number of syntheses were carried out in the same conditions as for obtaining α-PbSnF$_4$, i.e. without use of HF. Variable amounts of NaF were added to the SnF$_2$ solution used, in order to provide additional F$^-$ anion. In other sets of preparations, variable amounts of aqueous HCl were added to the SnF$_2$ solution. Many more preparations were carried out by addition of variable amounts of both NaF and HCl together, to provide both extra F$^-$ anion and protons. In all cases, only

α-PbSnF$_4$ was obtained. Therefore, the addition of either extra F$^-$ anions or extra protons, or both together, was unable to simulate the case when HF is added, and so o-PbSnF$_4$ was never obtained in these reactions. Thus, these experiments did not provide the answer about what part of HF, i.e. F$^-$ or H$^+$, is the key factor for initiating the orthorhombic distortion of PbSnF$_4$, or if both are necessary.

3.5.2. Bulk Density Measurements

In any system, a change in molar mass or unit-cell volume will change the density since the density is the ratio of the mass by the volume. The experimental density of PbSnF$_4$, for both the α-phase and the o-phase, versus the HF ratio, are shown on Table VIII. The density of each sample was measured three times and the spread of the three trials for each sample is well below the possible errors for such a high density [35]. Figure 23 shows the density of PbSnF$_4$ versus the HF volume ratios. The solid line is the theoretical density of PbSnF$_4$ that was calculated from the volume of the unit-cell and the

Table VIII: Experimental Densities of α and o-PbSnF$_4$ done in three trials

Vol. $_{HF}$/Vol. $_{HF + H_2O}$	Trial 1	Trial 2	Trial 3	Average	Δ_{max} (%)
0	6.52	6.58	6.55	6.55	0.85
0.005	6.54	6.56	6.59	6.56	0.76
0.020	6.59	6.54	6.58	6.57	0.76
0.380	6.54	6.55	6.56	6.55	0.31
0.570	6.57	6.56	6.59	6.57	0.46

$$\Delta_{max} = \frac{\rho_{max} - \rho_{min}}{\rho_{ave}} \times 100$$

where: ρ_{max} and ρ_{min} are the maximum and minimum values of the three trials

ρ_{ave} is the average density

molar mass assuming the chemical composition is $PbSnF_4$. The experimental points fall very close to the theoretical values i.e. there is no evidence of metal non-stoichiometry since the high density of Pb compared to Sn would make significant density changes if the Pb/Sn ratio is varied. The presence of HF molecules would decrease the density significantly. The fact that most of the experimental points as shown on figure 23 fall very slightly below the calculated density is expected because of imperfect degassing. Indeed, air trapped between the particles prevents CCl_4 from occupying that dead space and leads to overestimation of the volume, hence an underestimation of the density.

This problem is always present, although it is strongly minimized by wetting the sample while still under vacuum, by use of the specially designed glass vessel described in the experimental section. Since it leads to a tighter packing, $PbSnF_4$ is thermodynamically more stable than a mixture of SnF_2 and PbF_2 in the conditions of the reaction. However, if there is a substitution of tin by lead or vice versa, it would have been observed because lead is much more dense than tin. No change is observed other than the slight increase of density due to volume change at the $\alpha \rightarrow o$- transition. The absence of a detectable Sn/Pb substitution is evidenced by a nearly constant density.

Therefore, the density measurements corroborate chemical analysis results, i.e. it is unlikely that a chemical change occurs at the $\alpha \rightarrow o\text{-}PbSnF_4$ transition, unless it is concerned with only minor amounts of impurities or defects.

3.5.3. Scanning Electron Microscopy (SEM)

The very high preferred orientation observed in $PbSnF_4$, particularly in the

α-phase obtained by precipitation α-$PbSnF_4(aq_1)$, leads to believe that the shape of the

particles favors the stacking of crystallites along $\bar{c}$, since the $(00l)$ peaks are very

strongly enhanced in α-$PbSnF_4$ prepared by precipitation (fig.24-28). This is obvious

from the visual observation of the very thin sheet-like crystallites. Scanning electron

microscopy (SEM) was used in order to measure the thickness of the sheets, and also in

an effort to explain why preferred orientation in o-$PbSnF_4$, although substantial, is clearly

smaller than in α-$PbSnF_4(aq_1)$.

Figures 24-28 show the scanning electron micrographs of the tetragonal

and orthorhombic phases versus VR. It can be clearly seen that there are large thin plates

in α-$PbSnF_4$ as expected in the layered structure for VR = 0. This crystal habit originates

from the fact that the planes of lone pairs prevent interlayer bonds, and thus provide

planes of easy cleavage. The surface area of the plates decreases as VR increases. At HF

ratio VR = 0.57, the particles are much smaller, however, upon magnification, plates can

still be observed. Particle fractionning at the $\alpha \rightarrow$ o-transition takes place in such a way

that the surface area of the sheets parallel to the $(\bar{a}, \bar{b})$ plane is smaller. Since the strain

takes place in the $(\bar{a}, \bar{b})$ plane, through the transition from tetragonal to orthorhombic, it

is probably responsible for the breakage of the plates. This is analogous to the formation

of multidomain particles in ferroic phases, when $a_t \rightarrow a_o$ or b_o and $b_t \rightarrow a_o$ or b_o

hesitation takes place. Although the area of the plates decreases through the tetragonal to

3K
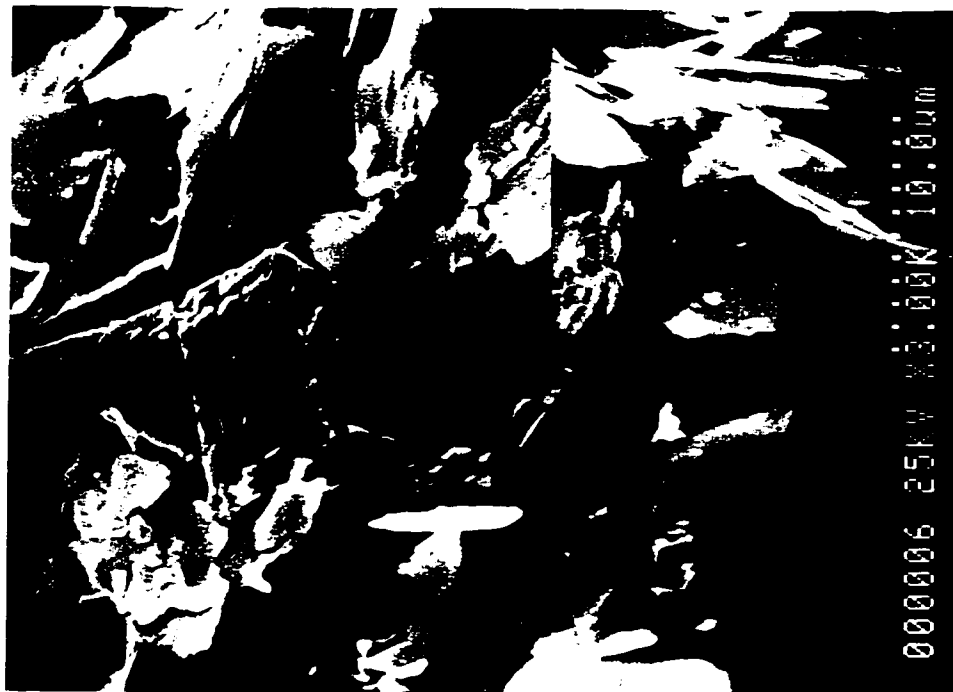
1K

Figure 24: Scanning Electron Microscopy photographs of tetragonal α-PbSnF$_4$ (VR= 0).

3K

1K

Figure 25: Scanning Electron Microscopy photographs of orthorhombic o-PbSnF$_4$ (VR= 0.01).

4K
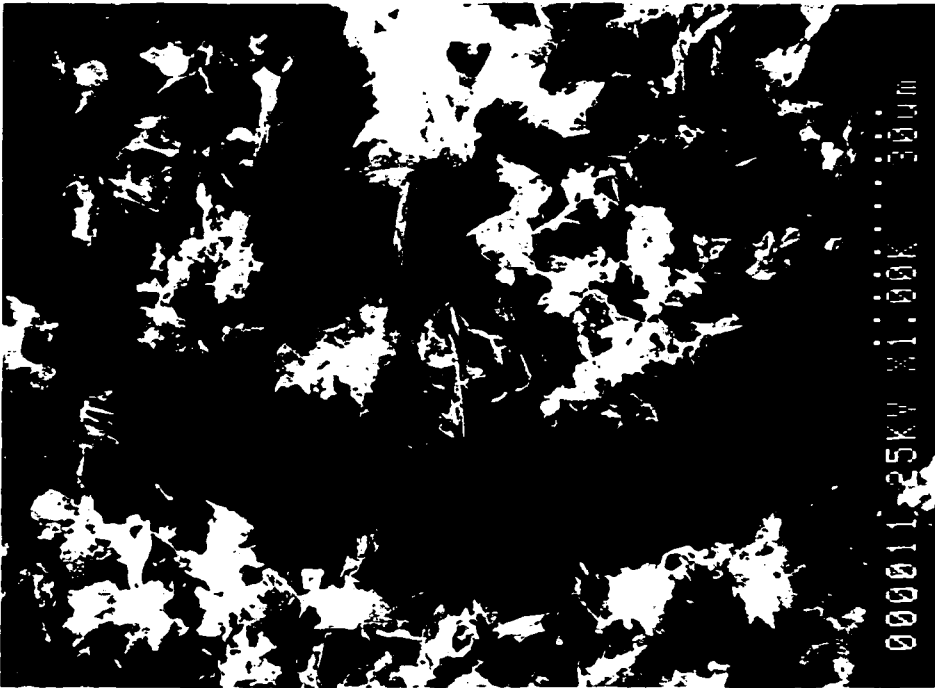
1K

Figure 26: Scanning Electron Microscopy photographs of orthorhombic o-PbSnF$_4$ (VR= 0.05).

88

4K
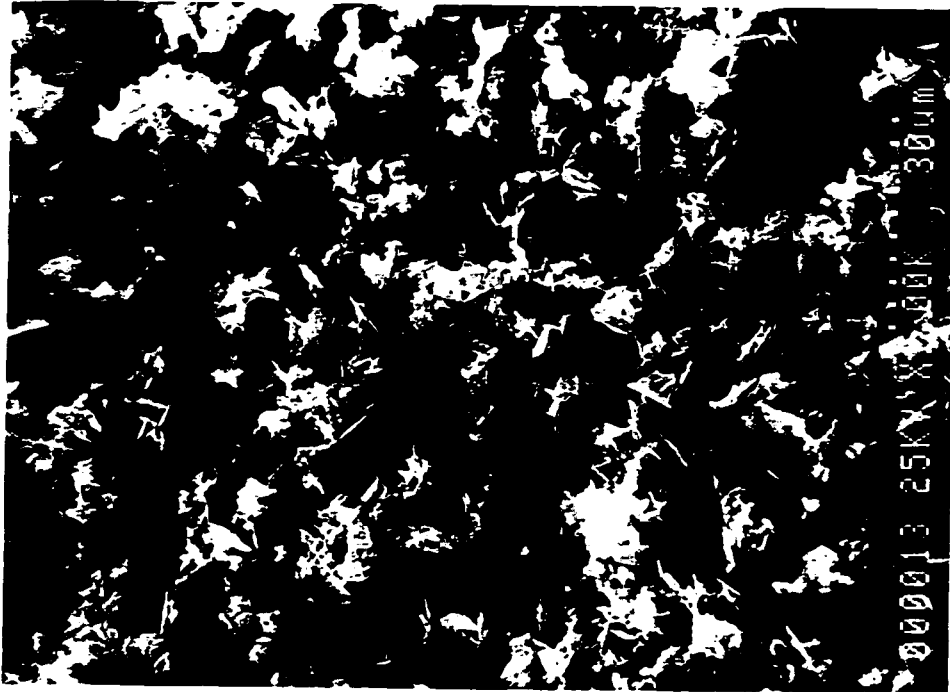
1K

Figure 27: Scanning Electron Microscopy photographs of orthorhombic o-PbSnF$_4$ (VR= 0.38).

89

4K
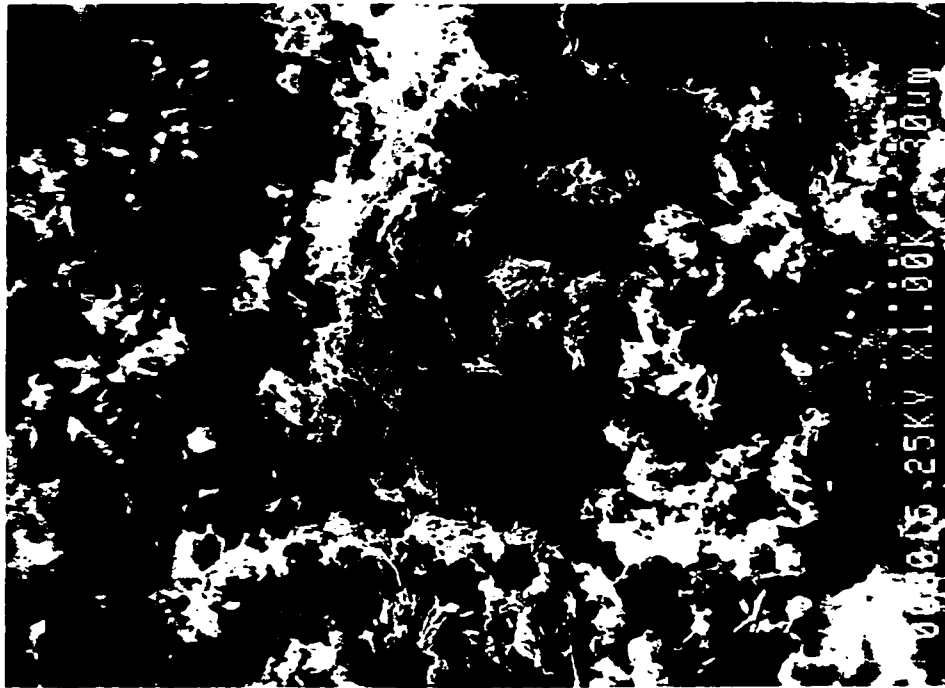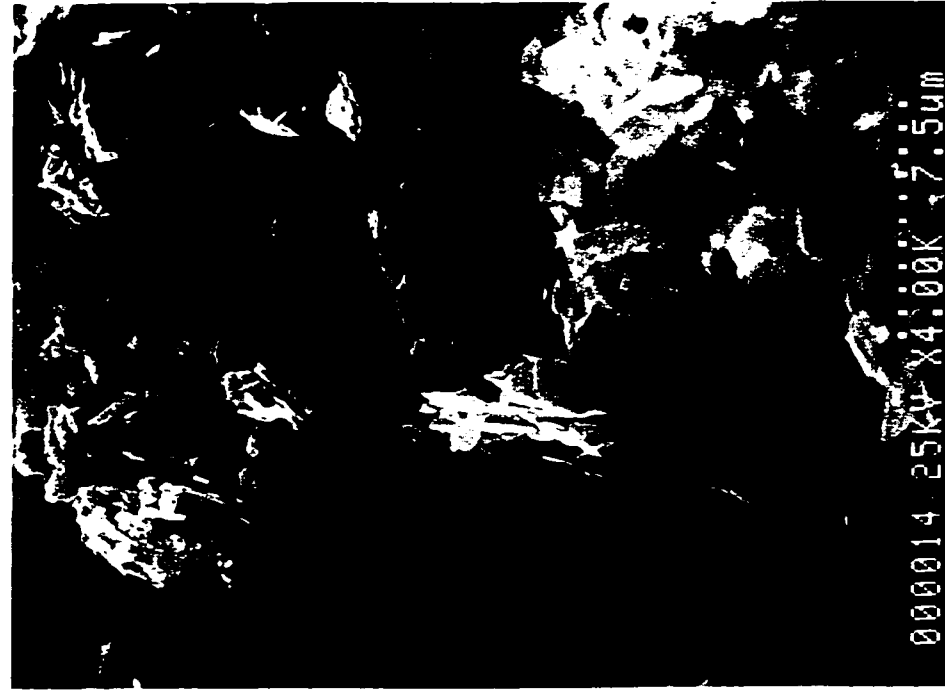
1K

Figure 28: Scanning Electron Microscopy photographs of fully split orthorhombic o-PbSnF$_4$ (VR= 0.57).

orthorhombic transition, their thickness shows little change. These results are in agreement with the texture observed during sample preparation and with the X-ray diffraction results which show a net decrease of preferred orientation in o-PbSnF$_4$ (the (00l) peaks are not as strong) as compared to α-PbSnF$_4$(aq$_1$) (fig.6).

During crystal growth, there is an instability due the strain in the transitional phase and in the orthorhombic phase at moderate VR ratios. The continuity of the sheets that are growing is broken down by permutation of the nearly equivalent $\bar{a}$ and $\bar{b}$ axes until the orthorhombic splitting is sufficiently large and the strain decreases. This is commonly encountered in ferroic phases i.e. ferroelastic, ferroelectric and ferromagnetic, with two unit-cell parameters nearly equivalent in the ferro-phase and exactly equivalent in the para-phase, and results in a severe fractioning of the particles.

As HF was added, the area of the particles is reduced much faster than the thickness of the sheet which shows that the main changes are taking place in the ($\bar{a},\bar{b}$) plane, in agreement with the unit-cell distortion observed by X-ray diffraction. There is no major reconstructing of the structure taking place at the $\alpha \rightarrow$ o-PbSnF$_4$ transition in accordance with previous observations[10-12]. This is just a displacive transition, i.e. atoms shifting to slightly different x,y,z coordinates without rearrangement of the whole structure. The preferred orientation observed in o-PbSnF$_4$ by X-ray diffraction is much less acute than in the α-phase due to the lower probability of stacking the particles parallel to one another in the orthorhombic, since the surface area of the plates, which is parallel to the ($\bar{a},\bar{b}$) plane is smaller. The fact that the plate thickness is about the same in both α-PbSnF$_4$(aq$_1$) and in o-PbSnF$_4$ suggests that the basic sheet structure is the

same in the orthorhombic phase as in α-PbSnF$_4$, the difference between the two structures being atomic shifts mostly parallel to the $(\bar{a},\bar{b})$ plane due to the ferroelastic transition, which allows a slightly more efficient packing along $\bar{c}$ (c decreases slightly).

3.6. INFLUENCE OF STIRRING RATE

The influence of the stirring rate of the SnF$_2$ solution during the addition of the lead nitrate solution was not studied in earlier works by others. However, its influence was shown recently to be a major parameter in the case of the reaction of calcium nitrate and SnF$_2$[40]. Therefore, it was quite appropriate to suspect that it might also have an influence on the preparation of PbSnF$_4$.

The influence of several stirring rates using different values of VR was studied in order to ensure the reproducibility of the preparation of PbSnF$_4$ and see how the stirring rate affects the $\alpha \rightarrow$ o-transition. More particularly, the influence of the stirring rate on the following was studied: (i) symmetry of PbSnF$_4$, (ii) linewidth of Bragg peaks (presence of strain and/or microcrystallinity), (iii) intensity of Bragg peaks (severity of preferred orientation and, (iv) presence of other phases. Three rates of stirring were studied and the results are as follows:

(i) Series 1: no stirring vs. VR - The X-ray powder diffraction (fig, 29) shows that at VR = 0 and 0.0005, only peaks α-PbSnF$_4$ are obtained and, the (102) peak is much broader than usual especially at the foot of the peak. At a higher value, e.g. VR $\approx$ 0.22, o-PbSnF$_4$ is obtained and extra peaks are observed which belong to Pb$_2$SnNO$_3$F$_5$·2H$_2$O
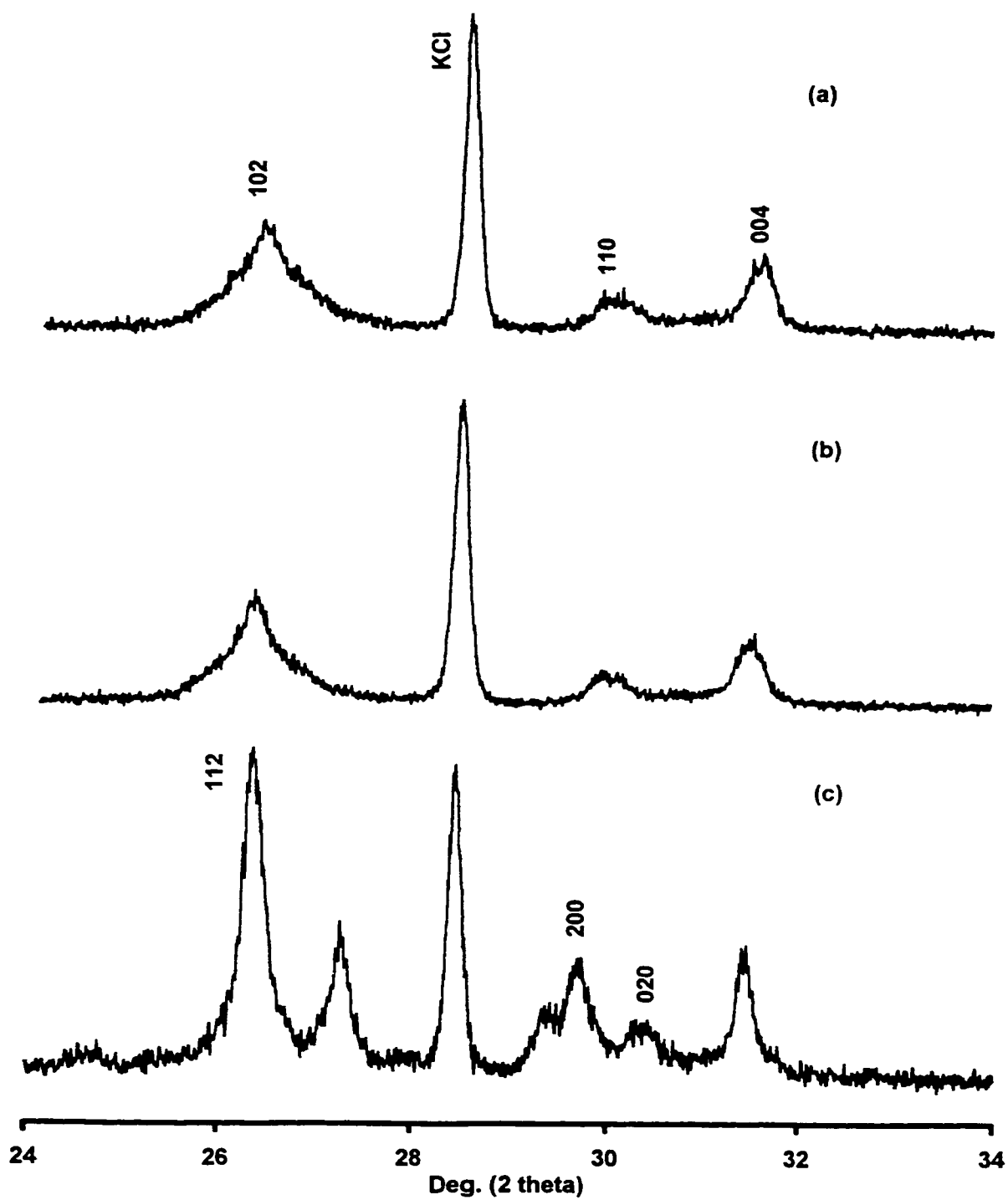
Figure 29: X-ray diffraction of PbSnF$_4$: no stirring
versus VR: (a) 0, (b) 0.0005, (c) 0.22

obtained by Donaldson and Senior by adding a solution of SnF_2 to a solution of lead nitrate[1]. In addition, the (112) peak of o-$PbSnF_4$ is much narrower than the (102) peak of α-$PbSnF_4$ observed for VR = 0 and 0.0005.

(ii) Series 2: slow stirring vs. VR (fig. 30) shows the same phases as when the mixture is not stirred, however, for VR = 0.22 only one peak of the $Pb_2SnNO_3F_5 \cdot 2H_2O$ is observed. Furthermore, the (102) peak is much narrower for VR = 0 than it is when the reaction mixture is not stirred.

(iii) Series 3: medium stirring vs. VR (fig. 31) shows that the X-ray powder patterns of α-$PbSnF_4$ is obtained again for VR = 0 and 0.0005 and o-$PbSnF_4$ at VR = 0.22. However, $Pb_2SnNO_3F_5 \cdot 2H_2O$ has completely disappeared and the $(102)_\alpha$ is narrower for VR = 0 than for no stirring but somewhat broader than for slow stirring. However, for all values of VR, the (102) peak has a very broad base, more particularly at VR = 0.0005, this is also true for the (112) peak.

(iv) Series 4: fast stirring vs. VR (fig. 32) shows that the results for fast stirring are similar to those observed at medium stirring i.e. no $Pb_2SnNO_3F_5 \cdot 2H_2O$ is observed and α-$PbSnF_4$ is obtained for VR = 0 and 0.0005, and o-$PbSnF_4$ for VR = 0.22. For VR = 0.0005, the $(102)_\alpha$ peak is much broader with shoulders on both sides.

The following conclusions can be drawn from these experiments:

(i) The formation of $Pb_2SnNO_3F_5 \cdot 2H_2O$ takes place only when $Pb(NO_3)_2$ is in excess in the reaction mixture compared to SnF_2, which is in agreement with the literature[1]. This does not occur here in a homogeneous mixture since x = Pb/Sn = 0.20, i.e. SnF_2 is in large excess and thus, $Pb_2SnNO_3F_5 \cdot 2H_2O$ is never observed for medium or
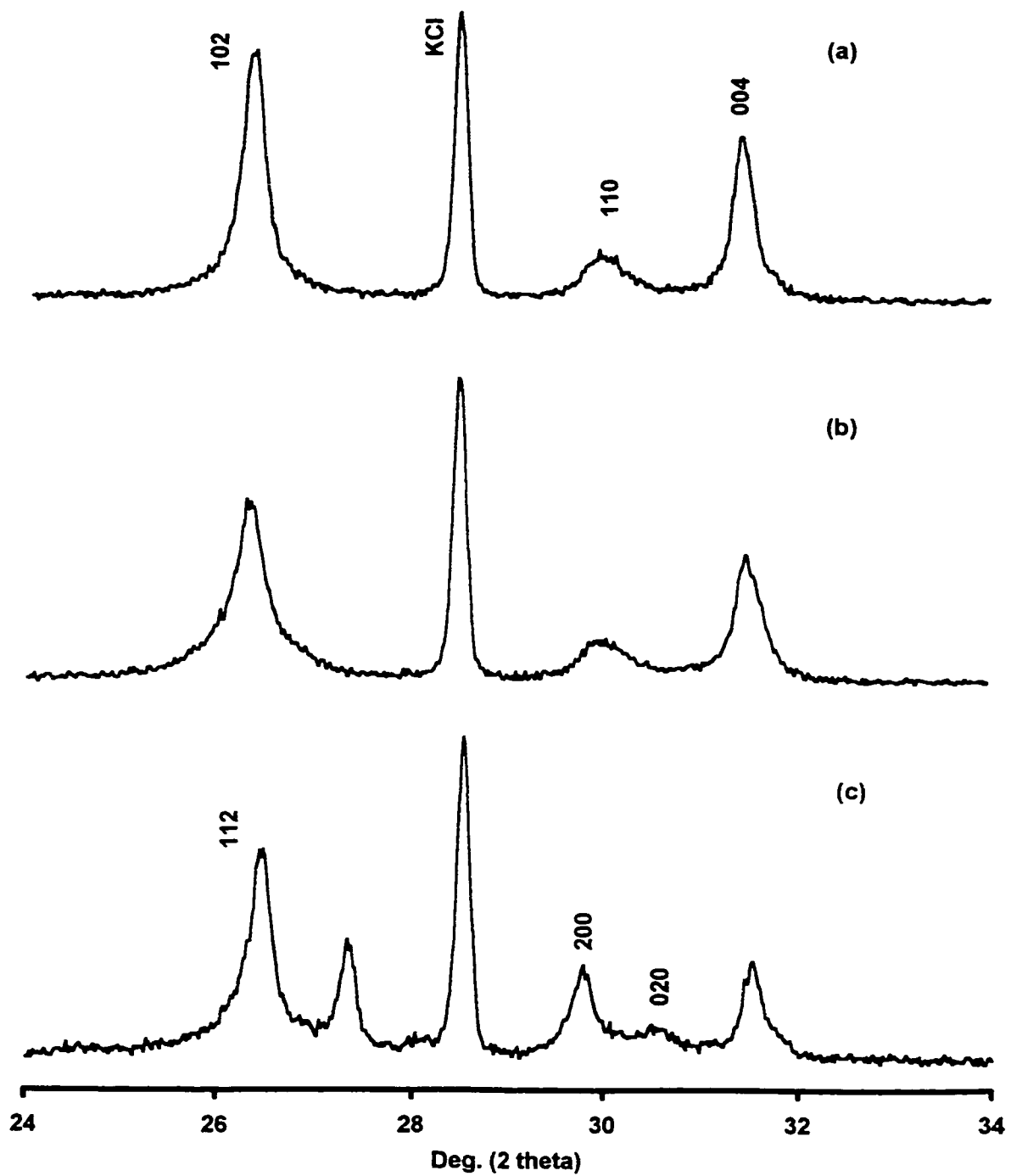
Figure 30: X-ray diffraction of PbSnF$_4$: slow stirring
versus VR: (a) 0, (b) 0.0005, (c) 0.22
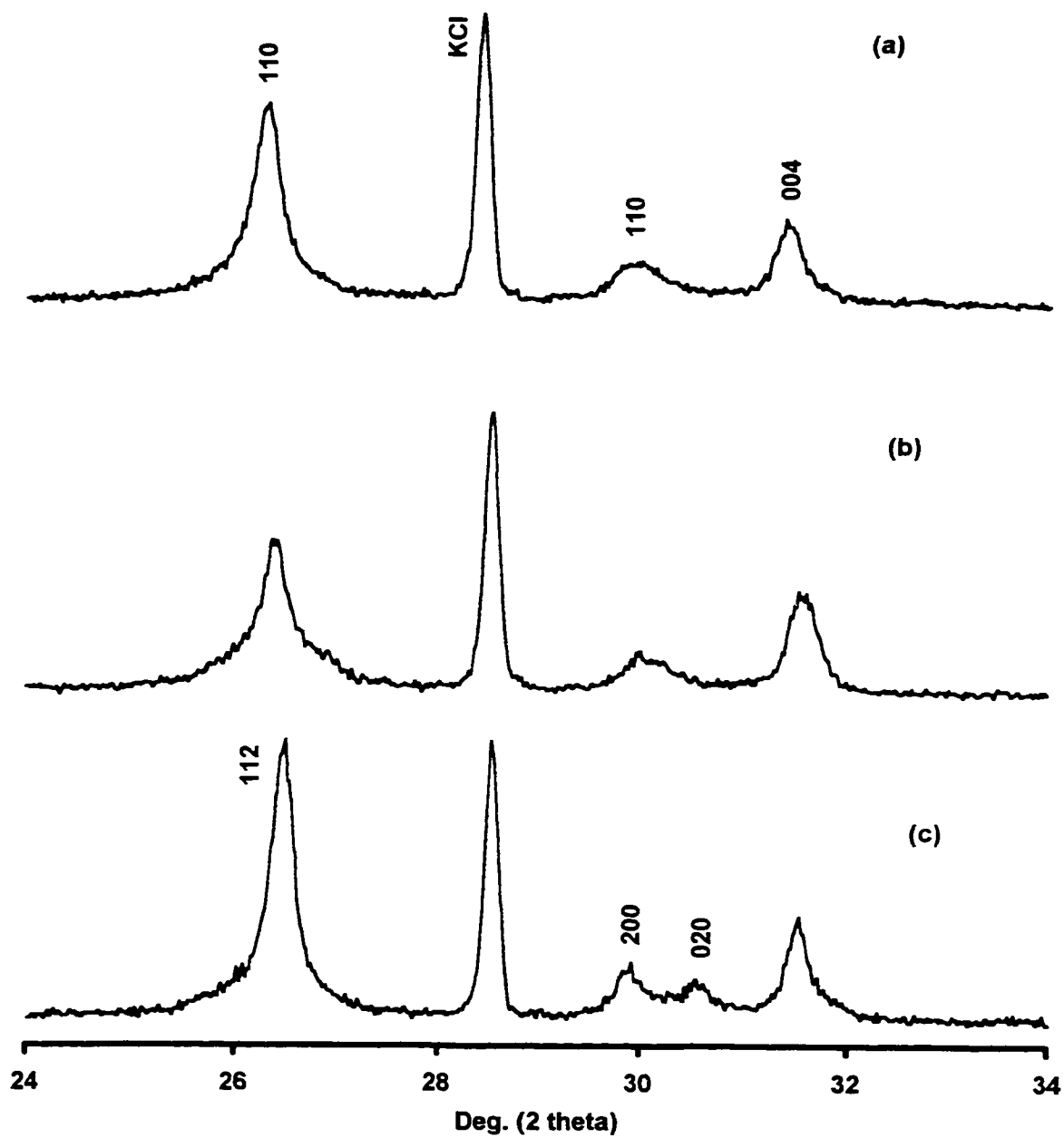
Figure 31: X-ray diffraction of PbSnF$_4$: medium stirring
versus VR: (a) 0, (b) 0.0005, (c) 0.22
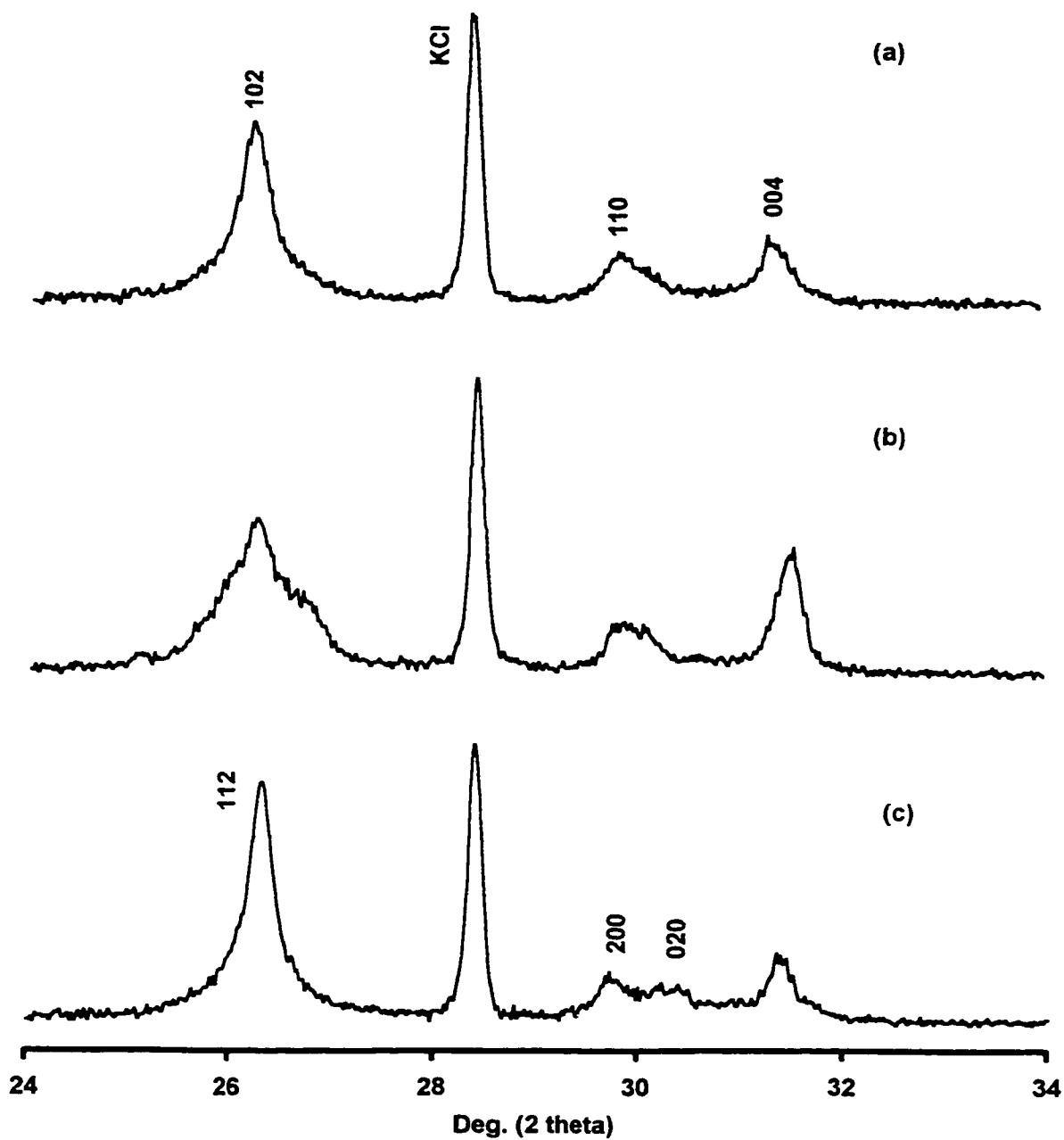
Figure 32: X-ray diffraction of PbSnF$_4$: fast stirring
versus VR: (a) 0, (b) 0.0005, (c) 0.22

fast stirring, which makes the mixture homogeneous. However, for slow stirring and when the reaction mixture is not stirred, at the interface of the drops of $Pb(NO_3)_2$ solution and the SnF_2 solution contained in the beaker, there is temporarily a large excess of $Pb(NO_3)_2$, until ion diffusion in the solutions homogenizes the mixture. However, this gives enough time to precipitate significant amounts of the material which is the most stable under excess $Pb(NO_3)_2$, i.e. $Pb_2SnNO_3F_5 \cdot 2H_2O$. As the stirring rate increases, the amount of $Pb_2SnNO_3F_5 \cdot 2H_2O$ produced decreases, due to more efficient homogenization. However, it is unclear why $Pb_2SnNO_3F_5 \cdot 2H_2O$ is obtained only when a large amount of HF is used (VR = 0.22). The contrary could have been expected, i.e. to obtain only fully fluorinated $PbSnF_4$ where excess fluoride ions are present.

(ii) For very low amount of HF (VR = 0.0005), the $(102)_\alpha$ peaks is very broad particularly when no stirring is performed and at a high stirring rate. Again, the lack of homogenizaton could be responsible for this, even at a very fast stirring rate. The centrifugal effect of fast stirring might result in a vertical layering of the two solutions that could hinder proper homogenization. In addition, it is interesting to note that the (102) peak is broad when no HF is used and the mixture is not stirred, however, it is much narrower as soon as stirring, even slow, is performed. This suggests that the $\alpha \rightarrow o$ transition is somewhat related to the broadening of (102), since at very low VR, the strain in the $(\bar{a}, \bar{b})$ plane is much larger than at VR = 0, and tetragonal α-$PbSnF_4$ is trying to become orthorhombic o-$PbSnF_4$. Interestingly, the $(112)_o$ peak at VR = 0.22 is never broader than $(102)_\alpha$, and it is much narrower when the mixture is not stirred. This indicates that the disturbance of the width of $(112)_o$ is higher in the strained phase (0 or very low VR) than in the fully orthorhombic phase (high VR). However, at this point, we

cannot offer an explanation for the reason of the very large broadening of $(102)_\alpha$ at VR = 0 and 0.0005.

(iii) The onset of the $\alpha \to$ o-transition at very low VR values maybe a function of stirring rate, such that sometimes, it is hard to tell whether $PbSnF_4$ is tetragonal α or orthorhombic for VR = 0.0005, at some stirring rates.

3.7. CONCLUSION

The detailed study of the $\alpha \to$ o phase transition of $PbSnF_4$ shows that it is a paraelastic $\to$ ferroelastic type of transition, driven by internal strain in the $(\bar{a}, \bar{b})$ plane. It is a bidimensional phase transition, the small change on c being just the response of layer packing to the large changes taking place in the $(\bar{a}, \bar{b})$ plane. Just a very minor amount of HF in the SnF_2 solution used for the synthesis is sufficient to initiate the transition. It starts with an increase of the strain in $(\bar{a}, \bar{b})$ and includes considerable hesitation about the definition of the $\bar{a}$ and $\bar{b}$ directions in orthorhombic, with possibly fluctuations between the two directions at low HF content. This behaviour is typical of ferroic type transitions. No variation of the chemical composition at the transition was detected. The layered structure of both phases results in large and very thin crystallite shape. Their thickness changes little through the transitions, but their surface area decrease somewhat, and this results in a reduced amount of preferred orientation in o- $PbSnF_4$. The considerable strain present in α-$PbSnF_4(aq_1)$ is most likely an indication of a "failed" o-$PbSnF_4$. Surprisingly, no strain is present in α-$PbSnF_4(ssr)$. The diffraction

pattern of precipitated α-PbSnF$_4$ varies with the stirring rate of the lead nitrate solution, with considerable broadening of (102) when no stirring or fast stirring, when no or little HF is used. This behaviour is not fully understood at the present time.

CHAPTER 4

RESULTS AND DISCUSSION : EFFECTS OF MECHANICAL ENERGY ON THE STRUCTURES AND PHASE TRANSITIONS OF PbSnF$_4$

4.1. TEXTURE, CRYSTALLINITY AND PHASE CHANGES VERSUS GRINDING TIME

Applying mechanical energy such as grinding, e.g. by use of ball milling, can cause profound changes in solids, such as: (i) induce phase transitions (e.g. the $\beta \rightarrow \alpha$ transition of SnF$_2$[46] or (ii) even chemical reactions, (iii) reduce the particle size and crystallinity and (iv) create a large number of crystal defects. We have ball milled the various phases of PbSnF$_4$ that are stable or metastable at ambient temperature, versus grinding time, in an attempt to obtain a randomly oriented sample, and maybe induce phase transitions. In all cases, a drastic change of the diffraction pattern was observed, and a reduced particle size was obtained. Then, the ground samples were annealed 200°C for 2 hours. In all cases, recrystallization leading to strain free well crystalline materials was observed. However, the way ball milling changed the samples is a function of the starting phase of PbSnF$_4$. The phases subjected to ball milling were α-PbSnF$_4$(aq$_1$) (precipitated from the reaction in aqueous medium), α-PbSnF$_4$(aq$_2$) (obtained by stirring solid α-PbF$_2$ in an aqueous solution of SnF$_2$), α-PbSnF$_4$(ssr) (prepared by solid state reaction (equation III)), o-PbSnF$_4$ and β-PbSnF$_4$.

4.1.1. α-PbSnF₄(aq₁) (fig. 33 and 34)

The X-ray diffraction pattern of α-PbSnF$_4$ (aq$_1$) versus ball milling time is shown on figure 33 and 34. It is observed that as the grinding time increases, the (00l) reflections are slowly suppressed until they completely disappear. A significant decrease of the (00l) peaks is observed after just 10 seconds (fig. 33b). This results in the enhancement of the perpendicular direction, i.e. (110). This is due to a decrease of the preferred orientation of the polycrystalline sample, which is very strong before grinding, owing to the layered structure (fig. 1b).

After 40s ball milling (fig. 33c), a significant line broadening is observed, while at the same time all peaks characteristic of tetragonal distortion are getting weak, although the magnitude of the tetragonal distortion remains unchanged. The (110) peak, which was already considerably broadened by the bidimensional stress in $(\bar{a},\bar{b})$ does not seem to broaden further on milling. The intensity of all the peaks characteristic of tetragonal distortion decreases rapidly as milling time increases. After 50s milling (fig.33d), the linewidth has increased further and every sign of tetragonal distortion and of superstructure has disappeared and the X-ray diffraction pattern can be fully indexed in the cubic system with an F lattice and is similar to that of β-PbF$_2$, i.e. Fm3m space group, with broadened peaks. It looks like milling has created microcrystalline β-PbF$_2$. Prolonged milling (e.g. 5 min. for fig. 34a), brings no further changes and particularly no further line broadening.
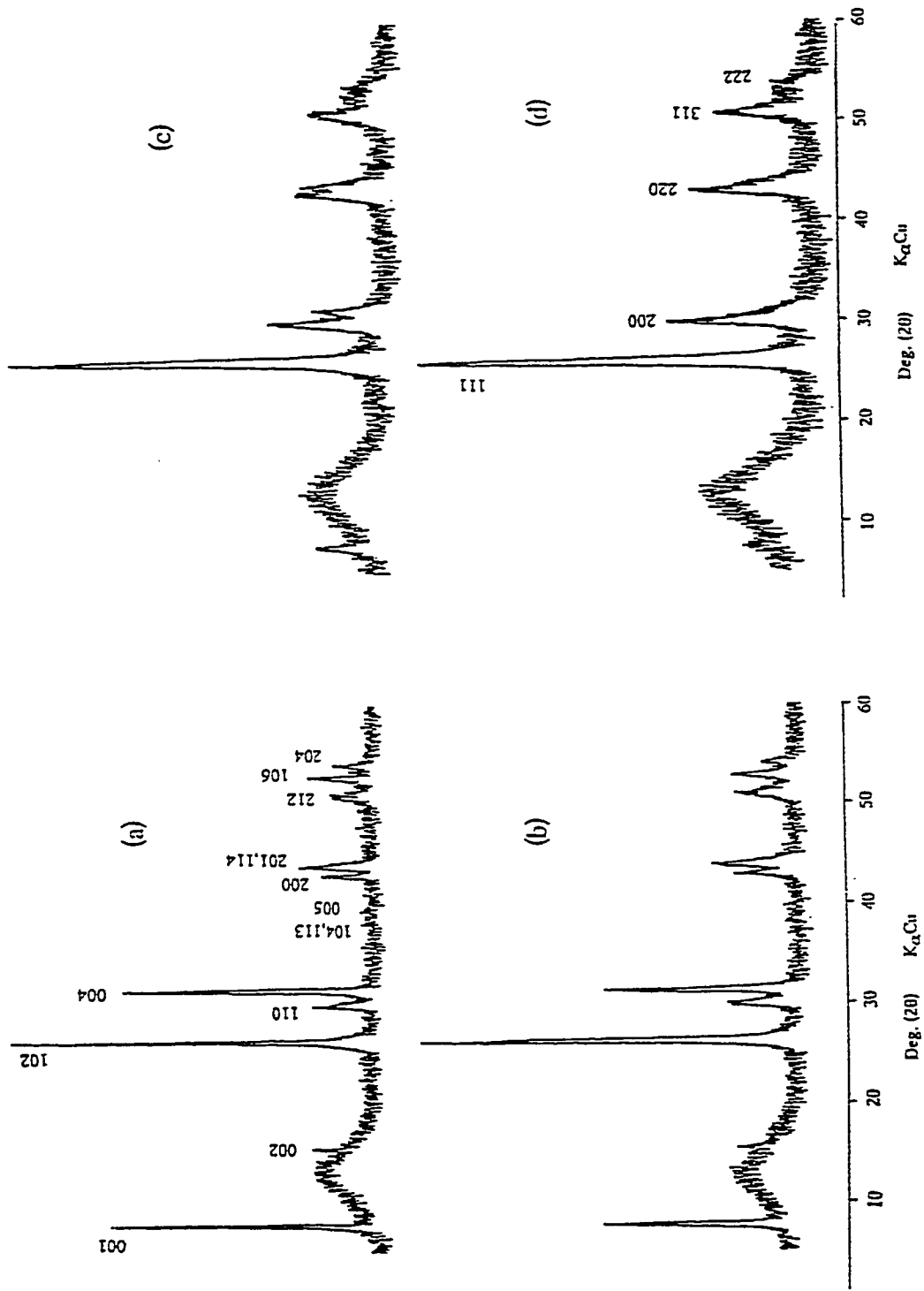
Figure 33: α-PbSnF₄(aq₁) versus grinding time: (a) 0, (b) 10s, (c) 40s, (d) 50s

Figure 34: α-PbSnF₄(aq₁) versus grinding time and annealing: (a) 5min., (b) 6min. grinding and then, heated at 200°C for 2 hours

4.1.2 α-PbSnF₄ (aq₂) (fig.35)

α-PbSnF$_4$(aq$_2$) prepared by adding solid α-PbF$_2$ to an aqueous solution of SnF$_2$, shows the same behaviour as α-PbSnF$_4$(aq$_1$) i.e. both are highly oriented (very strong (00l) peaks)) and both are strained in the ($\bar{a}$,$\bar{b}$) plane although α-PbSnF$_4$(aq$_1$) is more so. Upon milling, less preferred orientation is observed (i.e. the intensity of the (00l) peaks decreases) and the peaks broaden (the particle size decreases). After 60s ball milling, the superstructure reflections (00l) have disappeared and the peaks characteristic of tetragonal distortion have coalesced to give a single peak and the diffraction pattern looks like that of microcrystalline β-PbF$_2$, and thus is identical to that of α-PbSnF$_4$ (aq$_1$) after about the same grinding time.

4.1.3. α-PbSnF₄ (ssr) (fig. 36 and 37)

The α-PbSnF$_4$ phase obtained by direct reaction of SnF$_2$ and PbF$_2$ in a Cu tube under nitrogen, α-PbSnF$_4$ (ssr), has the same set of peaks, as α-PbSnF$_4$ (aq$_1$) and α-PbSnF$_4$(aq$_2$), thus it is tetragonal with the same Pb/Sn order (fig 36a), and with the same unit-cell parameters within experimental error (Table VI). In addition, the linewidth for α-PbSnF$_4$ (ssr) is clearly smaller, particularly for the (110). This indicates that α-PbSnF$_4$ (ssr) is strain free, or at least, is much less strained than α-PbSnF$_4$ (aq$_1$) and α-PbSnF$_4$ (aq$_2$). Furthermore, the (00l) peaks are much weaker, indicating a much lower degree of preferred orientation. This indicates that the surface area of the platelet
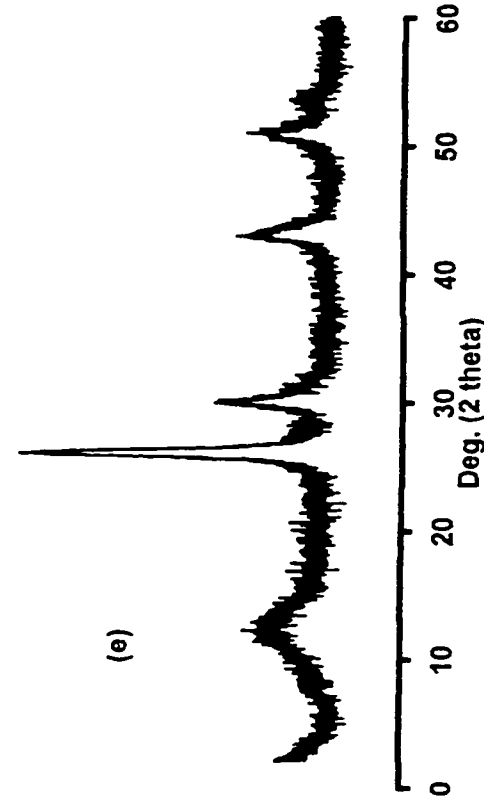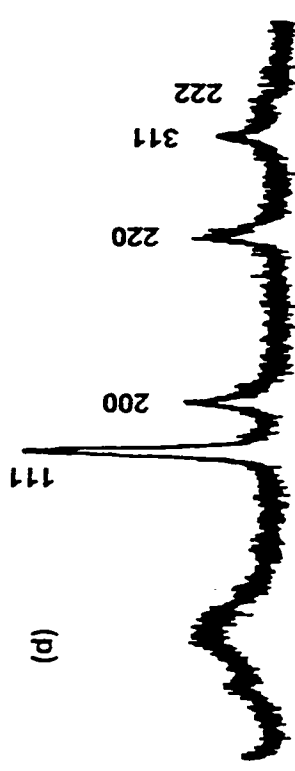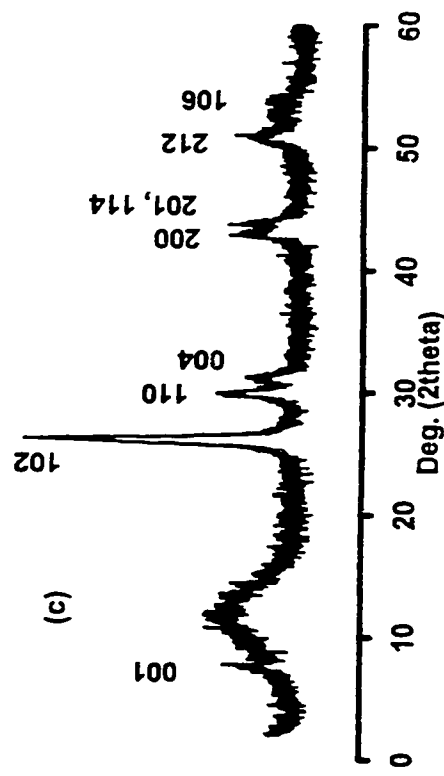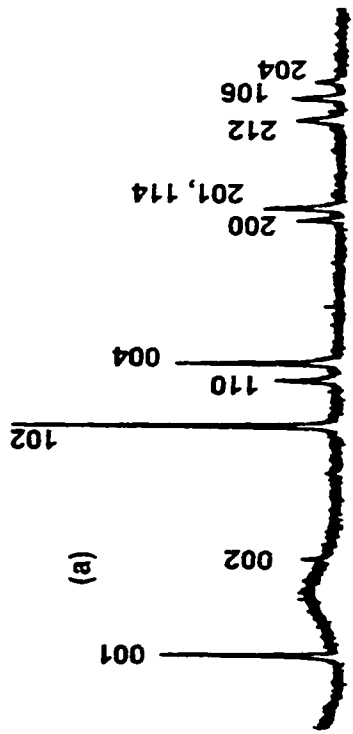
Figure 35: α-PbSnF$_4$(aq$_2$) versus grinding time (a) 0, (b) 10s, (c) 20s, (d) 50s, (e) 1min.
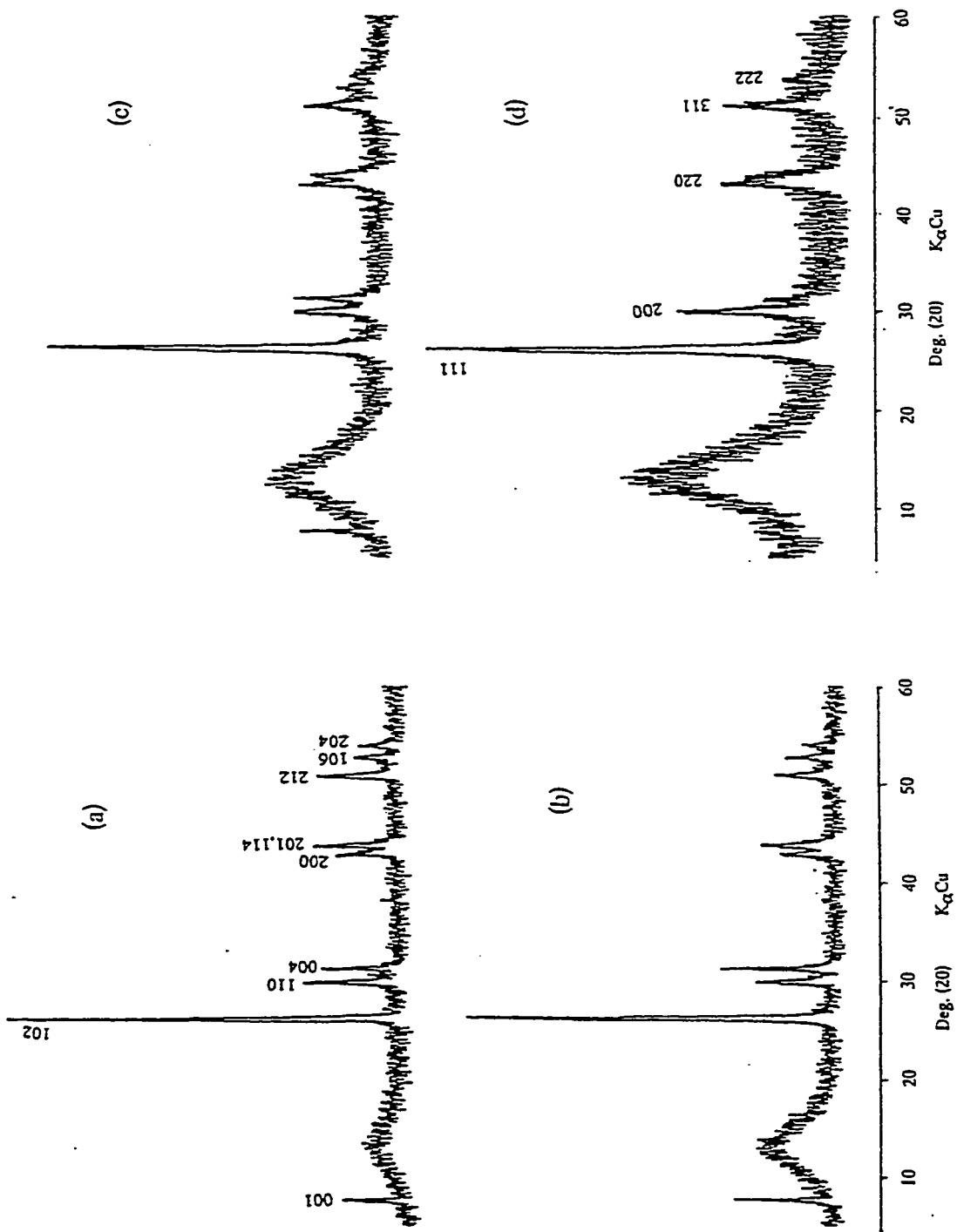
Figure 36: α-PbSnF₄(ssr) versus grinding time: (a) 0, (b) 10s, (c) 20s, (d) 50s

shaped crystallites is probably smaller. After 10s ball milling (fig. 36b), not much change is observed except a slight line broadening at high angles and some enhancement of the (00l) peaks. This is probably due to the particles being more favorably packed in the same orientation, thus enhancing the preferred orientation, which is not compensated by the particle fractionning after the short grinding time. However, after 20s (fig. 36c), the linewidth has increased and the intensity of the (00l) peak has decreased. After 50s (fig. 36d), all signs of Pb/Sn ordering and of tetragonal distortion have disappeared, and the diffraction pattern looks like that of microcrystalline β-PbF$_2$, and thus is identical to that of α-PbSnF$_4$ (aq$_1$) and α-PbSnF$_4$ (aq$_2$) after the same grinding time. In addition, grinding for longer periods of time brings about no significant change (fig. 37a & 37b), therefore the final result is the same as for α-PbSnF$_4$(aq$_1$) and α-PbSnF$_4$ (aq$_2$), i.e. the diffraction pattern of the final material looks like microcrystalline β-PbF$_2$ fluorite type.

4.1.4. o-PbSnF$_4$ (fig. 38 and 39)

The powder diffraction pattern of fully split o-PbSnF$_4$ (fig. 38a) looks much like that of α-PbSnF$_4$ with the exception that all peaks with $h \neq k$ are split due to orthorhombic distortion. The linewidth is smaller than for α-PbSnF$_4$ (aq$_1$) and (aq$_2$) due to its reduced amount of strain, and is somewhat similar to that of α-PbSnF$_4$ (ssr). Preferred orientation is less pronounced than in precipitated α-PbSnF$_4$, in agreement with the smaller surface area of the sheet like crystallites observed by SEM, hence weaker (00l) peaks due to less efficient parallel packing of the platelets. After 10s ball milling, significant broadening of the lines is observed (fig. 38b) which partially coalesce the
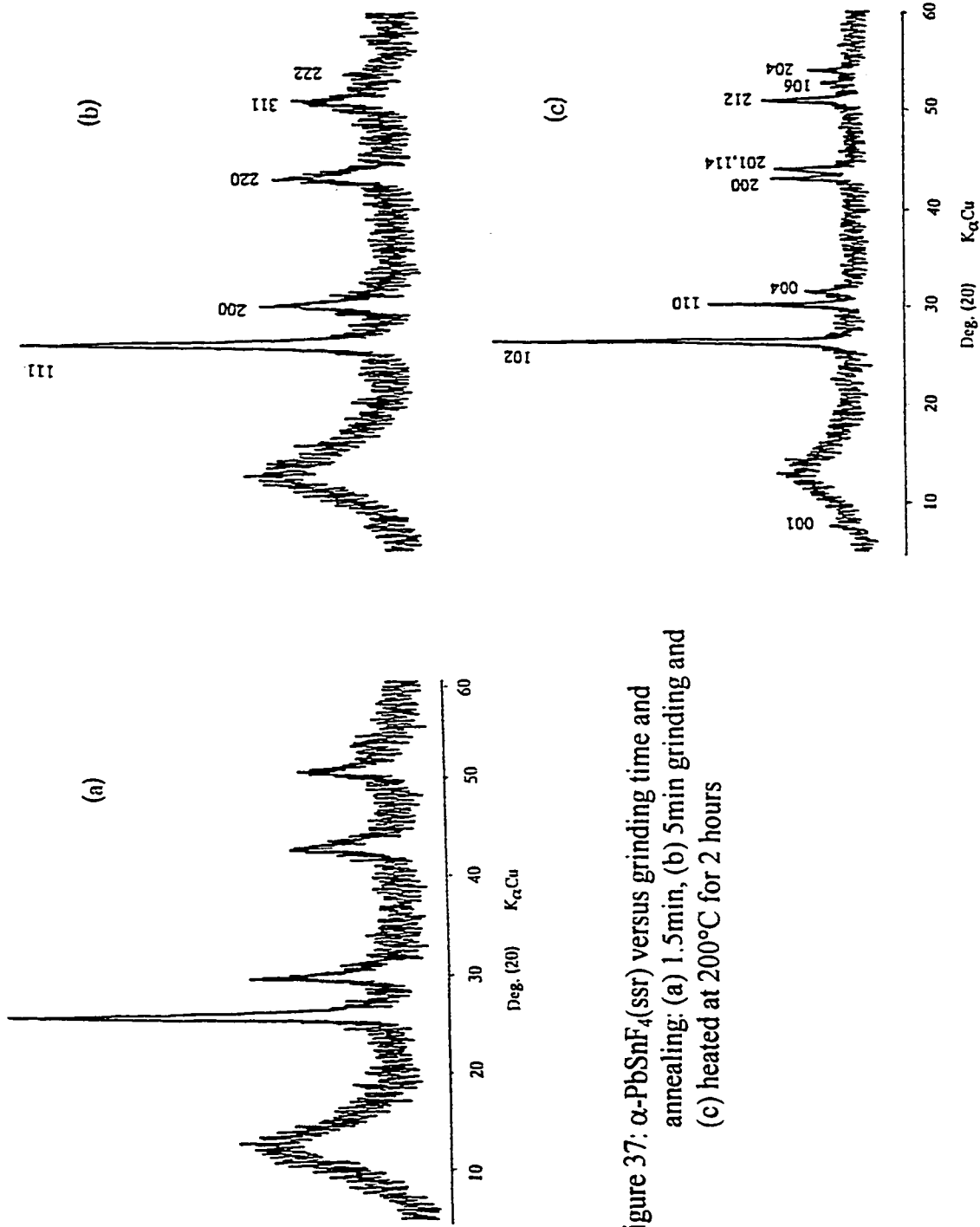
Figure 37: α-PbSnF₄(ssr) versus grinding time and annealing: (a) 1.5min, (b) 5min grinding and (c) heated at 200°C for 2 hours
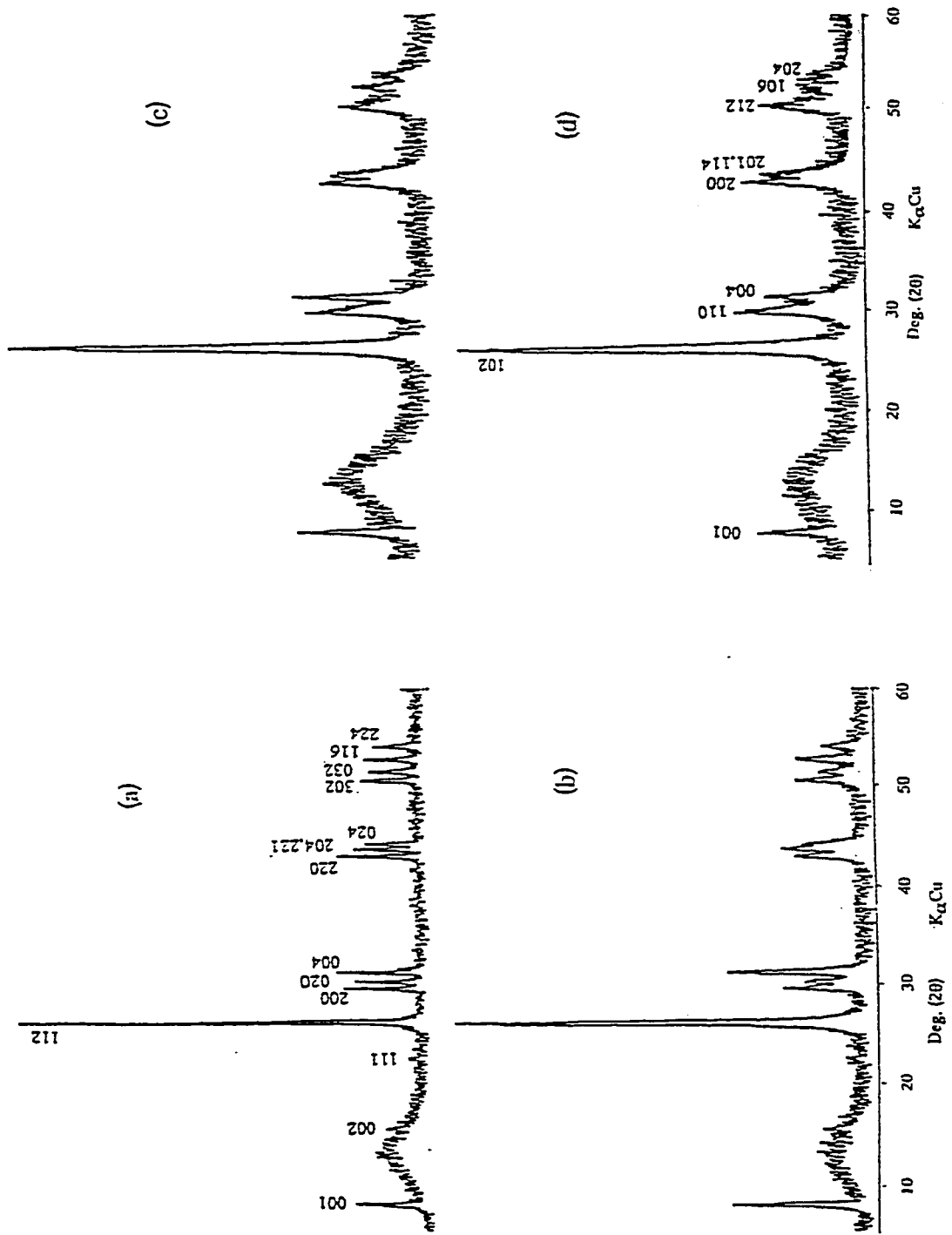
Figure 38: o-PbSnF$_4$ versus grinding time: (a) 0, (b) 10s, (c) 20s, (d) 30s

peak splitting responsible for orthorhombic distortion. In addition, the intensity of the

(00l) peak is significantly enhanced, due to increased preferred orientation, caused by a

more efficient alignment of the platelets parallel to one another after a short shaking

time. The same was observed in α-PbSnF$_4$(ssr). After 20s of milling (fig. 38c), further

line broadening is observed, the intensity of the (00l) peaks has decreased and the

orthorhombic distortion has disappeared, e.g. the (200)$_o$ and (020)$_o$ peaks have coalesced

to give (110)α. At this point, the diffraction pattern is the same as that of α-PbSnF$_4$ (aq$_1$)

and there is considerable strain in the ($\bar{a},\bar{b}$) plane (very broad (110)). After 30s milling,

the intensity of the (00l) peaks has decreased further (fig. 38d) and after 50s, all evidence

of lattice distortion has also disappeared (fig. 39a) and the X-ray diffraction pattern is

identical to all the milled α-PbSnF$_4$ samples, i.e. it looks like microcrystalline β-PbF$_2$.

Like in the case of α-PbSnF$_4$, overgrinding results in no further change (fig. 39b & c).

4.1.5. β-PbSnF$_4$ (fig. 40, 41 and 42)

The X-ray diffraction pattern of β-PbSnF$_4$ (fig.40a) is similar to that of α-PbSnF$_4$.

Like α-PbSnF$_4$, it shows a tetragonal distortion, just a little smaller. ($a_\beta \approx 4a_\alpha$; $c_\beta > 2c_\alpha$,

where a_α, c_α, a_β, c_β are the unit-cell parameters of α- and β-PbSnF$_4$, respectively), with

superstructures (x4 in the ($\bar{a},\bar{b}$) plane, x2 along $\bar{c}$). However, the (00l) peaks are much

weaker, indicating that there is much less preferred orientation in β-PbSnF$_4$, and its

Bragg peaks are narrower than those of α-PbSnF$_4$, particularly much narrower than those

of α-PbSnF$_4$(aq$_1$), which shows that β-PbSnF$_4$ has a much lower degree of strain, if any.
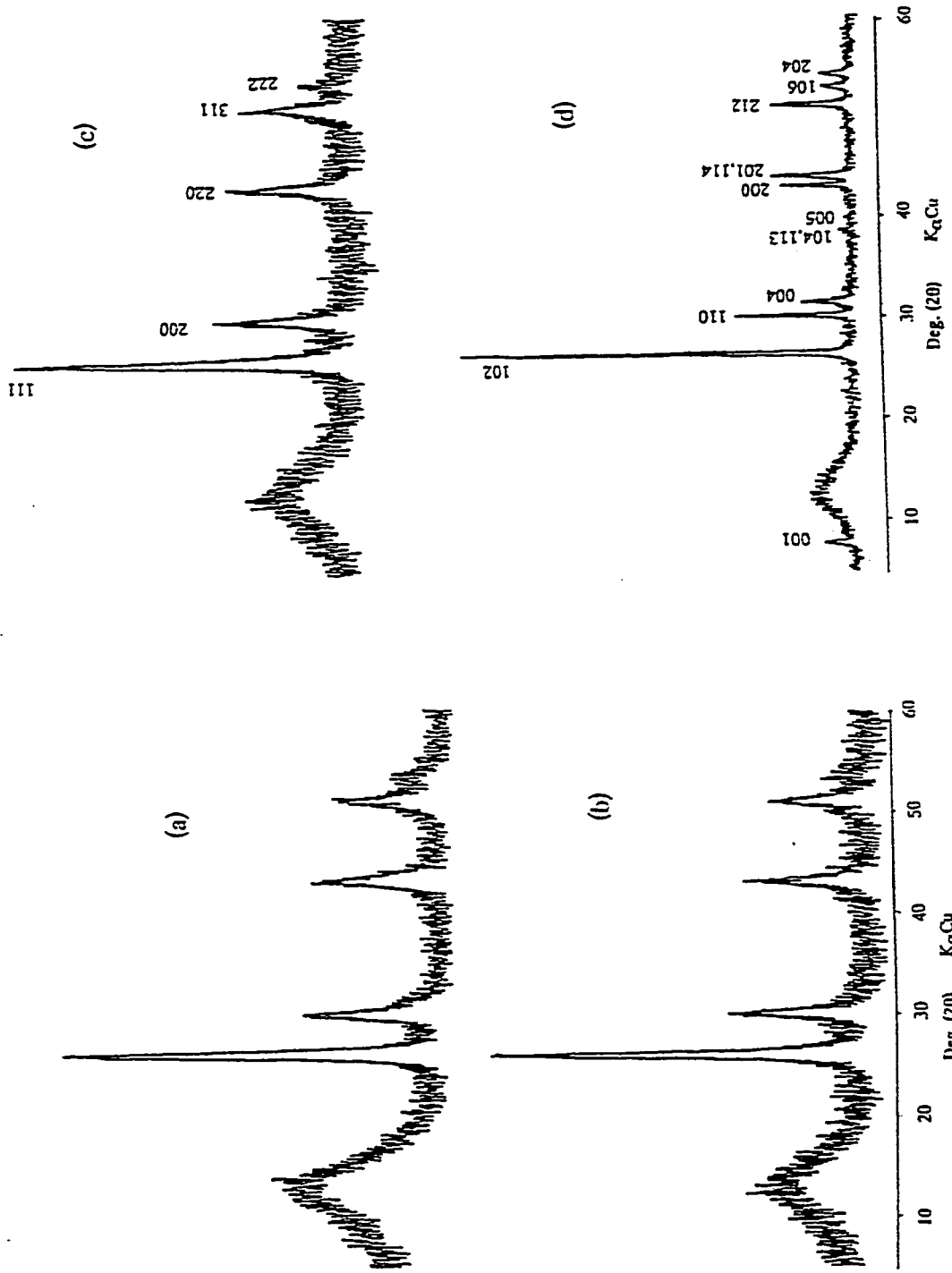
Figure 39: o-PbSnF$_4$ versus grinding time and annealing: (a) 50s, (b) 5min., (c) 10min., (d) 20min. grinding and then, heated at 200°C for 2 hours

112

Figure 40: β-PbSnF₄ versus grinding time: (a) 0, (b) 10s, (c) 20s, (d) 50s

113
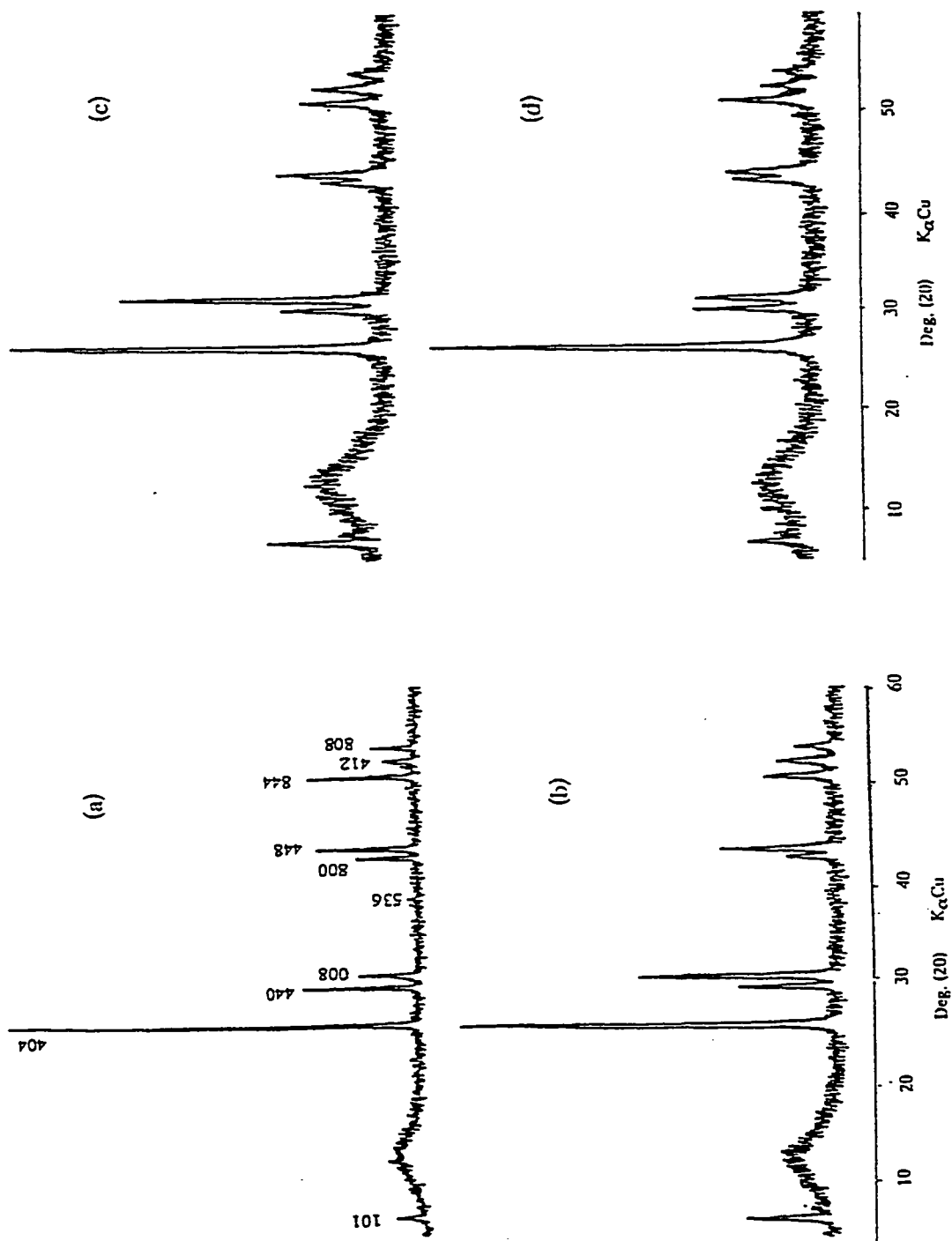
The superstructure reflection at high angle is not the same as for α-PbSnF$_4$, indicating that the Pb/Sn ordering is different from that of α-PbSnF$_4$. Grinding for 10s (fig. 40b) and 30s (fig. 40c) shows an increase of the linewidth, and also, a significant increase of the intensity of the (00l) peaks and of the superstructure reflection at low angle, like in α-PbSnF$_4$(ssr) and o-PbSnF$_4$. The same peaks show a net decrease of intensity after 50s milling, although they are still comparatively stronger than before milling (fig. 40d). The enhancement of the superstructure reflections and (00l) can be attributed, like in the previous cases, to a higher degree of preferred orientation due to a more efficient parallel alignment of the particles created by a short time shaking, a time too short to break up the particles sufficiently to cancel the effect of shaking. After 1min. grinding (fig. 41a), the intensity of the peaks is comparable to what it was before grinding however, the peaks are much broader, which can be attributed to a smaller particle size. After 3min. grinding (fig. 41b), the peak characteristic of the superstructure and of the tetragonal splitting are very weak, and after 5min. (fig. 41c), they have completely disappeared. At that stage, the diffraction pattern of milled β-PbSnF$_4$ is similar to that of microcrystalline β-PbF$_2$, i.e. it is identical to that of the other phases of PbSnF$_4$ after only 50s milling. Freshly prepared samples of β-PbSnF$_4$ must be used in the ball milling experiments, otherwise the results are not reproducible, i.e. the time required to obtain microcrystalline β-PbF$_2$ like diffraction patterns may vary. This is due to the metastability of the β-phase. Like for the other phases of PbSnF$_4$, prolonged milling causes no further change (fig. 42a).

In all the four phases of PbSnF$_4$ that were ball milled, overgrinding, i.e. grinding for much longer than the minimum time required to obtain the diffraction pattern of

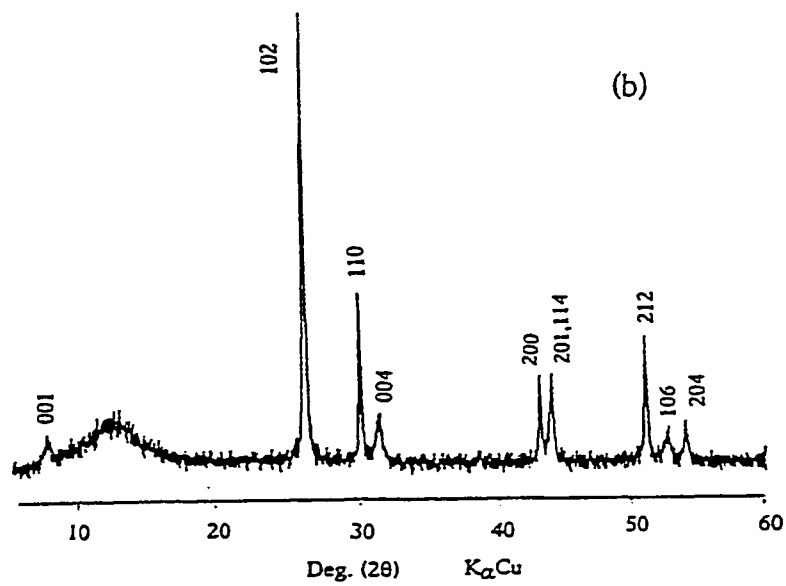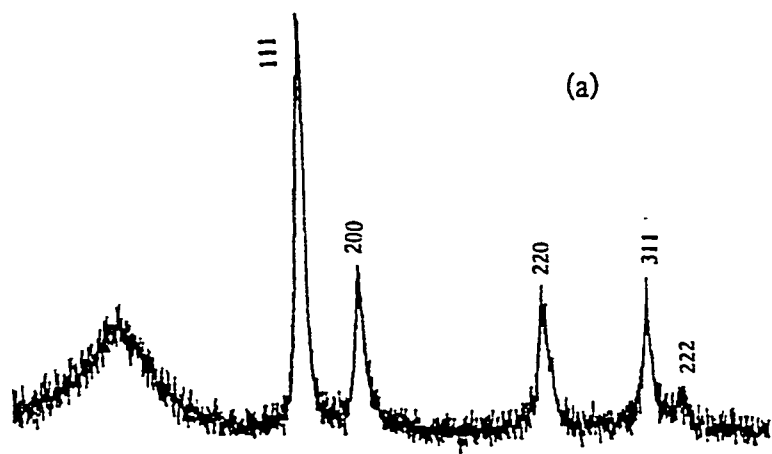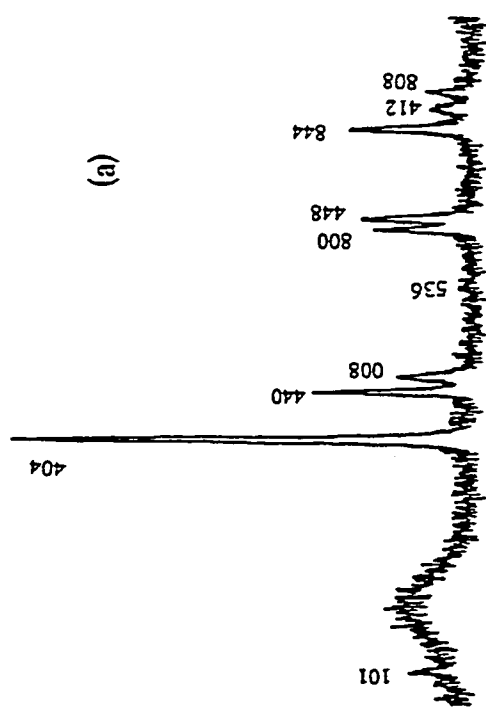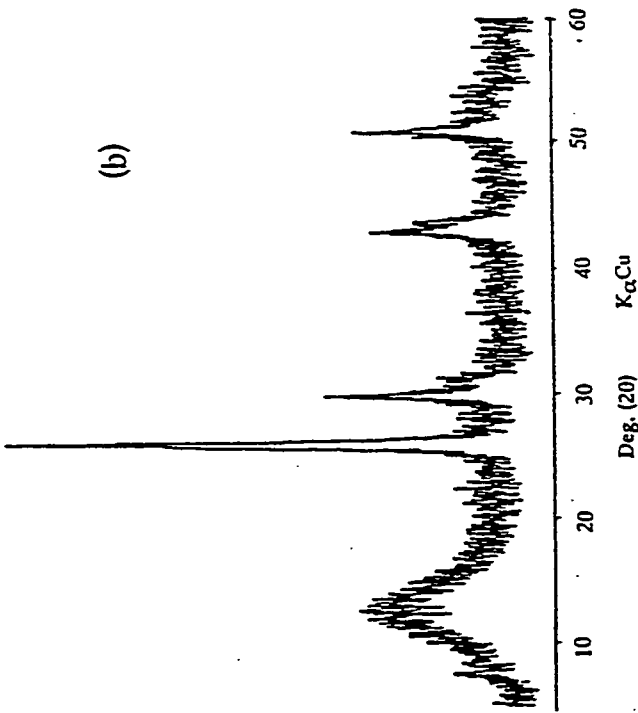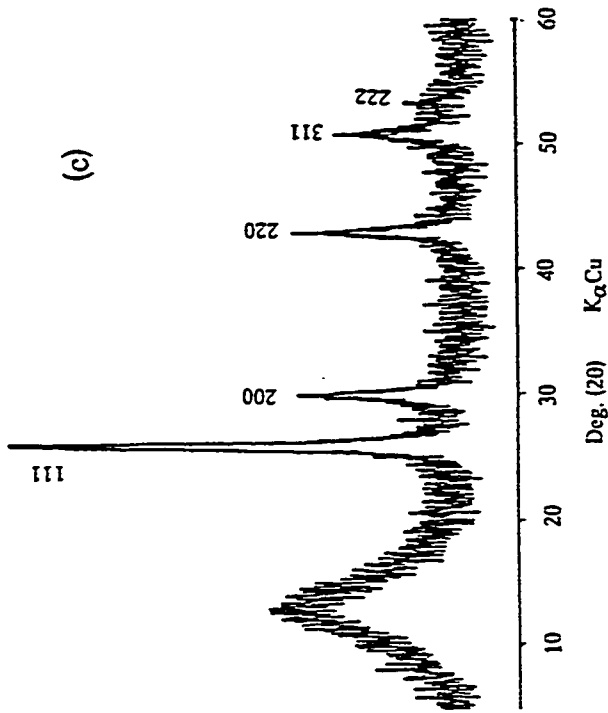Figure 41: β-PbSnF$_4$ versus grinding time: (a) 1min, (b) 3min grinding and (c) 5min.
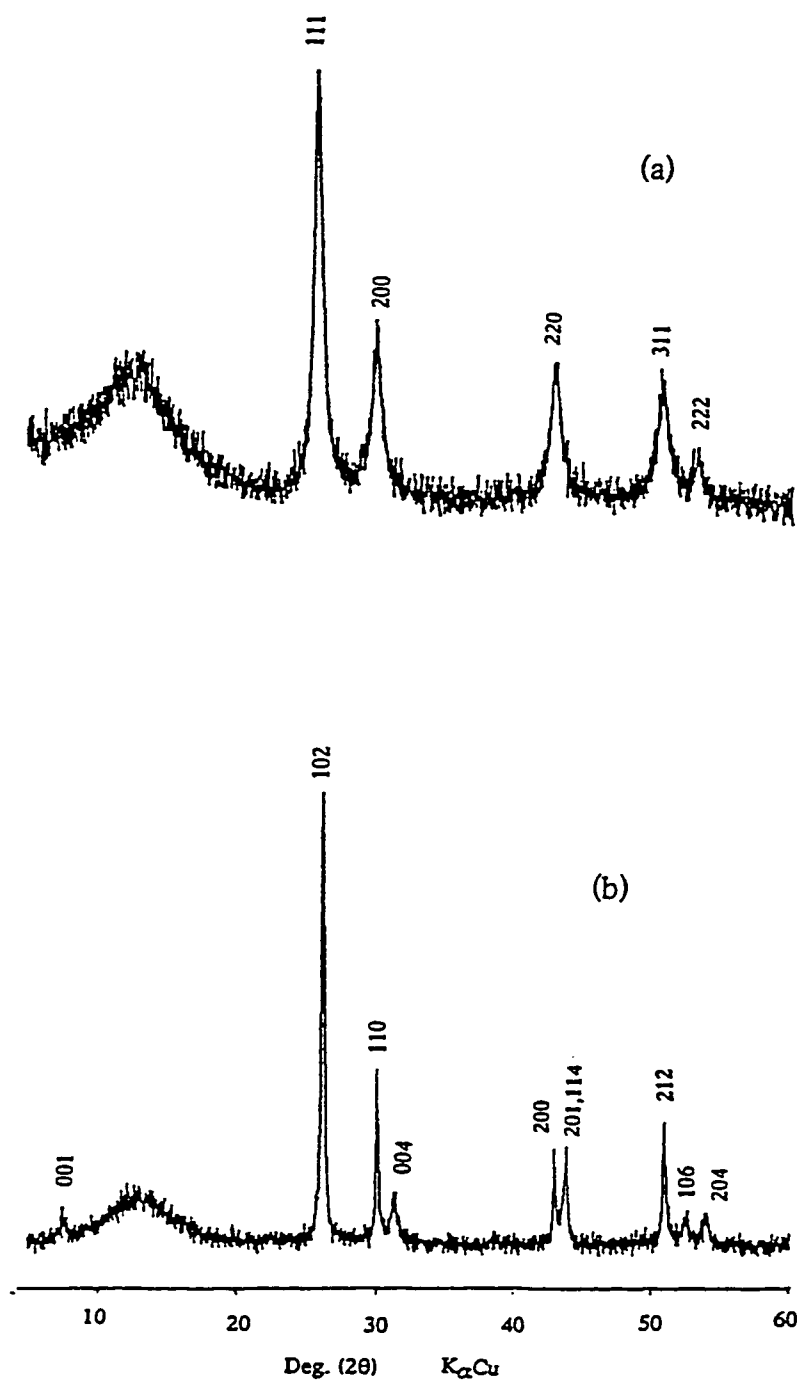
Figure 42: β-PbSnF₄ versus grinding time and annealing: (a) 20min.,
(b) 20min. grinding and then, heated at 200°C for 2 hours

microcrystalline β-PbF$_2$, does not bring about any other significant change, not even a further increase in the linewidth (fig. 34a, 37a & b, 39b & c, and 42a). To the contrary, a very slight narrowing might even occur in some cases, suggesting that the crystallinity of the phase formed increases slightly. These results imply that the microcrystallinity of the β-PbF$_2$-like material obtained is due to the transformation undergone by PbSnF$_4$ upon grinding and not just the breaking up of the crystallites by application of mechanical energy. If no phase transformation took place in the first minute (5minutes for β-PbSnF$_4$) of milling, then the particles would keep getting smaller on prolonged grinding, and eventually the samples would become completely amorphous to X-ray. In addition, the fact that all phases of PbSnF$_4$ gives the same diffraction pattern upon grinding suggests that the phase obtained is the same in all cases.

4.2. CHARACTERIZATION OF THE BALL MILLED PHASES
4.2.1. Describing the problem

Ball milling the four phases of PbSnF$_4$ has produced a microcrystalline phase, which looks identical regardless of the initial phase that was ground. This microcrystalline phase has a cubic unit-cell, an F Bravais lattice, and gives an X-ray diffraction pattern similar to that of β-PbF$_2$, except for the linewidth, and with approximately the same unit-cell parameter. Two possible transformations could have occurred upon ball milling:

- PbSnF$_4$ $\rightarrow$ microcrystalline β-PbF$_2$ + amorphous SnF$_2$: the SnF$_2$ formed would have to be amorphous since it is not detected by X-ray diffraction.

117

- $PbSnF_4$ → microcrystalline γ-$PbSnF_4$: crystalline γ-$PbSnF_4$ is obtained as a non-quenchable high temperature phase by heating $PbSnF_4$ above 390°C[4]. It might be possible that in this work γ-$PbSnF_4$ could be stabilized at room temperature in the metastable state. Stabilization might be made possible by the large number of defects generated upon grinding.

Now, we will try to differentiate between these two possibilities.

4.2.2. Unit-cell and particle size of the ground phases

The unit-cell parameter and average particle dimension of each ground phase was calculated from the position and linewidth of the (111) peak. The results are shown in Table IX.

Table IX: Crystallographic constants for ball milled $PbSnF_4$

Starting $PbSnF_4$ phase	Grinding Time (s) (a)	$a(Å)^{(b)}$	$\Delta V_1(\%)^{(c)}$	$\Delta V_2(\%)^{(d)}$	$D(Å)^{(e)}$
α-$PbSnF_4$ (aq$_1$)	50	5.968	+4.565	+2.241	117
α-$PbSnF_4$ (aq$_2$)	50	5.960	+3.977	+1.834	131
α-$PbSnF_4$ (ssr)	50	5.967	+4.504	+2.193	125
o-$PbSnF_4$	50	5.979	+5.807	+2.809	125
β-$PbSnF_4$	300	5.937	+2.698	+0.659	134
Pb_2SnF_6	600	5.936	+9.554	+0.616	117
β-PbF_2	-	5.924	-	-	-

(a) Minimum grinding time required to produce the cubic microcrystalline phase

(b) Unit-cell parameter measured from the position of (111)

(c) Relative volume change upon grinding, calculated as follows:
ΔV_1 (%) = 100 [V(after grinding) - V(before grinding)] / V(before grinding)

(d) Relative volume difference between ground $PbSnF_4$ and β-PbF_2, calculated as follows:
ΔV_2 (%) = 100 [V (after grinding) - V(β-PbF_2)] / V(β-PbF_2)

In all cases, the volume used is that of one $MSnF_4$ unit or two PbF_2 units.

(e) Average particle diameter

The following can be derived from Table IX:

(i) The unit-cell parameter of the ground phase varies significantly with the sample origin and is larger than that of β-PbF$_2$ in all cases. There is no significant difference between the three α-PbSnF$_4$ samples, however, the unit-cell parameter of ground o-PbSnF$_4$ is slightly larger, and that of ground β-PbSnF$_4$ is significantly smaller, and it is much closer to that of β-PbF$_2$. If the microcrystalline ground phase were β-PbF$_2$, it could have a unit-cell parameter slightly larger than 5.924Å since the creation of a large number of defects is known to increase the volume of the unit-cell. In addition, since the four samples have different structures, and probably have initially a different number of defects, the total number of defects in each might be different, hence a different unit-cell parameter.

Ground β-PbSnF$_4$ could be expected to have a larger unit-cell parameter than the others since it was ground for six times as long and thus, should have more defects. However, the kinetics of defect formation is certainly a function of bond strength (stronger bonds make it more difficult to generate defects) and since it took six times as long to grind β-PbSnF$_4$ to the microcrystalline cubic state, one can assume that the lattice of β-PbSnF$_4$ is much stronger than that of α-PbSnF$_4$ or o-PbSnF$_4$, and therefore, it is much more difficult to generate defects in β-PbSnF$_4$. Indeed, the structure of β-PbSnF$_4$ can be expected to be stronger than those of o- and α-PbSnF$_4$, since the latter are bidimensional with very effective cleavage planes (fig. 1b) whereas β-PbSnF$_4$ is believed to have a three-dimensional framework related to that of γ-PbSnF$_4$ (fig. 43), however, with Pb/Sn ordering in a fashion that is presently unknown[20].

119
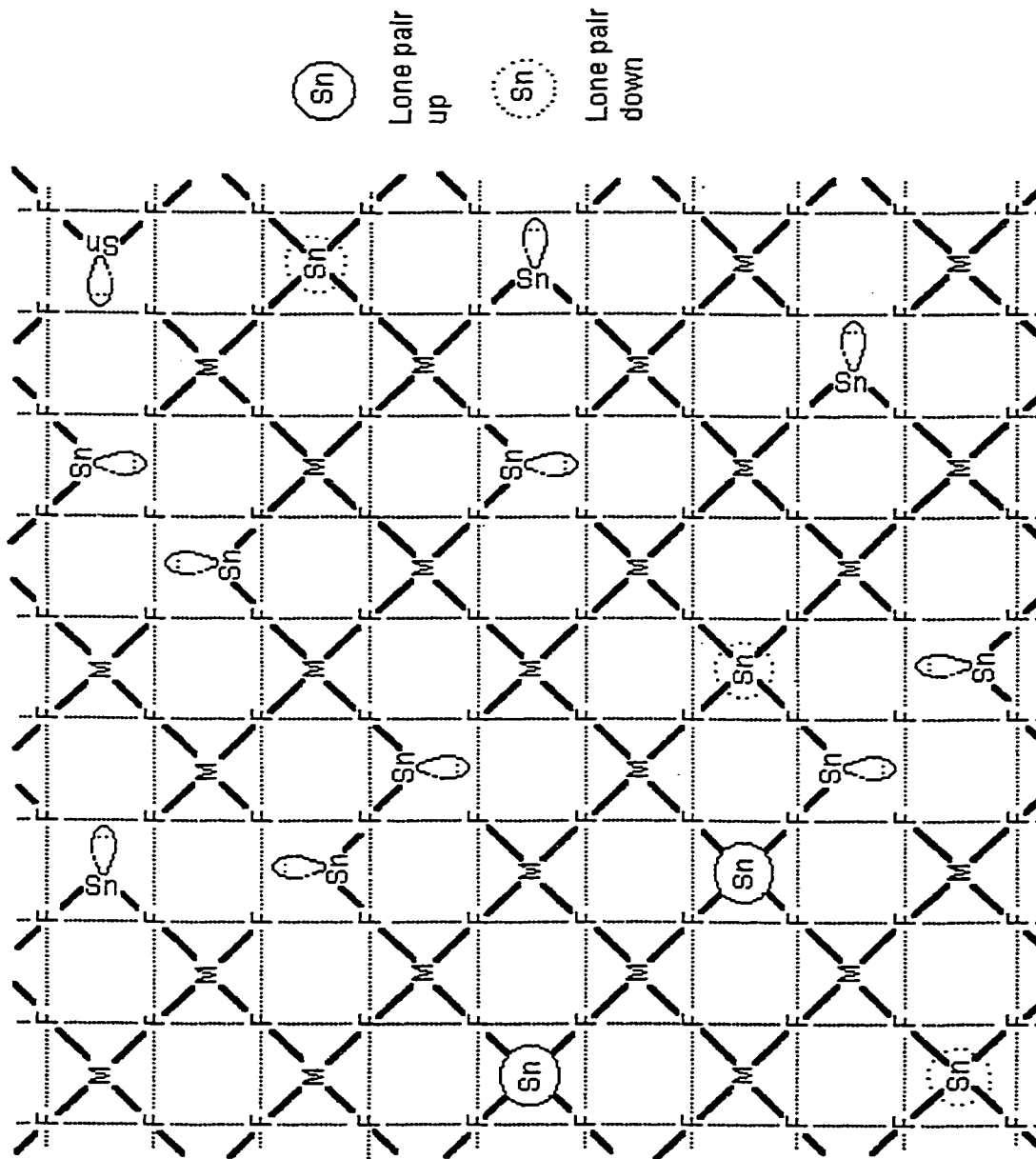
Figure 43: Model of the structure of γ-PbSnF$_4$ showing Pb/Sn disorder and random shift of tin parallel to the axes of the unit-cell

The comparison between the unit-cell of β-PbF$_2$ and each ground sample is also given in Table IX by the relative volume difference ΔV_2.

The above observations suggest very strongly that the milled samples are $\mu\gamma$-PbSnF$_4$, and not microcrystalline β-PbF$_2$ and amorphous α-SnF$_2$, however, further proof would be helpful. The fact that overgrinding does not increase either the unit-cell parameter or the linewidth shows that all changes (particle fractionning, phase transition, creation of defects) take place when the initial crystalline phase is subjected to the grinding effect, and the kinetics of defect formation is very slow once the microcrystalline cubic phase has formed. In addition, we checked that overgrinding β-PbF$_2$ results in an increasing linewidth and partial transformation to α-PbF$_2$. Since none of these is observed here, it is clear that it is not β-PbF$_2$ that is being ground, therefore the milled samples must be microcrystalline γ-PbSnF$_4$.

(ii) The relative volume change ΔV_1 at the transformation occuring upon grinding is a function of the starting PbSnF$_4$ phase. This is not surprising since both the starting phase and the ground phase have different unit-cell sizes. As expected, the differences between the three phases of α-PbSnF$_4$ is very small.

(iii) The average particle diameter D(Å) is similar for all ground samples, varying from 117 Å and 134 Å. The difference between the four samples is not significant, however, it is remarkable that all four samples give approximately the same particle size through the crystalline $\rightarrow$ microcrystalline transition obtained upon grinding regardless

of the structure of the initial crystalline phase, and regardless of the milling time.

4.2.3. Annealing the ground phases of PbSnF₄

The microcrystalline β-PbF$_2$ like materials obtained by ball milling the four phases of PbSnF$_4$ were heated at 200°C for 2 hours under nitrogen in a sealed copper tube container, in order to check their thermal stability. The results show that in all cases, α-PbSnF$_4$ is obtained (fig. 34b, 37c, 39d and 42b). Regardless of what was the phase of PbSnF$_4$ before grinding, annealing the ground samples gives α-PbSnF$_4$ which has little preferred orientation (($00l$) peaks are weak) and little strain (the (110) peak is very narrow), and with the same unit-cell parameters as those of α-PbSnF$_4$(aq$_1$) and α-PbSnF$_4$ (ssr). The absence of (or reduced) preferred orientation is probably due to the fact that the platelets of α-PbSnF$_4$ did not have enough time and thermal energy to grow in the ($\bar{a}$,$\bar{b}$) plane upon heating at 200°C for 2 hours. This is corroborated by the larger linewidth of the ($00l$) peaks which indicates microcrystallinity in the $\bar{c}$ direction, which is the direction of slow growth since $\bar{c}$ is perpendicular to the platelets. Transformation of $\mu\gamma$-PbSnF$_4$ to α-PbSnF$_4$ on heating is not surprising, since annealing is known to eliminate lattice defects and transform metastable phases back to lower temperature phases that are usually more ordered. Sintering of the crystallites also occur on annealing, however, the short heating time was not sufficient for this to occur efficiently.

4.2.4. Ball milling and annealing a mixture of SnF_2 + PbF_2

If the material obtained upon ball milling were a mixture of microcrystalline β-PbF_2 and nanocrystalline or amorphous SnF_2, these two materials could recombine in the mild conditions used for annealing, i.e. 2 hours at 200°C. These conditions give no reaction in a mixture of crystalline α-PbF_2 and α-SnF_2. However, small particles of both β-PbF_2 and α-SnF_2 would certainly increase significantly the contact surface between the two materials which could lead to a substantial increase of reactivity. In addition, the energy supplied by ball milling might be sufficient to induce the reaction of PbF_2 and α-SnF_2 and give $\mu\gamma$-$PbSnF_4$.

In order to simulate the annealing of ground $PbSnF_4$ samples and check if a mixture of microcrystalline β-PbF_2 and amorphous SnF_2 would react together to give α-$PbSnF_4$, a 1:1 mixture of β-PbF_2 and SnF_2, and a 1:1 mixture of α-PbF_2 and SnF_2 (the latter for comparison) were ground together and then, annealed at 200°C. When a 1:1 mixture of β-PbF_2 and SnF_2 is ground together the intensity of the peaks of both phases decreases (amorphization or reaction giving amorphous materials). No reaction is observed after 2 min. grinding (fig. 44a and 44b), however, after 30 min. grinding new peaks are observed (fig.44c). These are peaks of α-PbF_2. This could have been expected, since β-PbF_2 is a high temperature phase and has a higher volume than α-PbF_2, and thus, it is metastable at ambient conditions, and the β-$PbF_2 \rightarrow \alpha$-PbF_2 transition is expected to take place upon application of pressure or mechanical energy. However, no $PbSnF_4$ is formed. When these samples are annealed, reactions between SnF_2 and PbF_2 are observed if the mixture were milled prior to heating. When the mixture that was not
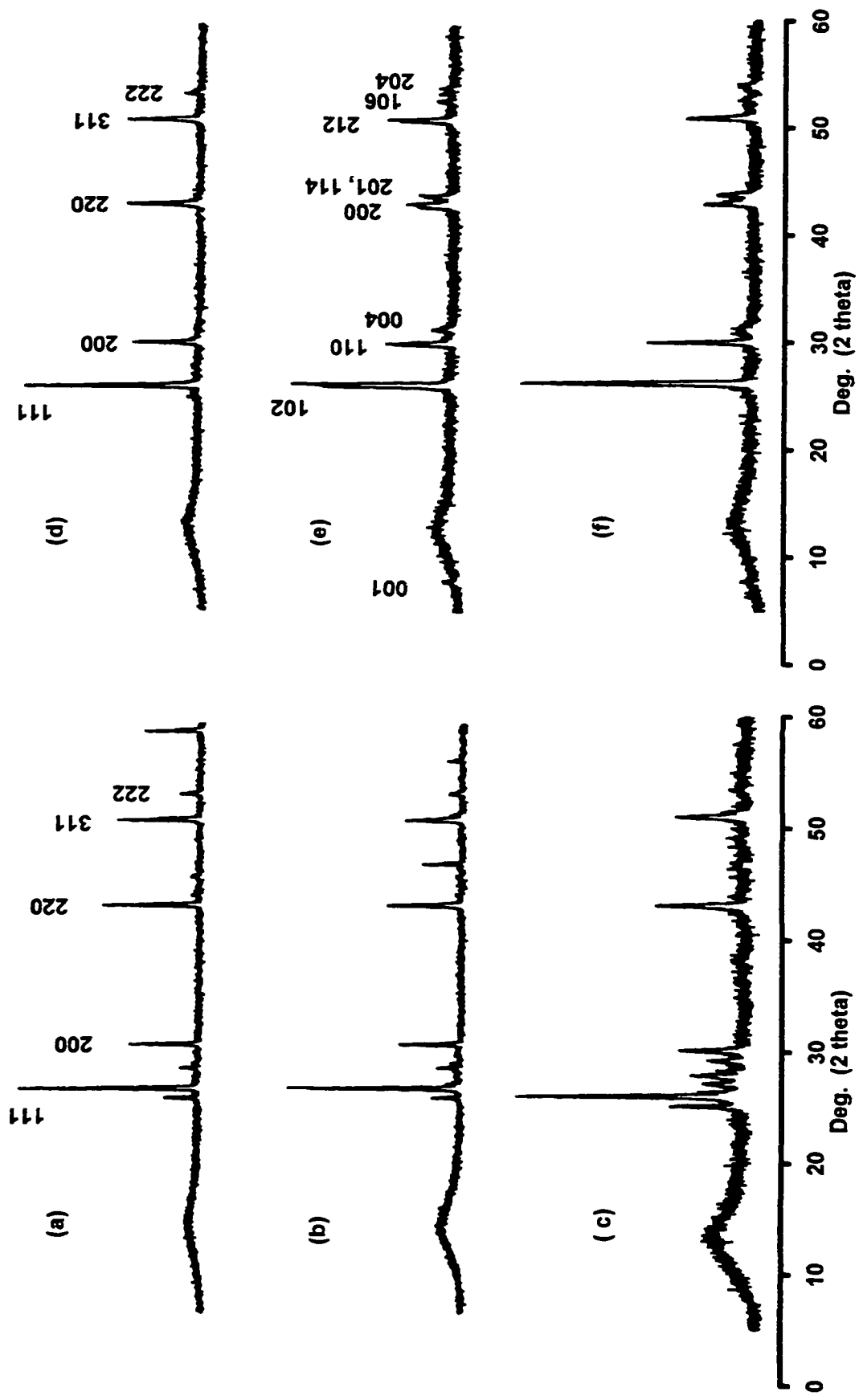
Figure 44: X-ray diffraction pattern of the mixture of β-PbF₂ and SnF₂ versus grinding time and annealing: (a) 0 grinding, (b) 2min., (c) 30min., (d), (e), (f) ground samples 0, 2, 30min. respectively, heated at 200°C for 24h

ground (fig. 44a) was annealed, only the β-PbF$_2$ X-ray pattern is observed together with very weak peaks (the strongest) of SnF$_2$ (fig. 44d). No PbSnF$_4$ has formed. The question here is: what happened to most of the SnF$_2$? Since the cubic pattern of PbF$_2$ has a slightly smaller unit-cell parameter than β-PbF$_2$, some SnF$_2$ was probably used to form the Pb$_{1-x}$Sn$_x$F$_2$ solution, which is cubic for x $\leq$ 0.30 and tetragonal β-PbSnF$_4$ type for 0.30 < x $\leq$ 0.50[39]. Some of it might be amorphous or microcrystalline and it is also harder to detect due to the lower scattering power of tin as compared to that of lead and to the lower intensities of the SnF$_2$ Bragg peaks because of its lower symmetry (monoclinic). For the ground mixtures, α-PbSnF$_4$ is observed after annealing in both cases (fig. 44e and 44f). In the case of the mixture ground for 30min. (fig. 44c), all the α-PbF$_2$ peaks disappear after annealing therefore, both the α-PbF$_2$ produced on milling and the remaining milled β-PbF$_2$ reacts with milled SnF$_2$ in our heating conditions. In addition, the (00l) peaks of α-PbSnF$_4$ are much broader than in the sample ground only 2min., which indicates that the platelet shaped crystallites are thinner. This is understandable since milling decreases the particle size of PbF$_2$ and SnF$_2$, thereby increasing the surface area of the crystallites. It results in a substantial increase of reactivity which favor crystal nucleation and does not provide enough time for crystal growth. When a 1:1 mixture of α-PbF$_2$ and SnF$_2$ is ground together the intensity of the peaks decreases, like when β-PbF$_2$ is used (fig. 45b and 45c). In addition, β-PbF$_2$ is formed. It seems contradictory that grinding β-PbF$_2$ gives some α-PbF$_2$ and grinding α-PbF$_2$ gives some β-PbF$_2$. However, this maybe understood by the fact that grinding gives enough energy to overcome the barrier that traps β-PbF$_2$ in the metastable state, and

125
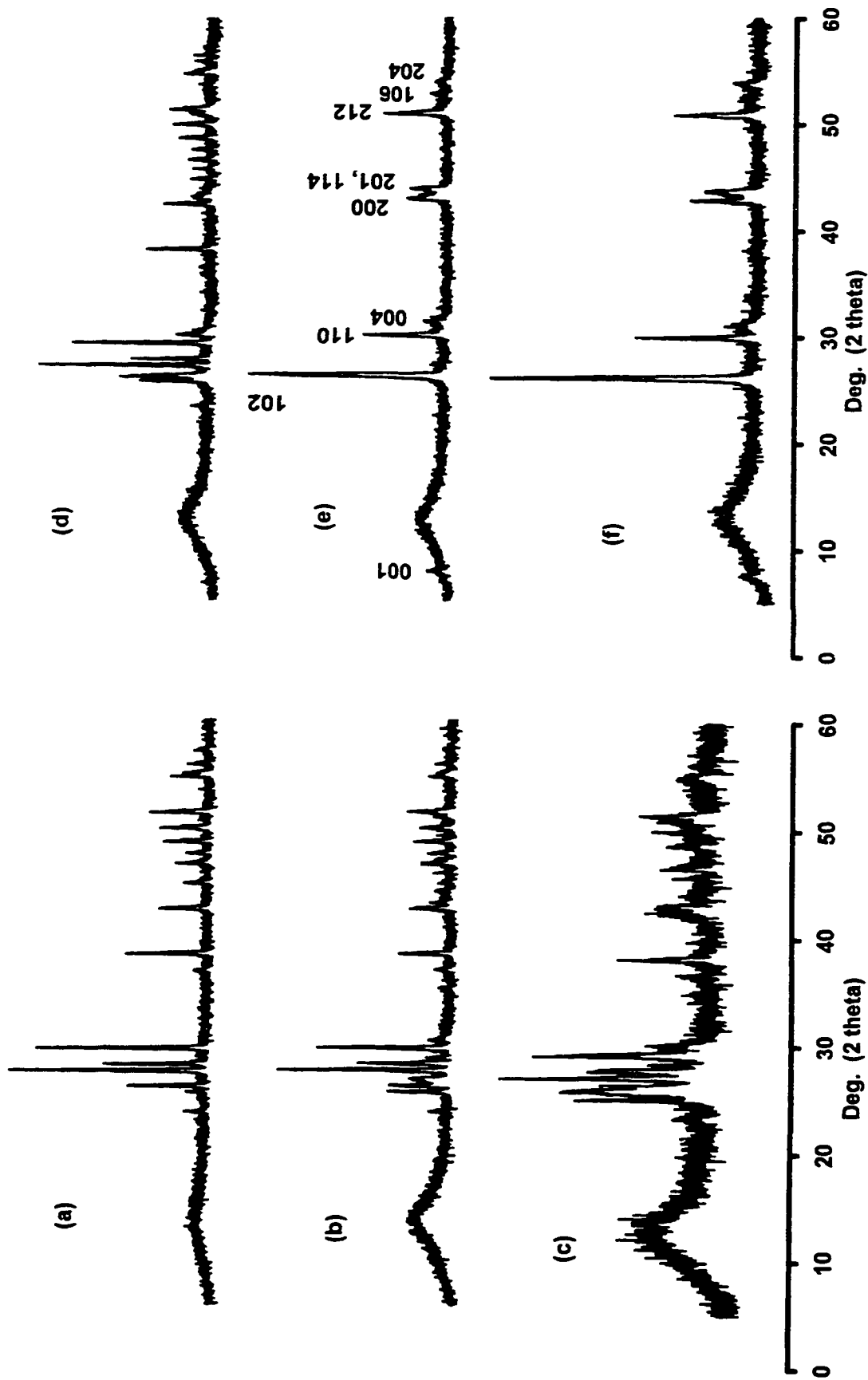
Figure 45: X-ray diffraction pattern of the mixture of α-PbF$_2$ and SnF$_2$ versus grinding time and annealing: (a) 0 grinding, (b) 2min., (c) 30min., (d), (e), (f) ground samples 0, 2, 30min. respectively heated at 200°C for 24h

it also provide enough energy to convert some α-PbF$_2$ to high temperature β-PbF$_2$. The conversions of α-PbF$_2$ to β-PbF$_2$, and of β-PbF$_2$ to α-PbF$_2$, on grinding, require the presence of SnF$_2$, as is described in **4.2.5**. Heating together the 1:1 mixture of α-PbF$_2$ and SnF$_2$ that was not ground (fig. 45d) gives also some β-PbF$_2$ unless it is α-PbSnF$_4$ (it is hard to say because of the similarity of their X-ray diagram and the large number of α-PbF$_2$ peaks that make detection of new weak peaks difficult). The ground samples give α-PbSnF$_4$ after annealing (fig. 45e and 45f).

Annealing ground mixtures of PbF$_2$ and SnF$_2$ produces α-PbSnF$_4$ at 200°C, when non-ground mixtures require 250°C, and although the ground β-PbF$_2$ started converting to α-PbF$_2$ instead of becoming microcrystalline. Therefore, the fact that α-PbSnF$_4$ is formed at 200°C after grinding suggests that milling and heating at 200°C cannot differentiate unambiguously between the two options for ground PbSnF$_4$ samples, i.e. are they microcrystalline γ-PbSnF$_4$ or a mixture of microcrystalline-β-PbF$_2$ and amorphous SnF$_2$? However, since overgrinding the PbSnF$_4$ samples does not produce α-PbF$_2$, whereas grinding β-PbF$_2$ does, it is clear that the ground PbSnF$_4$ samples are not microcrystalline β-PbF$_2$, therefore they are γ-PbSnF$_4$. Figure 44e, 44f, 45e and 45f show that the α-PbSnF$_4$ produced by heating the ground mixtures of PbF$_2$ and SnF$_2$ at 200°C for 24 hours is free of strain in the $(\bar{a},\bar{b})$ plane (narrow (110) peak) and shows no preferred orientation (very weak (00l) peaks). In addition, the platelet shaped crystallites are very thin (broad (00l) peaks).

4.2.5. Ball milling of both α-PbF₂ and β-PbF₂ versus time

Ball milling both forms of PbF_2 resulted in significant changes. Fig. 46 & 47 show the most relevant portion of the X-ray diffraction pattern $(24-31°(2\theta))$, where each phase has strong peaks which show little overlap. When β-PbF_2 was milled (fig. 46), the lines broadened slightly and new peaks appeared. The beginning of these changes are observed after just 2min. (fig. 46b) and after 30min. (fig. 46c), further broadening of the β-PbF_2 lines is observed. The new lines are stronger than those of β-PbF_2. After milling for 60min., the relative intensity of the new peaks has changed little, and in addition, all the peaks are much broader (fig. 46d). The new peaks observed are those of α-PbF_2, and they start appearing rapidly when β-PbF_2 is ball milled (after just 2min.). The transformation to α-PbF_2 is rapid in the first 30min. However, from 30 and 60min. milling, no further transformation is detected (no significant increase of the relative intensity of the α-PbF_2 peaks), which seems to indicate that a constant mixture of both phases has been obtained. No change is observed for even longer milling times (60min.).

On the other hand, the increasing peak linewidth at half height indicates that the particle dimension keeps decreasing at increasing milling time particularly for the α-PbF_2 formed at shorter milling time. For the remaining β-PbF_2, it is hard to tell whether the linewidth increases above 30min. milling because the line intensity is too small to make possible a reliable measurement of the linewidth. The average particle diameter of milled β-PbF_2 and of the α-PbF_2 being formed is given in Table X.
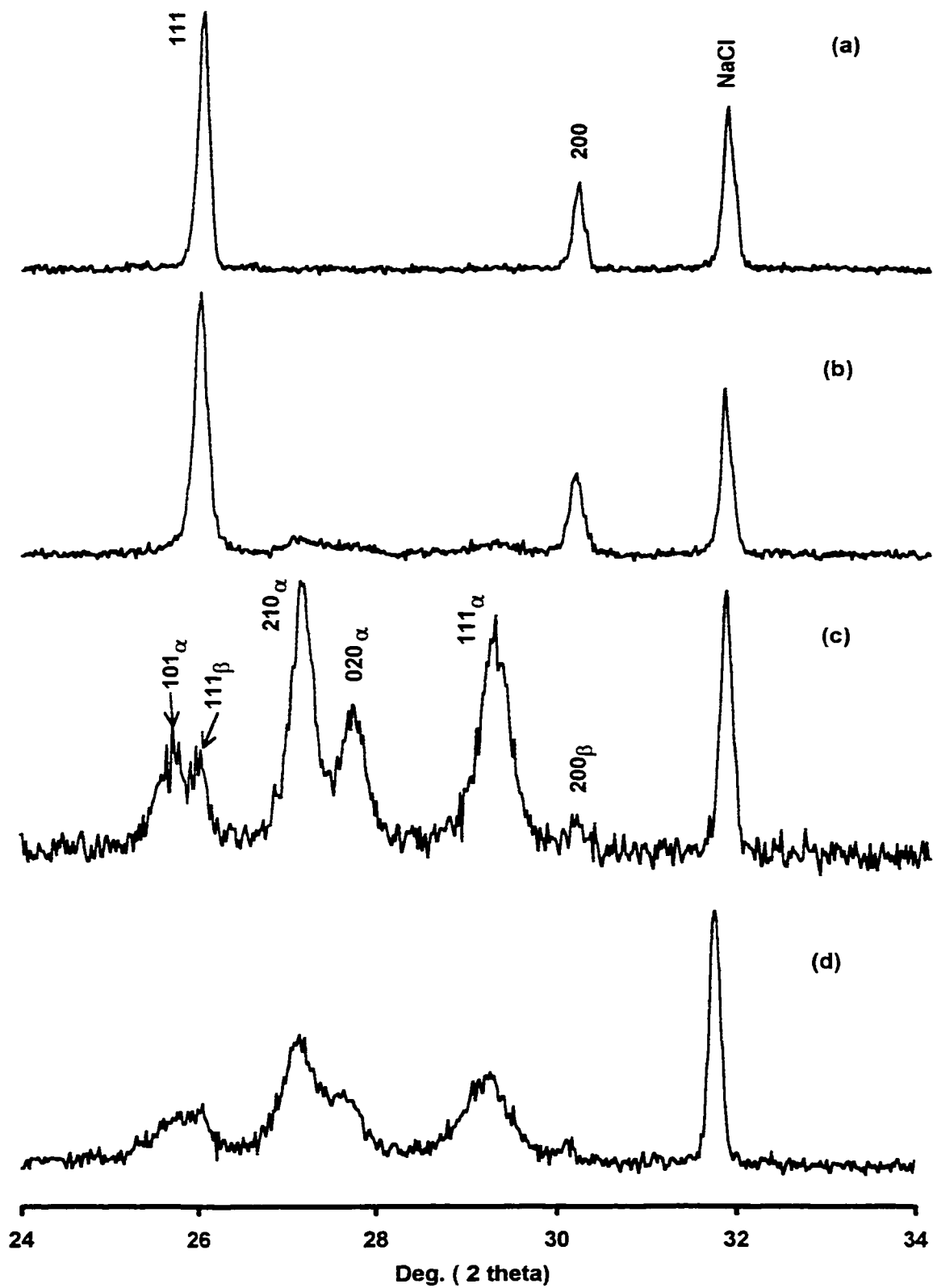
Figure 46: X-ray diffraction pattern of β-PbF₂ versus grinding time: (a) 0 grinding, (b) 2min., (c) 30min., (d) 1h. (NaCl is used for reference)
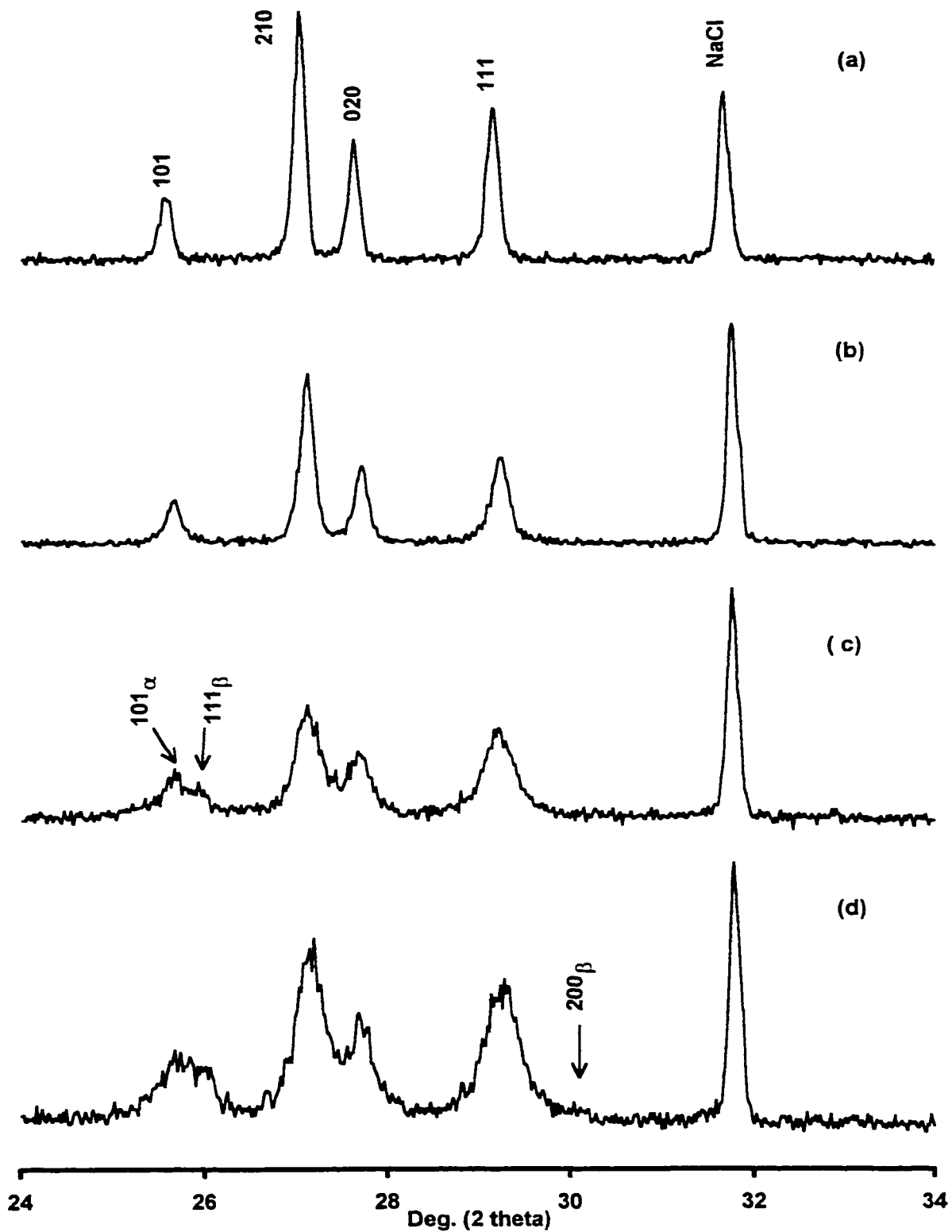
Figure 47: X-ray diffraction pattern of α-PbF$_2$ versus grinding time: (a) 0 grinding, (b) 2min., (c) 30min., (d) 1h. (NaCl is used for reference)

The X-ray diffraction pattern of α-PbF$_2$ versus ball milling time is shown on figure 47. It shows similar type of changes as that of β-PbF$_2$, i.e. first peaks get broader and then, new peaks appear. However, in this case, the new peaks are not observed yet after 2 min. ball milling and they never get as strong as the peaks of α-PbF$_2$ formed on milling β-PbF$_2$. The new peaks formed belong to β-PbF$_2$ and the ratio of the intensities of the peaks of the two phases seems to have reached nearly a constant value after 30min.

Table X: Average particle size diameter D_α (Å) of α-PbF$_2$ and D_β (Å) of β-PbF$_2$ versus ball milling

	Ball Milling time (min.)	D_α (Å)	D_β (Å)
α-PbF$_2$	2	451	-
	30	202	-
	60	202	-
β-PbF$_2$	2	-	770
	30	267	-
	60	129	-

(fig.47c). It also shows little change after milling an additional 30min. (fig.47d), like when β-PbF$_2$ is milled. The intensity of the peaks of the two phases seems to reach about the same ratio regardless of the starting phase, therefore, milling α-PbF$_2$ or milling β-PbF$_2$ result in about the same mixture of α- and β-PbF$_2$ after 30 min., which does change on further milling. Figures 46 & 47 and Table X show that the particles of

α-PbF$_2$ are much smaller after 60 min. milling β-PbF$_2$ (129Å) than those obtained after milling α-PbF$_2$ for the same time (202 Å). Furthermore, the particles of α-PbF$_2$ obtained in the $\beta \rightarrow \alpha$ transformation first grow to 267 Å after 30min. (fig. 46c) milling, and then decrease to 129 Å after a total milling time of 60 min.

4.2.6. Solubility test for ground and unground PbSnF$_4$

Another method for distinguishing between the two options $\mu\gamma$-PbSnF$_4$ or microcrystalline β-PbF$_2$ + amorphous SnF$_2$ is a solubility test. PbF$_2$ is poorly soluble at all temperatures, and probably so is PbSnF$_4$ since it is obtained by precipitation from aqueous solutions (for α- and o-PbSnF$_4$). On the other hand, α-SnF$_2$ is highly soluble. Thus, stirring slurries of ground PbSnF$_4$ samples in water could be expected to result in a minor weight loss if the samples are $\mu\gamma$-PbSnF$_4$, or in a more major weight loss if the samples are mixtures of microcrystalline β-PbF$_2$ and amorphous SnF$_2$, since SnF$_2$ would dissolve and only solid β-PbF$_2$ would be recovered by filtration. In both cases, the X-ray diffraction pattern should not change. The four samples were stirred in 40 mL of water at ambient temperature for 1 hour. Then, they were filtered, allowed to dry at ambient temperature, weighed and checked by X-ray diffraction. The weight losses for each sample and the % theoretical weight loss if all of SnF$_2$ and none of PbF$_2$ dissolved are given in Table XI.

The fact that the weight loss varies considerably from one sample to another is an indication that it is not just SnF$_2$ dissolving, since even if some PbF$_2$ dissolved, it should

be the same quantity since it has about the same particle size (Table IX). This is an indication that ground $PbSnF_4$ might be $\mu\gamma$-$PbSnF_4$. The % weight loss in o-$PbSnF_4$ and β-$PbSnF_4$ is observed to be lower than in the two α-$PbSnF_4$ phases and the two forms of α-$PbSnF_4$ show similar losses. For o-$PbSnF_4$, this might be due to the higher compacity (smaller volume) of the unground sample, although after grinding it has the highest volume, therefore it is more likely due to bonding. For β-$PbSnF_4$, it could be due to the fact that its structure is more closely related to that of insoluble β-PbF_2, and it is three-dimensional, therefore offering a lower surface exposed to water molecules. However, this interpretation implies that each ground phase keeps the memory of its origin, which is proven by X-ray diffraction of the ground samples before stirring and after stirring.

Table XI: % Weight loss of $PbSnF_4$ upon stirring in water for 1 hour

$PbSnF_4$ phase	Unground sample	Ground sample
α-$PbSnF_4$ (aq$_1$)	29	51
α-$PbSnF_4$ (ssr)	24	49
o-$PbSnF_4$	16	33
β-$PbSnF_4$	22	36
mixture of SnF_2 + α-PbF_2	36	-
mixture of SnF_2 + β-PbF_2	45	-
mixture of SnF_2 + PbF_2*	39	39

* theoretical value if all of SnF_2 and none of PbF_2 dissolves

The X-ray diffraction pattern of the ground samples after stirring in water was highly unexpected (fig. 48). Indeed, regardless of whether it is $\mu\gamma$-PbSnF$_4$ or microcrystalline β-PbF$_2$, it was not expected to change. To the contrary, a drastic change is observed, both kinds of α-PbSnF$_4$ and β-PbSnF$_4$ after grinding and stirring in water give α-PbSnF$_4$, whereas o-PbSnF$_4$ gives back o-PbSnF$_4$. This shows unambiguously that SnF$_2$ did not just dissolve and get washed out upon filtering. In addition, surprisingly, o-PbSnF$_4$ kept the memory of its origin after grinding, even though the ground material looked like the other phases of PbSnF$_4$ obtained after grinding. In addition, the broad lines indicates that the PbSnF$_4$ obtained after stirring is microcrystalline. This experiment proves that ground PbSnF$_4$ is $\mu\gamma$-PbSnF$_4$, and despite the fact they all look the same, some memory of their origin remains.

As a double check, samples of the four kinds of PbSnF$_4$ not ground were also stirred in water in the same conditions as for the ground samples (fig. 49). The % weight loss is smaller (about half) for unground samples (Table XI). This could be due to the fact that they are not microcrystalline (less surface exposed to water molecules and also their crystalline structure is different (different bond strength). In addition, their X-ray diffraction pattern is unchanged, i.e. they are well crystalline and preferred orientation is much higher, particularly in α-PbSnF$_4$ (aq$_1$).
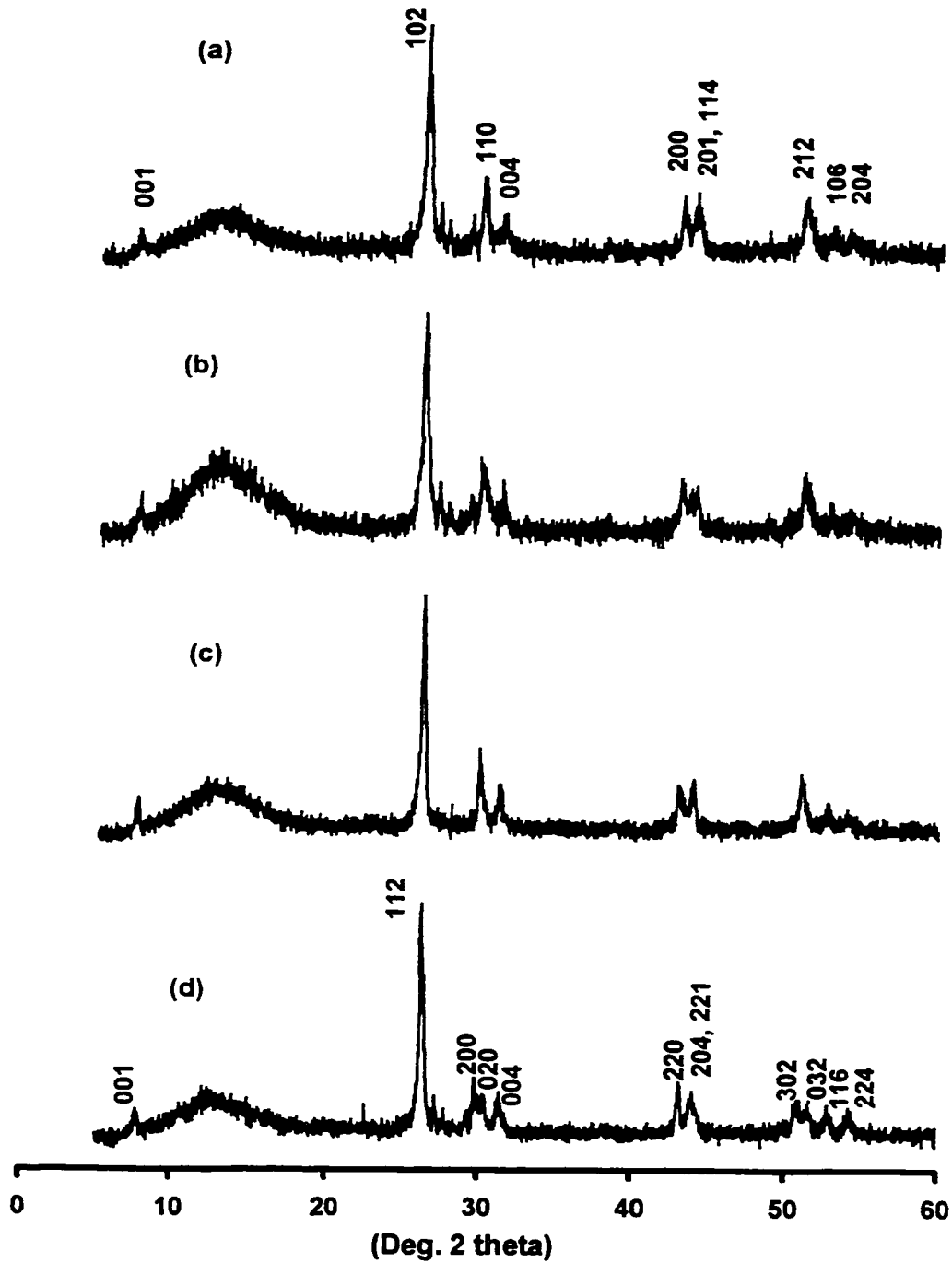
Figure 48: X-ray diffraction pattern of the different phases of PbSnF$_4$ milled and stirred in water for 1h: (a) α-PbSnF$_4$(aq$_1$), (b) α-PbSnF$_4$(ssr), (c) β-PbSnF$_4$, and (d) o-PbSnF$_4$
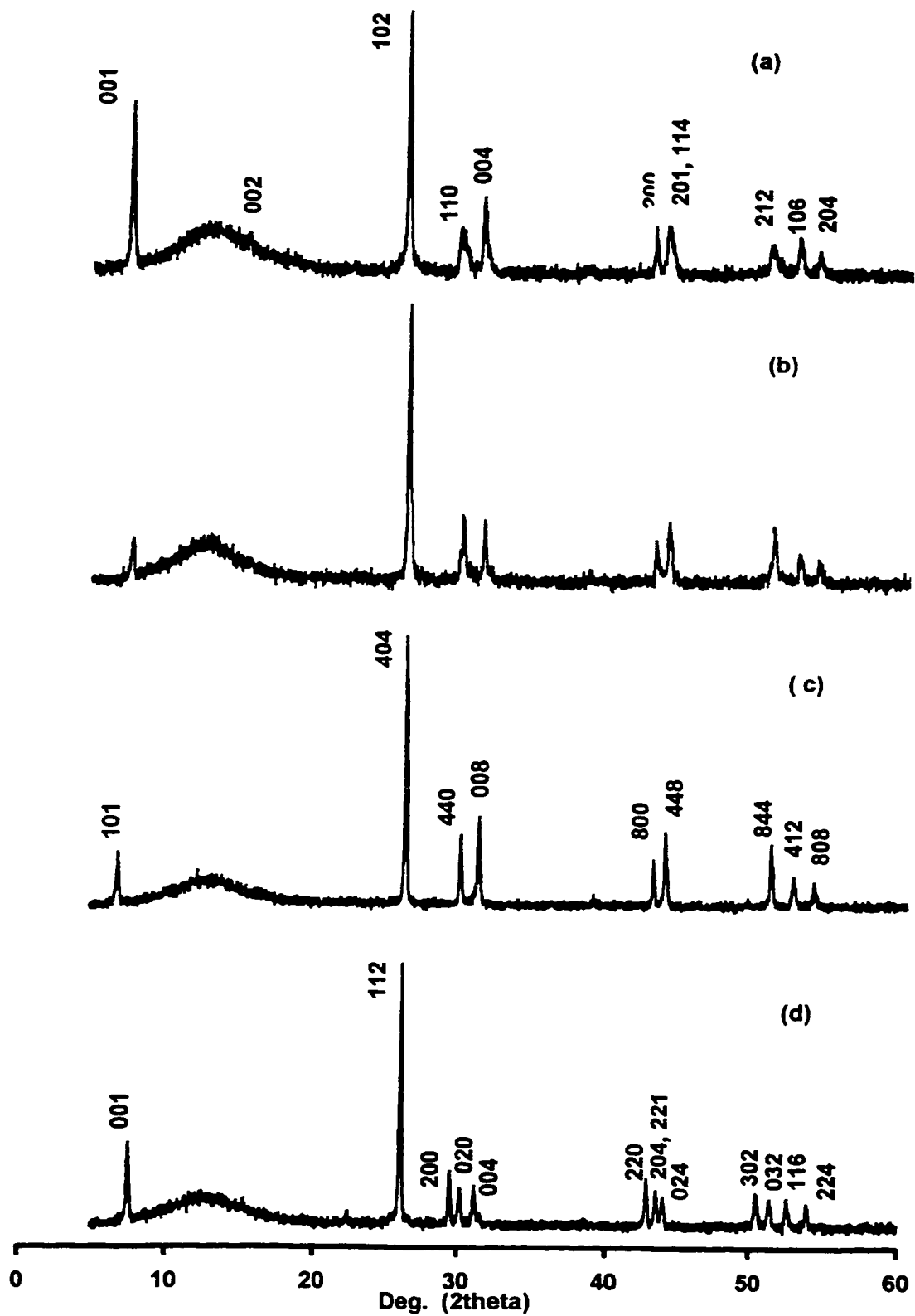
Figure 49: X-ray diffraction pattern of the four phases of PbSnF$_4$ not milled, after stirring in water: (a) α-PbSnF$_4$(aq$_1$), (b) α-PbSnF$_4$(ssr), (c) β-PbSnF$_4$, and (d) o-PbSnF$_4$

4.2.7. Stirring non-ground α- and β-PbF₂ in an aqueous solution of SnF₂

In order to check whether the α- and o-PbSnF$_4$ obtained by stirring ground PbSnF$_4$ in water was not due to a reaction between PbF$_2$ and SnF$_2$ in water, slurries of α-PbF$_2$ and β-PbF$_2$ were stirred in an aqueous solution of SnF$_2$, with a molar ratio PbF$_2$:SnF$_2$ = 1:1, for 1 hour at ambient temperature. β-PbF$_2$ showed no change upon stirring in a solution of α-SnF$_2$ and particularly, no PbSnF$_4$ was formed (fig. 50). On the other hand, for α-PbF$_2$, the result was very surprising (fig. 51). A significant change of diffraction pattern took place, although no PbSnF$_4$ was formed either (fig. 51b). All the α-PbF$_2$ peaks are conserved and one of them has its intensity very strongly enhanced (ca. doubled), and in addition, a few new peaks have appeared, some of them weak, between the α-PbF$_2$ peaks, and one new peak is at very low angle and is strong. This new peak cannot be indexed in the α-PbF$_2$ unit-cell, however, its d-spacing is four times that of the enhanced peak. In addition, the sample had gained weight. It appears that solid α-PbF$_2$ had incorporated tin in its structure to give a new material with Pb/Sn ordering in the direction represented by the enhanced peak.

This is a new material and its chemical composition is about 2Pb/1Sn. It is not a new phase of PbSnF$_4$ and its study is presented in more details in paragraph **4.3**. When solid β-PbF$_2$ is stirred in an aqueous solution of SnF$_2$, no reaction occurs and only the diffraction pattern of β-PbF$_2$ is observed (fig. 50b). Stirring both polymorphs of PbF$_2$ in a solution of SnF$_2$ for PbF$_2$:SnF$_2$ = 1:1 shows that the reactivity of α-PbF$_2$ is higher than that of β-PbF$_2$ and proves that PbF$_2$ and SnF$_2$ do not react in water to give α- or o-PbSnF$_4$

Figure 51: X-ray diffraction pattern of: (a) α-PbF$_2$,
(b) α-PbF$_2$ stirred for 1h in an aqueous solution
of SnF$_2$ (SnF$_2$/PbF$_2$ = 1)

Figure 50: X-ray diffraction pattern of: (a) β-PbF$_2$,
(b) β-PbF$_2$ stirred for 1h in an aqueous solution
of SnF$_2$ (SnF$_2$/PbF$_2$ = 1)

when stirred for one hour in a molar ratio 1:1, thereby proving that the ground samples of

PbSnF$_4$ are $\mu\gamma$-PbSnF$_4$ and not a mixture of microcrystalline β-PbF$_2$ and amorphous SnF$_2$.

In addition, it was also demonstrated that the four microcrystalline phases of γ-PbSnF$_4$

are not completely alike and some memory of their origin is imprinted in them. The

memory remains after grinding and can be expressed again when stirred in water.

4.2.8. Mössbauer Spectroscopy of the milled phases

The tin-119 nuclide (8.5% natural abundance) is used to probe the local situation

on the tin sublattice. Contrary to X-ray diffraction, it has the advantage of working,

regardless of crystallinity, however it require a sufficiently strong lattice, otherwise

phonons destroy the resonant reabsorption of the γ-rays. The spectra measured at

ambient temperature are all quite similar, i.e. they are made of a line at ca. 0 mm/s, and a

doublet at positive velocities (fig. 52). The peak at velocity zero is due to tin(IV), most

likely SnO$_2$, produced by surface oxidation of the particles. This is present in all

polycrystalline tin(II) compounds, however, it is not observed in large single crystals

where the surface is infinitely small relative to the bulk[16]. Dénès et al. studied it earlier

in details in SnF$_2$ and showed that it is a thin layer of SnO$_2$ that passivates the particles

against deeper oxidation[51-53]. The relative intensity of the tin(IV) Mössbauer signal

grossly overestimates the quantity of tetravalent tin in the materials.

Dénès showed earlier that the recoilless fraction of SnF$_2$ is much higher than that

of tin(II)fluoride (13 times as high as that of α-SnF$_2$), therefore the intensity of the tin(IV)

signal should be divided by more than 10 in order to obtain an estimate of the fraction of
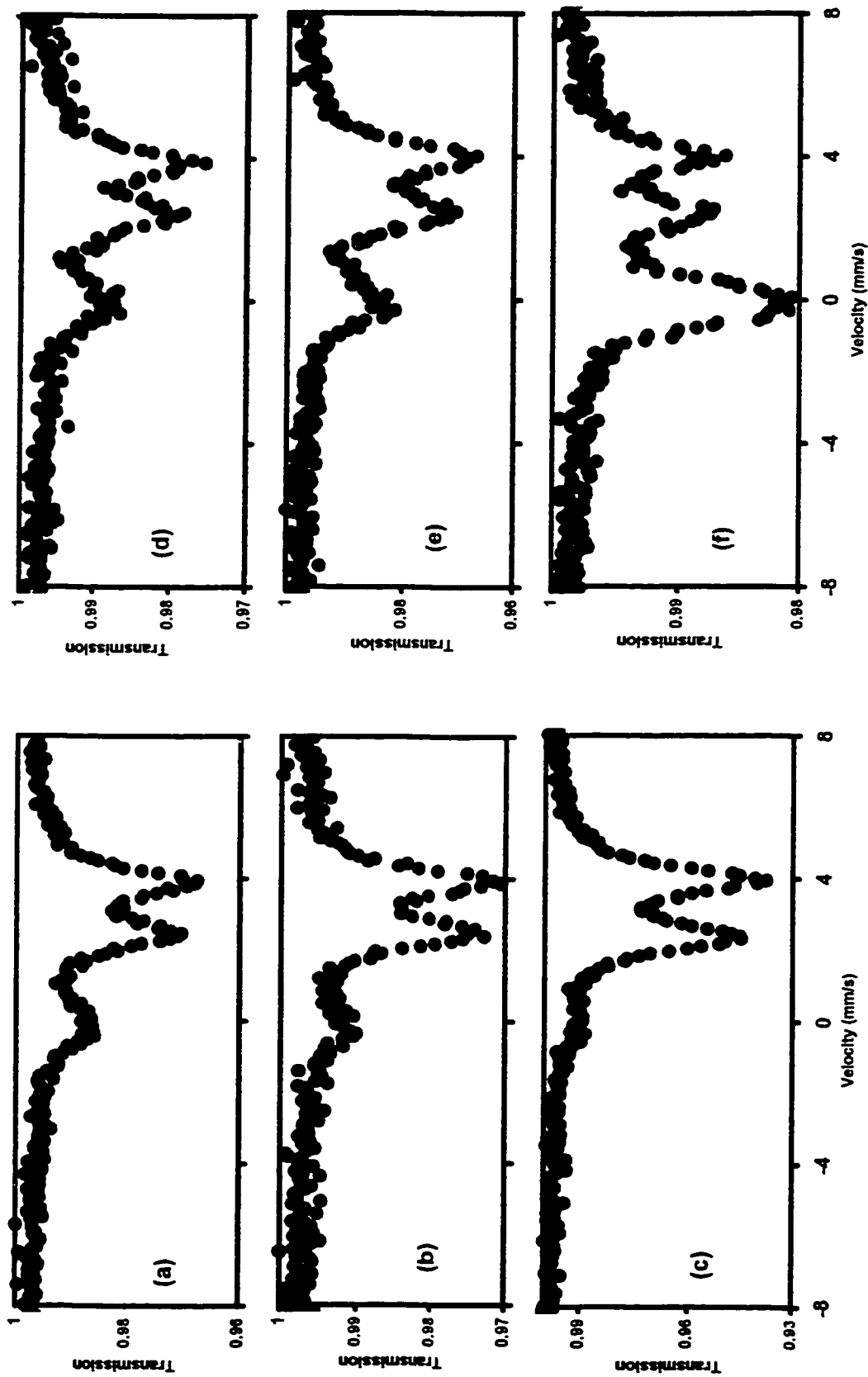
Figure 52: Mössbauer spectrum of the various phases of $PbSnF_4$: (a) α-$PbSnF_4(aq_1)$, (b) α-$PbSnF_4(ssr)$, (c) o-$PbSnF_4$, (d) β-$PbSnF_4$, (e) $\mu\gamma$-$PbSnF_4$, and (f) $\mu\gamma$-$PbSnF_4$ annealed for 2 hours at 200°C

SnO_2 in the materials, which is usually a few percent in the worst case, often less than 1%[28]. The larger amount of tin(IV) in the spectra of fig. 52d to 52f can be explained based on the factors that favor oxidation. Since β-PbSnF$_4$ (fig. 52d) requires heating at a higher temperature than α-PbSnF$_4$(ssr) (fig. 52b), a higher amount of tin(IV) can be expected. Milling increases the surface/bulk ratio, and thus increases the amount of tin(IV), even without heating (fig. 52e).

However, annealed $\mu\gamma$-PbSnF$_4$ combines two factors favoring oxidation, i.e. large surface area and high temperature, and therefore, a higher amount of tin(IV) could be expected (fig. 52f). However, the recoilless fraction of all phases PbSnF$_4$ is not necessarily the same, and this should be taken into account. Ordered phases like α- and o-PbSnF$_4$ are more compact, therefore they are most likely to have a more rigid lattice, thus a higher tin(II) recoilless fraction. As a result the tin(IV)/tin(II) signal ratio will be smaller, in agreement with observations (fig. 52a-52c). Since o-PbSnF$_4$ is more compact than α-PbSnF$_4$ (lower molecular volume), its tin(II) recoilless fraction could be higher, and its results in a lower tin(IV) signal (fig. 52c). Disordered systems like $\mu\gamma$-PbSnF$_4$, and maybe also in part β-PbSnF$_4$ (which is the limit of the Pb$_{1-x}$Sn$_x$F$_2$ solid solution), could be expected to be less rigid in accordance with their lower molecular volume, and therefore the lower tin(II) recoilless fraction results in a higher tin(IV) signal (fig. 52d & 52e), although the three-dimensionality of the structure β-PbSnF$_4$ should reinforce the rigidity of the structure, and therefore result in a lower increase of the Sn(IV) signal in comparison to what would be expected from the large volume.

The tin(II) signal is a large quadrupole doublet in all cases, with δ = 3.2 - 3.5 mm/s and Δ = 1.3 - 1.6 mm/s.

These values are typical of tin(II) covalently bonded to fluorine, with a highly axial stereoactive electron lone pair[16]. The lone pair contribution to V_{zz} is so high that, in many cases, the quadrupole splitting varies little with changes in coordination. It also results in similar 5s electron density being pulled away from the atom, such that for the same anion, changes in isomer shift are also small. The fact that the tin(II) signals are similar shows that the tin(II) coordination involves a stereoactive lone pair in all cases, similar to that observed in α-PbSnF$_4$ (fig. 1b)[12]. It is particularly important to learn from Mössbauer spectroscopy that the disordered systems such as $\mu\gamma$-PbSnF$_4$ (fig. 52f) contains covalently bonded tin(II) with a stereoactive lone pair on a hybrid orbital like in the case of ordered phases. This implies that tin cannot take the cubic coordination of lead, otherwise, the lone pair would not be stereoactive; it would be a 5s^2 unhybridized spherical orbital, which would make $V_{zz} \approx 0$, and thus $\Delta \approx 0$, i.e. a single tin(II) line would be observed, like in the case of SnCl$_2$ and of Ba$_{1-x}$Sn$_x$Cl$_{1+y}$F$_{1-y}$ solid solution[17,18,54-57].

4.3. REACTION OF α-PbF$_2$(s) + α-SnF$_2$(aq) VERSUS STOICHIOMETRY, STIRRING TIME AND TEMPERATURE

4.3.1. Synthesis

The reaction of α-PbF$_2$(s) + α-SnF$_2$(aq) was first carried out to check whether the α- and o-PbSnF$_4$ obtained by stirring the ground PbSnF$_4$ in H$_2$O were not due to a

reaction between α-PbF$_2$ and α-SnF$_2$ in water. As what was discussed earlier in section 4.2.7., β-PbF$_2$ stirred in an aqueous solution of SnF$_2$ showed no change upon stirring in a solution of SnF$_2$, and no PbSnF$_4$ was obtained.

However, surprisingly, a significant change of diffraction pattern was observed for α-PbF$_2$ stirred in an aqueous solution of SnF$_2$. The α-PbF$_2$ peaks are conserved and one of the peaks has its intensity strongly enhanced. Three new peaks also appear and one of them is at very low angle ($2\theta = 6.66°$)

The reaction of α-PbF$_2$ and α-SnF$_2$ was carried out at $X = \dfrac{PbF_2}{SnF_2} = 1$ for various stirring times in order to complete the reaction giving the material that has the peaks of α-PbF$_2$ and three new peaks and to know if at longer stirring times, another new phase or PbSnF$_4$ will be formed. It was observed that at a stoichiometric ratio rich in α-PbF$_2$ (from $X \geq 1$), the new material is obtained, and regardless of the length of stirring time, no change of phase is observed (i.e. no other new peaks appear) (fig. 53). However, the intensity of the enhanced peak, relative to the other peaks of α-PbF$_2$, increases fast in the first few hours (e.g. 0 to 6 hours) and then, it keeps increasing very slowly for higher reaction times. It was hoped to maybe determine that the reaction is completed when the ratio of the intensities does not change with the reaction time. However, this is made difficult by preferred orientation, which might be due to crystallite growth with increasing time. On the other hand, at a stoichiometric ratio rich in α-SnF$_2$ (from $X \leq 0.5$), α-PbSnF$_4$(aq$_2$) is obtained.
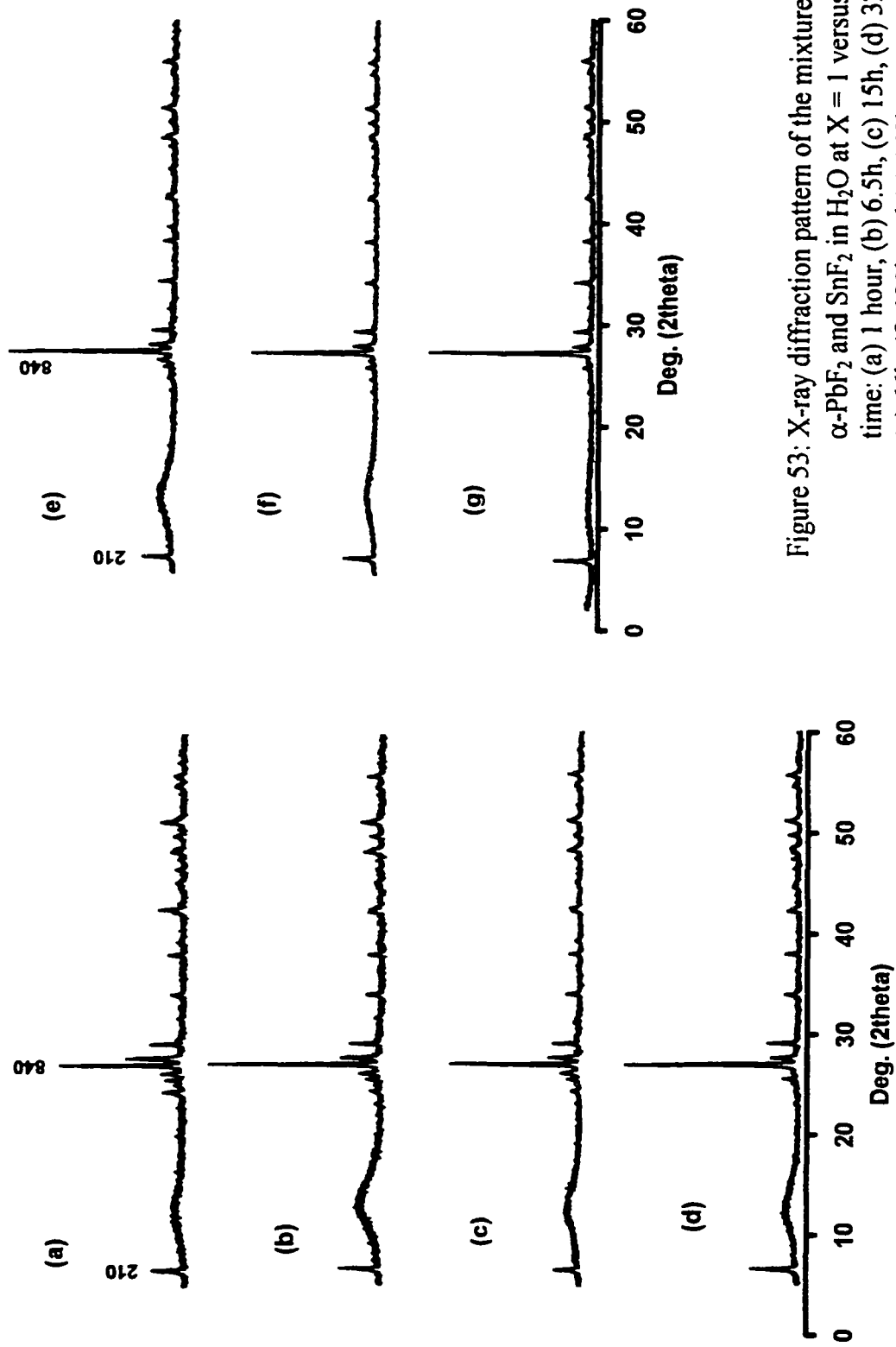
Figure 53: X-ray diffraction pattern of the mixture of α-PbF$_2$ and SnF$_2$ in H$_2$O at X = 1 versus stirring time: (a) 1 hour, (b) 6.5h, (c) 15h, (d) 32h, (e) 66h, (f) 120h and (g) 168h

4.3.2. Characterization of the new phase

4.3.2.1. Chemical analysis

The chemical analysis of the new material was carried out by AAS for the metals and using the F^- ion electrode for the fluoride ion analysis. Since the peaks of α-PbF$_2$ do not disappear, it is hard to judge when the reaction is complete, i.e. when all α-PbF$_2$ has reacted with SnF$_2$(aq) to give the new material. The reaction was assumed to be complete when the mass of the solid obtained reached a constant value (after 168 hours reaction time). The chemical analysis of the material obtained showed that it has the formula Pb$_2$SnF$_6$. In addition, DTA/TGA showed no weight loss characteristic of a hydrate, therefore the material is anhydrous.

4.3.2.2. Indexation and Unit-cell

The superstructure peak of the new material has a d-spacing four times as large as that of the peak, the intensity of which becomes very much enhanced, and which is indexed (210) in α-PbF$_2$. The superstructure, conserving the same direction of the unit-cell axes, makes the indexation of the enhanced peak to be (840), while the superstructure is indexed (210). This makes the supercell to be (4 a 4 b c), i.e. the number of MF$_2$ unit formulas and the volume are multiplied by 16.

145

4.3.3. Thermal Stability and Reactivity of the new phase

The thermal stability and reactivity of the new material obtained were checked by annealing in nitrogen and in air respectively, at different temperatures. The X-ray diffraction pattern of the samples heated for 15 hours at 100°C in air and in nitrogen are shown on figures 54b & 54c. In all cases, no significant change was observed i.e. no decomposition or formation of new phases seems to have taken place. The same observation was made for samples heated for 15 hours at 200°C under nitrogen (fig. 54d). However, after heating for 15 hours at 300°C, a significant change was observed (fig. 54e). A diffraction pattern similar to that of β-PbF$_2$ was obtained, with in addition a weak superstructure peak observed at very low angle and a splitting of the peaks with $h \neq l$, characteristic of a small tetragonal distortion (fig. 55). This is not surprising since this temperature is very close to the transition temperature of α-PbF$_2$ to β-PbF$_2$. The superstructure peak is at a lower angle than the superstructure peak of β-PbSnF$_4$, due to its larger tetragonal unit-cell: $a = 16.874$ Å, $c = 23.552$ Å, $Z_{\beta-PbF_2} = 4$, $c/a = 0.9869$ in β-PbF$_2$ axes, as compared to the following parameters for β-PbSnF$_4$: $a = 16.834$ Å, $c = 23.063$ Å, $c/a = 0.9688$.

This is the β-PbSnF$_4$ type solution Pb$_{1-x}$Sn$_x$F$_2$ with $x > 0.30$[39]. From the value of the tetragonal distortion and using the data from Dénès[39,58], the fractional substitution x of Pb by Sn can be estimated to be ≈ 0.33, which is in good agreement with the chemical composition of Pb$_2$SnF$_6$. Therefore, the following phase transition had taken place at 300°C:
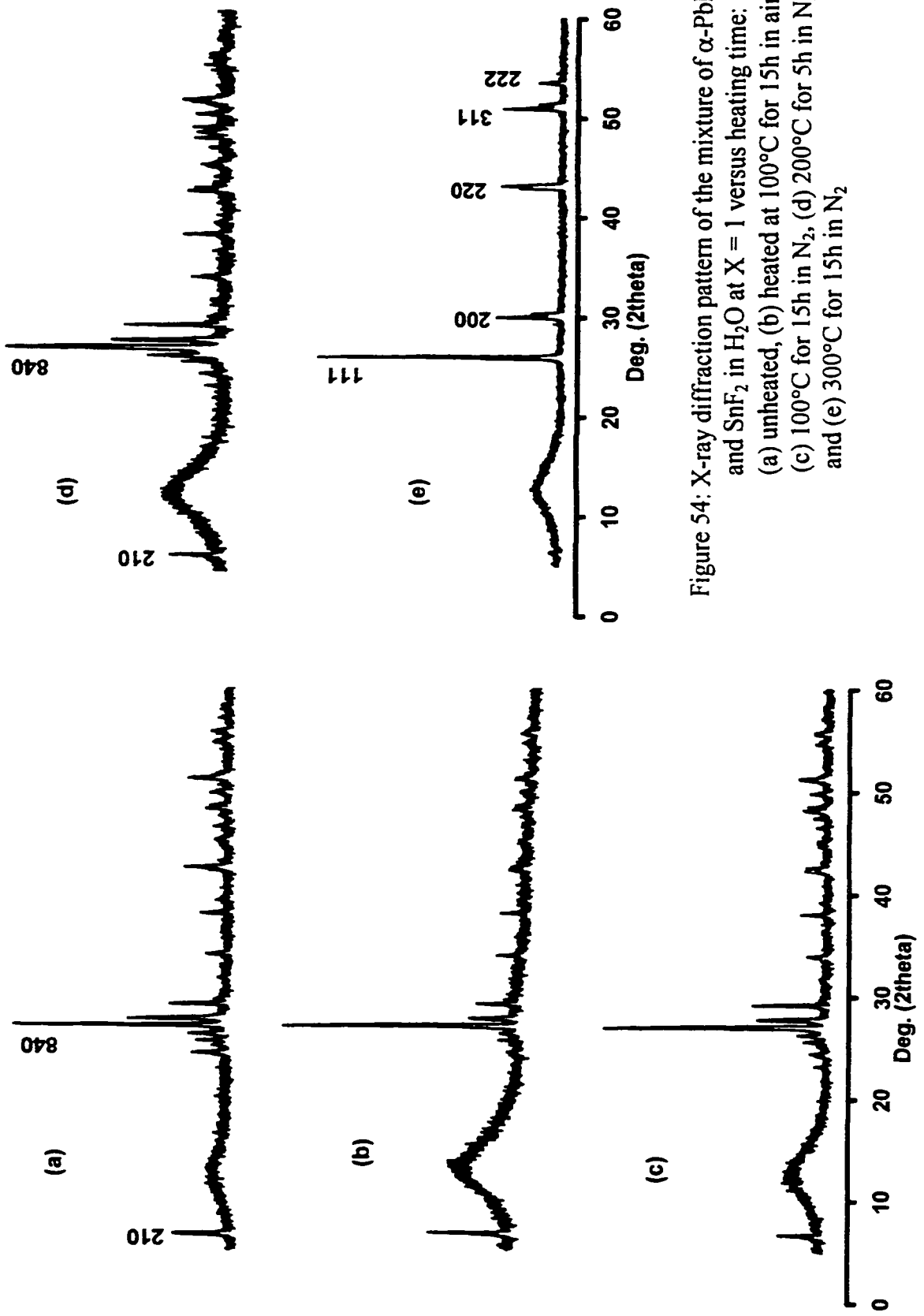
Figure 54: X-ray diffraction pattern of the mixture of α-PbF_2 and SnF_2 in H_2O at X = 1 versus heating time: (a) unheated, (b) heated at 100°C for 15h in air, (c) 100°C for 15h in N_2, (d) 200°C for 5h in N_2, and (e) 300°C for 15h in N_2

147
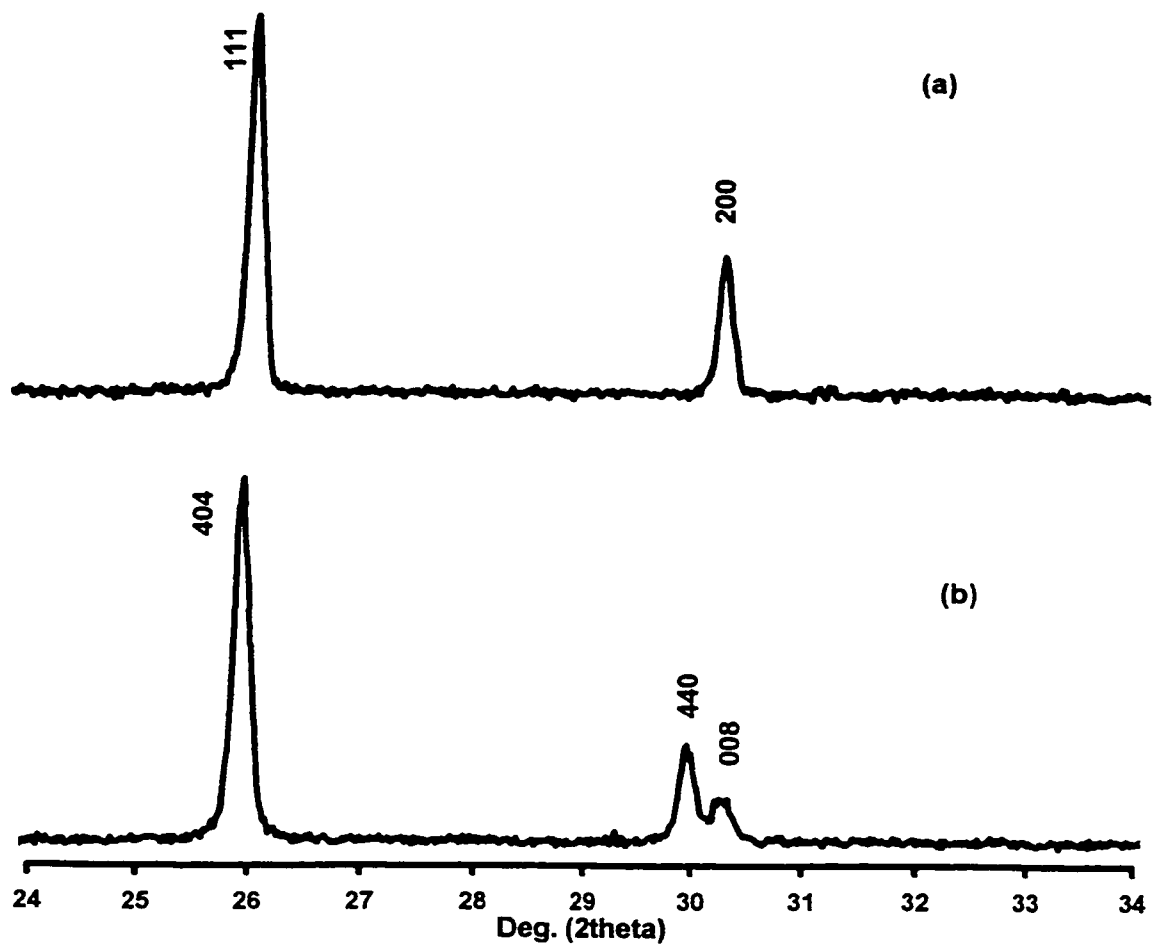
Figure 55: Details of the X-ray diffraction pattern: (a) β-PbF$_2$, and (b) Pb$_2$SnF$_6$ heated at 300°C under nitrogen

$$Pb_2SnF_6 \text{ (superstructure of } \alpha\text{-PbF}_2) \xrightarrow[N_2]{15h,300^\circ C} Pb_{1-x}Sn_xF_2 \text{ (}\beta\text{-PbSnF}_4 \text{ type)}$$
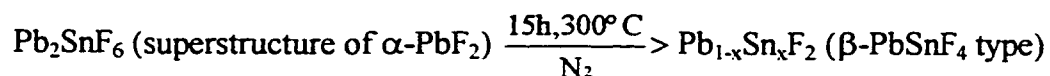
The $Pb_2SnF_6 \rightarrow Pb_{0.67}Sn_{0.33}F_2$ phase transition results in a 9.8% volume increase. Since the volume change of the transition increase, the transition is potentially reversible. This volume change is large compared to the 0.24% change at the α-PbSnF$_4$ $\rightarrow$ β-PbSnF$_4$ transition, and is 10% larger than the 8.9% volume change occuring at the α- $\rightarrow$ β-PbF$_2$ transition. It should be pointed out that the above calculation uses volumes of the phases measured at ambient temperature. The small volume increase (0.24%) measured in α- and β-PbSnF$_4$ at ambient temperature contrasts with the 1.7% increase measured in-situ at 300°C, at the transition point[4].

However, this difference is understood based on the thermal expansion coefficients of α- and β-PbSnF$_4$, which are the same in the $(\bar{a},\bar{b})$ plane for both phases, but the c parameter of β-PbSnF$_4$ shrinks rapidly on cooling from 300°C to ambient temperature, whereas c of α-PbSnF$_4$ decreases only slightly[4]. This reduces strongly the volume difference between the two phases at ambient temperature, compared to the difference measured at 300°C.

4.3.4. Ball milling of the new material versus time

The ball milling of the new material was carried out in order to know if a new phase will be obtained like in the case of PbSnF$_4$, and also to study possible microcrystallinity and randomization of the particle orientation.

Figure 56 shows that after 10s milling, the intensity of the most intense peak has started decreasing and after 20s, some broadening is observed which indicates particle fractionning. The relative intensity of all peaks keeps decreasing with increasing grinding time, while a few new very broad peaks appear. After about 10min. ball milling, all the peak of Pb_2SnF_6 have disappeared (fig. 56g). The new X-ray diffraction pattern obtained is similar to that of $\mu\gamma$-PbSnF$_4$ obtained by ball milling any other phase of PbSnF$_4$, i.e. it has a pattern similar to β-PbF$_2$, with highly broadened lines. Therefore, Pb_2SnF_6 undergoes a transformation to microcrystalline β-PbF$_2$-like phase resulting in complete disorder, like when PbSnF$_4$ is ball milled. The complete transformation requires a minimum of 10min., which is much longer than what is required by PbSnF$_4$ (50s for α- and o-PbSnF$_4$, 5min. for β-PbSnF$_4$).

The unit-cell parameter of ball milled Pb_2SnF_6 is 5.936Å (Table IX) which is within experimental error, the same as for β-PbSnF$_4$ (5.937 Å). This is not surprising since both phases have the same structure. The volume change on milling is much higher for Pb_2SnF_6 (9.554%) than for β-PbSnF$_4$ (2.698%). This is due to the fact that the structure of Pb_2SnF_6 is the same as for α-PbF$_2$ (with, in addition a superstructure), which is a more condensed phase than β-PbF$_2$ and the β-PbSnF$_4$, the structure of which is derived from β-PbF$_2$. The volume difference between the milled phases (β-PbF$_2$ like structure) and crystalline β-PbF$_2$ is slightly smaller for Pb_2SnF_6 (0.616%) than for β-PbSnF$_4$ (0.659%). The reason is the higher lead content in Pb_2SnF_6 (67% of the metal) than in β-PbSnF$_4$ (50% of the metal) since the volume per MF$_2$ unit is higher in crystalline $Pb_{0.67}Sn_{0.33}F_2$ than in β-PbSnF$_4$[58].
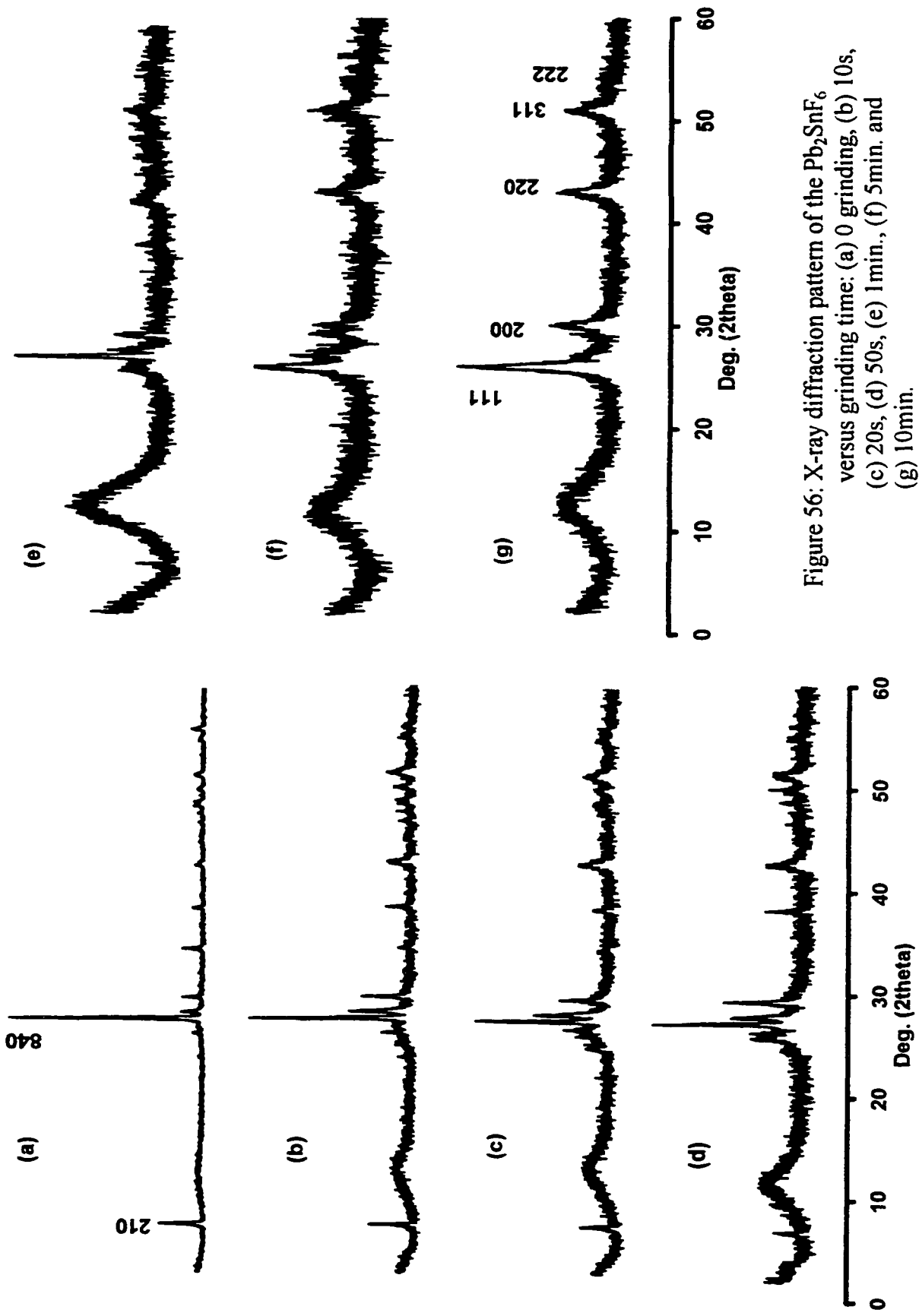
Figure 56: X-ray diffraction pattern of the Pb_2SnF_6 versus grinding time: (a) 0 grinding, (b) 10s, (c) 20s, (d) 50s, (e) 1min., (f) 5min. and (g) 10min.

The average particle size of μ- $Pb_{0.67}Sn_{0.33}F_2$ (117 Å) is similar to that of $\mu\gamma$-PbSnF$_4$ (117 – 134 Å).

4.4. CONCLUSION

Ball milling all phases of PbSnF$_4$ results in what looks like identical materials which have an X-ray diffraction pattern that looks like that of microcrystalline β-PbF$_2$, i.e., cubic Fm3m, with a unit-cell parameter that is a function of the starting phase of PbSnF$_4$ and is in all cases clearly larger than that of β-PbF$_2$. The particle size of the microcrystalline phase is similar in all cases ($\approx$120 – 130 Å average particle diameter). In all forms of α-PbSnF$_4$ and in o-PbSnF$_4$, the grinding time required to obtain this result is identical and very short (50s). This suggests that the strain has little influence on the efficiency of grinding since α-PbSnF$_4$ (aq$_1$) and (aq$_2$) are highly strained when α-PbSnF$_4$ (ssr) has none and o-PbSnF$_4$ obtained at high VR has much less than α-PbSnF$_4$ (aq$_1$) and (aq$_2$), and nevertheless, the same grinding time is required to get the X-ray diffraction pattern that looks like microcrystalline β-PbF$_2$. However, the case of β-PbSnF$_4$ is different. Although it gives ultimately the same results, i.e. a diffraction pattern like that of β-PbF$_2$, the time required to achieve it is much longer, i.e. ca. 5min., which is six times as long as for the other PbSnF$_4$ phases. This is probably due to the structure of each phase and their bond strength. Based on our observations of the $\alpha \rightarrow$ o-transition and the shape of the particles (from SEM), it is highly likely that o-PbSnF$_4$ has a sheet-like structure very similar to that of α-PbSnF$_4$, with sheets of lone pairs replacing sheets of fluorine atoms, which have moved to adjacent F$_8$ cubes not containing a metal atom.

On the other hand, since the β → γ-transition of PbSnF$_4$ is reversible with very little hysteresis, if any, it is likely that β-PbSnF$_4$, like γ-PbSnF$_4$ (isotypic to β-PbF$_2$ with complete Pb/Sn disorder), also has no such sheets of lone pairs and has the regular fluorite-type fluoride ion lattice, with local distortions. This would explain the sluggishness of the α → β-transition, and more particularly of the reverse transition (β → α) such that the β-phase can be quenched to ambient temperature[4]. The absence of layers of lone pairs makes it such that it is not a layered structure. This makes the overall bonding three-dimensional, and therefore stronger, which makes it much more resistant to changes upon milling, although the stereoactive lone pair still prevents bonding in the lone pair direction.

It appears that since the micro-β-PbF$_2$ like phase is actually microcrystalline PbSnF$_4$, and since it shows no type of Pb/Sn ordering, or ordering between different F sites, it is similar to γ-PbSnF$_4$, and therefore, we call it μγ-PbSnF$_4$ i.e. microcrystalline γ-PbSnF$_4$. Crystalline γ-PbSnF$_4$ cannot be quenched to RT since it reversibly gives β-PbSnF$_4$ upon cooling at ca. 380°C[4]. The reason μγ-PbSnF$_4$ is stable at ambient temperature, at least over several weeks, might be due to the large number of crystal defects which are most likely created upon milling. Stabilization of high temperature phases by quenching of crystal defects is a well known phenomenon. For example, zirconia ZrO$_2$ is monoclinic at ambient temperature, tetragonal (distorted fluorite type) above and cubic just below melting, at ca. 3000°C[37]. Chemical creation of anion vacancies by substituting some Zr with lower valence cations, e.g. Y, stabilizes the tetragonal or cubic phase at ambient temperature, and such a solid solution e.g. Zr$_{1-x}$Y$_x$O$_{2-x/2}$ is called "stabilized zirconia". Such high temperature phases stabilized by

defects are often metastable and slowly revert back to the stable phase as a sufficient number of defects are annealed. This seems to be the case of $\mu\gamma$-PbSnF$_4$, which partly converts back to α-PbSnF$_4$ over several weeks.

Overgrinding of the sample does not result in further microcrystallinity. The unit-cell parameter of each sample of $\mu\gamma$-PbSnF$_4$ is a function of the starting PbSnF$_4$ phase, and each keeps the memory of its origin. Upon annealing at 200°C, all give α-PbSnF$_4$. The same is obtained by stirring in water, except the sample originating from o-PbSnF$_4$, which gives back o-PbSnF$_4$. Milled PbF$_2$ + SnF$_2$ gives α-PbSnF$_4$ at 200°C, when non-milled mixtures require 250°C. β-PbF$_2$ gives α-PbF$_2$ upon milling and vice versa. Reactions of α-PbF$_2$ + SnF$_2$ in water at a stoichiometric ratio $X \geq 1$ gives a new phase rich in lead, Pb$_2$SnF$_6$, which is a superstructure (4a 4b c) of α-PbF$_2$ and at a ratio of $X \leq 0.5$, α- PbSnF$_4$ (aq$_2$) is obtained. On the other hand, β-PbF$_2$ does not react with aqueous solutions of SnF$_2$.

Ball milling of Pb$_2$SnF$_6$ results in a material identical to ball milled PbSnF$_4$, i.e. a microcrystalline β-PbF$_2$ like material, which is probably the Pb$_{1-x}$Sn$_x$F$_2$ solid solution ($x \approx 0.33$) stabilized in cubic symmetry by the lattice defects like $\mu\gamma$-PbSnF$_4$. The fact that the milling time required to achieve this (10min.) is longer than for PbSnF$_4$, even longer than for β-PbSnF$_4$ (5min.) can be explained by the fact that Pb$_2$SnF$_6$ is richer in lead than PbSnF$_4$, and thus has a stronger lattice, which requires more mechanical energy for reorganizing the solid and creating a sufficient number of defects to stabilize the disordered microcrystalline μ-Pb$_{1-x}$Sn$_x$F$_2$ phase. Ball milled Pb$_2$SnF$_6$ is very similar to ball milled β-PbSnF$_4$, however, it involves a much higher volume change, 9.554%, which

explains the longer milling time required.

Upon annealing non-ground Pb_2SnF_6 under nitrogen at 300°C, a tetragonal distortion of β-PbF_2 lattice is observed. The material obtained is tetragonal of the β-$PbSnF_4$ type, $Pb_{1-x}Sn_xF_2$ with $x \approx 0.33$, therefore the phase transition $Pb_2SnF_6 \rightarrow Pb_{1-x}Sn_xF_2$ (tetragonal) ($x \approx 0.33$) has taken place and involved a 9.8% volume change, which is a little higher than that of the α- $\rightarrow \beta$-PbF_2 transition, and much higher than that of the α- $\rightarrow \beta$-$PbSnF_4$ transition, in accordance with their crystal structures.

CHAPTER 5

RESULTS AND DISCUSSION: STUDY OF THE PHASE TRANSITIONS IN PbSnF₄ VERSUS TEMPERATURE AND TIME

5.1. INTRODUCTION

The recent fabrication of an oxygen sensor using $PbSnF_4$[25,26] makes it necessary to use a well characterized material, that is stable over the lifetime of the sensor. Any phase transition could lead to a modification of the properties of $PbSnF_4$, and a degradation of the sensor performances. However, there are many ways of preparing $PbSnF_4$, giving variable results, and the phase transitions published in the literature, some sluggish, raise doubts about the stability of $PbSnF_4$ unless a well stable and well characterized phase is used. The purpose of this work was to examine the possible phase changes taking place versus time and temperature. Other properties such as crystallinity, presence of strain, and preferred orientation can also alter the properties of polycrystalline samples, therefore, how they vary with time at various temperatures was also studied.

Second order phase transitions ($\Delta H = 0$; $\Delta Cp \neq 0$; $\Delta_a = \Delta_b = \Delta_c = \Delta v = 0$; $\alpha_a \neq \alpha_b \neq \alpha_c \neq \alpha_v \neq 0$), where α_a, α_b, and α_c are the linear expansion coefficients along the three axes of the unit-cell and α_v is the volume expansion) are perfectly reversible without hysteresis, by definition. They are continuous transitions preceded by premonitory effects and the space group of the lower symmetry phase is a subgroup of

the space group of the high temperature phase. This is the case of the β-SnF$_2$ → γ-SnF$_2$ phase transition[59,60] on heating and of the α → o-PbSnF$_4$ upon addition of HF to the SnF$_2$ solution used for the synthesis. On the other hand, first order phase transitions show discontinuities ($\Delta H \neq 0$; $\Delta_a \neq \Delta_b \neq \Delta_c \neq \Delta_V \neq 0$) although these can sometimes be so small as to escape detection. In addition, first-order phase transitions do not require group/subgroup relationships and can give rise to hysteresis when cycling around the transition point, but not necessarily so. For example, both the α → β and β → γ transitions of PbSnF$_4$ are first order ones. However, the β → γ transition shows no detectable discontinuity of the unit-cell parameters, although $\Delta H \neq 0$, and no measurable hysteresis was observed by X-ray diffraction[4], although about 1°C hysteresis was measured by neutron diffraction[6]. On the other hand, at the α → β transition, the c parameter and the volume increase while a shows no discontinuity. In addition, a very large hysteresis exists, such that, upon quenching, β-PbSnF$_4$ can be stabilized at ambient temperature in the metastable state for a long time (up to several months)[4]. The same is observed for the α-PbF$_2$ → β-PbF$_2$ transition. Other sequences of phase transitions in PbSnF$_4$ have been published by another group[3,5], particularly involving an orthorhombic to tetragonal, or monoclinic to tetragonal transition at 80°C, held responsible for the change of activation energy for the F$^-$ion transport in PbSnF$_4$. We have recently observed the same break of activation energy at ca. 80 °C[21,22]. In order to check the stability of each phase of PbSnF$_4$ versus time and versus temperature, and particularly, in order to check what happens to o-PbSnF$_4$ upon heating, i.e. o → α-PbSnF$_4$ or o → β-PbSnF$_4$, and characterize the phase transition at 80°C, we have carried out a study of the phase

157

transitions of PbSnF$_4$ versus temperature and time. Samples of each phase were heated versus time at selected temperatures and then studied by X-ray diffraction. In addition, the samples were studied by DTA in order to observe any phase change that would show a detectable enthalpy.

5.2. X-RAY DIFFRACTION

The X-ray powder diffraction was carried out on the different phases of PbSnF$_4$ versus temperature and time. This technique was used due to its sensitivity to lattice distortions and the presence of superstructures and therefore is very powerful for detecting and characterizing phase transitions. The behaviour and stability of each phase and possible transitions versus time upon heating at constant temperature was studied. KCl was used as an internal standard for line position and for linewidth.

5.2.1. α-PbSnF$_4$(aq$_1$) heated at different temperatures versus time

In order to test its stability relative to o- and β-PbSnF$_4$, α-PbSnF$_4$(aq$_1$) was heated at various temperatures i.e. 100°C - 290°C for times varying from 1 to 48 hours. The (110) peak α-PbSnF$_4$(aq$_1$), precipitated from aqueous solution is broad due to strain in ($\bar{a},\bar{b}$). It was observed to get narrower after heating at 100°C, therefore, the strain has been partially annealed (fig. 57a & 57b). In addition, a drastic decrease of the (00l) peaks is observed, which shows a considerable decrease of preferred orientation. Heating at 150°C for 1 hour, is sufficient to achieve the same result as at 100°C for

Figure 57: Room temperature X-ray diffraction pattern of α-PbSnF$_4$(aq$_1$) heated for various times at various temperatures: (a) unheated; (b) 100°C, 24h; (c) 100°C, 48h; (d) 150°C, 1h; (e) 200°C, 1.5h

24 hours, therefore strain annealing and particle breaking are fast at that temperature (fig. 57d). The same is true after heating for 1.5 hours at 200°C; the (110) peak gets narrower faster and the (00l) peaks get depressed faster; this is due to the stress being annealed and faster particle breakage at higher temperatures (fig. 57e). In addition, the intensity of the (00l) peaks decrease drastically upon heating even moderately (e.g. 24 hours at 100°C) showing that the preferred orientation of the particles has considerably decreased, probably due to fractionning of the sheets into smaller sheets of similar thickness. This breakage in ($\bar{a}, \bar{b}$) probably takes place when the strain, which is also in ($\bar{a}, \bar{b}$), is annealed. After 24.5 hours at 200°C (fig. 58b), the intensity of the (00l) peaks has been reduced further, therefore, much less preferred orientation is present. Further heating of the sample up to 48 hours at 200°C brings little further changes (fig. 58c). After heating at 250°C for 24 hours, however, further changes have taken place: partial transformation to the β-PbSnF$_4$ is observed (fig.58d). The (110) peak of α-PbSnF$_4$ as shown on fig. 58d, remains very narrow but the (004) peak, on the other hand, has become very poorly defined which is probably due to the complex reorganization taking place with a change in the ordering along $\bar{c}$. The best test for partial transformation of β-PbSnF$_4$ is the presence of (101)$_\beta$ at very low angle (ca. 7°(2θ)).

The $\alpha \rightarrow \beta$ transition can also be characterized by a decrease of the (00l)$_\alpha$ peaks and the growth of the (00l)$_\beta$ peaks at lower angles (in the range of 250-290°C). This was observed at the $\alpha \rightarrow \beta$ transition reported to take place in the temperature range of 260°-290°C when α-PbSnF$_4$ was heated and the X-ray diffraction pattern recorded in situ at high temperature, however, no such disorder along $\bar{c}$ was reported[4].
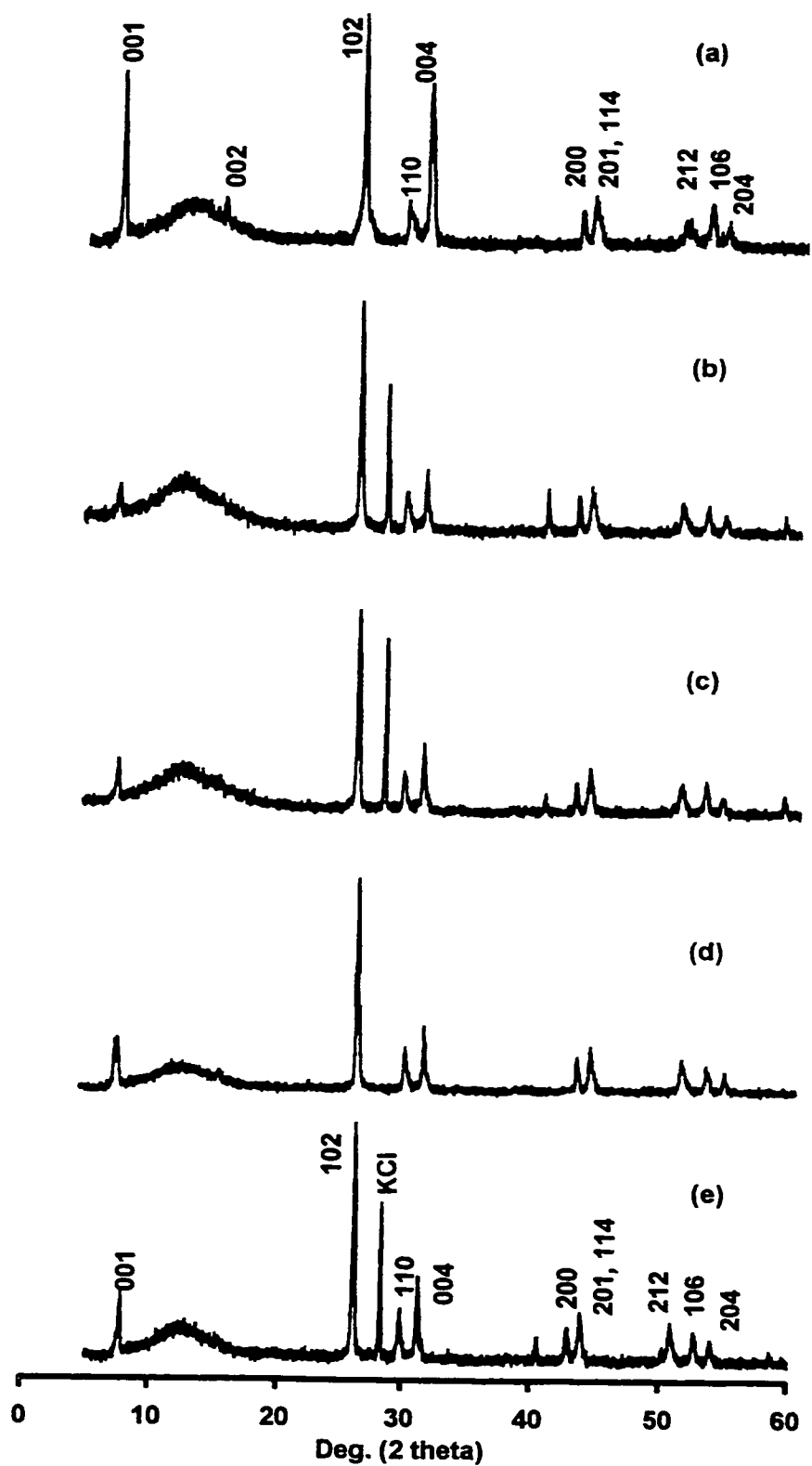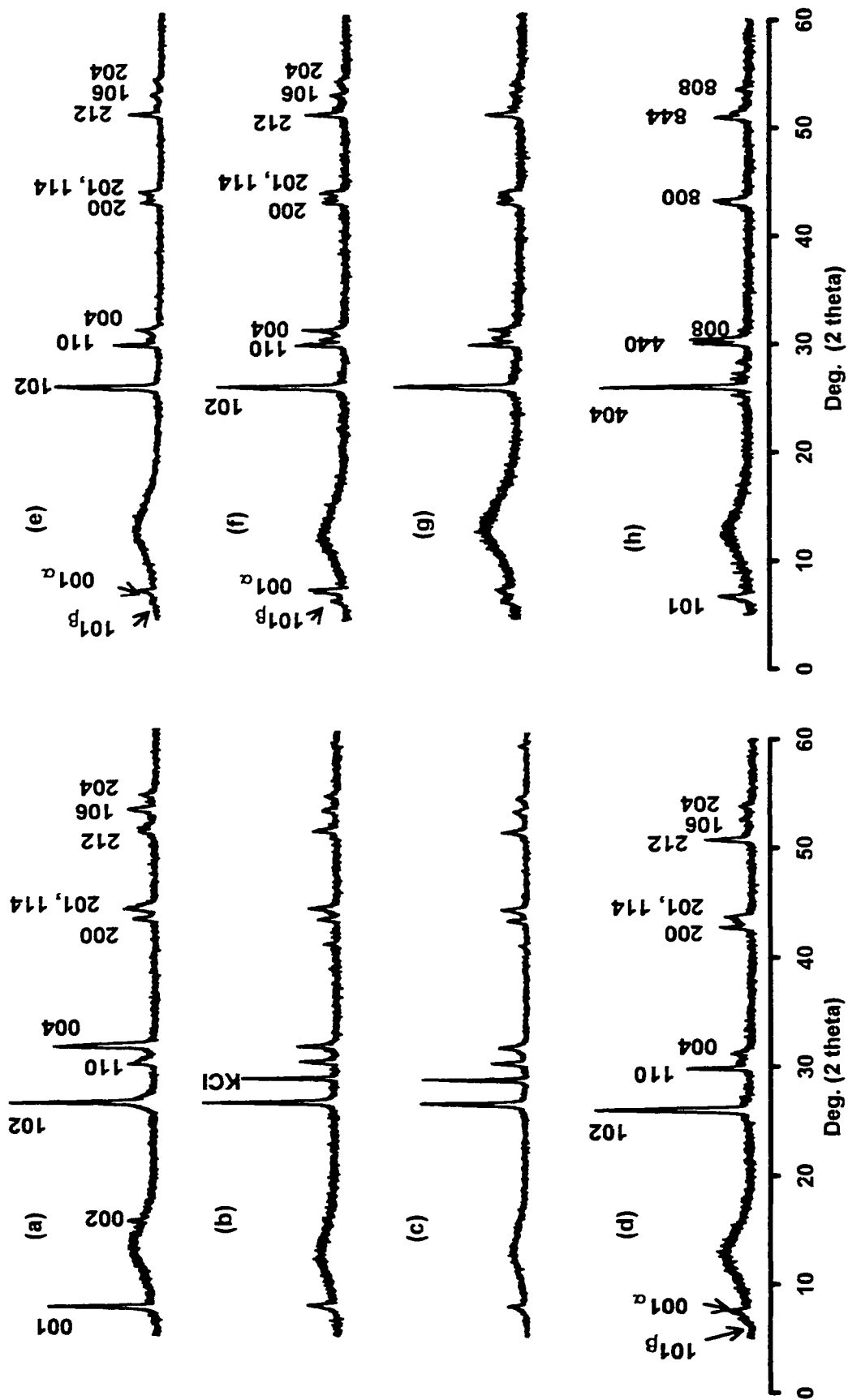
Figure 58: Room temperature X-ray diffraction pattern of α-PbSnF₄(aq₁) heated for various times at various temperatures: (a) unheated; (b) 200°C, 24.5h; (c) 200°C, 48h; (d) 250°C, 24h; (e) 270°C, 13h; (f) 280°C, 24h; (g) 290°C, 5h; (h) 290°C, 24h

However, it is not expected that the two methods should give exactly the same results since partial transformations can take place on quenching and the heating times are not necessarily the same, so this study also shows that heating and quenching does not necessarily substitute taking measurements in situ versus temperature, due to the additional effect of quenching, and the aging that follows, due to the metastability of some quenched phases.

Heating the sample for 13h at 270°C (fig. 58e) or 24h at 280°C (fig. 58f) or 5h at 290°C (fig. 58g) bring about little further changes since mixture of α and β are observed in various preparations with variable amounts of disorganization along $\bar{c}$. At 290°C after 24h. no more α-PbSnF$_4$ is observed since the $(001)_\alpha$ peak has disappeared and only $(101)_\beta$ characteristic of the β-PbSnF$_4$ superstructure is observed at low angles (fig. 58h) which is in agreement with the literature[4]. The tetragonal distortion seems to be very small (c/a in β-PbF$_2$ axes = 0.9905; compared to 0.9606 in β-PbSnF$_4$ and 0.9584 in unheated α-PbSnF$_4$) if the two main peaks between 30 and 31°(2θ) are indexed (440) and (008) respectively. However, the diffraction pattern shows a small peak at 31.2°(2θ), where the (008) peak of β-PbSnF$_4$ should be, but this peak is much stronger when β-PbSnF$_4$ is prepared according to literature procedure (reaction III)[4]. In the diffraction pattern of fig. 58h, two β-PbSnF$_4$ type phases can be considered as having a slight difference in the a parameter (a = 16.8104Å and a' = 16.6512 Å) if both main peaks between 30-31°(2θ) are the (440) peak of the two phases and if the $\bar{c}$ axis of both phases is highly disordered (fig. 58d to 58h). Such a disorder along the $\bar{c}$ axis has not ever been reported, however, unit-cell changes related to the SnF$_2$/PbF$_2$ ratio in the Pb$_{1-x}$Sn$_x$F$_2$ solid

solution have already been reported[39]. It is most likely that the sample heated a 290°C

for 24h contains two phases that have different SnF_2/PbF_2 ratio and with a similar

β-PbSnF$_4$ type structure, since $a \approx b$, i.e. $c/a \approx 0.99$ would require $Pb/(Pb+Sn) \approx 0.32$,

instead of 0.50 as in PbSnF$_4$[39]. After heating for 24h, weak unidentified peaks have

appeared (fig. 58h). If these impurity peaks belong to a phase richer in SnF_2 than PbSnF$_4$

then the β-PbSnF$_4$ phase is a composition within the tetragonal β-PbSnF$_4$ type $Pb_{1-x}Sn_xF_2$

with $x > 0.30$, and if x is small enough, it could explain that c/a is close to unity.

5.2.2. o-PbSnF$_4$ heated at different temperatures versus time

The o-PbSnF$_4$ obtained at a high VR is quite strain free in the $(\bar{a},\bar{b})$ plane as can

be seen by the small linewidth of (200) and (020) (fig. 59a). Upon heating at 100°C,

(020) broadens rapidly (after just 5 hours) (fig. 59b) probably due to internal strain along

the $\bar{b}$ axis, although it could also be due to the presence of domains with different values

of b. This is somewhat similar to the asymmetric broadening of $(110)_\alpha$ towards higher

angles observed when VR increases in the $\alpha \rightarrow o$ transition (fig. 19) which seem to be

due to the broadening of (020) whereas the width of (200) does not seem to change.

After 24 hours (fig. 59c) and 48 hours (fig. 59d) at the same temperature, broadening of

(020) has increased further, and then it seems to remain quite constant for longer heating

periods (at least up to 1500 hours) (fig. 60b to 60d) whereas there is little change

observed of the (200) peak. This indicates the presence of internal strain along $\bar{b}$ or a

distribution of the values of the b unit-cell parameter, (as mentioned above). The a

163
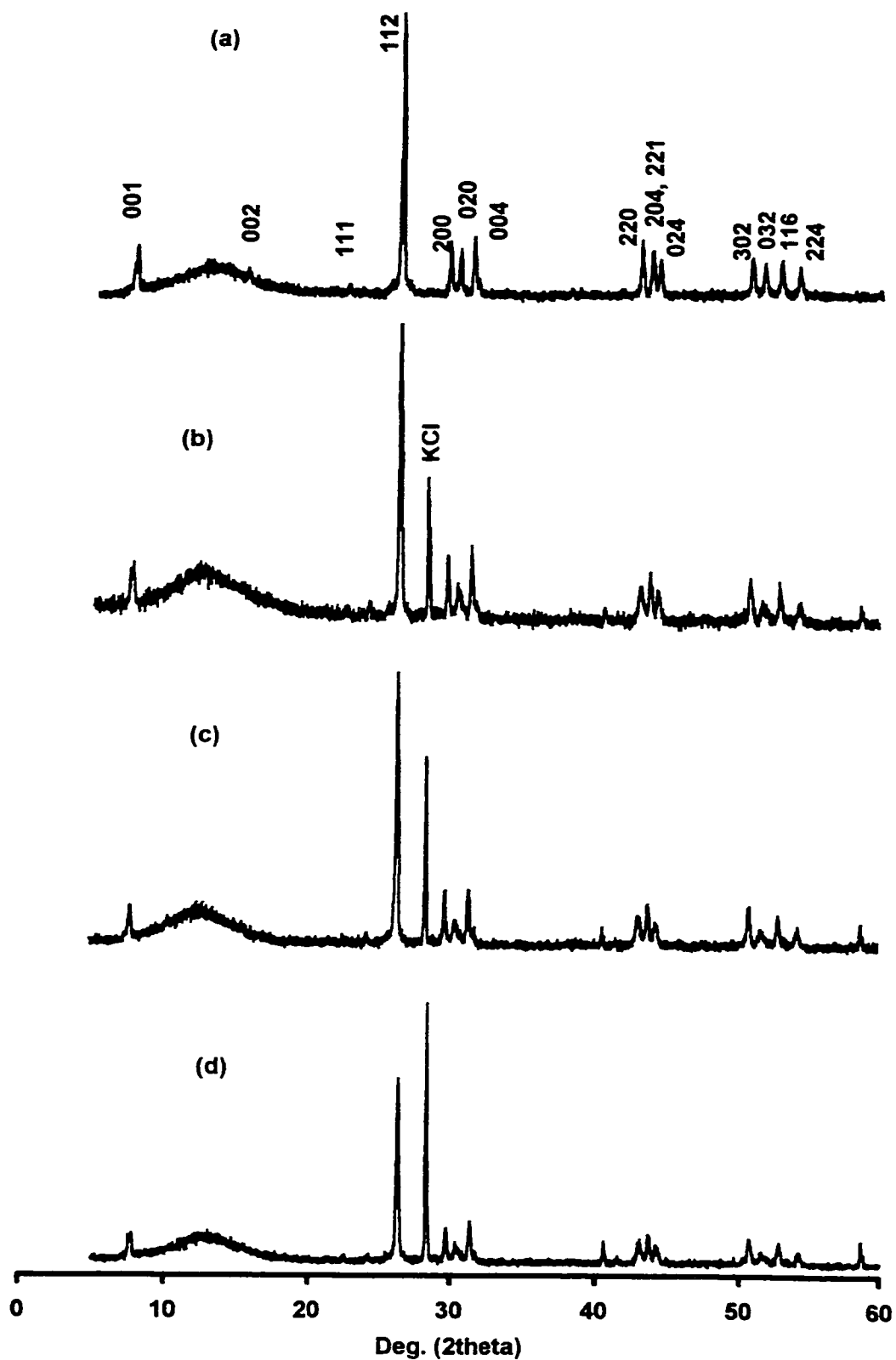
Figure 59: Room temperature X-ray diffraction pattern of o-PbSnF₄ heated at 100°C for various times: (a) unheated, (b) 5h, (c) 24h, (d) 48h
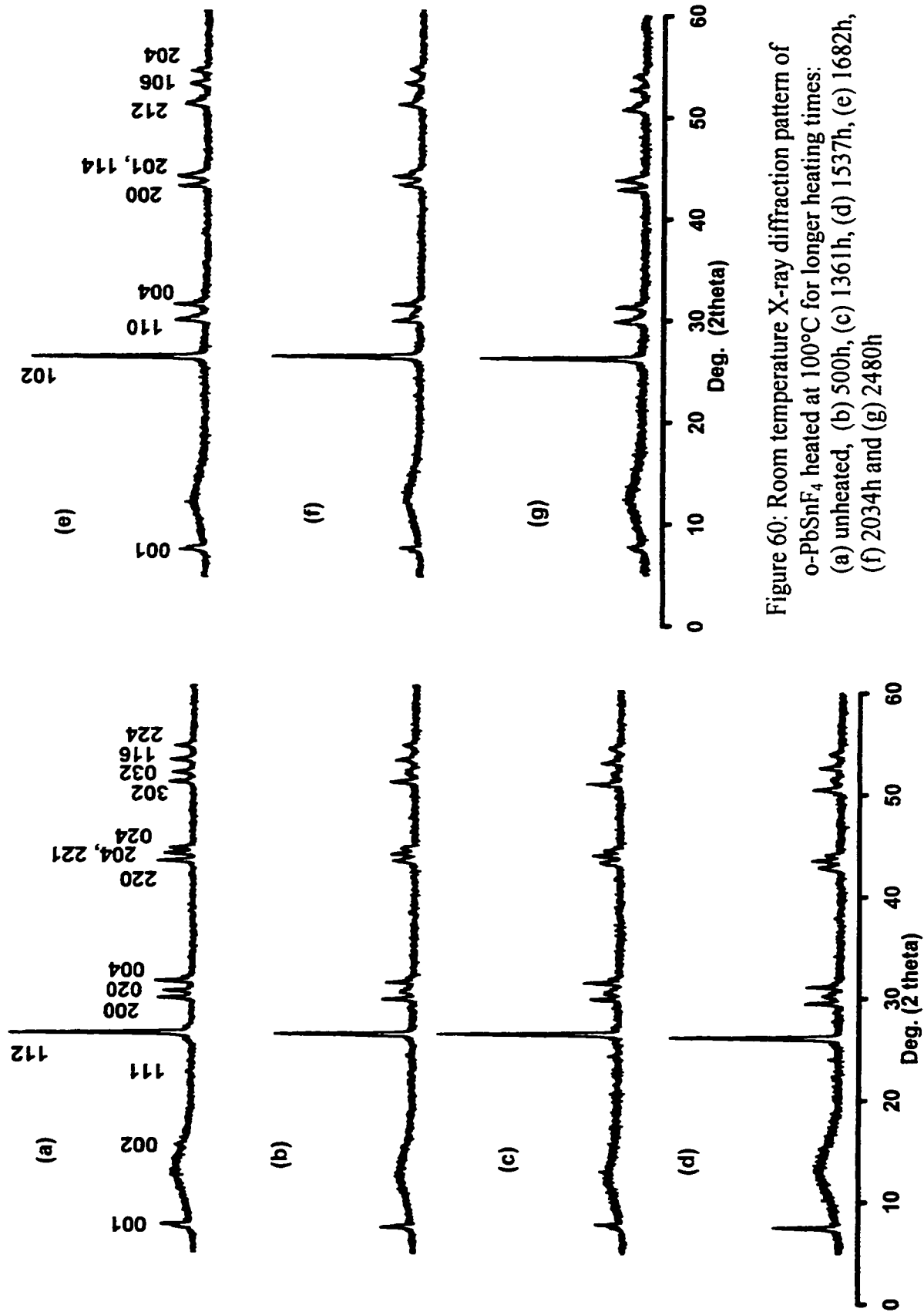
Figure 60: Room temperature X-ray diffraction pattern of o-PbSnF₄ heated at 100°C for longer heating times: (a) unheated, (b) 500h, (c) 1361h, (d) 1537h, (e) 1682h, (f) 2034h and (g) 2480h

165

parameter and the average b, however, did not change since no peak shift is observed. After 1682 hours at have coalesced to give the $(110)_\alpha$ peak of α-PbSnF$_4$ and the pattern is indexed in tetragonal. At this stage, the o → α transition has been completed. No significant additional change is observed by further heating at 100°C up to 2480h (fig. 60f & 60g).

The a parameter decreases as shown the (200) peak shift to a higher angle. On the other hand, the b parameter increases which is shown as the (020) peak shifts towards lower angles. Little motion of the (004) peak is observed, in accordance with the very minor change of the c parameter at the transition. This behaviour is in agreement with the ferroic nature of the orthorhombic to tetragonal transition.

After completion of the o → α transition, the (110) peak is broad therefore there is much strain in ($\bar{a}, \bar{b}$). Figures 61b & 61c show the behaviour of o-PbSnF$_4$ at 150°C versus heating time. The broadening of the (020) peak is no longer observed because coalescence of (200) and (020) to give $(110)_\alpha$ occurs much more rapidly. It is already well on the way after just one hour at 150°C and is complete after 3 hours (fig. 61b). The $(110)_\alpha$ peak obtained after 3 hours is highly broadened; indicating the presence of a large amount of strain. After 65.5 hours, it has narrowed down considerably (fig. 61c), therefore, this α-PbSnF$_4$ has little stress in ($\bar{a}, \bar{b}$); the stress has decreased due to annealing. In addition, since the intensity of the (001) peak changes little at the o → α transition, the preferred orientation remained the same and therefore, no growth of the ($\bar{a}, \bar{b}$) plane of the particles took place. However, the (00l) peaks are much broader (fig. 61c) which show that much disorder has appeared along $\bar{c}$, like in the case

Figure 61: Room temperature X-ray diffraction pattern of o-PbSnF₄ heated for various times at various temperatures: (a) unheated; (b) 150°C, 3h; (c) 150°C, 65.5h; (d) 200°C, 1h; (e) 200°C, 3h; (f) 200°C, 10h

of heated α-PbSnF$_4$. At 200°C (fig. 61d to 61f), the results are similar to those observed at 150°C. At longer times, (10 hours), the (110) peak characteristic of α-PbSnF$_4$ starts getting narrower, showing the beginning of the annealing of the strain, which is probably more efficient at higher temperatures.

For the samples heated for 24 hours in the range of 250-290°C (fig. 62), the following was observed:

(i) 250 to 280°C (fig. 62b to 62e) - the diffraction pattern is that of α-PbSnF$_4$, with a very narrow (110) peak and weak and broad (00l) peaks. These observations indicate that there is no strain in the $(\bar{a},\bar{b})$ plane and there is little preferred orientation, like in α-PbSnF$_4$ (ssr). However, in addition, the (00l) peaks are broadened. The samples are still α-PbSnF$_4$ as can be seen by the (00l) superstructure reflection at ca. 8°(2θ). This is different from the α-PbSnF$_4$ heated in the same conditions that gives a mixture of α and β-PbSnF$_4$ as shown on figure 58. The broadening could be due to the c parameter starting to change in order to form β-PbSnF$_4$, since c increases at the $\alpha \rightarrow \beta$ transition, i.e. the (00l) peaks shifts to lower angles. A distribution of values of c (and therefore of (00l) positions) is obtained, probably stabilized by quenching, and the sample is most likely multidomain. The very narrow (110) peak does not contradict this hypothesis since there is no discontinuity of a at the transition[4].

(ii) 290°C (fig. 62f & 62g) - The o $\rightarrow$ α transition is completed in less than one hour and the $\alpha \rightarrow \beta$ transition takes place slowly. After 24 hours, the transformation to β-PbSnF$_4$ is completed (fig. 62g) like in the case of α-PbSnF$_4$ also heated at 290°C for 24 hours. Most particularly, the tetragonal splitting appears to be very small in both

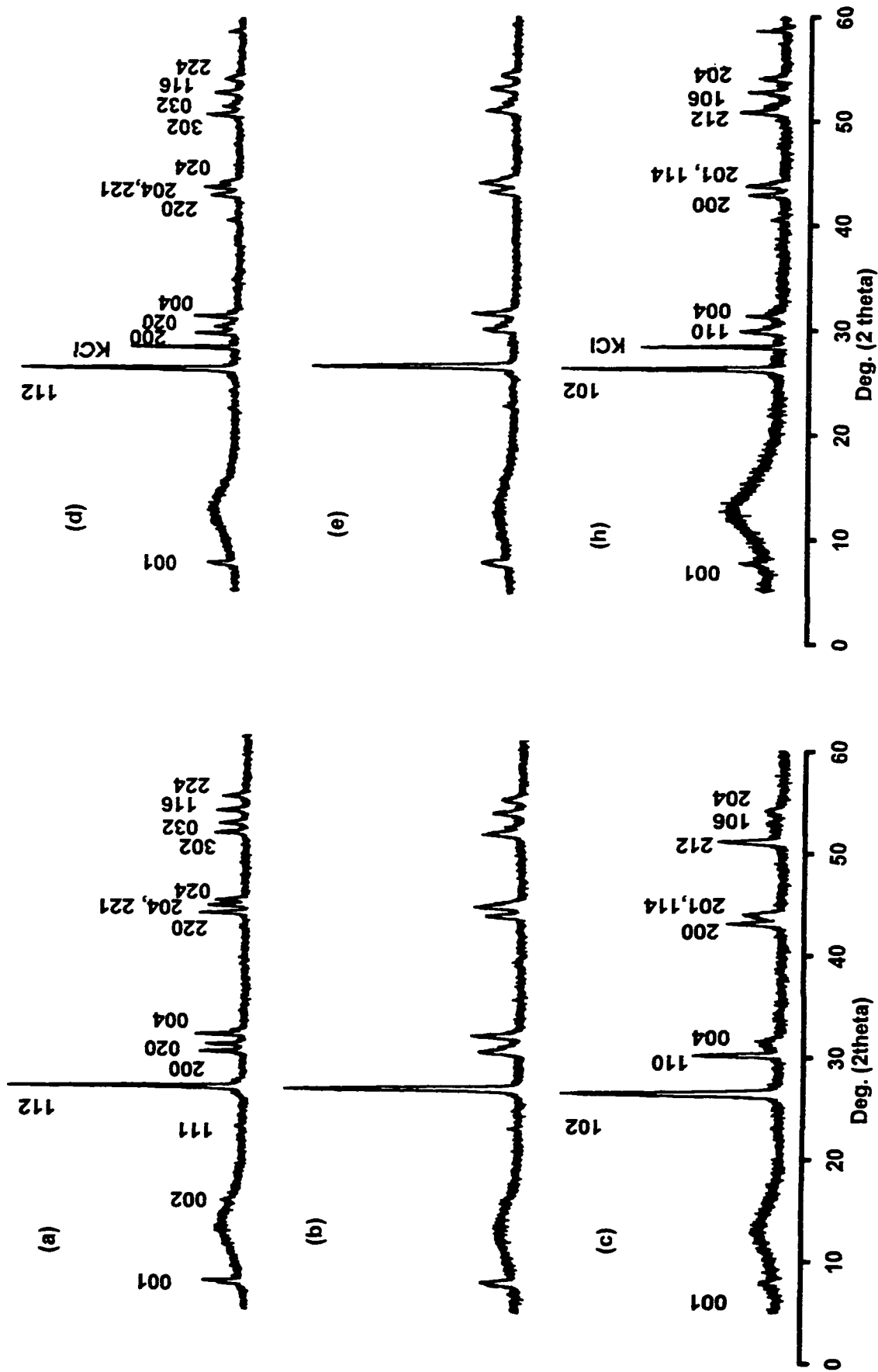Figure 62: Room temperature X-ray diffraction pattern of o-PbSnF$_4$ heated for various times at various temperatures: (a) unheated; (b) 250°C, 24h; (c) 260°C, 24h; (d) 270°C, 24h; (e) 280°C, 24h; (f) 290°C, 24h; (g) 290°C, 1h; (g) 290°C, 24h

cases (≈ 0.99), however, it is more likely that there are two values of a and the value of c is not measurable due to too much disorder. The β-phase is characterized by the superstructure reflection (101) which occurs at a lower angle than $(001)_\alpha$ and the tetragonal distortion at ambient temperature is slightly smaller, due to an increase of c, with no change of a.

From these observations, it appears that there is no direct o $\rightarrow$ β-PbSnF$_4$ transition below the $\alpha \rightarrow \beta$-PbSnF$_4$ transition temperature, i.e. $\leq 270°C$. Heating at 280° and 290°C for shorter periods of time would be necessary to check if there is a direct o $\rightarrow$ β-PbSnF$_4$ transition in that temperature range, or if α-PbSnF$_4$ is formed for a short period of time, i.e. if the sequence o $\rightarrow$ α $\rightarrow$$\beta$ takes place. However, as temperature increases above 270°C, the formation of β-PbSnF$_4$ will accelerate such that it might be impossible to differentiate between the two possibilities.

5.2.3. β-PbSnF$_4$ heated at different temperatures versus time

PbSnF$_4$ is a high temperature phase that can be quenched to room temperature, where it exists as a metastable phase[4]. Although it has been observed to be stable at ambient conditions for long periods of time (months), some changes were also noticed with time such as loss of crystallinity and line broadening. This is not surprising since a metastable phase can change uncontrollably to the stable phase. Such a spontaneous transition to the thermodynamic stable phase is usually a function of particle size, thermal history and mechanical treatments, particularly grinding. This has been previously observed for metastable β-SnF$_2$[46] which makes the observations versus

temperature and time not well reproducible. Therefore, β-PbSnF$_4$ can be expected to transform back to the α-form at any temperature below the $\alpha \rightarrow \beta$ transition temperature. i.e. < 270°C. However, the atomic motion required to undergo the $\beta \rightarrow \alpha$ transition requires energy, that is why the β phase appears like if it were stable at ambient conditions for some periods of time. This explains why samples of β-PbSnF$_4$ stored at room temperature after long periods of times (weeks or months) sometimes start changing very slowly to α-PbSnF$_4$.

The X-ray powder diffraction pattern of β-PbSnF$_4$ upon heating versus time relative to the unheated sample is shown on figure 63. Metastable β-PbSnF$_4$ is completely transformed to α-PbSnF$_4$ after heating at 250°C for 24 hours(fig. 63b). Partial transformation to the α-phase was observed at 260°C for 1 hour (fig. 63c), which shows the importance of the time factor compared to 10°C higher. The partial transformation is characterized by the broadening of $(008)_\beta$ (due to partial overlap with $(004)_\alpha$, a weakening of $(101)_\beta$, and the appearance of $(001)_\alpha$. After heating for 24 hours at 260°C (fig. 63d), transformation to stable α-PbSnF$_4$ is completed, which shows again the sluggishness of the $\beta \rightarrow \alpha$ transition. No further change is observed after 13 hours at 270°C (fig. 63e); however, after 24 hours at the same temperature, the $(00l)$ peaks are much weaker and broader (fig. 63f). This is also the case after 24 hours at 280°C (fig. 63g). The same, indicating a higher disorder along $\bar{c}$, was observed when o- and α-PbSnF$_4$ were heated at the same temperature. At higher temperature such as 290°C for 1 hour (fig. 63h), a mixture of a α- and β-PbSnF$_4$ is observed, which is in agreement with the observations on heated α- and o-PbSnF$_4$. At longer heating times, 290°C for 24 hours
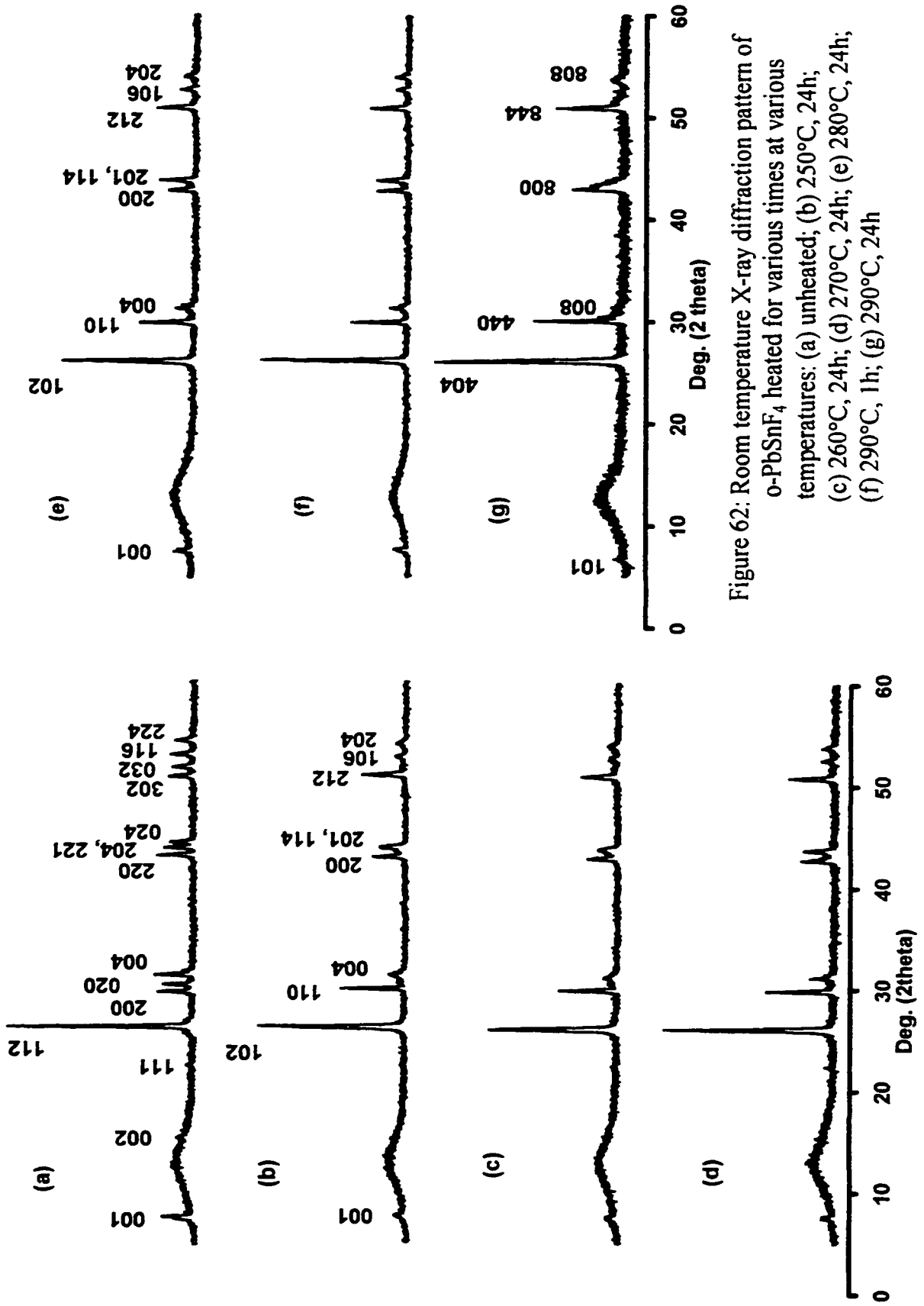
171
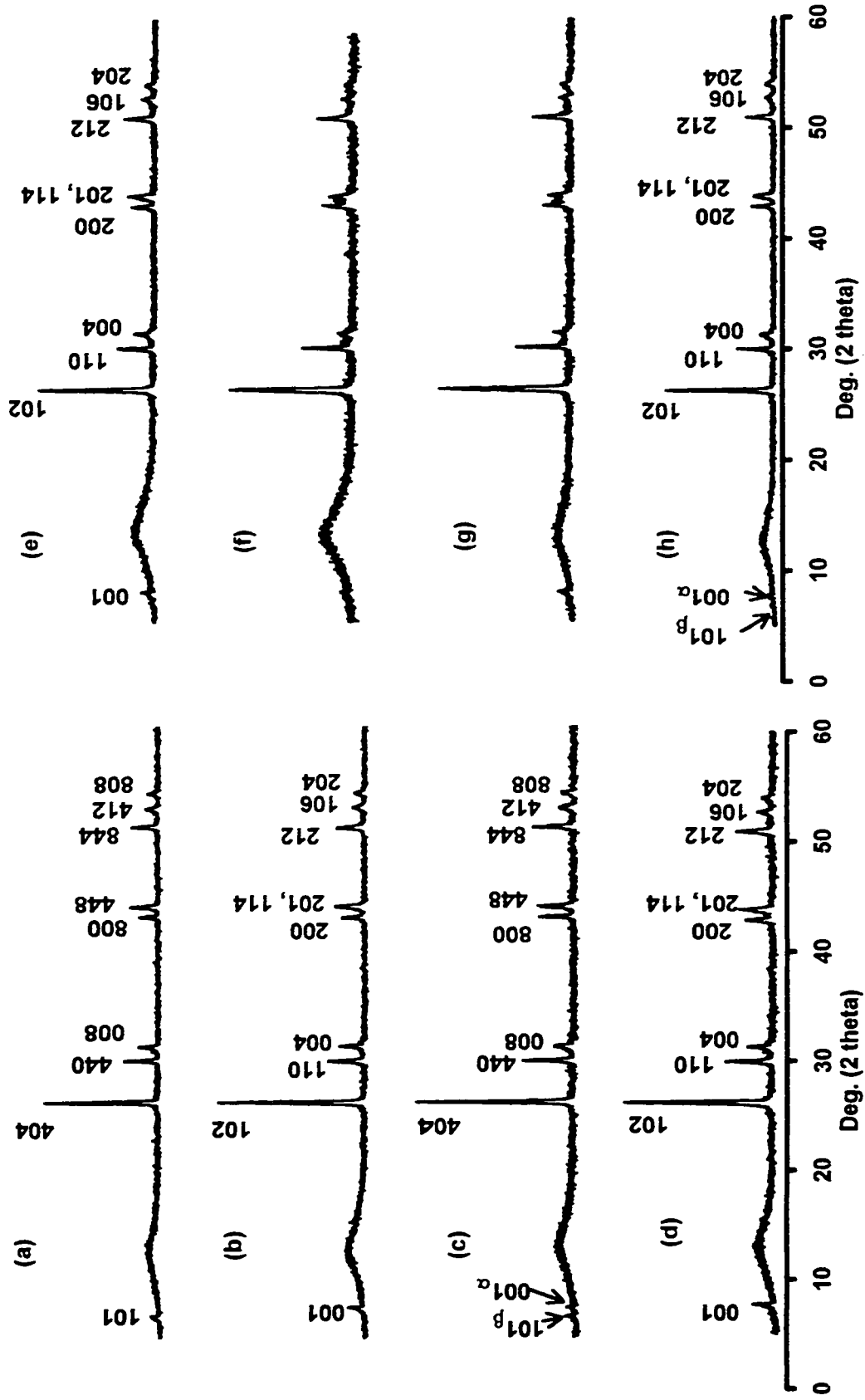
Figure 63: Room temperature X-ray diffraction pattern of β-PbSnF₄ heated for various times at various temperatures: (a) unheated; (b) 250°C, 24h; (c) 260°C, 1h; (d) 260°C, 24h; (e) 270°C, 13h; (f) 270°C, 24h; (g) 280°C, 24h; (h) 290°C, 1h

172

(fig. 64b) only α-PbSnF$_4$ and no trace of β-PbSnF$_4$ is observed. At this temperature, the $\alpha \rightarrow \beta$ transition is nearly completed when the data are recorded in situ[4]. However, since 290°C is not in the region where the β phase is well stabilized, and cooling the tubes in air is not an efficient way of quenching, so the β phase formed could have retransformed to the α-phase. This also illustrates the fact, that due to the sluggishness of the $\alpha \rightarrow \beta$ and $\beta \rightarrow \alpha$ transitions, results are not always perfectly reproducible.

5.2.4. $\mu\gamma$-PbSnF$_4$ heated

$\mu\gamma$-PbSnF$_4$ gives α-PbSnF$_4$ when heated 2 hours at 200°C. The α-PbSnF$_4$ phase obtained is strain-free in ($\bar{a}, \bar{b}$) and has little, if any, preferred orientation. See **4.2.3.** for details.

5.3. THERMAL ANALYSIS

The crystalline phases of PbSnF$_4$ were analyzed using DTA in order to study the first order transitions ($\Delta H \neq 0$) taking place on heating. Figure 65 shows the DTA curves of the different phases. The orthorhombic phase (figure 65a) is observed to have a very small endothermic peak $\approx$ 70°C which is not observed in the other phases. This is in agreement with DSC results[22] which show two overlapping broad endothermic peaks, the strongest being at 73°C. A similar but much broader peak was also observed for α-PbSnF$_4$(aq$_1$) by DSC, however, this could not be seen by DTA, probably because it is
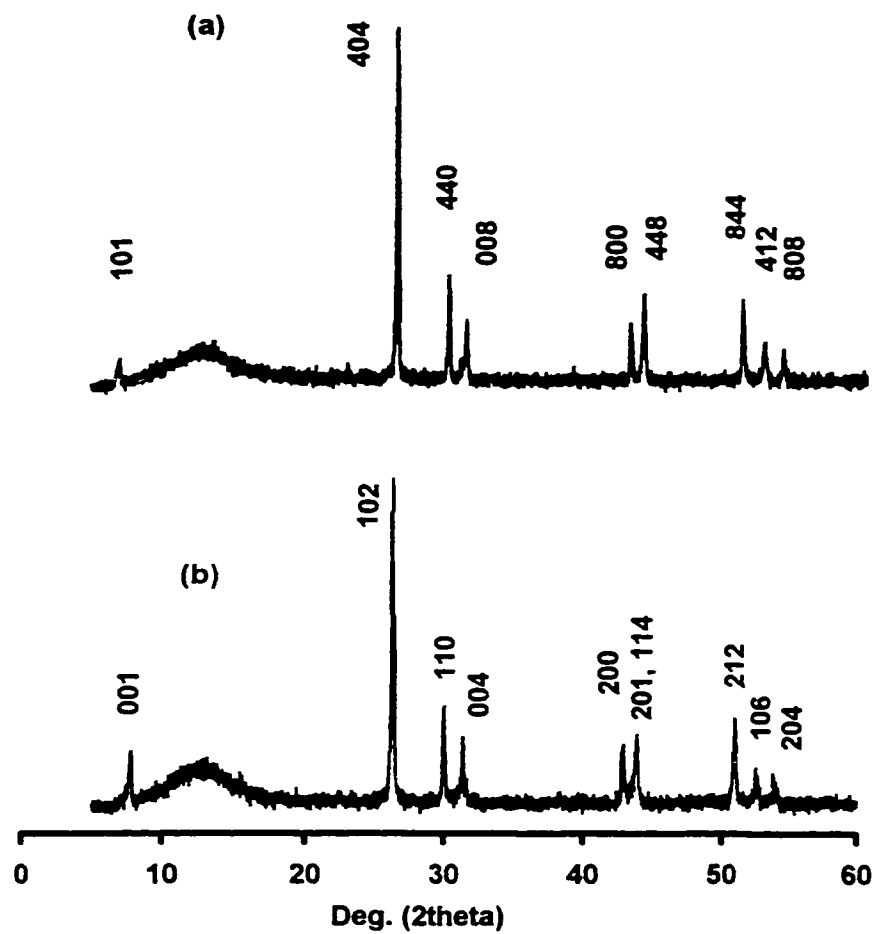
Figure 64: Room temperature X-ray diffraction pattern of β-PbSnF₄:
(a) unheated; (b) heated at 290°C for 24h

ENDO

(a)

(b)

(c)

(d)

100   200   300   400

Temperature °C
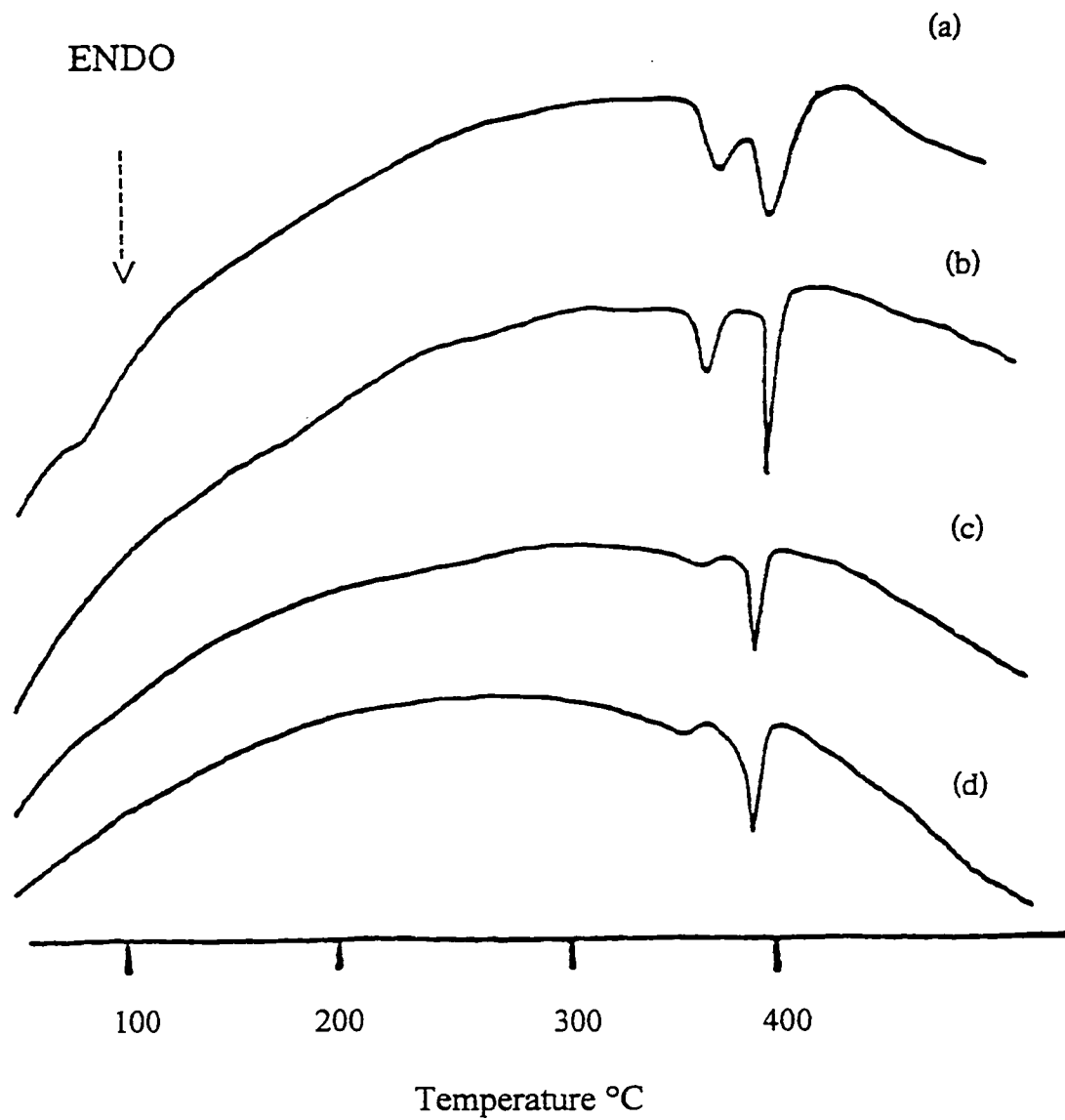
Figure 65: DTA curves of (a) o-PbSnF$_4$, (b) stressed α-PbSnF$_4$(aq$_l$), (c) unstressed α-PbSnF$_4$(ssr), and (d) β-PbSnF$_4$.

175

much more diffuse. The $\alpha \rightarrow \beta$ and $\beta \rightarrow \alpha$ transition are also too diffuse to be observed by DTA. The sluggishness of these transitions was shown by X-ray diffraction [4, and this work]. Results on the electrical conductivity measurements of both o- and α -PbSnF$_4$[3, 5, 21 and 22] show that a break in the behaviour of the conductivity was observed at ca. 80°C which results in a much lower activation energy above 80°C, and this had been interpreted as occurring at the o $\rightarrow \alpha$[3] or monoclinic $\rightarrow \alpha$ phase transition[5]. However, since our results have shown there is no phase transition at this temperature, we hypothesize that it is due to F$^-$ delocalization. Such delocalization was observed recently by neutron diffraction [10,11]. The two endothermic peaks observed at higher temperature 360-400°C are the $\beta \rightarrow \gamma$ transition and melting. We do not understand at this point why the $\beta \rightarrow \gamma$ transition is more diffuse in α-PbSnF$_4$ (ssr) and in β-PbSnF$_4$ than in α-PbSnF$_4$ (aq$_1$) and in o-PbSnF$_4$. Is it related to the fact that α-PbSnF$_4$ (ssr) and in β-PbSnF$_4$ both prepared from solid state reaction are stress free? Comparison between α-PbSnF$_4$ (aq$_1$) and o-PbSnF$_4$ shows that the narrowest $\beta \rightarrow \gamma$ peak is observed for highly stressed α-PbSnF$_4$ (aq$_1$). It results that the narrower the DTA peak for the $\beta \rightarrow \gamma$ transition, the more stressed the structure. Indeed, highly stressed α-PbSnF$_4$ (aq$_1$) has the narrowest peak, strain-free α-PbSnF$_4$(ssr) and in β-PbSnF$_4$, have a very broad peak indicating a more diffuse transition, and moderately stressed o-PbSnF$_4$ is in between. This could mean that, since a stressed structure is less stable, it can undergo the $\beta \rightarrow \gamma$ transition more easily, whereas unstressed structures are more stable and therefore, require more thermal energy, or at least prior creation of a large number of crystal defects before they can undergo the transition. However, this interpretation is just

tentative since the starting PbSnF$_4$ should have transformed to stress-free β-PbSnF$_4$ upon heating, prior to undergoing the β → γ transition, although the high heating rate used in DTA might have been too fast to allow the sluggish α → β transition to reach completion, and the stress to anneal. Indeed, comparison of fig. 63b and 63c show that heating time can be a more important factor than heating temperature for speeding up some of the β → α-PbSnF$_4$ transition, i.e. for destabilizing the β-phase. Therefore, it is quite possible that the very broad β → γ transition observed for stress-free α-PbSnF$_4$(ssr) and β-PbSnF$_4$ is due to the fact that these unstressed phase must first have enough defects to destabilize the β-phase. Creation of these defects absorbs heat, hence a much broader peak results.

5.4. CONCLUSION

The present study has shown that PbSnF$_4$ can exist under various forms, depending on the method of preparation and on various treatments. Phase changes are observed to take place spontaneously at ambient temperature and are not controllable (e.g. metastable β-PbSnF$_4$ → α-PbSnF$_4$), or under moderate heating (o → α, μγ- → α, or annealing of the strain in α-PbSnF$_4$).

When all phases of PbSnF$_4$ are heated, phase changes take place versus temperature and time. When α-PbSnF$_4$(aq$_1$) is heated at 100°C, the strain is annealed and preferred orientation is drastically reduced. Prolonged heating at 250°C triggers the beginning of the α → β transition, however, it is not completed until 290°C.

Heating o-PbSnF$_4$ at 100°C results in uniaxial strain parallel to $\bar{b}$ or a distribution of **b** parameters after just 24 hours. For over much longer periods of time, a slow conversion to non-oriented, strained α-PbSnF$_4$ is observed (completed after 2480 hours). Heating at 150°C or above anneals the strain present in $(\bar{a},\bar{b})$. Above 250°C, partial transformation to β-PbSnF$_4$ is observed, which is completed at 290°C. β-PbSnF$_4$ is obtained by quenching from 300°C or above. Its metastable conditions below ca. 290°C makes observations not exactly reproducible since its metastability can be a function of parameters which sometimes are hard to control, such as thermal and mechanical histories and particle size. Heating up to 250°C was observed to result in no change. However, at 260°C, it converts to stable α-PbSnF$_4$, and at higher temperature, it starts transforming back to β-PbSnF$_4$.

A common feature observed for all phases heated in the range 260-280°C is the broadening of the (00*l*) peaks, particularly (004), such that it becomes hardly visible in some cases. This has been attributed to disorder parallel to $\bar{c}$, which is in agreement with the observations that, with the exception of the strain and orthorhombic distortions in $(\bar{a},\bar{b})$, most of the transformations undergone by PbSnF$_4$ involve atomic shifts parallel to $\bar{c}$. The differences observed between the measurements carried at ambient conditions on quenched or annealed samples in this work, and those measured in-situ versus temperature by others are understood if one takes into account the difference of conditions and the thermal expansion coefficients of each phase.

CHAPTER 6

CONCLUSIONS

From the results presented, we can say that the addition of a very minor amount of HF in the solution of SnF_2 used for the preparation of $PbSnF_4$ is sufficient to change the symmetry of the material from tetragonal to orthorhombic. From this study, no monoclinic distortion is observed as claimed in one earlier publication.

A replacement of a very minor amount of H_2O by HF in the reaction mixture is enough to give an orthorhombic splitting. This transition occurs via an intermediate phase we call "*transitional phase*" and, at the early stage of the $\alpha \rightarrow o$ transition, the transitional $PbSnF_4$ contains much more strain than the starting α-$PbSnF_4$. A significant amount of strain remains in the orthorhombic phase, even at a much higher HF volume ratios, although substantially less than in α-$PbSnF_4$ (aq$_1$). It was observed that as HF is added to the SnF_2 solution, the strain increases. For larger HF volume ratios where fully split orthorhombic $PbSnF_4$ is obtained, the strain decreases.

The $\alpha \rightarrow o$-$PbSnF_4$ transition is mostly bidimensional taking place in the $(\bar{a}, \bar{b})$ plane. The parameter **a** increases; **b** decreases and the $(\bar{a}, \bar{b})$ plane shrinks. The changes taking place in the $(\bar{a}, \bar{b})$ plane are driven by the amount of stress acting in the same plane. The presence of HF in the solution seems to overcome the tetragonal symmetry constraints. The decrease in symmetry increases the number of degrees of freedom for the atomic positions, therefore, this allows an increase in packing efficiency of the sheets which is observed in the form of a slight decrease in the **c** parameter. However, since no

measurable composition change occurs at the tetragonal to orthorhombic transition this is a structural phase transition. There could have been some Pb/Sn substitution and this was checked by chemical analyses and bulk density measurements.

SEM was used in order to relate the observed decrease of preferred orientation to the $\alpha \rightarrow o$ phase transition. It was observed that, like α-PbSnF$_4$, o-PbSnF$_4$ is a sheet-like structure with smaller sheets, although their thickness is comparable. The results showed that the particles of both α and o-PbSnF$_4$ are thin flat sheets which is in agreement with the crystal structure of α-PbSnF$_4$ and of our observations that $\alpha \rightarrow o$ is a ferroic type transition with just a minor displacement of the atoms; no drastic structural rearrangement takes place at the transition. The surface area of the sheets decreases drastically at the tetragonal to orthorhombic transition, due to the strain present in the $(\bar{a},\bar{b})$ plane and the near equivalence of the **a** and **b** parameters in the orthorhombic phase, which creates a pull in both $\bar{a}$ and $\bar{b}$ direction in the transitional phase, until one direction sets as being $\bar{a}$ and the other as being $\bar{b}$.

One preparation parameter that was not scrutinized by Parris[7] is the stirring rate . For this work, the influence of stirring was also studied and we observed that in order to have reproducible results the stirring rate must be closely monitored. Without stirring, with high HF added to the solution, Pb$_2$SnNO$_3$F$_5$·2H$_2$O and all peaks are broader. This is due to strong local inhomogeinity when the drops of Pb(NO$_3$)$_2$ solution come in contact with the SnF$_2$ solution. The diffraction pattern of precipitated α-PbSnF$_4$ varies with the stirring rate of the lead nitrate solution, with considerable broadening of (102) under no stirring or at fast stirring, when no or little HF is used. Therefore, a medium to fast

stirring rate is needed to obtain clean $PbSnF_4$. This behaviour is not fully understood at the present time.

The effects of mechanical energy on the different phases of $PbSnF_4$ have been studied and it was observed that upon ball milling α-, o- and β-$PbSnF_4$ give a microcrystalline fluorite type phase. There is not much difference in the grinding time required for the different phases in order to give a microcrystalline fluorite type phase except for β-$PbSnF_4$. o-$PbSnF_4$ gives α-$PbSnF_4$ first on grinding then the microcrystalline fluorite type. β-$PbSnF_4$ requires a much longer grinding time than the other phases but at the end, it also gives a microcrystalline fluorite type phase. All the different phases were annealed after grinding and it was observed that all phases gave α-$PbSnF_4$. This α-$PbSnF_4$ had little if any preferred orientation and was not strained.

From this study, we tried to know if the microcrystalline fluorite type phase is a mixture of β-PbF_2 and amorphous α-SnF_2 or a microcrystalline $PbSnF_4$ with Pb/Sn disorder similar to crystalline γ-$PbSnF_4$ observed only above 390°C. It was found that it is a microcrystalline $PbSnF_4$ which we called $\mu\gamma$-$PbSnF_4$.

Stirring the microcrystalline fluorite type phase obtained from ball milling, in an attempt to remove the amorphous SnF_2 it could contain, resulted in the formation of unstressed non-oriented α-$PbSnF_4$, except for the $\mu\gamma$-$PbSnF_4$ obtained by ball milling o-$PbSnF_4$, which went back to o-$PbSnF_4$. Milling α and β-PbF_2 for comparison showed that both the $\beta \rightarrow \alpha$ and $\alpha \rightarrow \beta$ transitions take place upon milling and give, in both cases, a constant mixture of a major amount of α-PbF_2 and a minor amount of β-PbF_2, both of which are microcrystalline. In further tests that were carried out, stirring α-PbF_2

both of which are microcrystalline. In further tests that were carried out, stirring α-PbF$_2$ in an aqueous solution of α-SnF$_2$ resulted in the formation of α-PbSnF$_4$(aq$_2$) or Pb$_2$SnF$_6$ depending on the PbF$_2$/SnF$_2$ ratio. On the other hand, no reaction occurs with β-PbF$_2$.

The unit-cell parameter of Pb$_2$SnF$_6$ is a (4a   4b   c) superstructure of α-PbF$_2$. Heating at 300°C gives a β-PbSnF$_4$ type tetragonal Pb$_{1-x}$Sn$_x$F$_2$ phase, and upon milling, a $\mu\gamma$-PbSnF$_4$ like phase, μ-Pb$_{1-x}$Sn$_x$F$_2$ is obtained.

The mechanism of phase transitions were studied for all the phases. Orthorhombic PbSnF$_4$ was observed to transform to α-PbSnF$_4$ at 100°C after a very long time ca. 2480 hours. Above 250°C, partial transformation to β-PbSnF$_4$ is observed, which is completed at 290°C. When α-PbSnF$_4$(aq$_1$) is heated at 100°C, the strain is annealed and preferred orientation is reduced. The beginning of the $\alpha \rightarrow \beta$ transition is observed above 250°C, however, it is not completed until 290°C.

CHAPTER 7

SUGGESTIONS FOR FUTURE WORKS

Our study has led to a significant progress in the understanding of the phase transitions undergone by $PbSnF_4$. It has also resulted in the discovery of new phase transitions, like $\alpha\text{-} \rightarrow \mu\gamma\text{-}$, o- $\rightarrow \mu\gamma\text{-}$ and $\beta\text{-} \rightarrow \mu\gamma\text{-}$ upon ball milling , and from $\mu\gamma\text{-} \rightarrow \alpha\text{-}$ (or $\mu\gamma\text{-} \rightarrow$ o-) upon annealing or stirring in water. We have shown that most, if not all, changes are related either to Pb/Sn order-disorder phenomena, strain and/or preferred orientation. Our investigations have also shown a very important fact: the more we learn about $PbSnF_4$, the more remains to be done. Many questions remain unanswered and will require further studies:

1. Crystal structure of each phase of $PbSnF_4$ and of Pb_2SnF_6.

Up to now, the structure of $\alpha\text{-}PbSnF_4$ is known by isotypy to $BaSnF_4$. Crystal structures have also been studied versus temperature by neutron diffraction, however, it is difficult to be sure what was the phase in each case. The structure of $\gamma\text{-}PbSnF_4$ is also known to be fluorite type with full Pb/Sn disorder, since this is the only option for this cubic F lattice with no lattice distortion or superstructure. Presumably, the structure of $\mu\gamma\text{-}PbSnF_4$ obtained upon ball milling is the same. The structure of o-$PbSnF_4$ is not known, but we derived it to be a small bidimensional distortion of $\alpha\text{-}PbSnF_4$. The structure of $\beta\text{-}PbSnF_4$ was shown to be more closely related to $\beta\text{-}PbF_2$. However, the

exact atomic position in both phases and the type of order present in β-PbSnF$_4$ remains unknown. Solving the crystal structure of Pb$_2$SnF$_6$ would show how the superstructure of α-PbF$_2$ is formed. This is the first of this kind. The structural studies of these phases poses a formidable challenge, due to the crystal habit, and the resulting preferred orientation, the presence of high strain in some of the phases, the very high scattering power of lead for X-rays, and the disorder present on some of the fluorite sites. Nevertheless, in order to gain a clearer understanding of these phases, their properties and the phase transitions, structural studies will be necessary. This will require trying to grow single crystals of acceptable quality for single crystal X-ray diffraction and, now that we have designed a method for preparing polycrystalline samples with a low amount of strain and of preferred orientation, neutron powder diffraction could be used (Rietveld profile refinement).

2. Mechanism of the phase transitions at the atomic level.

We have shown that the α → o phase transition is caused by the addition of HF to the SnF$_2$ solution used for the preparation, however, we could not establish why this happens. Testing with F- anions, acids, or even both together did not yield the answer. We also showed that α → o is a bidimensional, most likely ferroic type, transition driven by the presence of a large amount of strain. However, since the atomic positions in o-PbSnF$_4$ are not known, we could not relate the two structures, and establish unambiguously the displacive and ferroic nature of the transitions, and fully explain the presence of strain.

The knowledge of the crystal structure of β-PbSnF$_4$ would make possible to understand the mechanism of the $\alpha \rightarrow \beta$ and of the $\beta \rightarrow \gamma$ transition. It would also lead to the key to the metastability of the β phase and the reversibility of the $\beta \rightarrow \gamma$ phase transition.

Knowing the crystal structures of all the phases may also open the door to the understanding of the formation of $\mu\gamma$-PbSnF$_4$ upon milling, and explain the much longer grinding time required for β-PbSnF$_4$. Other transitions, such as $\mu\gamma$-PbSnF$_4 \rightarrow \alpha$-PbSnF$_4$ upon annealing or stirring in water also need further investigation, as well as $\mu\gamma$-PbSnF$_4 \rightarrow$ o-PbSnF$_4$ upon stirring in water, and the mechanism of the memory effect. Another phase transition of interest is the Pb$_2$SnF$_6$ $\xrightarrow{\Delta}$ Pb$_{0.67}$Sn$_{0.33}$F$_2$.

During this work, we have also observed that the metastable phases β-PbSnF$_4$ and $\mu\gamma$-PbSnF$_4$ show slow transformations on aging at ambient conditions. These phenomena should be investigated in details.

3. Electrical Conductivity

PbSnF$_4$ is the highest performance fluoride ion conductor known to date. This is probably due to the combination of covalently bonded tin(II) with the ionic β-PbF$_2$ structure, creating lattice distortion, superstructures, and a large amount of disorder on the fluorine lattice. However, the conductivity mechanism is still not very clear. Neutron powder diffraction and ^{19}F solid state NMR would be very useful probes and have already been used on some of the phases. Up to now, conductivity measurements have been done on the o- and α-phases. Measurements should also be carried out on the

other phases, i.e. β-, γ-, and μγ-PbSnF$_4$, the latter versus the phase it originated from. In order to compare conductivity of each phase and to understanding the change of conductivity and/or activation energy at each phase transition, the crystal structure of each of the phases must be known. In addition, changes occur even when there is no phase transition, e.g. at ca. 70°C, where an increase of F$^-$ disorder takes place, as we have shown, and not a phase transition, as claimed earlier by others.

The high anisotropy of the orthorhombic and tetragonal structures is highly likely to result in a strong anisotropy of the F$^-$ ion mobility. Indeed, it should be easier for the fluoride ions to move parallel to the plane, where the network of fluorine sites and their defects exist. On the other hand, it should be more difficult for the fluoride ions to move parallel to the $\bar{c}$ axis since they would have overcome the barrier created by the planes of negatively charged tin lone pairs. The conductivity of a polycrystalline sample, should be equal to the average of the three crystallographic axes σ$_{av}$ if a perfectly randomly oriented sample is used. However, this has probably never been measured since before this study, randomly oriented sample could not be obtained, because of the sheet structure and the resulting enhanced preferred orientation. We have found that by ball milling to get μγ-PbSnF$_4$ and subsequent annealing or stirring in water, highly randomized samples of α-PbSnF$_4$ are obtained. Conductivity measurements on these samples should be performed in order to obtain values as close as possible to the true random polycrystalline case. Furthermore, it would be interesting to measure the anisotropy of the conductivity, i.e. in σ$_\perp$ ($\bar{a},\bar{b}$) and σ$_{||}$ along $\bar{c}$. This would normally require large single crystals, which have not been obtained up to date and would be difficult to obtain considering the crystal habit and the presence of a large number of

phase transitions. However, we have developed a method for obtaining quasi-perfect alignment of the crystallites perpendicularly to $\bar{c}$, which would allow the measurement of $\sigma_{\parallel}$. Having already measured σ_{av} for randomly oriented polycrystalline sample, σ_{rs}, and since $\sigma_{rs} = \sigma_{av}$ (where: $\sigma_{av} = (2 \sigma_{\perp} + \sigma_{\parallel})/3$, one could determine $\sigma_{\perp}$, and thus obtain the anisotropy of the conductivity.

4. Other studies

Many other studies could be performed as extensions of the work presented here. For example, during the development of this work, we have discovered and partly characterized several new crystalline phases, which are not reported here. Recrystallization of o-PbSnF$_4$ in HNO$_3$ also give several new phases (probably at least 3 or 4) all of which give also very thin sheet-like crystallites. Their exact composition has not been determined, but they contain Pb, Sn, F, and NO$_3$. Furthermore, by adding a solution of SnF$_2$ to a solution of Pb(NO$_3$)$_2$, Pb$_2$SnNO$_3$F$_5\cdot$2H$_2$O was obtained, when PbSnF$_4$ is obtained by adding a solution of Pb(NO$_3$)$_2$ to a solution of SnF$_2$. Much more work remains to be done on all these new phases and Pb$_2$SnNO$_3$F$_5\cdot$2H$_2$O, including determining their formula (except for Pb$_2$SnNO$_3$F$_5\cdot$2H$_2$O), and solving their crystal structures, investigating the possibility of the existence of phase transitions on heating and by ball milling, and studying their conducting properties.

In addition, the study of preferred orientation in the materials we have obtained should be carried out using mainly X-ray powder diffraction and Mössbauer spectroscopy. Furthermore, since the fluoride ion conductivity is thermally activated and

PbSnF$_4$ has already been used in the fabrication some practical devices, and since several phase transitions take place at high temperature, it is suggested to study the stability of the material when heated in air. We have already carried out preliminary experiments that show an amorphous passivating layer similar to that observed earlier in SnF$_2$ by Dénès et al. is formed. Further investigations are required.

REFERENCES

1. J.D. Donaldson and B.J. Senior, *J.Chem.Soc* (A), 1821 (1967).

2. G. Dénès, J. Pannetier and J. Lucas, *C.R. Acad. Sc. Paris C*, **280**, 831 (1975).

3. J.M Réau, C. Lucat, J. Portier, P.Hagenmuller, L. Cot and S. Vilminot, *Mat. Res. Bull.*, **13**, 877 (1978).

4. J. Pannetier, G. Dénès and J. Lucas, *Mat. Res. Bull.*, **14**, 627 (1979).

5. G. Perez, S. Viminot, W. Granier, L. Cot, C. Lucat, J.M Réau, J. Portier and P. Hagenmuller, *Mat. Res. Bull.*, **15**, 587 (1980).

6. T. Birchall, G. Dénès, K. Ruebenbauer and J. Pannetier, *Hyperfine Interact.*, **29**, 1331 (1986)

7. J. M Parris, *M.Sc. Thesis*, Concordia University Montréal, Quebec Canada (1988).

8. G. Dénès, M.C. Madamba and J.M. Parris "Solid State Ionics IV", *Mat. Res. Soc. Symp. Proc.*, **369**, 463 (1995).

9. R. Kanno, S. Nakamura, K. Ohno and Y. Kawamoto, *Mat. Res. Bull.*, **26**, 1111 (1991).

10. Y. Ito, T. Mukuyama, H. Funatomi, S. Yoshikado and T. Tanaka, *Solid State Ionics*, **67**, 301 (1994).

11. R. Kanno, K. Ohno, H. Izumi, Y. Kawamoto, T. Kamiyama, H. Asano and F. Izumi, *Solid State Ionics*, **70/71**, 253 (1994).

12. G. Dénès , Y.H. Yu, T. Tyliszczak and A.P. Hitchcock, *J. Solid State Chem.*, **91**, 1 (1991).

13. J.E. Callanan, R.D. Wier, and E.F. Westrum, Jr., *Can. J. Chem.*, **66**, 549 (1988).

14. G. Dénès, T. Birchall, M. Sayer, and M.F. Bell, *Solid State Ionics* , **13**, 213 (1988).

15. G. Dénès, "Solid State Ionics IV", *Mat. Res. Soc. Symp. Proc.*, **369**, 295 (1995).

16. T. Birchall, G. Dénès, K. Ruebenbauer and J. Pannetier, *J. Chem Soc. Dalton Tr,.* 2296 (1981).

17. G. Dénès, D. Le Roux, and A. Muntasar, *J. Radioanal. Nucl. Chem. Articles*, **190**, 431 (1995).

18. A. Muntasar and G. Dénès, *Mössbauer Spectroscopy in Material Science*, (1998) in press.

19. J. Barrett, S.R.A. Bird, J.D. Donaldson and J. Silver, *J. Chem. Soc.* **(A)**, 3105 (1971).

20. G. Dénès, M.C. Madamba, A. Muntasar, A. Peroutka, K. Tam and Z. Zhu, *Mössbauer Spectroscopy in Material Science*, (1998) in press.

21. G. Dénès, G. Milova, M.C. Madamba, and M. Perfiliev, *Solid State Ionics*, **77**, 86-88 (1996).

22. G. Milova, G. Dénès, M.C. Madamba, and M. Perfiliev, *Mat. Res. Soc. Symp. Proc.*, **398**, 525 (1996).

23. G. Villeneuve, P. Echegut, C. Lucat, J.M. Réau and P. Hagenmuller, *Phys. Stat. Solidi*, **(b) 97**, 295 (1980).

24. M. Durand-Le Floch, J. Pannetier and G. Dénès, *Phys. Rev. B*, **33**, 632 (1986).

25. A. Wakagi and J. Kuwano, *J. Mat. Chem.*, **41**, 973 (1994).

26. A. Wakagi , J. Kuwano, M. Kato and H. Hanamoto, *Solid State Ionics*, **70/71**, 601 (1991).

27. G. Dénès , Y.H. Yu, T. Tyliszczak and A.P. Hitchcock, *J. Solid State Chem.*, **104**, 239 (1993).

28. G. Dénès, *J. Solid State Chem.*, **77**, 54 (1988).

29. W. Parrish, E.A. Hamacher, and K. Lowitzsch, Philips Tech. Rev. **16**, 123 (1954).

30. Joint Committee for Powder Diffraction Standards (JCPDS), International Centre for Diffraction Data, Swarthmore, PA.

31. Micro-Powder Diffraction Search Match (μPDSM) Fein-Marquat Associates, Inc., Baltimore, MD.

32. E.W Nuffield, *X-ray Diffraction Methods*, John Wiley & Sons, NY (1966).

190

33. G.D Christian, Analytical Chemistry, (1986).

34. E.S Gladney and W.E Goode, *Analytica Chimica Acta*, **91**, 411 (1977).

35. G. Dénès, M.A Dénès, F. Lenay, D. LeScorner, to be published.

36. A. Vaillancourt, *M.Sc. Thesis*, Concordia University Montréal, Québec Canada, 1990.

37. A.R West, *Solid State Chemistry and its Applications*, J. Wiley & Sons, New York, pp. 102-108, 363, 365, 466 and 663 (1984).

38. N.N. Greenwood and T.C. Gibb, *Mössbauer Spectroscopy*, Chapman and Hall, London (1971).

39. G. Dénès, *Proc. of the 2nd Nassau Mössbauer Conf.*, (ed) C.I. Wynter and E.E. Alp, W.C Brown Publishers, 109 (1994).

40. Z. Zhu, *M. Sc. Thesis*, Concordia University Montréal, Québec Canada, 1990.

41. G. Dénès, A. Muntasar and Z. Zhu, *Hyperf. Interact. C*, **1**, 468 (1996).

42. B.D Cullity, *Elements of X-ray Diffraction*, 3rd Ed. (Addison-Wesley Reading), pp. 263-269, 444-453 (1959).

43. G. Dénès, R. Le Van Mao and A. Vaillancourt, *Mat. Res. Soc. Symp. Proc.*, **356**, 105 (1995).

44. K. Aizu, *J. Phys. Soc. Japan*, **27**, 387 (1969).

45. K. Aizu, *Phys Rev. B*, **2**, 754 (1970).

46. G. Dénès, *Mat. Res. Bull.*, **15**, 807 (1980).

47. G. Dénès, *J. Solid State Chem.*, **36**, 20 (1981).

48. T.G. Warlton and R.A. Beyertein, Phys. Rev. B, **12**, 1899 (1975).

49. S. Gobon, Acta Chem. Scand. A **30**, 745 (1976).

50. T. Birchall and G. Dénès, *Can. J. Chem.*, **62**, 591 (1984).

51. G. Dénès and E. Laou, *Hyperf. Interact.*, **92**, 1013 (1994).

52. G. Dénès and E. Laou, *Mater. Res. Symp. Proc.*, **357**, 109 (1995).

53. G. Dénès, A. Gueune, E. Laou and S. Le Huérou, "High Temp. Electrochem." *Ceramics and Metals Proc. 17th Riso International Symp. on Materials Sciences*, 223 (1996).

54. G. Dénès and A. Muntasar, *Proc. Inter. Conf. Appl. Mössbauer Effect: ICAME-95*, ed. I. Ortalli, **50**, 83 (1996).

55. A. Muntasar and G. Dénès, *Proc. Inter. Conf. Appl. Mössbauer Effect: ICAME-95*, ed. I. Ortalli, **50**, 127 (1996).

56. G. Dénès, J. Bratigny, D. Le Roux and A. Muntasar, *Mater. Res. Soc. Symp. Proc.*, **453**, 177 (1997).

57. G. Dénès and A. Muntasar, *Materials Structure*, **3**, 246 (1996).

58. G. Dénès, in preparation.

59. G. Dénès, *J. Solid State Chem.*, **37**, 16 (1981).

60. J. Pannetier, G. Dénès, M. Durand and J.L. Bueroz, *J. Physique*, **41**, 1019 (1980).

ARTICLES PUBLISHED FROM THIS WORK

1. G. Dénès, M. C. Madamba and J. M. Parris,
   "Strain Driven Two-Dimensional Phase Transition in PbSnF$_4$ Superionic Conductor."
   "Solid State Ionics", *Mat. Res. Soc. Symp. Proc.*, Vol. **369**, 463-468 (1995).

2. G.Dénès and M. C. Madamba,
   "Kinetics of Phase Transitions in Superionic PbSnF$_4$ versus Temperature."
   "Thermodynamics and Kinetics of Phase Transformations", *Mat. Res. Soc. Symp. Proc.*, Vol. **398** , 525 (1996).

3. G. Dénès, M. C. Madamba, G. Milova and M. Perfiliev,
   "Electrical Characterization of the Structure, Texture and Other Phenomena in Superionic PbSnF$_4$." "Electrically Based Microstructural Characterization", *Mat. Res. Soc. Symp, Proc.*, Vol. **411**, 151 (1996).

4. G. Dénès, G. Milova, M. C. Madamba and M. Perfiliev,
   "Structure and Ionic Transport of PbSnF$_4$ - Superionic Conductor."
   Solid State Ionics, Vol. **86-88**, 77-82 (1996).

5. G.Dénès and M.C. Madamba,
   "X-ray Diffraction Study of Phase Transformations in Superionic PbSnF$_4$ upon Milling and Subsequent Annealing." *Materials Structures in Chemistry, Biology, Physics and Technology*, Vol. **3**, 246 (1996).

6. R. Calandrino, A. Collins, G. Dénès , M. C. Madamba and J. M. Parris,
   "Phase Stability and Properties of Superionic PbSnF$_4$ as a Function of the Method of Preparation. "Solid State Chemistry of Inorganic Materials", *Mat. Res. Soc. Symp, Proc.*, Vol. **453**, 585-590 (1997).

7. G. Dénès and M. C. Madamba,
   "Phase Transitions in Lead(II)Fluoride upon milling","Phase Transformations and Systems driven far from Equilibrium", *Mat. Res. Soc. Symp. Proc.*, Vol. **481**, 673-678 (1998).

8. G. Dénès, D. Le Roux and M. C. Madamba,
"Phases driven far from Equilibrium by applying Mechanical energy: Phase transformations to $\mu\gamma$-PbSnF$_4$ upon Ball Milling","Phase Transformations and Systems driven far from Equilibrium", *Mat. Res. Soc. Symp. Proc.*, Vol. **481**, 667-672 (1998).

9. G. Dénès, M. C. Madamba, A. Muntasar, A. Peroutka, K. Tam and Z. Zhu,
"Application of Mössbauer Spectrocopy to the Study of the Structure, Order/Disorder Phenomena and Conduction Mechanism of Fluoride Ion Conductors.", *Proc. MSMS98 - Mössbauer Spectrocopy in Materials Science*", NATA Advanced Research Workshop, in press (1998).

10. A. Collin, G. Dénès, D. Le Roux, M.C. Madamba, J.M. Parris and A. Salaün,
"Understanding the Phase Transitions and Texture in Superionic PbSnF$_4$: The Key to Reproducible Physical Properties. ", *Proc. IM98- First International Conference on Inorganic Materials*, submitted (1998).

11. G. Dénès, M. C. Madamba and A. Muntasar,
"Reactivity of SnF$_2$ with Fluorite type MF$_2$ versus M: Synthesis of High Performance Fluoride Ion Conductors", "Solid State Chemistry of Inorganic Materials II", *Mat. Res. Soc. Symp. Proc.*, in press (1999).

12. G. Dénès, M. C. Madamba and A. Muntasar,
"Reactivity and Stability of Superionics MSnF$_4$ at High Temperature in various Media", "Solid State Chemistry of Inorganic Materials II", *Mat. Res. Soc. Symp. Proc.*, in press (1999).

13. G. Dénès, M. C. Madamba, A. Muntasar, A. Peroutka, K. Tam and Z. Zhu,
"Use of Mössbauer Spectrocopy for the Characterization of Order/Disorder Phenomena in Tin(II) Containing Ionic Conductors and for Making Predictions Regarding Possible Electron Contribution to the Conduction", Solid State Ionics", *Mat. Res. Soc. Symp. Proc.*, in press (1999).

14. R. Calandrino, A. Collin, G. Dénès and M. C. Madamba,
"Reactivity of Fluoride Ion Conductor PbF$_2$: A Comparative Study of the Reactivities of α- and β-PbF$_2$ in the Synthesis of Superionic Conductors", "Solid State Chemistry of Inorganic Materials II", *Mat. Res. Soc. Symp Proc.*, submitted (1999).

15. G. Dénès, H. Merazig, M. C. Madamba, A. Muntasar,
    W. Nanayakkara, A. Peroutka, K. Tam and Z. Zhu,
    "Search for New Fluoride Ion Conductors with Inorganic Polymeric Networks",
    "Solid State Ionics", *Mat. Res. Soc. Symp. Proc.*, submitted (1999).

16. G. Dénès, M. C. Madamba, A. Muntasar and Z. Zhu,
    "Crystal Structure and Characterization of Order/Disorder in Ionic Conductors: A
    Combination of techniques is Required", "Solid State Ionics", *Mat. Res. Soc. Symp.
    Proc.*, submitted (1999).

17. G. Dénès and M. C. Madamba,
    "Design of a Method for Measuring the Conductivity Anisotropy of $PbSnF_4$ Fluoride
    Ion Conductor from Polycrystalline Material", "Solid State Ionics", *Mat. Res. Soc.
    Symp. Proc.*, submitted (1999).

18. G. Dénès and M. C. Madamba,
    "Thermodynamic Stability and Phase Transitions in Fluoride ion Conductors Derived
    from the Fluoride type Structure", "Solid State Ionics", *Mat. Res. Soc. Symp. Proc.*,
    submitted (1999).